# Biochemical Studies on the Mechanism of Action of Remdesivir and Other Nucleotide Analog Polymerase Inhibitors during the COVID-19 Pandemic

by

Calvin Joel Gordon

A thesis submitted in partial fulfillment of the requirements for the degree of

Doctor of Philosophy

in

Virology

Department of Medical Microbiology and Immunology

University of Alberta

Abstract

Several disease-causing RNA virus families, capable of infecting humans, remain a significant global health threat due to the lack of effective medical countermeasures. This was perhaps best exemplified early in the COVID-19 pandemic when spread of severe acute respiratory syndrome coronavirus 2 (SARS-CoV-2) went unperturbed. To counteract future outbreaks, epidemics, and pandemics, effective antiviral drugs available for immediate use are needed. However, pharmaceutical intervention strategies are challenged by the diverse nature of the RNA viruses. Therefore, a proactive approach is required, directing research efforts toward prototypic RNA viruses representing different viral families. Placing emphasis on broadly acting antiviral agents can help amplify preparedness efforts. Required for viral genome replication, the viral RNA-dependent RNA polymerase (RdRp), specifically the highly conserved catalytic active site, represents a logical therapeutic target for broad-spectrum nucleoside analogs. To this end, remdesivir (RDV), β-D-$N^4$-hydroxycytidine (NHC), and GS-7682, have demonstrated antiviral activity against several different RNA virus families. This thesis details the biochemical characterization of the active 5′-triphosphate (TP) form of the aforementioned nucleoside analogs against various viral RdRp.

Aligning with the prototypic framework, chapter 3 presents the investigation of RDV-TP against Middle East respiratory syndrome coronavirus (MERS-CoV) RdRp initiated before the COVID-19 pandemic. Here, I help illustrate the first mechanism of action of RDV-TP against a model coronavirus RdRp. I found that RDV-TP is incorporated more efficiently than its natural counterpart ATP and inhibits RNA synthesis via delayed chain termination. Importantly, these studies enabled the timely transition into pandemic rapid response efforts and the investigation of SARS-CoV-2 when vaccines and antivirals were not available. Chapters 4 and 5 present a more

complete mechanism of action for RDV-TP against SARS-CoV-2 RdRp, identifying two different modes of inhibition during virus replication. Exemplifying the utility of our biochemical techniques, I also investigated other clinically relevant broad-spectrum nucleotide analogs, providing an early indication of their efficacy that preclinical and clinical studies would later confirm.

The intravenous administration of RDV inherently restricts treatment regimens to hospitalized patients. Considering this, molnupiravir, the prodrug of NHC, represented an orally available treatment for COVID-19. In chapter 6, I show the first biochemical mechanism for molnupiravir against SARS-CoV-2, explaining the mutagenic effect observed in previous studies. Crucial to this investigation was the ability to monitor base pairing tendencies during RNA virus transcription and replication that facilitate error catastrophe. Together, my investigation of RDV and molnupiravir supported their approval and authorization for the treatment of COVID-19 by the Food and Drug Administration, respectively.

RDV contains a 1′-cyano modification and stands as the preferred treatment for coronavirus infection. Conversely, GS-7682 is a novel 4′-cyano modified nucleoside prodrug that targets other high priority RNA viruses, namely picorna- and pneumoviruses. In chapters 7 and 8, RDV-TP and GS-646939, the active metabolite of GS-7682, are investigated against a panel of viral RdRp. We show that efficient incorporation is required to elicit an antiviral effect, RDV-TP universally inhibits RNA synthesis when embedded in the template-strand, and GS-646939 acts predominately as an immediate chain terminator. The observed mechanistic differences between RDV-TP and GS-646939 offer assurance that 1′- and 4′-cyano modified nucleotides are viable candidates to target a spectrum of RNA viruses. These insights will guide the development of nucleotide analogs as effective therapeutics available for the next pandemic.

## Preface

Permissions – The American Society for Biochemistry and Molecular Biology (ASBMB) States: Effective with initial submissions from January 1, 2018, authors must agree that if their manuscript is accepted, they will grant ASBMB an exclusive, irrevocable License to Publish their work; the copyright remains with the authors. Authors of manuscripts, submitted at any time, need not contact the journal to request permission to reuse their own material. Authors are allowed to do the following:

1. To use all or part of the work in compilations or other publications of the Authors' own commercial and noncommercial works (includes theses/dissertations), to use figures, photos, and tables created by them and contained in the work, to present the work orally in its entirety, and to make copies of all or part of the work for the Authors' use for lectures, classroom instruction or similar uses. If the author is employed by an academic institution, that institution also may reproduce the article for teaching purposes.
2. To post the accepted manuscript version of the work, the "Paper in Press," on the author's personal web page, their personal or institutional repository, or their funding body's archive or designated noncommercial repository, provided that a link to the article on the journal site is included.
3. To post a manuscript version of the work on not-for-profit preprint servers provided that the Authors retain distribution rights to the work, that ASBMB formatted final files are not posted, and that a link to the article on the journal site is included.
4. To post the final edited PDFs, created by ASBMB, to their own departmental/university websites, provided that the posting does not happen until 12 months after publication of the work, and that a link to the article on the journal site is included.

This thesis is an original work by Calvin Gordon under the supervision of Dr. Matthias Götte. The research presented in the data chapters was originally published in the Journal of Biological Chemistry and completed through collaboration with others to maximize output and aid pandemic rapid response efforts. Author contributions and project funding are detailed at the beginning of each data chapter.

A portion of chapters 2 & 3 of this thesis have been published as "Gordon CJ[#], Tchesnokov EP[#], Feng JY, Porter DP, Götte M. The antiviral compound remdesivir potently inhibits RNA-dependent RNA polymerase from Middle East respiratory syndrome coronavirus. J Biol Chem. 2020; 295:4773-4779. © the authors."

A portion of chapters 2 & 4 of this thesis have been published as "Gordon CJ[#], Tchesnokov EP[#], Woolner E, Perry JK, Feng JY, Porter DP, Götte M. Remdesivir is a direct-acting antiviral that inhibits RNA-dependent RNA polymerase from severe acute respiratory syndrome coronavirus 2 with high potency. J Biol Chem. 2020; 295:6785-6797. © the authors."

A portion of chapters 2 & 5 of this thesis have been published as "Tchesnokov EP[#], Gordon CJ[#], Woolner E, Kocincova D, Perry JK, Feng JY, Porter DP, Götte M. Template-dependent inhibition of coronavirus RNA-dependent RNA polymerase by remdesivir reveals a second mechanism of action. J Biol Chem. 2020; 295:16156-16165. © the authors."

A portion of chapters 2 & 6 of this thesis have been published as "Gordon CJ, Tchesnokov EP, Schinazi RF, and Götte M. Molnupiravir promotes SARS-CoV-2 mutagenesis via the RNA template. J Biol Chem. 2021; 297:100770. © the authors."

A portion of chapters 2 & 7 of this thesis have been published as "Gordon CJ[#], Lee HW[#], Tchesnokov EP[#], Perry JK, Feng JY, Bilello JP, Porter DP, and Götte M. Efficient incorporation and template-dependent polymerase inhibition are major determinants for the broad-spectrum antiviral activity of remdesivir. J Biol Chem. 2022; 298:6785-6797. © the authors."

A portion of chapters 2 & 8 of this thesis have been published as “Gordon CJ, Walker SM, Tchesnokov EP, Kocincova D, Pitts J, Siegel D, Perry JK, Feng JY, Bilello JP, and Götte M. Mechanism and spectrum of inhibition of a 4′-cyano modified nucleotide analog against diverse RNA polymerases of prototypic respiratory RNA viruses. J Biol Chem. 2024; 300:107514. © the authors.”

[#]Authors contributed equally to this work.

Dedication

This thesis is dedicated to my parents Michelle, Scott, Craig, and Chandelle.

Acknowledgements

The completion of this thesis would not have been possible without with the support of several people both inside and outside the lab.

I would first like to thank my supervisor, Dr. Matthias Götte, for the unconditional support throughout my studies. You taught me that the ability to collaborate with others and proficiently communicate my research are skills equally valuable to the benchwork itself. I appreciate the freedom you gave me to pursue different ideas that may not have been pertinent to my ongoing projects but allowed me to learn and improve as independent investigator; and the invaluable experience I gained through travel and presenting my research to different audiences. I wish you nothing but the best in the years to come.

I would next like to thank Dr. Egor Tchesnokov. I am grateful for all the skills you taught me at the lab bench and for helping me think of different and creative approaches to answer difficult questions. Your dedication to science and consistency in the lab does not go unnoticed and is something I strive to emulate. You have undoubtably helped me grow as a scientist and as an individual. I wish you the best of luck on your future endeavors.

Chapters 3, 4, and 5 included in this dissertation represents some of the most fun I have had doing science. For this I would like to thank our outstanding collaborators Dr. John Bilello, Dr. Jason Perry, and Dr. Joy Feng, much of the work presented in this thesis does not happen without your support.

Next, I would like to extend my gratitude to Dr. Kalyan Das for hosting me as a visiting researcher. Working in your group underscored the importance of fostering a supportive work environment, where I forged friendships that I will always cherish.

I would like to thank current and former members of the Götte lab for their friendship and support: Kieran Maheden, Parisa Raesimakiani, Brendan Todd, Hery Lee, Jalisa Kassam, Arlo Loutan, Simon Walker, Emma Woolner, Dr. Dana Kocincova, and Dr. Maulik Badmalia.

Thank you to the MMI department, students and staff you all made coming to the lab an enjoyable experience that I will surely miss.

Finally, I am forever grateful to my family and friends for their unwavering support, with special thanks to my parents and my partner Tifanny.

Table of Contents

List of Tables

# List of Figures

## Chapter 1: Introduction



## Chapter 3: The antiviral compound remdesivir potently inhibits RNA-dependent RNA polymerase from Middle East respiratory syndrome coronavirus



## Chapter 4: Remdesivir is a direct-acting antiviral that inhibits RNA-dependent RNA polymerase from severe acute respiratory syndrome coronavirus 2 with high potency

Chapter 5: Template-dependent inhibition of coronavirus RNA-dependent RNA polymerase by remdesivir reveals a second mechanism of action



Chapter 6: Molnupiravir promotes SARS-CoV-2 mutagenesis via the RNA template



Chapter 7: Efficient incorporation and template-dependent polymerase inhibition are major determinants for the broad-spectrum antiviral activity of remdesivir

List of Abbreviations

ATP – adenosine triphosphate

ADK – adenosine kinase

AZT – 3′-azido-3′-deoxythymidine

BEVS – baculovirus expression vector system

CCHFV – Crimean-Congo hemorrhagic fever virus

CHIKV – chikungunya virus

COVID-19 – Coronavirus disease 2019

CTP – cytidine triphosphate

CVB3 – coxsackievirus B3

DAA – Direct-acting antiviral

DENV– Dengue virus

DNA – deoxyribonucleic acid

EBOV – Ebola virus

EDTA – ethylenediaminetetraacetic acid

EFdA – 4′-ethynyl-2-fluoro-2′-deoxyadenosine

ETV – entecavir

EUA – emergency use authorization

EV – Enterovirus

EVD – Ebola virus disease

ExoN – exonuclease

FDA – Food and Drug Administration

FMDV – foot-and-mouth disease virus

FluB – influenza B

FVP – favipiravir

GTP – guanosine triphosphate

HBV – hepatitis B virus

HCV – hepatitis C virus

HIV-1 – human immunodeficiency virus 1

HMPV – human metapneumovirus

h-mtRNAP – human mitochondrial RNA polymerase

HPIV-3 – human parainfluenza virus 3

HRV-16 – human rhinovirus type 16

HSV – herpes simplex virus

IMPDH – inosine monophosphate dehydrogenase

JEV – Japanese encephalitis virus

Kb – kilobases

KCl – potassium chloride

kDa – kilodalton

LASV – Lassa virus

L – large protein subunit

MeV – Measles virus

MERS-CoV-2 – Middle East respiratory syndrome coronavirus

MHV – murine hepatitis virus

MP – Monophosphate

MTase – methyltransferase

NaCl – sodium chloride

NIAD – National Institute of Allergy and Infectious Diseases

Ni-NTA – nickel nitrilotriacetic acid

NiRAN – Nidovirus RdRp-Associated Nucleotidyltransferase

NiV – Nipah virus

Nsp – non-structural protein

N-site – nucleotide-binding site

PA – polymerase acidic

PB – polymerase basic

P – phosphoprotein

PIV-5 – parainfluenza virus 5

PV – poliovirus

PPi – inorganic pyrophosphate

P-site – priming site

RBV – ribavirin

RDV – remdesivir

RDV-TP – remdesivir triphosphate

RdRp – RNA-dependent RNA polymerase

RNA – ribonucleic acid

RSV – respiratory syncytial virus

RT – reverse transcriptase

RVFV – Rift Valley fever virus

SARS-CoV – severe acute respiratory syndrome coronavirus

SARS-CoV-2 – severe acute respiratory syndrome coronavirus 2

SDS-PAGE – sodium dodecyl sulfate-polyacrylamide gel electrophoresis

TEV – Tobacco Etch virus

TP – triphosphate

UTP – uridine triphosphate

VP35 – viral protein 35

WHO – World Health Organization

WNV – West Nile virus

YFV – Yellow fever virus

ZIKV – zika virus

2′-F,2′-Me – 2′-α-fluoro,2′-β-methyl

2′-F,4′-$ClCH_2$ – 2′-fluoro,4′-chloromethyl

4′-F U – 4′-fluorouridine

# Chapter 1: Introduction

## 1.1 RNA viruses of interest and their public health burden

Several disease-causing RNA virus families remain a significant threat to human health due to the lack of effective medical countermeasures. To counteract this, the World Health Organization (WHO) and the National Institute of Allergy and Infectious Diseases (NIAID) have published a framework to direct research and development efforts[1, 2]. These strategies are proactive, emphasizing the need to research prototype RNA viruses from important families. The success of this approach is best demonstrated by pandemic response efforts to severe acute respiratory syndrome coronavirus 2 (SARS-CoV-2), the causative agent of coronavirus disease 2019 (COVID-19) and member of the *Coronaviridae* family[3, 4]. Prior to the COVID-19 pandemic, research on related coronaviruses, SARS-CoV and Middle East respiratory syndrome coronavirus (MERS-CoV), allowed for rapid advancement of COVID-19 vaccines[2]. As detailed by the WHO and NIAID, additional RNA virus families that possess high pandemic potential are *Picornaviridae*, *Flaviviridae*, *Filoviridae*, *Paramyxoviridae*, *Orthomyxoviridae*, and five virus families belonging to the *Bunyavirales* order (*Arena*-, *Hanta*-, *Nairo*-, *Peribunya*-, and *Phenuiviridae*). Although not included in this list, RNA viruses within the *Pneumoviridae* family are often associated with acute lower respiratory infections and present a global health burden to children and older adults[5, 6]. Collectively, these families encompass positive-sense, non-segmented negative-sense, and segmented negative-sense single-stranded RNA viruses. They are classified according to their genome structure and translatability (Fig. 1.1)

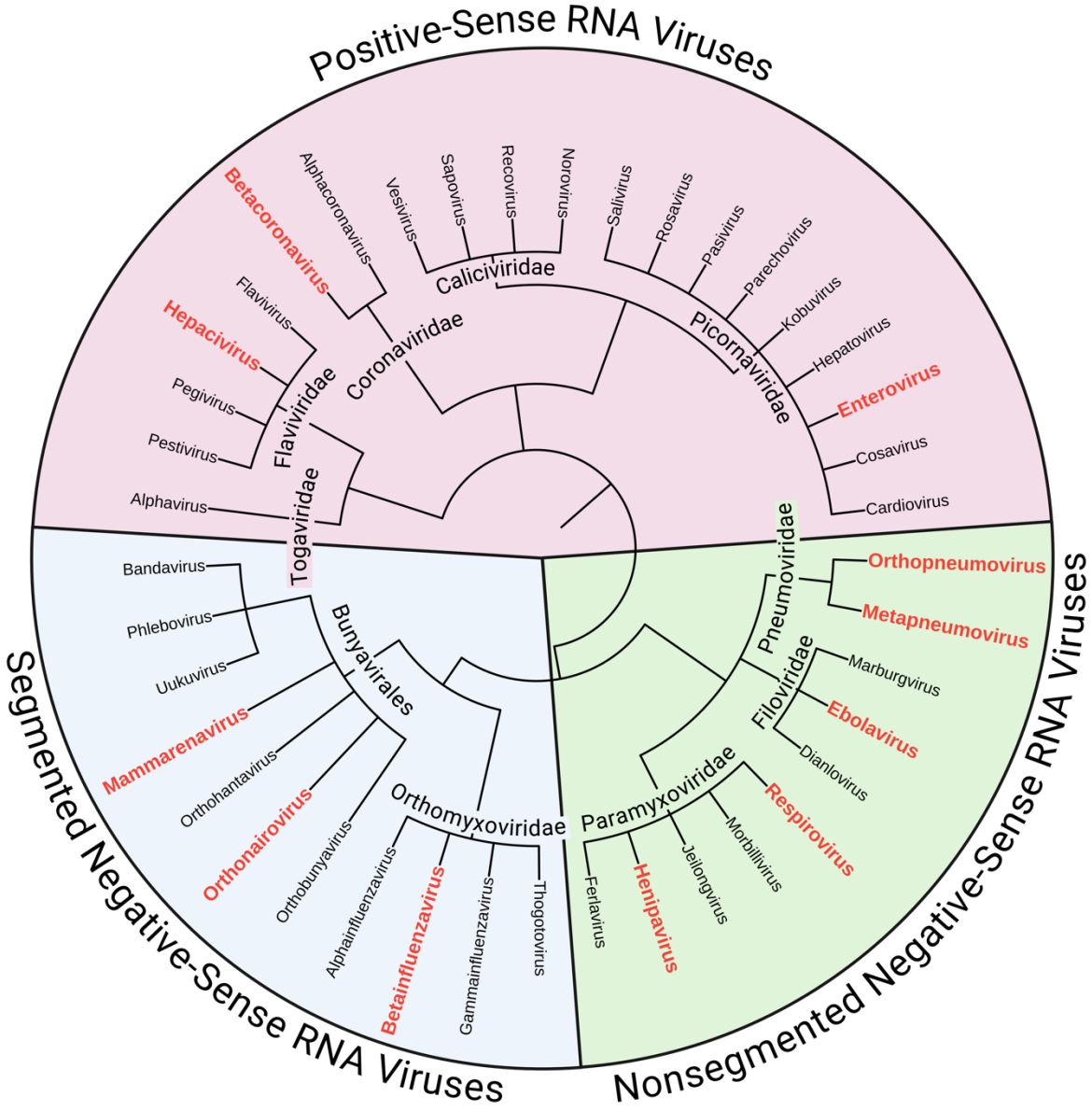


**Figure 1.1. A phylogenetic tree demonstrating the relatedness of different single-stranded RNA virus families discussed in this thesis**. Maximum likelihood phyolgenetic tree was generated using the conserved cataltyic motifs of the viral RNA-dependent RNA polymerase. The genomic structure and polarity are displayed outside the circle, viral families are denoted by "-viridae", and the five clades below *Bunyavirales* (top down) represent *Phenu-*, *Arena-*, *Hanta-*, *Nairo-*, and *Peribunyaviridae*, respectively. The RdRp investigated in the data chapters of this thesis belong to an RNA virus from the genus shown in red. This phylogenetic tree was visualized using Interactive Tree of Life (iTOL) v6[7] and BioRender.com. The data file required to create the phylogenetic tree was provided by Dr. Bart Hazes.

To accommodate different replication strategies, RNA viruses have evolved replication machinery that often contains several functional domains. This variation inherently stifles the development of effective medical countermeasures. However, central to the replication of all RNA viruses, the viral RNA-dependent RNA polymerase (RdRp) represents a common therapeutic target. Despite the structural variations of these enzymes across viral families, there is relatively consistent preservation of both the active site and the mechanisms underlying nucleic acid synthesis. Therefore, the cumbersome task of antiviral development can be lessened by nucleoside analogs that offer broad-spectrum antiviral activity against multiple RNA virus families. Historically, nucleoside analogs constitute a large proportion of approved treatments for viral infection[8, 9]. Exemplifying their success, nucleoside analog prodrugs are a standard of care against human immunodeficiency virus 1 (HIV-1), herpes simplex virus (HSV), hepatitis B virus (HBV), and hepatitis C virus (HCV) infection. The data chapters presented in this thesis describe the biochemical parameters of three different nucleotide analogs that allow them to effectively target the RdRp of different RNA viruses.

## 1.2 Viral RNA-dependent RNA polymerases

The biosafety measures required for the investigation of nucleoside analogs against live RNA viruses, although essential, can delay therapeutic development. To mitigate this, direct antiviral targets like the RdRp of RNA viruses can be recombinantly expressed and investigated using more accessible biochemical techniques. This approach offers several advantages, such as high-throughput screening, target validation, and mechanism of action studies. The latter of which is supplemented by detailed kinetic and structural investigation. Essential to these endeavours is a catalytically competent polymerase active site, which may require additional cofactors to support RNA synthesis. Discussed below are the RdRp and accessory proteins of important positive- and negative-sense RNA virus families required for the biochemical investigation of nucleotide analogs and their inhibition of RNA synthesis.

### 1.2.1 *Picornaviridae*

The *Picornaviridae* positive-sense genome is relatively small (7 to 8 Kb) compared to other single-stranded RNA viruses. The RdRp also referred to as $3D^{pol}$, is monomeric and does not require additional cofactors[10, 11] (Fig. 1.2*A*, *top*). Conserved at the core of most other viral RdRp, the simplicity inherent to picornavirus replication has allowed $3D^{pol}$ to serve as an archetype to investigate single-stranded RNA virus replication[12, 13]. Readily expressed in bacteria, the $3D^{pol}$ has supported the investigation of RNA synthesis fidelity, initiation, and elongation. Poliovirus (PV), coxsackievirus B3 (CVB3), enterovirus (EV), and human rhinovirus (HRV) $3D^{pol}$ are most often employed for biochemical studies. The first RdRp structure solved belonged to PV and confirmed the presence of the evolutionarily conserved subdomains fingers, palm, and thumb that house the catalytic motifs required for nucleic acid synthesis[14] (Fig. 1.2*B*). $3D^{pol}$-mediated RNA synthesis can be investigated *in vitro* using short oligonucleotide substrates to form elongation complexes.

### 1.2.2 *Flaviviridae*

The *Flaviviridae* family is comprised of the *Hepacivirus*, *Flavivirus*, *Pegivirus*, and *Pestivirus* genera, their positive-sense genome can vary in size from 9 to 13 Kb. HCV is a well-studied human pathogen that can be subdivided into six genotypes. HCV replication relies on non-structural protein 5B (NS5B) (Fig.1.2*A*, *middle*) and has been the subject of extensive biochemical characterization. Crystallographic studies of HCV NS5B provided the first indication of an encircled active site[15-17] (Fig. 1.2*C*), a structural feature shared with the picornavirus RdRp[18]. Important to these studies was the realization that the removal of 21 hydrophobic residues from the C-terminus improved the solubility of a catalytically active NS5B[19, 20]. HCV infection can often be treated successfully with the nucleoside prodrug sofosbuvir[21, 22]. Consequently, therapeutic development efforts have now pivoted to mosquito-borne flaviviruses capable of causing human disease. These include Dengue virus (DENV), Japanese encephalitis virus (JEV), Yellow fever virus (YFV), West Nile virus (WNV) and Zika virus (ZIKV). Translation of the flavivirus genome generates a single polyprotein comprised of three structural and seven non-structural proteins[23]. Non-structural protein 5 (NS5) contains two therapeutic targets, the methyltransferase (MTase) and RdRp domain at the N- and C-terminus, respectively. Like picornavirus $3D^{pol}$, biochemical investigation of NS5-catalyzed RNA synthesis does not require additional protein cofactors. However, reduced RdRp activity in the absence of the MTase domain

suggests their activities are coupled during RNA synthesis[24, 25]. Expressed in *E. coli*[26] or baculovirus-infected insect cells[27], NS5 is capable of RNA synthesis *in vitro* using an oligonucleotide primer, enabling the investigation of elongation complexes[28-30]. With the support of structural and biochemical studies, many of the mechanisms pertaining to picornavirus RNA synthesis can be extended to the *Flaviviridae*[31].

### 1.2.3 *Coronaviridae*

The *Coronaviridae* positive-sense genome is the largest (~30 Kb) of any known RNA virus[32, 33]. To accommodate the replication of their large genome, coronaviruses have evolved a replication complex made of several components[34]. Tasked with maintaining RNA synthesis fidelity are Nsp12, the RdRp, and Nsp14, the 3′ to 5′ proofreading exoribonuclease (ExoN). Located at the N-terminus of Nsp12 is the Nidovirus RdRp-Associated Nucleotidyltransferase (NiRAN) domain (Fig. 1.2*A*, *bottom*) which is essential for viral replication[35]. Functions ascribed to the NiRAN domain are nucleotidylation of Nsp9[36, 37] and subsequent viral RNA capping[38, 39]. Existing as a tetramer, Nsp12 forms a complex with one Nsp7 and two Nsp8 cofactors required for Nsp12-dependent RNA synthesis[40-44] (Fig. 1.2*D*). Active recombinant Nsp7, -8, and -12 complexes have been generated in prokaryotic and eukaryotic expression systems. Different strategies include bacterial expression of Nsp7 and -8, individually or linked, and Nsp12 may be expressed in bacteria or insect cells before complex assembly *in vitro*[41, 43, 45, 46]. Others have had success using a single bacterial expression plasmid containing all three non-structural proteins[47, 48]. Alternatively, the expression of a large polyprotein containing Nsp5, -7, -8, and -12 in baculovirus-infected insect cells results in the formation of an active RdRp complex following the post-translational cleavage by the protease Nsp5[49, 50]. The proofreading ExoN represents an additional hurdle for nucleotide analogs targeting the RdRp domain of Nsp12. Responsible for excising mismatched base pairs, the ExoN supports fidelity during viral replication and transcription[51]. Indeed, ExoN inactivation *in vitro*[52, 53] and *in vivo*[54] leads to increased mutations, an observation that biochemical studies have corroborated[55]. Like Nsp12, the ExoN activity relies on its association with a cofactor, Nsp10[55-57].

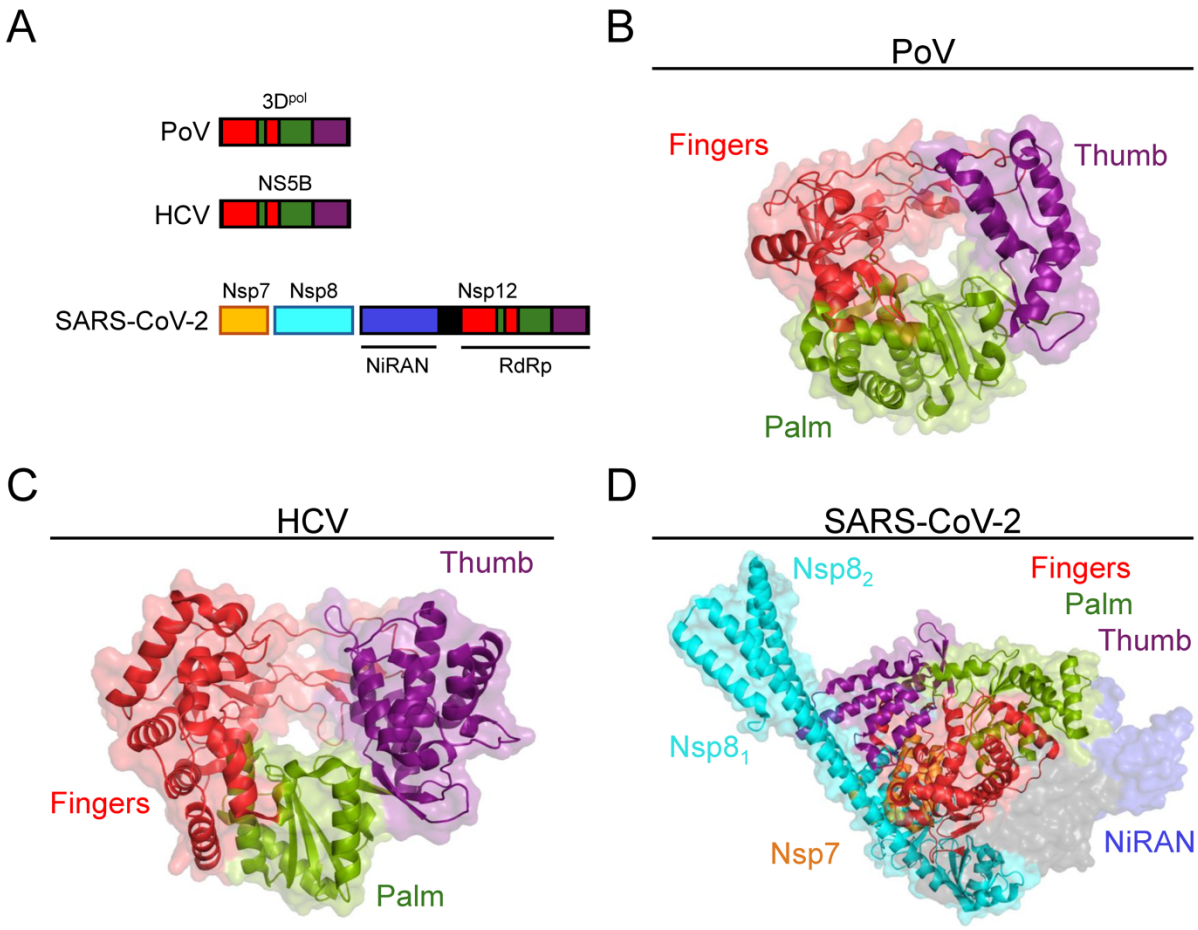


**Figure 1.2. Structural comparison between positive-sense RNA virus RdRp and RdRp complex**. ***A***, linear organization of the PoV 3D$^{pol}$, HCV NS5B, and SARS-CoV-2 RdRp complex. PoV (***B***) and HCV (***C***) RdRp shown here are monomeric and do not require additional cofactors for template-dependent RNA synthesis. ***D***, SARS-CoV-2 RdRp complex shown is comprised of two Nsp8 subunits (*light blue*), one Nsp7 subunit (*orange*), and one Nsp12 subunit (*black*) that contains the NiRAN domain (*dark blue*). The RdRp subdomains fingers (*red*), palm (*green*), and thumb (*purple*) support RNA synthesis. Protein Data Bank identifier numbers used to construct the images are 4WTA (HCV), 1RA6 (PoV), 6YYT (SARS-CoV-2). Structures were created using PyMOL[58].

### 1.2.4 Replication machinery of nonsegmented negative-sense RNA viruses

Nonsegmented negative-sense RNA viruses within the *Filo*-, *Paramyxo*-, and *Pneumoviridae* families represent high-priority pathogens. Unlike positive-sense RNA viruses, their genome must first be transcribed before translation. Therefore, the necessary components contained within the virion are the nucleocapsid protein (NP), phosphoprotein (P), and the large (L) protein, which contains the RdRp active site[59]. Replication relies on the L protein for

performing RNA synthesis, capping, and methylation[60-64]. Defined according to their amino acid sequence, six conserved regions can be found in the L protein. Not to be confused with the RdRp motifs responsible for RNA catalysis, these regions play a role in the complete architecture of the L protein, supporting its multiple enzymatic activities. P (or VP35 in the case of EBOV), on the other hand, is catalytically inactive and as a tetramer forms a complex with L to stimulate RNA synthesis activity[65] (Fig. 1.3). Recent L/P complex structures include Ebola virus (EBOV) RdRp associated with RNA duplex[66], two pneumoviruses, respiratory syncytial virus (RSV)[67-69] and human metapneumovirus (HMPV)[70], and the paramyxoviruses human parainfluenza virus 3 (HPIV-3)[71] and parainfluenza 5 (PIV-5)[72]. Aside from its N-terminus, the L protein is well conserved, but increased variation is observed for P[73]. Notably, it is the N-terminus of L that interacts with P. These studies have begun to illustrate the intramolecular interactions involved in initiation, early elongation, and processive elongation[60]. The first HPIV-3 L/P complex structure was recently published and reported the dimerization of two L proteins[71]. Similar observations have been made for other nonsegmented negative-sense RNA viruses and suggest this intermolecular interaction may be implicated in replication but not transcription[71, 74, 75]. Essential for structural and biochemical studies is a catalytically active L/P complex. The size of L (~250 kDa) and the likely need for phosphorylation of P[76, 77] exceed the demands of a prokaryotic expression system. Therefore, recombinant L/P complexes are often expressed in insect cells using the baculovirus expression system[78].

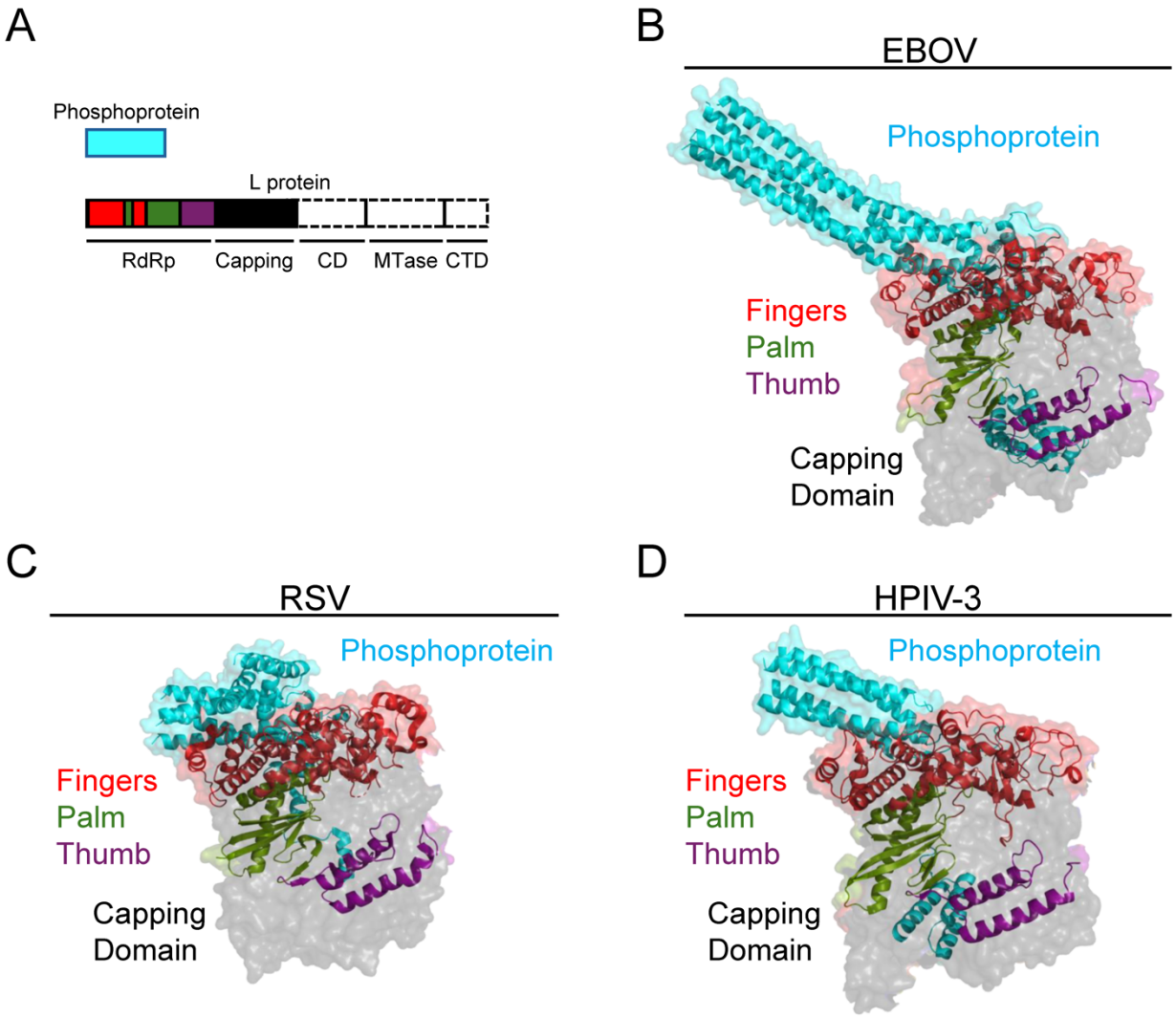


**Figure 1.3. Structural comparison between nonsegmented negative-sense L/P complexes**. ***A***, linear organization of the phosphoprotein subunit (*blue*) and large (L) protein subunit. The EBOV (***B***), RSV (***C***), and HPIV-3 (***D***) L/P replication complexes shown are composed of four phosphoprotein subunits (*blue*), one L protein subunit containing the RdRp fingers (*red*), palm (*green*), and thumb (*purple*) subdomains which support RNA synthesis. Also shown is the capping domain (*black*), the remaining L protein connecting (CD), MTase, and carboxy-terminal (CTD) domains are not shown because the density for these regions has not been solved for all structures. Protein Data Bank identifier numbers used to construct the images are 7YER (EBOV), 6PZK (RSV), and 8KDC (HPIV-3). This figure was adapted from Ouizougun-Oubari et al[60], structures were created using PyMOL[58].

### 1.2.5 Replication machinery of segmented negative-sense RNA viruses

Replication strategies of segmented negative-sense RNA viruses are significantly different compared to their nonsegmented counterparts. Many of the mechanisms ascribed to segmented negative-sense RNA virus replication were pioneered by structural studies targeting the replication machinery of influenza[79-84]. Together, the polymerase basic 1 (PB1) which contains the RdRp domain, polymerase basic 2 (PB2), and polymerase acidic (PA) subunits constitute the ~250 kDa heterotrimer responsible for orthomyxovirus replication and transcription[85] (Fig. 1.4*A*). Also classified as segmented negative-sense RNA viruses, the *Bunyavirales* order encompasses several pathogenic RNA viruses, including, Lassa virus (LASV), Rift Valley fever virus (RVFV), and Crimean-Congo hemorrhagic fever virus (CCHFV). Unlike orthomyxoviruses, bunyavirus replication relies on a single polypeptide termed the Large (L) protein[86, 87]. Although different structurally, the L protein and polymerase complex of influenza exhibit the same dynamic modalities required for RNA synthesis[88]. Importantly, segmented negative-sense RNA viruses lack intrinsic capping and methyltransferase activities. As a result, they have evolved a cap-snatching mechanism where the virus must sequester capped host cellular RNA to facilitate RNA synthesis. The structural investigation of the influenza heterotrimer by Reich et al. detailed the mechanisms tailored to cap-snatching[80]. More recent structural and biochemical studies have illuminated the molecular underpinnings of bunyavirus cap-snatching[86, 89]. Snapshots of the LASV and other bunyavirus L proteins have identified key intricates involved in bunyavirus promoter binding and genome replication and transcription[90-92]. Together, these studies revealed the dynamic monomer resembles the heterotrimeric influenza replication complex, possessing an N-terminus endonuclease, RdRp core, and C-terminus cap-binding domain (Fig. 1.4*B*). Structural information for CCHFV RdRp remains limited, relying on in silico modelling[93]. Currently, the only RVFV L protein structure available is in an inactive state[94]. Like nonsegmented L/P complexes, insect cell expression systems have been instrumental for studying the mechanisms pertaining to orthomyxo- and bunyavirus replication.

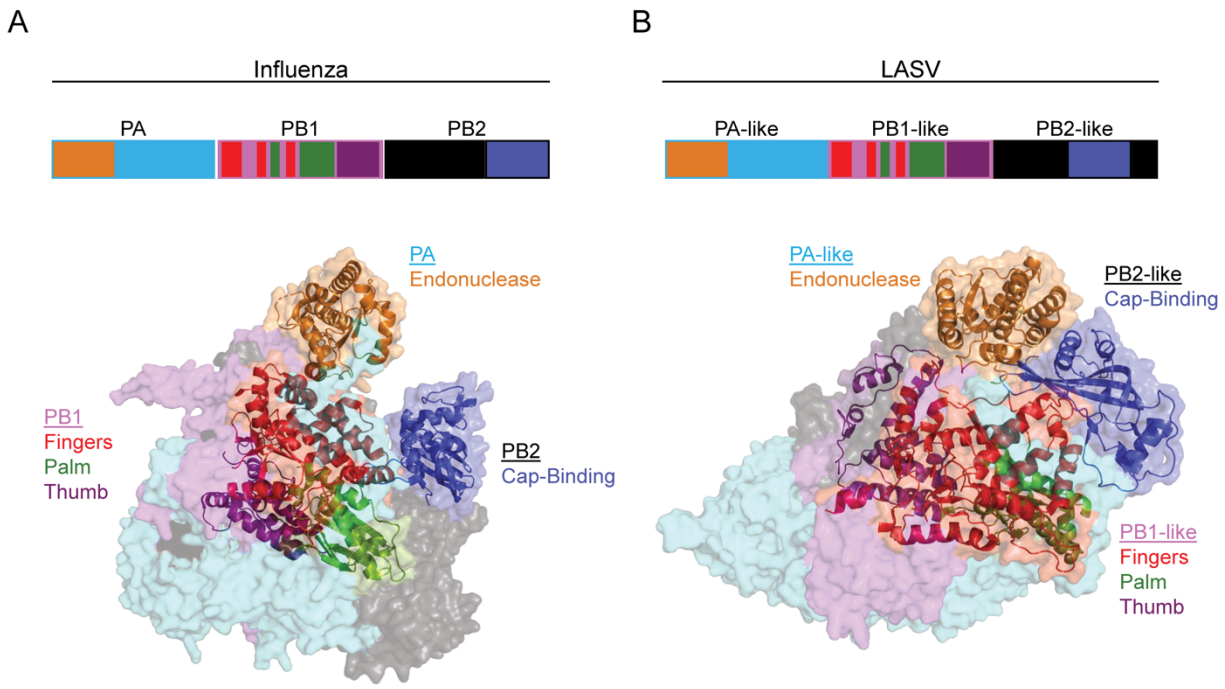


**Figure 1.4. A structural comparison between the influenza heterotrimeric replication complex (*A*) and the LASV L protein (*B*).** The two viruses exhibit similar replication machinery possessing a PA or PA-like (*light blue*), PB1 or PB1-like (*pink*), and PB2 or PB2-like (*black*) domain. The endonuclease (*orange*) and cap-binding (dark *blue*) subdomain are contained within PA and PB2, respectively. The fingers (*red*), palm (*green*), and thumb (*purple*) subdomains that support RNA synthesis are found in the PB1 or PB1-like subdomain. Protein Data Bank identifier numbers used to construct the images are 4WSA (influenza) and 7OJN (LASV). This figure was adapted from Reich et al.[80] and Kouba et al.[90], structures were created using PyMOL[58].

### 1.2.6 RdRp motifs and RNA catalysis

As shown above, the structural variation of viral RdRp and RdRp complexes coincides with genomic replication strategies. However, regions engaged in template-dependent RNA synthesis are relatively well conserved[95-98]. The tertiary structure of the RdRp consists of the subdomains palm, fingers and thumb which take on a "right-handed" fold[18]. Contained within these subdomains are seven amino acid sequence-derived catalytic motifs, denoted A through G, fundamental to viral RdRp-mediated RNA synthesis[98, 99] (Fig. 1.5). Found in the palm subdomain, motifs A through E undergo metal-induced rearrangement to facilitate nucleotide triphosphate (NTP) binding and catalysis. Motifs F and G reside in the fingers subdomain, which forms the NTP tunnel[17]. Lacking any conserved motifs, the thumb subdomain is thought to stabilize the RNA template and interact with the fingers subdomain[100].

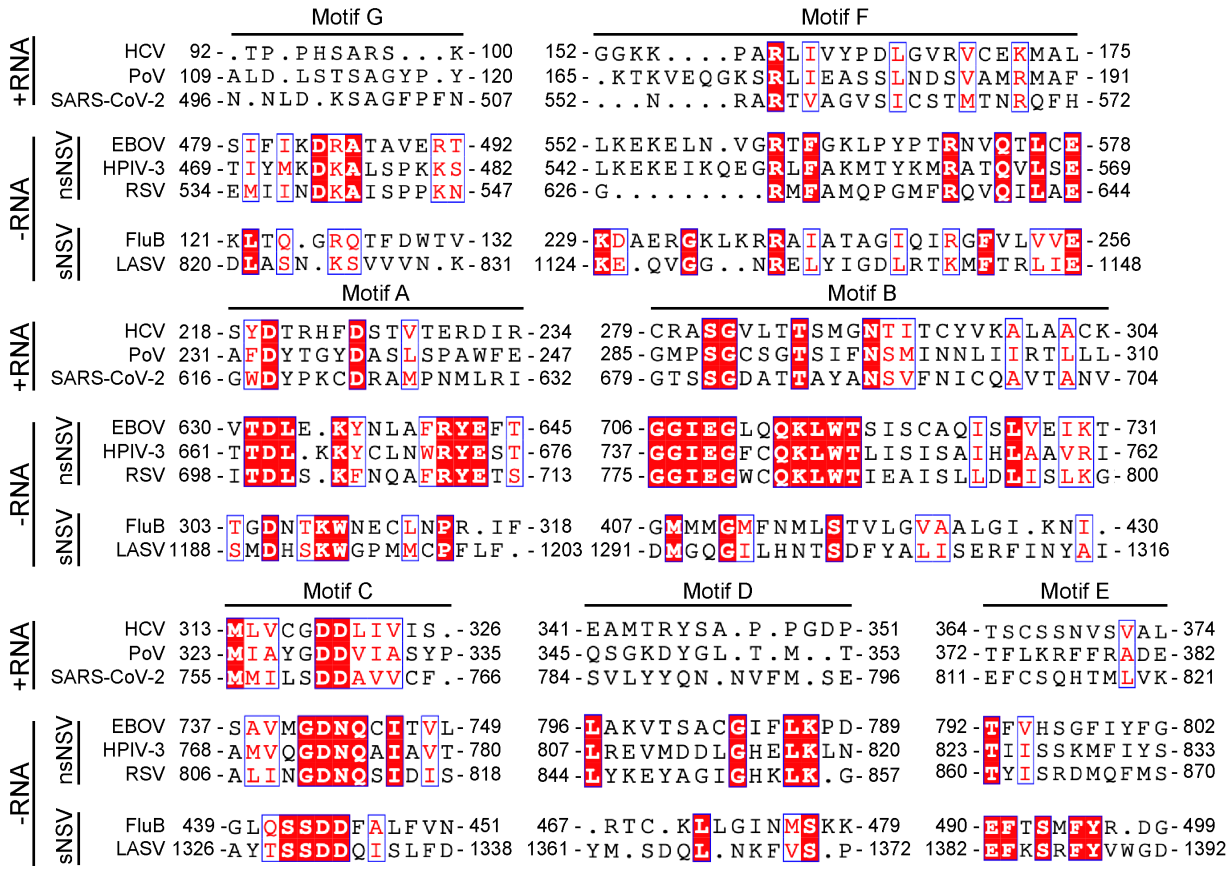


**Figure 1.5. Structure-based alignment of RdRp catalytic motifs from select positive-sense (+RNA), nonsegmented negative-sense (-RNA, nsNSV), and segmented negative-sense (-RNA, sNSV) RNA viruses**. Due to the large nature of some of these proteins, alignments were confined to the RdRp domain. Protein Data Bank identifier numbers used to generate the structure-based alignment: 4WTA (HCV), 1RA6 (PoV), 7BV2 (SARS-CoV-2), 7EYR (EBOV), 8KDC (HPIV-3), 6PZK (RSV), 4WSA (FluB), 7OJN (LASV). Structural alignments were conducted using Chimera UCSF software and visualized in ESPript 3.0[101, 102].

In motifs A and C, two aspartates are coordinated by two divalent cations accompanying the NTP into the active site[97] (Fig. 1.5). Interacting solely with the two metal ions, these aspartate residues assist in deprotonating the 3′-hydroxyl of the nascent RNA primer strand for a nucleophilic attack on the α-phosphate of the correctly positioned NTP[97]. This “two-metal-ion” mechanism was proposed in 1993[103] and has since been a paradigm for the active site chemistry of all polymerases[104]. Later work extended this model to include protonation of the pyrophosphate by motif D before release[105, 106]. Moreover, the flexibility of motif D ensures the catalytic residues do not take on their active conformation before correct NTP recognition and therefore, has been implicated in RdRp fidelity and efficiency[107-109]. Critical for RdRp-mediated RNA synthesis, is

the ability to differentiate between ribonucleotides and deoxyribonucleotides. While several motifs have a role in NTP discrimination, the recognition of the 2′-hydroxyl of the incoming NTP is performed by a conserved aspartate and asparagine residue found in motifs A and B in positive-sense RNA viruses, respectively[110, 111] (Fig. 1.5). Less is known about the key RdRp residues involved in negative-sense RNA virus NTP discrimination which lack the conserved asparagine. More recent studies have begun to associate motif B with motifs F and G, facilitating translocation[112-114]. Specific to viral RdRp, the role of motif E remains largely unknown; it is believed to be involved in positioning the 3′-hydroxyl of the primer[96, 115]. Motif F contains positively charged residues that stabilize the incoming NTP and the template RNA strand[116]. Not involved in phosphodiester bond formation, motif G is believed to regulate post-chemistry RdRp "shuttling" along the RNA duplex[114]. Together, these structurally dynamic motifs support the chemistry required for phosphodiester bond formation central to the multistep catalytic process of RNA synthesis. Pre-chemistry steps include an "open" RdRp-RNA complex that can accommodate NTP binding, followed by active site closure[116]. Once the phosphodiester bond has formed, the viral RdRp can "thread" the RNA duplex downstream, effectively translocating to the next templating base position[114]. Importantly, when describing the translocation of the RdRp, is the position of the 3′-end of the RNA primer in relation to the nucleotide-binding site (N-site)[117, 118]. Pre-translocation can be defined as the 3′-end of the RNA primer occupying the N-site. Conversely, when the N-site is unoccupied, and the 3′-end of the RNA primer is registered one position back, in the priming site (P-site), the RdRp is in a post-translocated state. High-resolution structures are necessary to identify the 3′-end of the primer within an RdRp ternary complex, and biochemical techniques used to probe for pre- and post-translocation conformations can assist these structural efforts.

Taken together, the structural dynamics universal to RdRp-catalyzed RNA synthesis highlight several points of consideration for the development of effective nucleotide analogs. The potency of nucleotide analogs will be determined at various stages in the phosphoryl transfer reaction. Although the structural dynamics of these motifs are believed to be universal, the sequence variation amongst different RNA virus families will impact the broad-spectrum efficacy of nucleotide analogs. Therefore, target validation and determining a nucleotide analog's mechanism of action remain important steps in therapeutic development.

## 1.3 Nucleotide analog activation

External to the viral RdRp, a nucleoside analog's efficacy relies on efficient entry into the host cell, subsequent phosphorylation by host cell kinases and limited off-target effects[119]. Nucleoside analogs often possess a prodrug moiety that serves to target the relevant cell type and improve diffusion through the cell's hydrophobic bilayer. The prodrug moiety can also mask a 5′-monophosphate, which bypasses the rate-limiting step in the phosphorylation pathway[120]. Finally, it is important to consider the cell tropism when developing a prodrug and investigating its efficacy against viral infection. The endogenous kinases present within different cellular environments can vary and could have altered chemical preferences, ultimately impacting the metabolic activation of a nucleoside analog[121].

In their active 5′-triphosphorylated form, nucleotide analogs mimic and, thereby, compete with one or more of the four natural ribonucleotides required for RNA synthesis. Once incorporated into the growing RNA chain, the nucleotide analog can inhibit viral replication[122]. The mechanism of inhibition depends on the chemical structure of the nucleotide analog and the nature of the polymerase. If incorporation of the nucleotide analog results in premature termination of RNA synthesis, then it can be defined as an “obligate” or “non-obligate” chain terminator. The former lacks a 3′-hydroxyl and therefore cannot support the chemistry required for the incorporation of the next nucleotide. The selective requirement for the 3′-hydroxyl has made this class of nucleotide analogs a poor substrate for the viral RdRp. Conversely, “non-obligate” chain terminators, such as sofosbuvir and remdesivir, have proven to be successful inhibitors of RNA virus replication. However, the presence of a 3′-hydroxyl suggests RNA synthesis beyond the incorporated nucleotide analog is possible. Therefore, a “non-obligate” chain terminator can inhibit RNA synthesis by preventing incorporation of the next nucleotide (i.e. immediate chain termination) or at a site downstream from incorporation (i.e. delayed-chain termination). Finally, mutagenic nucleotide analogs are distinct from chain terminators because they do not terminate RNA synthesis; instead, they promote base pair mismatches culminating in error-catastrophe or lethal mutagenesis.

Recently reviewed by Seley-Radtke et al. and Yates et al., nucleotide analogs have evolved substantially since the 1960s[123, 124]. As a result, an extensive repertoire of different modifications can be found in the literature. Discussed below are the relevant clinical, *in vitro*, and biochemical data of prominent broad-spectrum nucleotide analogs modified at the base or sugar moiety, including the 1′-, 2′-, and 4′-location (Fig. 1.6). Emphasis will be placed on the biochemical parameters and mechanism of action that facilitate the observed antiviral effect against important RNA virus families. Mechanisms of resistance will also be discussed as this can often provide further insight into the properties that make a nucleotide analog effective.

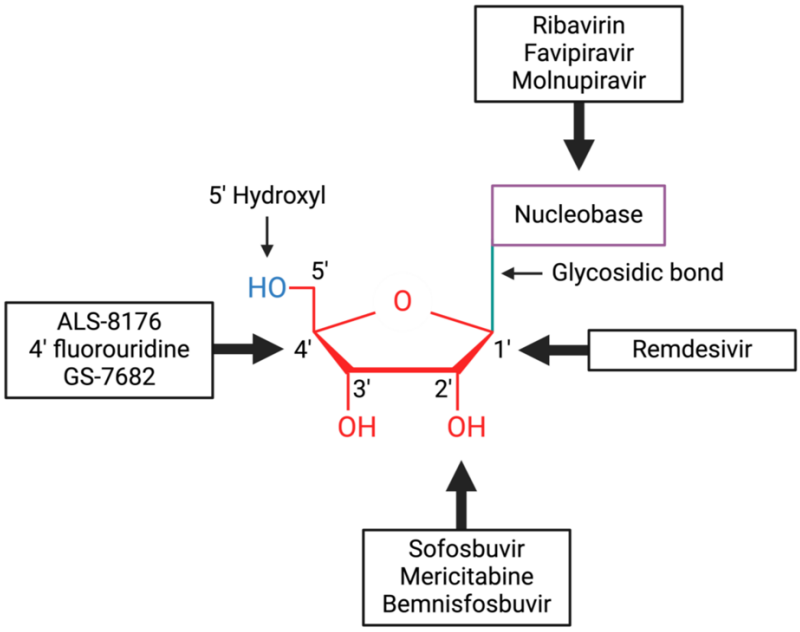


**Figure 1.6. Schematic representation of the modification sites of different nucleoside analogs**. Modified regions for nucleoside analog development include the 5′-hydroxyl (*blue*), the sugar moiety (*red*), the glycosidic bond (*green*), and the nucleobase (*purple box*). The nucleoside analogs discussed in this thesis are shown inside the black boxes, the large arrows indicate the position of their modification. This figure was adapted from Seley-Radtke et al.[123]

## 1.4 Base-modified mutagenic nucleotide analogs

Driven largely by their error-prone RdRp, RNA viruses have a natural propensity to mutate, ensuring their evolution necessary for survival[125, 126]. However, the mutation rate amongst RNA viruses is delicate and disrupting this balance can effectively attenuate or inactivate the virus[127]. Base-modified nucleotide analogs often target this mutational threshold via ambiguous base

pairing to promote error catastrophe. Existing as tautomers, this class of nucleotide analogs can present two conformations about the base moiety[128] to target RdRp fidelity and promote mismatched base pairs[129, 130]. Notably, the mutagenic effect evoked by this class of nucleotide analogs does not rely on the termination of RNA synthesis but on subsequent embedment in newly synthesized viral genome templates where the mutagenic mechanism can be realized. Ribavirin, favipiravir, and molnupiravir are prominent base-modified nucleotide analogs that demonstrate a broad spectrum of antiviral activity against RNA viruses.

### 1.4.1 Ribavirin

Discovered in 1972[131], ribavirin (RBV) (Fig. 7.1*A*, *left*) has been examined in the clinic against HCV[132], RSV[133, 134] and LASV[135]. Combined with pegylated interferon alpha, RBV was the basis for HCV treatment until more effective direct-acting antivirals (DAAs) were discovered[132, 136]. Despite the poor treatment efficacy, RBV remains the only DAA approved for treating RSV infection[137-139]. RBV has also demonstrated antiviral activity against other high-interest RNA viruses, including influenza[140], and RVFV[131, 141]. However, the broad-spectrum antiviral activities of this purine-like nucleotide analog cannot be explained by one mechanism[142-146].

### 1.4.2 Ribavirin mechanism of action

Independent of the virus, it has been suggested that RBV-monophosphate (MP) competes with GMP for metabolism by inosine monophosphate dehydrogenase (IMPDH) to reduce the cellular concentration of GTP[147], while others propose it modulates host T-cell responses[148]. However, RBV can be efficiently phosphorylated in the host cell to its active triphosphate form (RBV-TP) (Fig. 7.1*A*, *right*)[149]. As a result, several studies have attributed its antiviral activity to effects mediated by the viral polymerase. RBV treatment of several RNA virus families, including *Picornaviridae*[129, 150], *Flaviridae*[151], *Arenaviridae*[152], and *Orthomyxoviridae*[153], promoted G to A and C to U transitions. Biochemically, the PV and HCV polymerase could incorporate RBV-TP opposite cytidine and uridine with equivalent efficiency[129, 154] (Fig. 1.7*B*). Instrumental to its mutagenic mechanism, the incorporation of RBV-TP does not terminate RNA synthesis, therefore, RBV-MP residues can become embedded in templating genomic RNA strands where it can base pair with CTP or UTP[129, 154] (Fig. 1.7*C*). In agreement with these observations, RBV treatment had

no effect on PV translation or replication but did reduce virus infectivity[130]. Sequence analysis of HCV-infected patients who had undergone RBV monotherapy revealed an increase in G to A and C to U transitions, affirming error catastrophe as a mechanism of RBV-directed inhibition[155, 156]. Taken together, RBV exerts its mutagenic effect when it does not terminate RNA synthesis following incorporation as a G-analog, where it can then base pair with UTP when acting as the templating base (C:R:U or G:C:R:U:A).

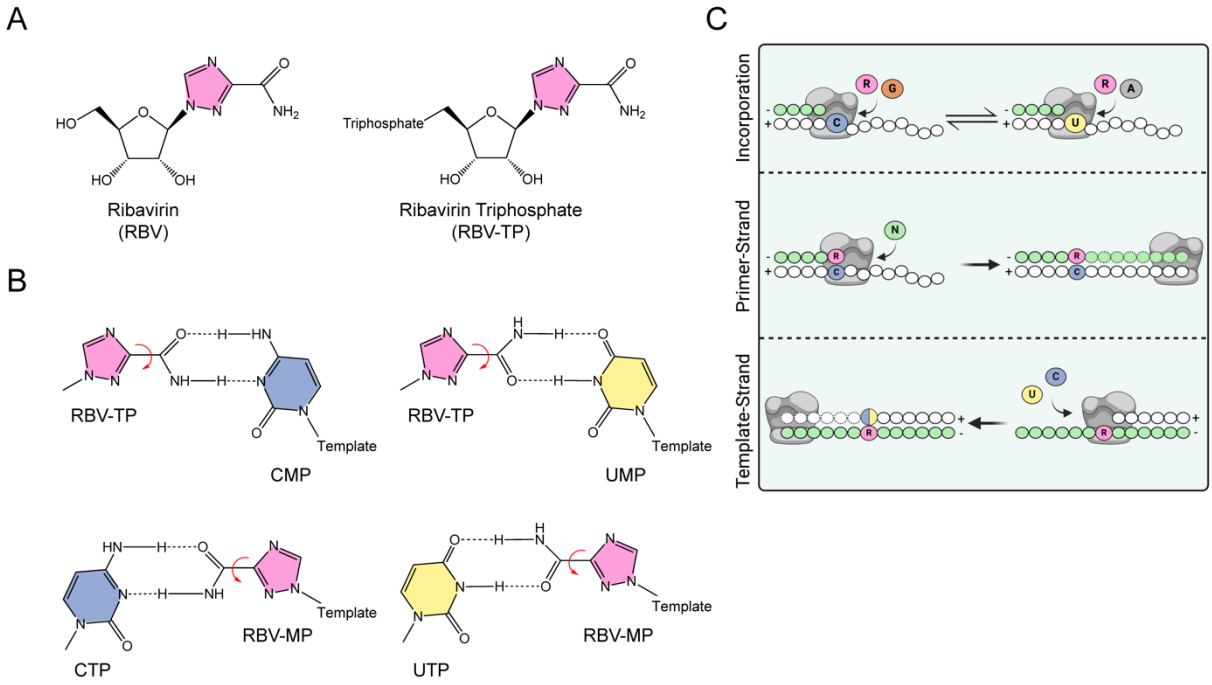


**Figure 1.7. Mutagenesis model of RBV against PV**. ***A***, Nucleoside prodrug (*left*) and triphosphate (*right*) form of RBV. ***B***, Alternative base pairing of RBV-TP as a substrate (*top*) and as a templating base (*bottom*). ***C***, Schematic representation of PV RdRp (*grey*)-mediated nucleotide incorporation into RNA primer (*green circles*)/template (*white circles*). Plus and minus signs indicate RNA sense. Letters A, C, G, and U refer to natural bases, letter R refers to ribavirin. RBV-TP is incorporated opposite CMP or UMP (*top*) and does not inhibit RNA synthesis (*middle*); therefore it can exert its mutagenic mechanism when embedded in the template-strand (*bottom*). Adapted from Crotty et al.[130] and created with BioRender.com.

The proofreading 3′ to 5′ ExoN possessed by coronaviruses presents an extra challenge in the development of anti-coronavirus nucleotide analogs. Intrinsic to RBV's mutagenic mechanism is the absence of chain termination following incorporation. This could prevent recognition by the ExoN and therefore, promote base pair mismatches during viral replication. Nonetheless, RBV proved to be ineffective against SARS-CoV-2 *in vitro*[157, 158]. This can likely be attributed to inefficient incorporation by the SARS-CoV-2 RdRp[49] and excision by the SARS-CoV ExoN[159].

*In vitro*, an ExoN-deficient coronavirus demonstrated increased sensitivity to RBV treatment[160]. However, these effects could be tied to both inhibition of RNA synthesis and decreased intracellular GTP pools[160].

### 1.4.3 Ribavirin resistance

The gold standard in DAA target identification is the generation of resistance. Serially passaging PV at increasing RBV concentrations resulted in the resistance-conferring mutation G64S in the viral polymerase[161]. Located in the fingers subdomain, the backbone of Gly-64 is predicted to participate in a hydrogen bond network with motif A[162], a sequence of residues essential for correct NTP selection[13]. Substituting glycine for serine at this position demonstrated improved fidelity, effectively reducing the frequency of RBV-TP incorporation to a tolerable level[161, 162]. G64S did not appear to significantly diminish viral replication and promoted genomic homogeneity amongst the viral population[127]. As a result, this high-fidelity mutant generated an attenuated virus due to reduced evolutionary capacity[127]. The analogous mutation in EV-71 (Gly-62), another picornavirus, confirmed this residue's conserved role in replication fidelity[163]. Inversely, a mutator phenotype due to the substitution H273R in PV RdRp rendered the virus more susceptible to RBV treatment[164]. Like the high-fidelity mutant G64S, H273R PV demonstrated decreased virulence compared to the WT[165]. Together, RdRp fidelity is a predictor of RBV efficacy, and RdRp mutations to this end can impact susceptibility. However, owing to the delicate balance of viral genomic diversity, mutations that impact RdRp fidelity can attenuate the virus.

Generating RBV resistance in an HCV replicon resulted in resistant mutations not located in the polymerase but instead NS5A as well as the host cell[166]. The many functions of NS5A delineate an exact mechanism of resistance. Interestingly, the cell-derived mechanism caters to RBV resistance by reducing RBV import or intracellular stability[166]. However, this may be inherent to Huh-7 cells commonly used to investigate HCV replication. Adenosine kinase (ADK) is reported to play a key role in the metabolism of RBV-MP, a competitive inhibitor of IMPDH[167]. It was demonstrated that endogenous ADK expression in Huh-7 cells is lower than other classical cell lines used to monitor RBV antiviral activity[167]. Indeed, the efficacy of RBV against PV in Huh-7 cells was less than that observed in HeLa cells[166]. Finally, the inhibition or knockdown of ADK reduced RBV anti-HCV activity[167] , while inhibition of IMPDH did not have any effect on

HCV replicon activity, but when combined with RBV, improved anti-HCV activity[168]. While these RBV studies against HCV do not provide any additional insight into the mutagenic mechanism, they highlight the importance of cell type consideration when investigating nucleoside analogs.

### 1.4.4 Favipiravir

Favipiravir (FVP) (Fig. 1.8*A*, *left*), also known as T-705, is currently licensed in Japan for the treatment of pandemic influenza virus strains and strains resistant to other approved medical countermeasures[8]. The antiviral activity and clinical efficacy of FVP prior to the COVID-19 pandemic have been covered extensively by Delang and colleagues[169]. Briefly, clinical studies of FVP have demonstrated that it is well tolerated in healthy individuals. However, *in vivo* studies have identified teratogenic risks associated with FVP treatment and, therefore, should not be used to treat individuals who are or may become pregnant. The antiviral activity of FVP *in vitro* and *in vivo* is widespread. RNA viruses susceptible to favipiravir treatment include positive-sense RNA viruses (corona-, flavi-[170] and picornaviruses[171, 172]); nonsegmented negative-sense RNA viruses (filo-[173], parmyxo-[174], and pneumoviruses[174]); and several segmented negative-sense bunyaviruses (arena-[175], nairo-[176, 177], and phenuivirus[178, 179]).

More recent clinical data has emerged evaluating FVP for the treatment of COVID-19. Consistent with previous reports, treatment was well tolerated in healthy individuals. However, several randomized controlled trials deemed FVP ineffective for the treatment of COVID-19[180-184]. These findings are consistent with pre-clinical studies that demonstrate an elevated effective concentration ($EC_{50}$) of FVP (>10 μM) is required to inhibit SARS-CoV-2 replication in cell culture[45, 157, 158, 185, 186]. Like RBV, the antiviral effects of FVP cannot be attributed to one specific mechanism of action.

### 1.4.5 Favipiravir mechanism of action

The observed mutagenic pattern resulting from FVP treatment varies. For WNV[187] and norovirus[188], A to G and U to C were reported as the dominant transitions. Conversely, G to A and C to U transitions were observed in HCV[189], influenza[190, 191], EBOV[192], and SARS-CoV-2[45]. Although picornaviruses were susceptible to FVP treatment in cell culture, no dominant transitions could be identified[193] or an increase in genomic transitions was not observed[194]. FVP in its active

triphosphate form (FVP-TP) (Fig. 1.8*A*, *right*), operates as a purine analog against SARS-CoV-2[45] and influenza[195] RdRp, incorporating opposite a templated cytidine or uracil (Fig. 1.8*B*). Influenza polymerase incorporates FVP-TP as a G- and A-analog, 19- and 30-fold less efficiently than the natural counterpart, respectively[195] (Fig. 1.8*C*, *top*). Confounding the base pairing tendencies, PV RdRp can incorporate FVP-TP opposite adenosine, cytidine, and uracil[164]. Against SARS-CoV-2 RdRp complex, FVP-TP incorporation is relatively inefficient[49, 196], but its incorporation does not appear to terminate RNA synthesis[45, 197, 198], consistent with the proposed mutagenic mechanism. Notably, a more processive pattern of RNA synthesis was observed when PV[164] or SARS-CoV-2[45] RdRp incorporated FVP-TP opposite cytidine; whereas incorporation opposite uridine stalled RdRp elongation (Fig.1.8*C*, *middle*). For influenza RdRp, single[199] or consecutive[195, 200] incorporation events of FVP-TP can stall or terminate RNA synthesis.

To adequately define the mutagenic mechanism of FVP, natural NTP incorporation tendencies opposite a templated FVP-MP must be considered. When embedded in the template strand, FVP-MP drives two patterns of PV RdRp-catalyzed RNA synthesis[164]. Incorporation of CTP opposite the analog prevents subsequent NTP incorporation, whereas RNA synthesis is unperturbed following the U:FVP-MP base pair (Fig.1.8*C*, *bottom*). Incorporation of ATP opposite FVP-MP is not evident. Therefore, the C to U and G to A transitions are likely realized when favipiravir is incorporated opposite cytidine (C:F:U or G:C:F:U:A). This outcome is contingent on efficient extension of the incorporated FVP-MP and UTP base pairing opposite FVP-MP when embedded in the viral genome.

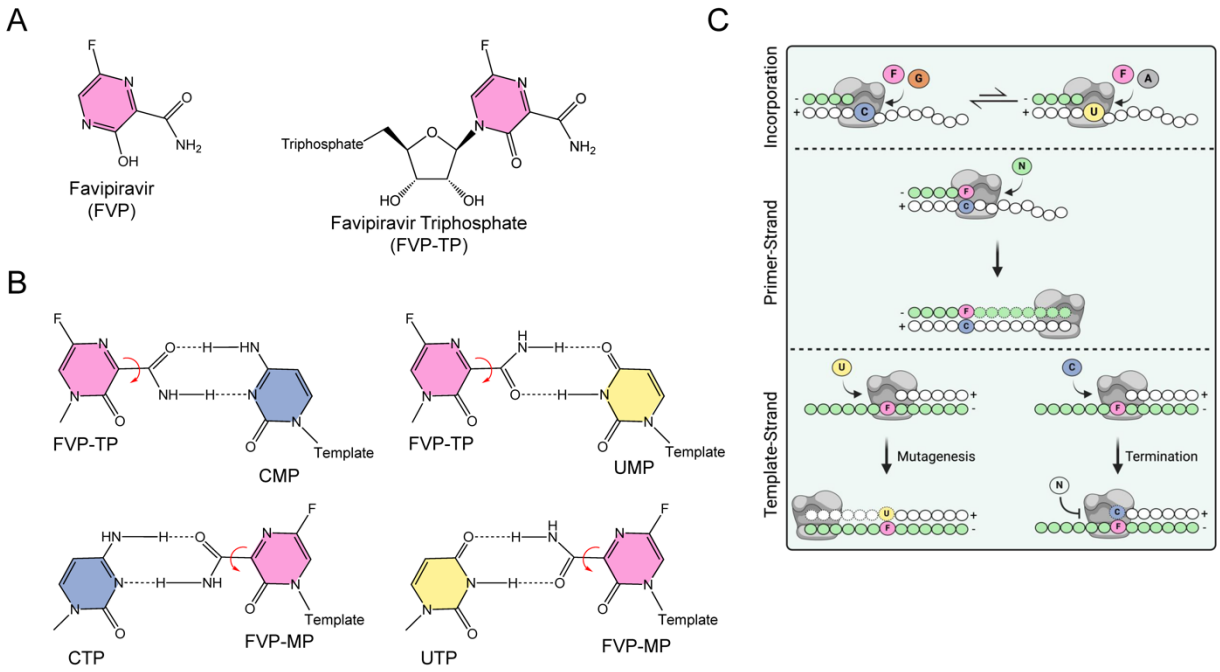


**Figure 1.8. Mutagenesis model of FVP**. ***A***, Nucleoside prodrug (*left*) and triphosphate (*right*) form of FVP. ***B***, Alternative base pairing of FVP-TP as a substrate (*top*) and as a templating base (*bottom*). ***C***, Schematic representation of influenza RdRp (*grey*)-mediated nucleotide incorporation into RNA primer (*white circles*)/template (*green circles*). Plus and minus signs indicate RNA sense. Letters A, C, G, and U refer to natural bases. Letter F refers to FVP. FVP-TP is favorably incorporated opposite CMP (*top*) and does not inhibit RNA synthesis (*middle*). The mutagenic mechanism is realized when UTP can base pair opposite a template embedded FVP residue (*bottom*, *left*). CTP incorporation opposite FVP-MP inhibits RNA synthesis (*bottom*, *right*). Created with BioRender.com.

An advanced biophysical assay measuring the force of tension on an RNA template proposes an alternative mechanism of action for FVP-TP. Employing magnetic tweezers, Dulin et al. show that FVP-TP incorporation can promote PV RdRp backtracking[164], an observation that could be later extended to EV-71 RdRp[194]. Backtracking is likely induced by unstable protein-RNA interactions resulting in the release of the 3′ end of the RNA-template duplex and backward shuttling of the RdRp[194, 200]. Backtracking has been proposed to assist RNA polymerase fidelity[201-203]. However, FVP exposure increased EV-71 genomic recombination, which could generate viral genomes unable to support replication[194]. It is not known which base pair, FVP-MP:C or FVP-MP:U, induces picornavirus RdRp backtracking events, but biochemical studies suggest

backtracked signatures align with the stalled PV RdRp ternary complex observed when FVP-TP is incorporated opposite a templated uridine[164, 200].

Recently, a backtracked influenza structure has been captured in the presence of FVP-TP[200]. In agreement with previous biochemical assays[195], the authors conclude that backtracking occurs in response to two successive FVP-TP incorporation events[200]. Moreover, the FVP-MP:U base pair resembles the G:U wobble base pair, whereas the FVP-MP:C resembles the canonical G:C base pair[200]. Against SARS-CoV-2 RdRp complex, FVP-TP did not promote backtracking[198] and its incorporation has only been structurally observed opposite CMP[196, 197]. However, it has been shown that SARS-CoV-2 RdRp complex backtracking is mediated by the helicase, which could enable intervention by the proofreading 3′ to 5′ ExoN[204-206]. FVP-induced backtracking has yet to be investigated against a SARS-CoV-2 replication complex that contains the helicase.

Taken together, the structural, biochemical, and biophysical evidence demonstrates that the antiviral activity of FVP is mediated through multiple mechanisms and can differ between RNA viruses. Against influenza, there are potentially two mechanisms of action: lethal mutagenesis and chain-termination. The promiscuous base pairing and increased mutations support the former, but the latter cannot be dismissed due to the abrogation of RNA synthesis. However, the probability of chain-termination decreases if two consecutive incorporation events are required. Future studies should evaluate the NTP base pairing tendencies of influenza RdRp complex opposite an embedded FVP-MP residue.

The mechanism of action for FVP against coronaviruses is likely lethal mutagenesis. Error catastrophe would be evoked when FVP behaves as a G-analog, which does not terminate or stall RNA synthesis, thereby escaping ExoN recognition. As an A-analog, FVP-TP incorporation hinders RNA synthesis, an event that would anticipate ExoN recognition and subsequent excision. Investigating the susceptibility of an ExoN-deficient coronavirus to FVP would help delineate its primary mechanism of action against coronaviruses.

Against picornaviruses, FVP treatment may or may not promote mutagenesis in cell culture[193, 194]. For foot-and-mouth disease virus (FMDV), a clear mutational genomic pattern could

not be identified, but FVP treatment did decrease specific infectivity, a hallmark of lethal mutagenesis[193]. Conversely, FVP promoted EV-71 genomic recombination, which would subsequently result in defective viral genomes; single-molecule experiments suggest this is due to increased RdRp backtracking[194].

### 1.4.6 Favipiravir resistance

*In vitro* selection experiments with chikungunya virus (CHIKV)[207], a positive-sense alphavirus, and influenza[208] revealed a conserved lysine to arginine substitution within motif F confers resistance to FVP. However, these mutations were associated with a fitness cost and required a compensatory mutation. For CHIKV, K291R-containing isolates were up to 9.6-fold less susceptible to FVP treatment[207]. Difficulties expressing active recombinant CHIKV RdRp have limited further mechanistic studies. K229R, together with the compensatory substitution P653L in the PA domain, reduced influenza susceptibility to FVP 30-fold[208]. Biochemically, only K229R improved discrimination against FVP-TP ~2-fold[208]. In a minigenome assay, K229R did not demonstrate cross-resistance to RBV or altered mutation frequency in the absence of FVP, suggesting this mutation does not improve fidelity[208].

Studies with the picornavirus CVB3 found the analogous mutation (K159R) unstable; to maintain a viable virus, the compensatory mutation A239G was required[209]. However, the double mutant (K159R and A239G) and A239G alone proved to be 3.4- and 2-fold more susceptible to FVP treatment, respectively. The single K159R substitution rendered the CVB3 polymerase inactive, and activity could only be restored by A239G[209]. An extensive site-directed mutagenesis study had previously identified several low-fidelity mutations, including A239G[210]. Found in motif A, Asp-238 is adjacent to Ala-239, a key residue in a hydrogen bonding network responsible for positioning the NTP and promoting catalysis[13, 211]. Finally, the double mutant (K159R and A239G) remained sensitive to RBV treatment, demonstrating that K159 and, perhaps more broadly motif F, is specific to the mechanism involved in FVP inhibition[209].

The impact of RdRp fidelity on the efficacy of FVP remains unclear. Previously identified high-fidelity (G64S) and low-fidelity (H273R) $3D^{pol}$ substitutions did not alter PV susceptibility to FVP[164]. Conversely, high-fidelity mutations in CVB3 $3D^{pol}$ (A372) and influenza PB1 (V43I)

reduced FVP antiviral activity[153, 209, 212]. This highlights that, like RBV, improved fidelity may be suitable to support resistance. However, this may not provide an evolutionary advantage. Like G64S in PV 3D$^{pol}$, V43I reduced basal mutation frequency and influenza pathogenicity[153, 212]. Several studies have shown that decreased genomic diversity supported by high-fidelity RdRp mutations attenuates the virus[127, 213, 214]; therefore, it could be inferred that A372V would attenuate CVB3.

Considering FVP treatment resulted in defective viral genomes, a resistant phenotype could arise from a substitution that reduces recombination. In EV-71 3D$^{pol}$, substituting tyrosine for histidine at position 276 (Y276H) resulted in a recombination-defective mutant[194]. Not associated with a catalytic motif, Tyr-276 is located in the fingers subdomain. Y276H improved the stability of the EV-71 elongation complex likely by enhanced interactions with the 3′ end of the RNA primer[194]. Adjacent to Tyr-276, Arg-277 was shown to have an integral role in RNA binding and elongation complex stability[215]. Affirming the relationship between backtracking and recombination, EV-71 Y276H 3D$^{pol}$ demonstrated reduced kinetic signatures associated with FVP-induced backtracking[194]. EV-71 Y276H was ~2-fold less susceptible to FVP in cell culture, suggesting recombination-defective phenotypes can support resistance to FVP[194].

### 1.4.7 Molnupiravir

In December 2021, molnupiravir (MK-4482/EIDD-2801) received emergency use authorization (EUA) from the FDA for the treatment of mild-to-moderate COVID-19 in adults at risk for severe disease progression[216]. Authorization was supported by a clinical trial that found molnupiravir reduced hospitalization and deaths[217]. However, more recent clinical data suggest molnupiravir has limited efficacy against vaccinated patients[218, 219]. There are concerns surrounding the potential off-target effects of molnupiravir. The parent compound of molnupiravir, β-D-N$^4$-hydroxycytidine (NHC, EIDD-1931), was shown to be mutagenic in mammalian cells[158, 220]. This could potentially be attributed to the 5′-diphosphate intermediate which is a metabolic precursor for the synthesis of ribonucleoside triphosphates and deoxyribonucleoside triphosphates[221]. It is the active ribonucleotide triphosphate form of NHC (NHC-TP), which acts as a substrate for RNA polymerases[130, 222-224]. Developed initially as an anti-influenza

compound[113], NHC has demonstrated antiviral activity against several positive- and negative-sense RNA viruses[222, 223, 225-228].

### 1.4.8 Molnupiravir mechanism of action

Extensive pre-clinical studies of NHC and molnupiravir against SARS-CoV-2 have defined the drug's mechanism of action. Acting as a pyrimidine mimic, NHC treatment *in vitro* promoted G to A and C to U transitions in SARS-CoV-2[229] and Influenza[223]. Interestingly, the mutagenic pattern differed for RSV, A to G transitions were the most prevalent, followed by G to A and then C to U[223]. Illustrated by SARS-CoV-2 structural and biochemical studies, the incorporation of NHC-TP is favoured opposite GMP and is notably more efficient than RBV-TP and FVP-TP[49, 130, 224]. Once incorporated, NHC-MP does not terminate RNA synthesis[130, 224]. Embedded in newly synthesized viral genome copies, ATP and GTP can incorporate opposite NHC-MP[130]. It is the base pairing of ATP opposite an RNA-embedded NHC residue that supports the G to A and C to U transitions. Confirming its mutagenic mechanism, SARS-CoV-2 isolates collected from COVID-19-infected patients following molnupiravir treatment found increased C to U and G to A transitions[230, 231].

To further delineate the parameters that facilitate the anti-coronavirus activity of NHC compared to RBV and FVP, consider the following studies. Against SARS-CoV-2, NHC proved to be 100-fold more effective than FVP or RBV[158]. Moreover, an ExoN deficient murine hepatitis virus (MHV), an orthologous coronavirus, did not significantly affect the efficacy of NHC[226], but did improve the potency of RBV ~100-fold[160]. Taken together, the improved efficacy of NHC can be attributed to its efficient incorporation and limited ExoN recognition. The molecular underpinnings that enable CoV ExoN recognition of one mutagenic nucleotide and not another remain unknown. These mechanisms are likely coupled to other components of the CoV replication transcription complex.

### 1.4.9 Molnupiravir resistance

In addition to target validation, *in vitro* resistance selection experiments often provide key insights into the molecular mechanism of a given nucleotide analog. However, NHC has demonstrated a high barrier to resistance against several RNA viruses. Against influenza,

passaging at sub-lethal NHC concentrations did not identify any resistance mutations that could be maintained in the viral population[113]. For Venezuelan equine encephalitis virus (VEEV), a positive-sense alphavirus, more than 15 passages were required before resistance was observed[232]. Several substitutions were discovered in the RdRp, however these resistant strains remained susceptible to NHC mutagenesis. Considering the library of key residues implicated in FVP and RBV resistance described above, it would be of interest to know if the analogous high- or low-fidelity mutations impact NHC susceptibility. Future biophysical studies should investigate kinetic signatures of NHC-TP against coronavirus RdRp complex.

### 1.4.10 Considerations for mutagenic nucleotide analogs

Base-modified mutagenic nucleotide analogs offer a plausible solution to treat RNA virus infection. However, the ambiguous nature of these analogs, both for their metabolism and mechanism of action, requires a cautionary approach[221]. Fundamentally, if the mutagenic nucleotide does not significantly enhance mutation rates to induce lethal mutagenesis, its treatment could, in theory, improve viral fitness. Indeed, exposing SARS-CoV-2 to molnupiravir promoted mutations that enabled escape from neutralizing antibodies[233, 234]. Moreover, base-modified mutagenic nucleotide analogs often lack specificity which raises concerns about off-target effects. The incorporation of nucleotide analogs by human polymerases can provide insight into potential toxicities[235, 236]. Biochemically, NHC-TP can act as a substrate for human mitochondrial RNA polymerase (h-mtRNAP) and does not impede RNA primer extension[237]. However, the embedded NHC-MP does appear to impact translation as treatment reduced protein expression[237]. Conversely, FVP-TP can act as a substrate for the h-mtRNAP, but it does not inhibit RNA or protein synthesis[238].

## 1.5 1′-modified nucleotide analogs

The poor stability of 1′-substituted *N*-nucleoside analogs as antiviral agents hindered their preclinical development[124, 239]. However, Cho and colleagues demonstrated that stability could be improved by linking the sugar and base through a C-C bond[240]. The resulting 1′-cyano-modified *C*-nucleoside analog demonstrated the greatest potency and widest spectrum of antiviral activity, as opposed to the 1′-methyl, -vinyl, and -ethynyl substituents[240]. These findings would ultimately support the development of the broadly acting nucleoside analog prodrug remdesivir (Fig. 1.9*A*).

### 1.5.1 Remdesivir

Remdesivir (RDV), formerly referred to as GS-5734, is a 1′-cyano modified *C*-adenosine monophosphate prodrug derived from the parent nucleoside GS-441524 (Fig. 1.9*B*). Originally discovered in 2012, GS-441524 demonstrated activity against HCV, YFV, HPIV-3, and SARS-CoV, but was ineffective against influenza[240]. Subsequent development led to the discovery of RDV, which showed considerable antiviral activity against EBOV[241]. As a result, RDV was subjected to a randomized clinical phase 3 trial for the treatment of Ebola virus disease (EVD)[242]. This trial ultimately concluded two monoclonal antibody therapies were more effective, but the human safety data allowed for the compassionate use against COVID-19 in January 2020[243]. RDV was the first antiviral drug to receive approval from the US Food and Drug Administration (FDA) for the treatment of COVID-19[244].

RDV is administered intravenously, this inherently restricts the therapeutic window preventing treatment early in the course of infection. To mitigate this limitation, two orally available prodrug derivatives of GS-441524 have since been generated: GS-621763[245] (Fig. 1.9*C*), ATV006[246]/GS-5245[247] (Fig. 1.9*D*). ATV006 and GS-5245 are identical prodrug formulations identified by independent groups and have demonstrated activity against several coronaviruses *in vitro*[246, 248]. GS-5245, also referred to as obeldesivir, exhibited anti-SARS-CoV-2 activity in a non-human primate (NHP) model[247], and is currently in phase 3 trials for COVID-19[249]. Consistent with the parent nucleoside spectrum of antiviral activity, GS-5245 demonstrated anti-filovirus activity and a 10-day course treatment afforded NHPs 100% protection against lethal Sudan ebolavirus infection[250].

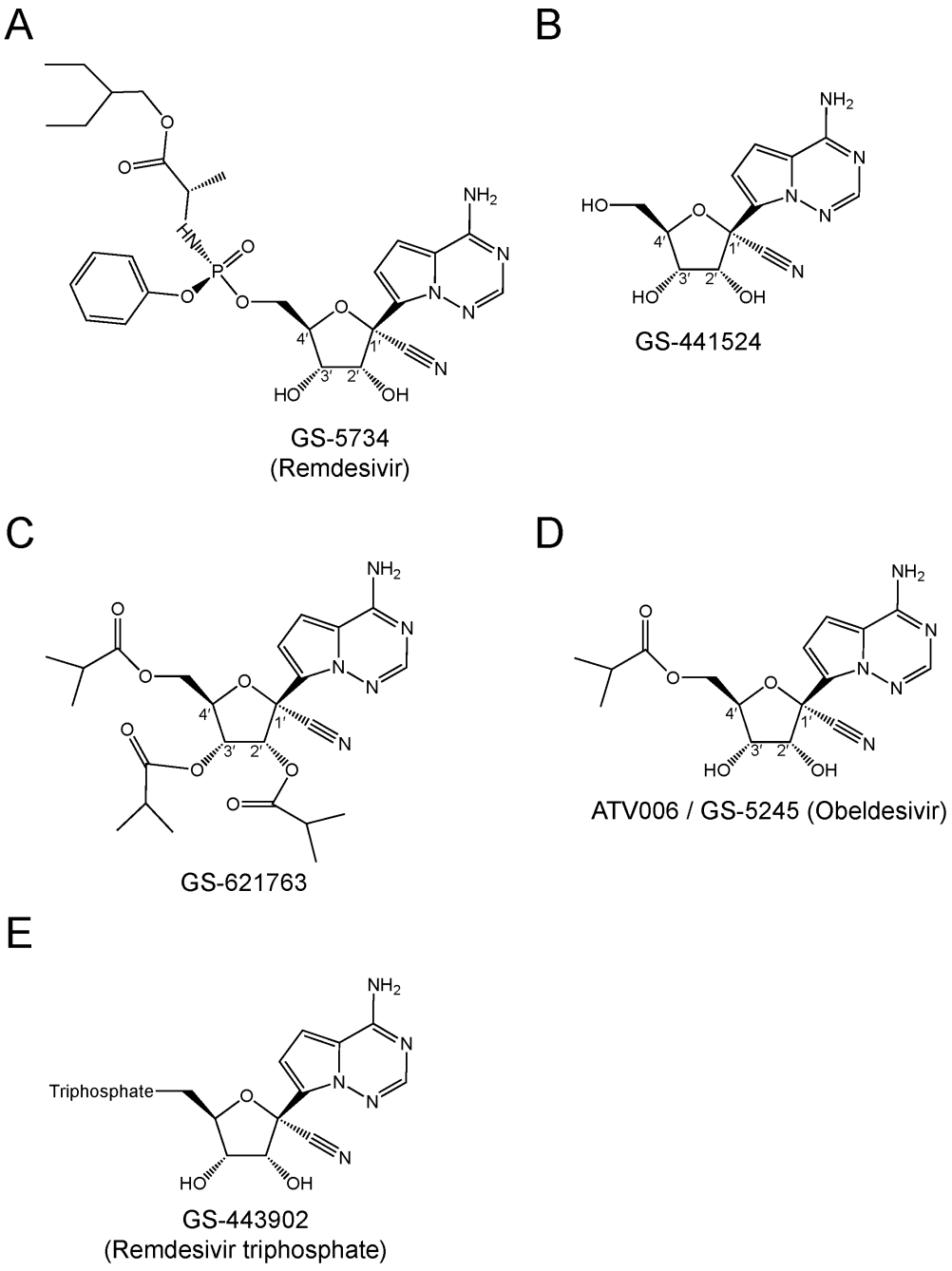


**Figure 1.9. Chemical structures of GS-5734 (*A*), GS-441524 (*B*), GS-621763 (*C*), ATV006 or GS-5245 (*D*), and GS-443902 (*E*).**

In cell culture, GS-441524 and RDV have demonstrated antiviral activity against positive-sense RNA viruses, including members of the *Coronaviridae*[157, 251-254], *Flaviviridae*[255], and *Picornaviridae*[255, 256], and nonsegmented negative-sense RNA viruses from the *Filoviridae*[241, 250, 257], *Penumoviridae*[257, 258], and *Paramyxoviridae*[240, 257]. However, limited activity was observed against the segmented negative-sense RNA virus families *Arenaviridae*, *Orthomyxoviridae*, and *Nairoviridae*[240, 257, 259]. Like the other nucleotide analogs discussed, the antiviral activity of GS-441524 and its prodrug derivatives cannot be credited to one explicit mechanism of action.

### 1.5.2 Remdesivir mechanism of action

The active metabolite of GS-441524, herein referred to as GS-443902 (Fig. 1.9*E*), competes with ATP for incorporation by the viral polymerase. Extensive structural and biochemical GS-443902 studies help to explain its prodrug derivatives' broad-spectrum antiviral activity. Investigating a panel of representative viral RdRp revealed efficient GS-443902 incorporation is a prerequisite for downstream antiviral activity[260]. Notably, GS-443902 outcompetes ATP, 2- to 3-fold for incorporation by SARS-CoV-2 RdRp[49, 50, 198, 261]. These efficient rates of incorporation can be explained by a polar pocket comprised of Thr-687, Asn-691, and Ser-759, which is particularly well adept to support the 1′-cyano of GS-443902[40]. Once incorporated, a heterogenous pattern of inhibition is observed amongst several viral RdRps[260, 262]. For coronavirus and picornavirus, GS-443902 incorporation at position "i" is followed by the incorporation of three nucleotides downstream before RNA synthesis comes to arrest at position "i+3"[49, 262-264]. A steric clash between the 1′-cyano group of GS-443902 and a conserved serine at position 861 (SARS-CoV-2 numbering) in the RdRp is responsible for primer strand inhibition[49, 263-266]. Likewise, inhibition at position "i+5" is observed following the incorporation by EBOV and RSV RdRp[267]. In all cases, delayed chain-termination is not absolute and can be overcome with elevated NTP concentrations that may better recapitulate what is present in the cell[49, 198, 263-266]. Therefore, it is conceivable that newly synthesized RNA viral genome copies could contain embedded GS-443902 residues. Interestingly, no termination was observed following GS-443902 incorporation by HCV[103] and several insect-borne flavivirus RdRp[112]. Further emphasizing an alternative mechanism of action independent of primer-strand termination. Although unlikely given the inefficient rates of incorporation, the extension of GS-443902 by segmented negative-

sense viral RdRp (CCHFV, LASV, and influenza) did not demonstrate inhibition of RNA synthesis[260].

Template-dependent mechanisms of inhibition have been previously described for other nucleotide analogs[154, 164, 268, 269]. When utilized as a template for subsequent rounds of replication, RNA synthesis by several viral RdRp opposite the embedded GS-443902 residue is inhibited[260, 265]. These observations support template-dependent inhibition as a universal mechanism of action. SARS-CoV-2 RdRp modelling suggests that a clash between the embedded RDV residue and the backbone of Ala-558 within motif F obstructs the incorporation of UTP opposite RDV[265]. Additional structural studies are required to define the structural conflict responsible for template-dependent inhibition.

Specific to coronaviruses, eliminating ExoN activity rendered MHV 4.5-fold more susceptible to RDV treatment *in vitro*[251]. Thus, subsequent nucleotide incorporation following GS-443902 incorporation does not offer complete protection from the ExoN. However, the mechanisms that facilitate RDV excision by the ExoN are still unclear. Notably, GS-443902 is only susceptible to excision in absence of the RdRp complex, which when associated with the RNA duplex appears to block ExoN access[270]. This barrier to excision is likely alleviated by the helicase which engages the template strand to unwind the RNA duplex[204, 205]. This action simultaneously backtracks the RdRp and pushes the 3′-terminus of the primer through the NTP tunnel to, in theory, meet the ExoN[207]. Using molecular tweezers, it was concluded that GS-443902 incorporation in the nascent RNA strand can promote RdRp backtracking in the absence of the helicase[198]. To fully understand how RDV is excised, further studies evaluating the interplay between the RdRp, helicase, and ExoN are warranted. Taken together, the anti-coronavirus activity of GS-443902 is likely due to embedment in the newly synthesized viral genome, where it is presumed go undetected by the ExoN.

### 1.5.3 Remdesivir resistance

*In vitro* selection experiments with GS-441524 and RDV against MHV, SARS-CoV-2 and EBOV identified resistant mutations that target nucleotide analog incorporation and template-dependent inhibition. For MHV, two mutations in the RdRp conferred 5.6-fold resistance to GS-441524, F476L and V553L[251]. Intriguingly, V553I improved MHV fidelity and was resistant to base-modified mutagenic nucleotide analogs[271]. However, V557L in SARS-CoV-2 RdRp (analogous to V553L) did not alter discrimination against GS-443902[265]. Instead, V557L supported ~5-fold resistance against template-dependent inhibition, underscoring the biological relevance of this mechanism[265]. Structural studies have implicated Val-557 and Ala-558 in RNA stabilization at the templating base position to facilitate NTP incorporation[42-44]. Computational modelling identified that V557L may alleviate translocation hindrance evoked by the template-embedded GS-443902 residue[272]. Additional SARS-CoV-2 resistance studies identified two complementary substitutions that support RDV resistance, S759A and V792I[273]. Reverse genetics found that alone, the analogous mutations conferred ~2-fold resistance in MHV but combined provided at least 25-fold reduced susceptibility[273]. Located in the active site, S759A supports resistance by increasing discrimination 5- to 10-fold against GS-443902[40, 273]. The altered preference could be explained by the disruption of the hydrogen bonding network formed by the hydrophilic pocket[40]. On the other hand, V792I alleviates template-dependent inhibition, but how exactly it drives this mechanism of resistance remains unknown. Importantly, V792I is a clinically relevant mutation and was identified in an immunocompromised patient 24 days after receiving RDV treatment[274].

For Ebola, six remdesivir-treated lineages demonstrated a 3.7- to 5.2-fold decrease in RDV effective concentration[275]. Appearing early in selection experiments, F548S remained a consistent substitution present in all resistant isolates after 35 passages. Biochemically, F548S promoted a subtle increase in discrimination against RDV-TP (1.4-fold)[275]. Like Val-557 in SARS-CoV-2 and Val-553 in MHV RdRp, Phe-548 is found in the evolutionarily conserved motif F, and therefore, its mechanism of resistance could be specific to template-dependent inhibition[275]. Characterization of these resistance-conferring mutations provides evidence that efficient incorporation and template-dependent inhibition are the primary parameters contributing to the antiviral efficacy of RDV.

## 1.6 2′-modified Nucleotide Analogs

As a scaffold, 2′-substituted nucleotide analogs have undergone extensive investigation. Initially developed as chemotherapies, altering the conformation of the 2′-hydroxyl to the "up" position was discovered to have an antiviral effect[123, 124]. This class of nucleotide analogs are referred to as arabinose or "Ara" nucleotide analogs. Due to toxicities, Ara nucleotide analogs have not progressed to the clinic as antiviral therapies but are frequently employed as controls alongside other investigational nucleotide analogs. An abundance of biochemical data has been generated over the past two decades for 2′-substituted nucleotide analogs. For brevity, this section will focus on clinically relevant 2′-α-fluoro,2′-β-methyl nucleotide analogs, namely sofosbuvir, mericitabine, and bemnifosbuvir (Figure 1.10). Perhaps most important from these studies are two mechanisms of resistance, increased nucleotide analog discrimination and phosphorolytic excision.

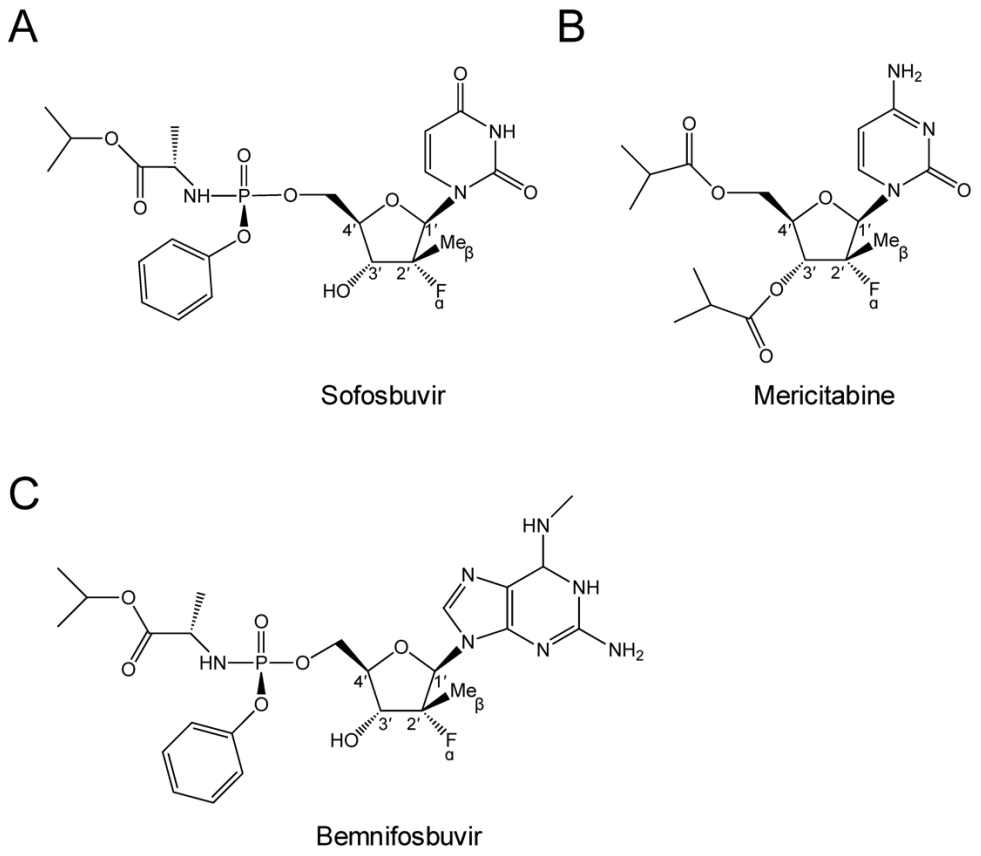


**Figure 1.10. Chemical structures of sofosbuvir (*A*), mericitabine (*B*), and bemnifosbuvir (*C*).**

### 1.6.1 Sofosbuvir

Discovered in 2010[276], sofosbuvir is a 2′-α-fluoro,2′-β-methyl uridine monophosphate prodrug approved for the treatment of HCV infection[21, 22]. Its approval was largely based on a clinical trial that demonstrated a 12-week regime of sofosbuvir and ribavirin, independent of interferon, offered a 100% cure rate[277]. As expected given the RdRp catalytic motif conservation observed amongst the *Flaviviridae* family[31], sofosbuvir demonstrated antiviral activity against several mosquito-borne flaviviruses, including DENV, JEV, WNV, YFV, and ZIKV in cell culture[278-282]. Moreover, the uncontrolled, off-label use of sofosbuvir improved YF disease outcomes in two patients[283]. However, in a controlled setting, sofosbuvir's anti-YFV activity was only maintained *in vivo* when administered prophylactically[284]. Investigation of sofosbuvir efficacy against other high-interest RNA viruses remains sparse. Computational modelling

concluded sofosbuvir could be a potential anti-SARS-CoV-2 agent[285]; but *in vitro*, sofosbuvir did not inhibit SARS-CoV-2 replication[157], likely due to inefficient incorporation by the SARS-CoV-2 RdRp complex[49, 286].

### 1.6.2 Sofosbuvir Mechanism of Action

The active metabolite of sofosbuvir, 2′-α-fluoro,2′-β-methyluridine triphosphate (2′-F,2′-Me UTP), competes with UTP for incorporation by the viral polymerase. Previous reports have shown that HCV RdRp incorporated 2′-F,2′-Me UTP 45-fold to 150-fold less efficiently than UTP[287, 288]. The differences in incorporation efficiency could be attributed to the different strains employed[288]. Acting as a non-obligate immediate chain terminator, 2′-F,2′-Me UTP inhibits HCV and multiple insect-borne flavivirus RdRp-mediated RNA synthesis at the site of incorporation[29, 278, 289]. Investigating several 2′-substituted UTP analogs against HCV NS5B, Fung et al. demonstrate 2′-F,2′-Me UTP-induced inhibition is mediated by the 2′-β-methyl and not the 2′-α-fluoro substituent[287]. Independent of the viral RdRp, the 2′-α-fluoro modification may be most important for cellular metabolism. The ribose conformation also referred to as the "sugar pucker"[290], has important implications for nucleotide analog activation and recognition by host enzymes[123, 124]. The electronegativity of the 2′-fluoro group locks the sugar in a 3′-endo position, mimicking the conformation of ribonucleotides[291, 292], and can improve the stability of the glycosidic bond[293]. The exact structural intricates that facilitate chain termination by 2′-β-substituted nucleoside analogs remain convoluted. It was initially posed that a 2′-F,2′-Me UMP-terminated primer prevented incorporation of the next nucleotide by HCV NS5B[294]. However, more recent work monitoring key residues using solution-state NMR concluded that the 2′-β-methyl ATP prevents PV $3D^{pol}$ active site closure[295].

### 1.6.3 Sofosbuvir Resistance

Early work using an HCV replicon system discovered that the substitution S282T conferred resistance to structurally related 2′-β-methyl-substituted ribonucleotide analogs, including sofosbuvir[294, 296-299]. However, this mutation has been observed infrequently in the clinic and is associated with a replication fitness cost[300]. The analogous substitution in DENV, WNV, and ZIKV RdRp generated a sofosbuvir-resistant phenotype *in vitro*[278, 289, 301]. Biochemical characterization of the mutated HCV and DENV RdRp found resistance is conferred at the level

of nucleotide incorporation[278, 302]. Contained within motif B, Ser-282 interacts with the 2′-hydroxyl of the incoming nucleotide[303]. It was also shown that the interaction between Ser-282 and the adjacent Gly-283 helps position the incoming nucleotide and template[302]. The interaction between Gly-283 and the 2′-hydroxyl of the templating base appears to be essential for improved discrimination against 2′-F,2′-Me UTP by HCV S282T RdRp[302]. Therefore, this substitution could disrupt fundamental interactions supporting the incorporation of 2′-F,2′-Me UTP and related 2'-β-methyl-substituted ribonucleotide analogs. Intriguingly, the HCV S282T replicon remained susceptible to the guanosine counterpart of sofosbuvir[297, 304]. This observation points to subtle differences between the incorporation of nucleotide analogs that differ in their base moiety but possess the same ribose modifications.

Another mechanism of resistance to chain-terminating nucleotide analogs is pyrophosphorolysis or ATP-dependent excision. Pyrophosphorolysis is the reversal of the phosphoryl transfer reaction whereby a pyrophosphate donor (ATP or inorganic pyrophosphate [PPi]) performs a nucleophilic attack to release the 3′-terminal nucleotide. Foundational cross-linking and footprinting assays with human immunodeficiency virus type 1 reverse transcriptase (HIV-1 RT) have helped guide our understanding of pyrophosphorolysis and its relationship to polymerase translocation[305-307]. These kinetic studies show that i) pyrophosphorolysis can only occur when the 3′-end of the primer is positioned in the N-site (i.e. pre-translocation)[307] and ii) HIV-1 RT maintains an equilibrium between pre- and post-translocation satisfying the Brownian ratchet model of polymerase translocation[117, 305, 306]. Extending these observations to mechanisms of resistance, consider the well-described HIV-1 RT nucleoside inhibitors 3′-azido-3′-deoxythymidine (zidovudine or AZT) and entecavir (ETV). AZT is an obligate chain terminator that prevents the incorporation of the next nucleotide, therefore favoring a pre-translocated conformation[308]. Structural and biochemical studies of HIV-1 RT have demonstrated ATP-mediated excision as a mechanism of resistance against AZT[309, 310]. Conversely, ETV is a non-obligate delayed-chain terminator, the incorporation of subsequent nucleotides ultimately protects against excision[268]. Similarly, HCV NS5B has demonstrated excision-competent complexes capable removing obligate chain terminators and non-obligate 2′-β-methyl-modified nucleotide analogs[311, 312]. A key observation amongst these studies was NTP binding in the active site after a

chain-terminating nucleotide protected against excision by forming a stable dead-end complex[311, 312].

Mericitabine is the cytidine counterpart to sofosbuvir and in its active trisphosphate form (2′-F,2′-Me CTP) inhibits HCV RNA synthesis in the same fashion as 2′-F,2′-Me UTP[313]. However, clinical trials determined mericitabine less effective than sofosbuvir at reducing patient response to HCV infection[314-316]. Considering the two analogs share identical sugar modifications, the difference in the clinic was unexpected. Offering one potential explanation, 2′-F,2′-Me CTP was found to be more susceptible to HCV NS5B pyrophosphorolytic excision than 2′-F,2′-Me UTP[288]. Moreover, the binding affinity of 2′-F,2′-Me CTP and 2′-F,2′-Me UTP were equivalent, and rates of excision were due to differences in pyrophosphate binding efficiency[288]. The observed differences in pyrophosphate binding efficiencies may relate to base-dependent structural changes that influence the translocation equilibrium proceeding phosphodiester bond formation. 2′-F,2′-Me UMP-terminated primers could prevent pyrophosphate access to the active site, but how this would be accomplished remains unknown. Monitoring the dynamics of key residues (i.e. Cryo-EM or solution-state NMR) in combination with dead-end complex formation and/or rescue experiments could provide valuable insight into the structural and chemical requirements that facilitate the excision of 2′-α-fluoro,2′-β-methyl CTP but not 2′-α-fluoro,2′-β-methyl UTP.

### 1.6.4 Bemnifosbuvir

Bemnifosbuvir, also referred to as AT-527, is currently in a phase 3 clinical trial for the treatment of high-risk COVID-19 in an outpatient setting (NCT05629962) and a phase 2 clinical trial evaluating its efficacy in combination with ruzasvir in patients with chronic HCV (NCT05904470). Bemnifosbuvir, is an orally available 2′-α-fluoro,2′-β-methyl guanosine monophosphate prodrug with ribose modifications identical to sofosbuvir and mericitabine. Moreover, AT-527 and AT-752 (the diastereomer of AT-527) have demonstrated antiviral activity against coronaviruses[317], HCV[304], and several insect-borne flaviviruses[318, 319]. Limited antiviral activity was observed against representative RNA viruses from the *Picornaviridae*, *Pneumoviridae*, and *Orthomyxoviridae* families[304, 318].

### 1.6.5 Bemnifosbuvir mechanism of action

Metabolic activation of AT-572 or AT-752, results in the active triphosphate AT-9010, herein referred to as 2′-F,2′-Me GTP, which competes with GTP to target the viral polymerase[304, 318]. Notably, 2′-F,2′-Me GTP has been shown to target different functional domains of SARS-CoV-2 Nsp12[286] and DENV NS5[318, 320]. Considering the SARS-CoV-2 RdRp domain, 2′-F,2′-Me GTP is incorporated ~5-fold less efficiently than GTP, a significant improvement compared to its uracil counterpart[286]. Like its cytidine and uracil counterparts, 2′-F,2′-Me GTP is a non-obligate chain-terminator that inhibits RNA synthesis as the site of incorporation[286]. Although not entirely resistant to SARS-CoV-2 ExoN-mediated excision, 2′-F,2′-Me GTP is excised less efficiently than 2′-F,2′-Me UTP[286]. Replacement of the non-bridging oxygen of the 5′-α-phosphate with a sulfur atom rendered 2′-F,2′-Me GTP resistant to ExoN excision but reduced incorporation efficiency by the RdRp complex[321]. Conflicting observations have yet to determine if the RdRp complex positioned at the 3′-end of the primer protects against excision[270, 321]. Structurally, 2′-F,2′-Me GDP was discovered in the NiRAN active site in an orientation that resembled the preferred natural substrate GTP[40, 286]; this, in turn, may prevent the capping mechanism integral to SARS-CoV-2 replication[39].

Similarly, two targets have been identified against DENV NS5[320]. First, 2′-F,2′-Me GTP targets the RdRp active site of NS5 and is incorporated ~7- to ~11-fold less efficiently than GTP by DENV NS5 depending on the serotype[318, 320]. Conversely, the same study found incorporation

of 2′-F,2′-Me UTP was not evident[320], which opposed a previous observation that DENV NS5 could incorporate 2′-F,2′-Me UTP[278]. However, this is likely due to the presence of a different divalent metal cation[29]. Second, 2′-F,2′-Me GTP bound to the NS5 MTase domain improved stability, this may result in the inhibition of the RNA capping[320]. Taken together, 2′-F,2′-Me GTP is an adequate substrate for SARS-CoV-2 nsp12 and DENV NS5, acting universally as a non-obligate immediate chain terminator[286, 304, 318, 320]. The incorporation differences observed between 2′-F,2′-Me GTP and its uracil counterpart are peculiar, given they possess identical sugar modifications. It has been postulated that the discrepancy observed between 2′-F,2′-Me GTP and 2′-F,2′-Me UTP incorporation is due to differences in motif D of HCV NS5B when compared to SARS-CoV-2 Nsp12 and DENV NS5[31, 320].

### 1.6.6 Bemnifosbuvir mechanism of resistance

Resistant mutations specific to bemnifosbuvir have yet to be evaluated in the literature, but previous HCV S282T cross-resistance studies can offer valuable insight. Using the HCV replicon system, it was determined that the S282T substitution confers cross-resistance to 2′-β-methyl ATP, 2′-β-methyl CTP, 2′-β-methyl GTP, and 2′-α-fluoro,2′-β-methyl CTP but not 2′-α-fluoro,2′-β-methyl GTP[294, 297, 304]. These observations indicate that the nucleotide base and sugar-pucker are necessary components to alleviate cross-resistance. It is not known if the analogous sofosbuvir-resistant conferring mutation in DENV NS5 (S604T) follows the same phenotypic pattern as HCV S282T and remains susceptible to the guanosine counterpart.

Taken together, 2′-α-fluoro,2′-β-methyl modifications elicit their antiviral effect via immediate chain-termination, but incorporation discrepancies can be observed when the ribose is attached to a purine or pyrimidine nucleobase (Fig. 1.11). Future studies should consider a parallel investigation of all four nucleobase analogs possessing these 2′-substitutions. In addition, mutagenic studies targeting motif D are warranted to better understand its role in nucleotide discrimination and the different incorporation patterns of 2′-F,2′-Me UTP and 2′-F,2′-Me GTP.

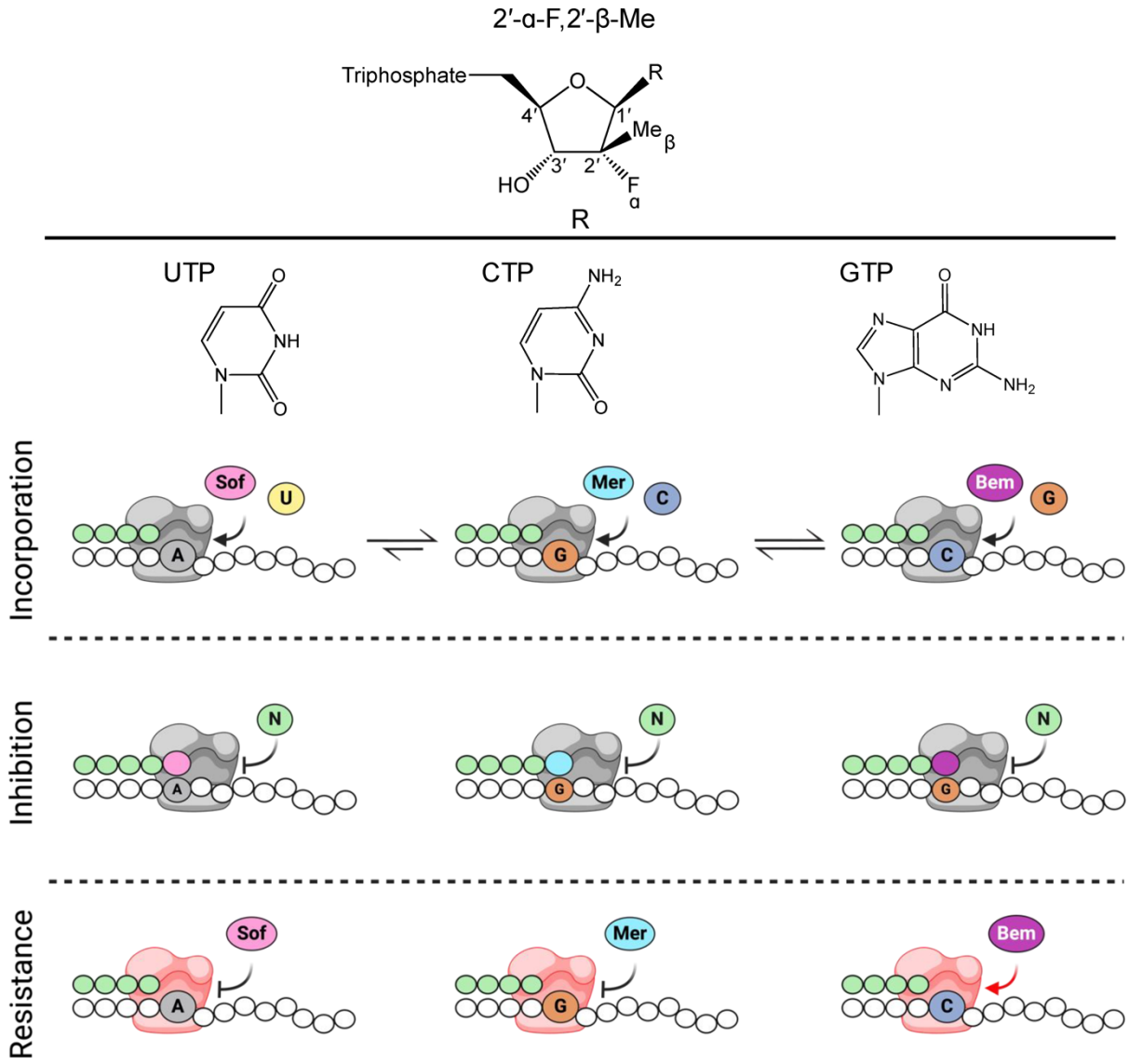


**Figure 1.11. Mechanism of action of sofosbuvir, mericitabine, and bemnifosbuvir**. All nucleotide analogs share the 2′-α-fluoro,2′-β-methyl-substituted ribose responsible for the inhibition of RNA synthesis (*top*). Schematic representation of viral RdRp (*grey*)-mediated nucleotide incorporation into RNA primer (*green circles*)/template (*white circles*). Letters A, C, G and U refer to natural bases. Incorporation, 2′-F,2′-Me UTP (pink circle) is incorporated less efficiently than 2′-F,2′-Me CTP (light blue circle) and 2′-F,2′-Me GTP (*purple circle*). Inhibition, all 2′-α-fluoro,2′-β-methyl-substituted nucleotide analogs behave as non-obligate chain terminators. Resistance, HCV mutant (S282T) RdRp (*red*) confers resistance to 2′-F,2′-Me UTP and 2′-F,2′-Me CTP, but remained susceptible to 2′-F,2′-Me GTP. Created with BioRender.com.

## 1.7 4′-modified nucleotide analogs

Within the family of ribose-substituted ribonucleotide analogs, the 4′-modification remains relatively underexplored. As a result, few have progressed to clinical trials for the treatment of RNA virus infection. This section will discuss two different 4′-modified nucleoside analogs that have demonstrated potent activity against different classes of RNA viruses, ALS-8176 and 4′fluorouridine.

### 1.7.1 ALS-8176

Derived from the parent compound ALS-8112 (Fig. 1.12*A*), ALS-8176 (Fig. 1.12*B*), also referred to as lumicitabine, is a 2′-F,4′-$ClCH_2$ cytidine nucleoside prodrug that was developed for the treatment of RSV infection[322]. A phase 1 RSV challenge study involving 62 participants older than 18 years of age found that continued treatment with ALS-8176 reduced viral load[323]. Unfortunately, ALS-8176 did not progress beyond phase 2 clinical trials due to toxicity concerns in infants[324]. Although unsuccessful, several lessons can be learned from the pre-clinical investigation of ALS-8112. In cell culture, ALS-8112 demonstrated activity against nonsegmented negative-sense viruses that belong to the *Pnuemoviridae* and *Paramyxoviridae* families[325]. In an African green monkey model, ALS-8176 effectively reduced RSV viral load[325]. However, limited activity was observed against positive-sense (*Flaviviridae* and *Picornaviridae*) and segmented negative-sense (*Orthomyxoviridae*) RNA viruses[325].

### 1.7.2 ALS-8176 mechanism of action

ALS-8176, in its active 5′-triphosphate form (2′-F,4′-$ClCH_2$ CTP), is incorporated 13-fold less efficiently than CTP by RSV RdRp[325]. Once incorporated, 2′-F,4′-$ClCH_2$ CTP inhibits RNA synthesis via immediate chain termination[325] (Fig. 1.12*C*). Aligning with the *in vitro* activity spectrum, 2′-F,4′-$ClCH_2$ CTP did not inhibit HCV or influenza RdRp but did inhibit PIV-1 RdRp[325]. Investigating other CTP analogs revealed that the 2′-fluoro modification, although not responsible for the inhibition of RNA synthesis, was crucial for 2′-F,4′-$ClCH_2$ CTP RSV RdRp specificity. In fact, 4′-$N_3$, 2′-F-4′-$N_3$, 2′-diF-4′$N_3$, and 4′-$ClCH_2$ CTP could inhibit both RSV and HCV RdRp[325]. Moreover, 4′-$N_3$ CTP and 2′-F CTP could be incorporated by h-mtRNAP, suggesting the 4′-$ClCH_2$ modification is responsible for mediating the limited off-target effects. Substituting the nucleobase of 2′-F,4′-$ClCH_2$ CTP for guanosine (2′-F,4′-$ClCH_2$ GTP) improved

incorporation efficiency but somewhat alleviated inhibition of RNA synthesis[326]. Conversely, 2′-F,4′-$ClCH_2$ ATP was incorporated as efficiently as 2′-F,4′-$ClCH_2$ CTP and resulted in immediate chain termination[326]. It is not known why changing the nucleobase impacts the sugar-driven inhibitory effect.

### 1.7.3 ALS-8112 mechanism of resistance

Following *in vitro* selection experiments, four combinatorial amino acid substitutions (M628L, A789V, L795I, and I796V) located in the RdRp domain reduced ALS-8112 anti-RSV activity 39-fold[325]. Resistance was specific to the 4′-$ClCH_2$ substitution and supported at the level of nucleotide incorporation. Biochemically, the RSV RdRp mutant incorporated 2′-F,4′-$ClCH_2$ CTP and 4′-$ClCH_2$ CTP approximately 4-fold and 24-fold less efficiently than the wildtype RdRp, respectively; no change was observed against 2′-F CTP. Located in motif B, A789V, L795I, and I796V provide cross-resistance to other 4′-halomethylated substitutions[326]. Of the four substitutions, A789V is closest to the nucleotide-binding site and is the greatest contributor to the resistant phenotype. Both wild-type and mutant RSV RdRp remained equally susceptible to 2′-F,4′-$N_3$ CTP in a luciferase reporter assay[326]. The structural examination of the RSV L/P complex revealed that A789V, L795I, and I796V are oriented away from the active site, suggesting resistance is likely conferred by a general architectural change of the active site[67, 68]. Intriguingly, the four-substitution mutant remained susceptible to 2′-F,4′-$ClCH_2$ ATP but conferred resistance to the 2′-F,4′-$ClCH_2$ GTP[326] (Fig. 1.12*C*). These observations, like S282T against 2′-α-fluoro,2′-β-methyl purine and pyrimidine analogs, highlight that the molecular mechanisms of resistance are not solely due to the sugar-modifications responsible for termination of RNA synthesis. Presumably, it is the conformational change of the active site that is impacting the recognition of CTP- and GTP-analogs, but not ATP-analogs.

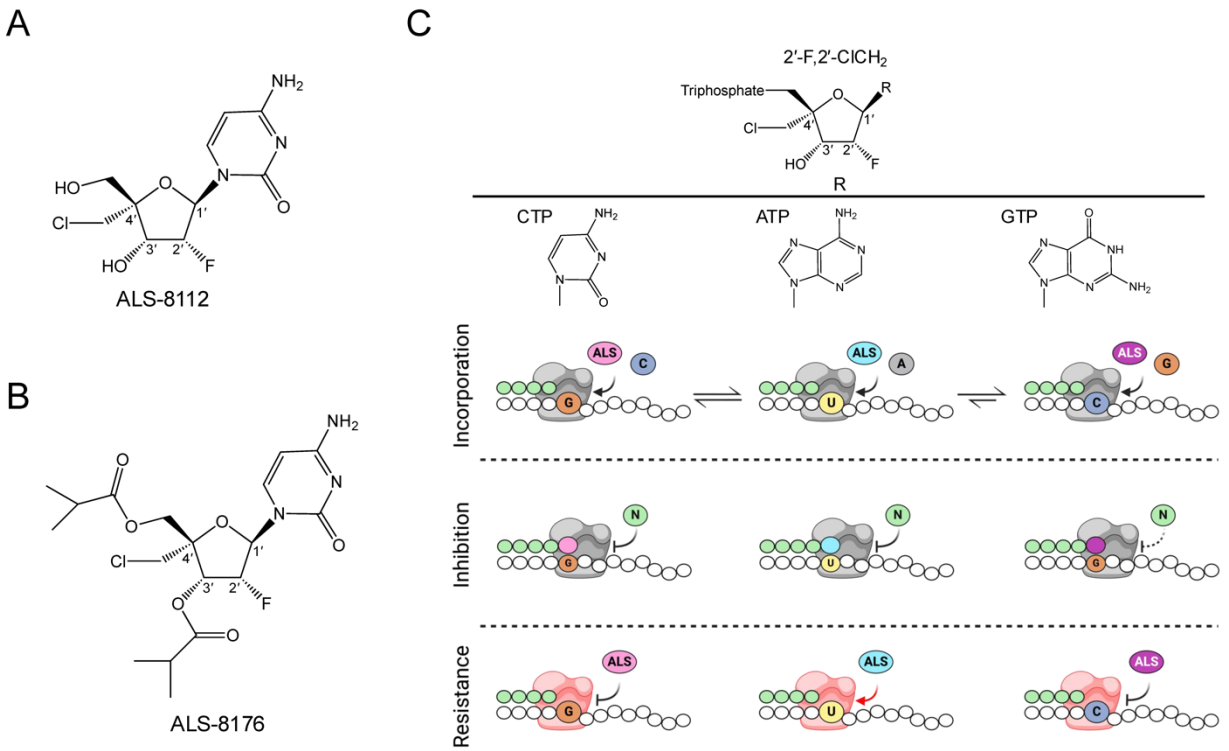


**Figure 1.12. Chemical structures and mechanism of action of ALS-8176 against RSV**. Chemical structure of the parent compound ALS-8112 (***A***) and its prodrug derivative ALS-8176 (***B***). ***C***, mechanism of action of the triphosphate form of ALS-8176 (*top*) against RSV based on experimental data from Deval et al.[325, 326]. Schematic representation of RSV WT RdRp (*grey*)-mediated nucleotide incorporation into RNA primer (*white circles*)/template (*green circles*). Letters A, C, G, and U refer to natural bases. "ALS" refers to the nucleotide analog ALS-8112-TP possessing identical ribose-modifications on a cytidine (*pink*), adenosine (*light blue*), and guanosine (*purple*) nucleobase. Incorporation, RSV RdRp incorporates ALS-8112 GTP slightly more efficiently than its CTP and ATP counterparts. Inhibition, ALS-8112 CTP and ATP inhibit RNA synthesis via immediate chain termination, whereas termination by ALS-8112 GTP is somewhat alleviated. Resistance, RSV mutant (M628L, A789V, L795I, and I796V) RdRp (*red*) confers resistance to ALS-8112 CTP and GTP at the level of nucleotide incorporation. However, RSV mutant RdRp remains susceptible to ALS-8112 ATP. Created with BioRender.com.

### 1.7.4 4′-fluorouridine

4′-fluorouridine (4′-F U) (Fig. 1.13*A*) exhibited antiviral activity against SARS-CoV-2[327], picornaviruses[328]; and several non-segmented negative-sense RNA viruses, including RSV, HPIV-3, NiV, and measles virus (MeV)[327]. Various seasonal and pandemic influenza strains, a segmented negative-sense RNA virus, were also susceptible to 4′F U treatment[329]. Like base-modified mutagenic nucleotide analogs, the lack of specificity observed for 4′F U may raise some questions about the potential for off-target effects. However, 4′F U treatment of various human and animal cell lines did not present any cytotoxic effects[327].

### 1.7.5 4′-fluorouridine mechanism of action

4′-F U in its active triphosphate form (4′-F UTP) (Fig. 1.13*B*) can act as a substrate for SARS-CoV-2, RSV, and influenza RdRp, competing with UTP for incorporation[327, 329]. Both RSV and influenza RdRp incorporate 4′-F UTP approximately 4-fold less efficiently than its natural counterpart[327, 329]. Biochemically, 4′-F UTP elicits different mechanisms of inhibition that are dependent on the viral polymerase and the sequence of the template (Fig. 1.13*C*). Against SARS-CoV-2 RdRp complex, a single incorporation of 4′F UTP does not impede RNA synthesis, while a second non-adjacent incorporation event results in immediate chain termination[327]. To determine the more likely mechanism of action against SARS-CoV-2, it is important to consider these observations in the context of the 3′ to 5′ proofreading ExoN. Sequence-dependent immediate chain termination would likely result in the recognition and excision of 4′-F UMP, thereby mitigating its antiviral effect. However, if no chain termination were to occur, then 4′-F UMP could become embedded in the newly synthesized viral genome strands. Acting as a templating base, NTP incorporation across 4′F UMP could facilitate a template-dependent mechanism of inhibition, but this has yet to be investigated. Employing an ExoN-deficient coronavirus has proven to be a valuable tool for investigating chain-terminating and mutagenic nucleotide analogs. To help delineate the mechanism of action, future studies should evaluate the potency of 4′-F U against an ExoN-deficient coronavirus. This would provide additional insight into the RNA synthesis termination effects of 4′F UTP.

The extension of single 4′-F UMP by RSV RdRp promotes the formation of intermediate product three nucleotides downstream[327]. Interestingly, two non-adjacent templated AMPs resulted in immediate chain termination following the first 4′F UTP incorporation event. Against influenza RdRp, it was concluded that 4′-F UTP promotes immediate chain termination[329]. However, the reduction of the overall signal at elevated 4′-F UTP concentration makes interpretation of its exact mechanism difficult. Additional mechanistic studies to solidify the inhibitory mechanism(s) of 4′-F UTP are required. Although it is assumed to bind to the picornavirus RdRp active site, a direct mechanism of action has yet to be determined[328]. To further corroborate the limited toxicity observed *in vitro*, 4′-F UTP should be evaluated as a substrate for human polymerases.

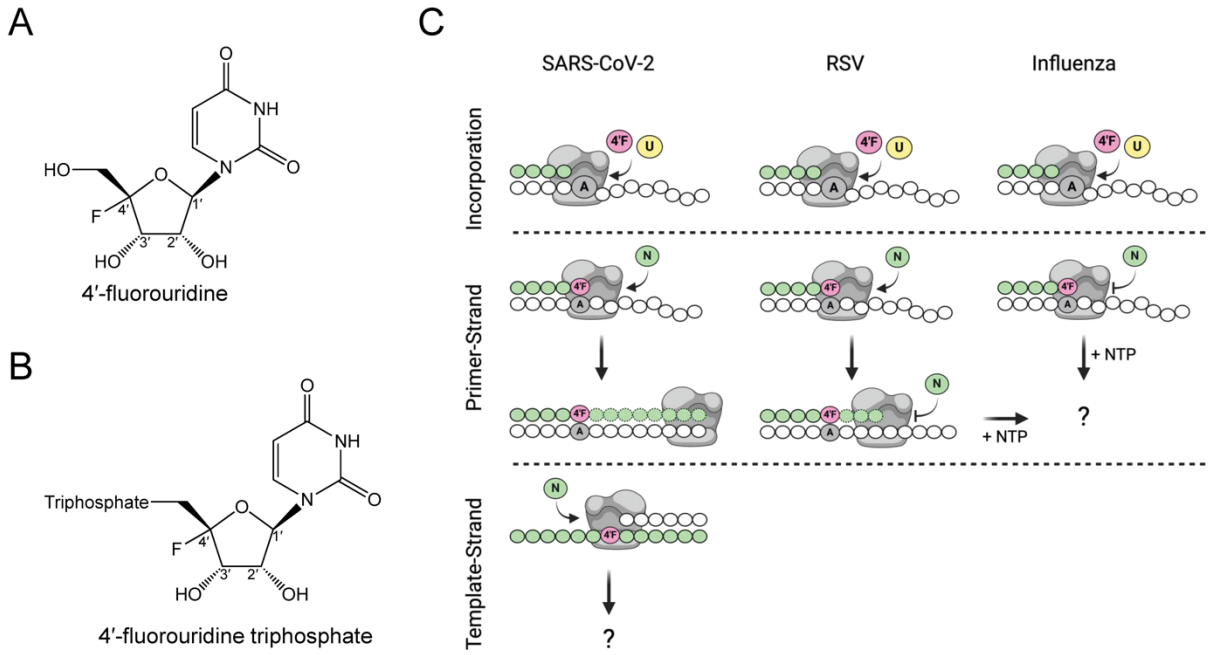


**Figure 1.13. Mechanism of action of 4′-fluorouridine (*A*).** Following intracellular metabolization the active metabolite 4′-fluorouridine triphosphate (***B***) can act as substrate for SARS-CoV-2, RSV, and influenza RdRp. ***C***, schematic depicting 4′-fluorouridine's mechanism of action against SARS-CoV-2 (*left*), RSV (*middle*), and influenza (*right*) RdRp based on experimental data by Sourimant et al.[327] and Lieber et al.[328]. Schematic representation of RdRp (*grey*)-mediated nucleotide incorporation into RNA primer (*white circles*)/template (*green circles*). Letter U refers to natural UTP and "4′F" refers to 4′-fluorouridine triphosphate. Different RNA synthesis patterns have been observed following a single incorporation event. Against SARS-CoV-2 incorporation of 4′-F UTP does not result in chain termination and therefore could become embedded in newly synthesized viral genome template-strands, a template-dependent mechanism has yet to be investigated. Against RSV and influenza RdRp 4′-F UTP acts as a delayed-chain terminator and immediate chain terminator, respectively. It is not known if termination can be overcome with increased subsequent nucleotide substrate concentration facilitating the formation of template-embedded 4′-F UMP residues. Created with BioRender.com.

### 1.7.6 4′-fluorouridine mechanism of resistance

A biochemical mechanism of resistance has yet to be described for 4′-F UTP. In cell culture, different 4′-F U resistant lineages of influenza were isolated, mutations were not specific to the RdRp (PB1) and could be found in all three functional domains[330]. The two substitutions of interest were V285I in PB1 and Y488C in PB2, both were identified independently in different resistant strains. V285I supported the greatest increase in $EC_{90}$ value, Y488C required compensatory mutations[330]. Both V285I and Y488C disappeared rapidly when co-infected with wildtype, likely due to a fitness cost associated with the substitution[330]. An influenza strain

containing favipiravir resistance-conferring mutations K229R in PB1 and P653L in PA remained sensitive to 4′-F U treatment[330]. V285I supported slight resistance to favipiravir but was more susceptible to molnupiravir[330]. Finally, resistance can be maintained *in vivo*, but 4′F U resistance coincides with viral attenuation[330]. RdRp resistance-conferring mutations that resulted in virus attenuation have been shown to impact RdRp fidelity. Future studies should consider investigating these resistant mutations at the level of nucleotide incorporation. It is hypothesized that the RdRp resistance-conferring substitutions alter active site geometry to better accommodate the secondary structure introduced by 4′-F UMP[330]. This would imply that 4′-F UTP is still incorporated by the mutant polymerase and RNA synthesis continues uninhibited. Therefore, the analog could become embedded in subsequently synthesized genomic RNA strands where its exact effects have yet to be determined.

## 1.8 Research project aims

Target validation and mechanism of action studies have proven to be instrumental for the discovery and development of DAAs. As exemplified by HIV-1 and HSV, the viral polymerase is an effective target for therapeutic intervention. However, similar endeavors against high-priority RNA viruses are lacking. This is in large part due to reactive research practices that are challenged by (1) the inherent diversity between different RNA virus families and (2) their difficult to express viral RdRp and RdRp complexes. Therefore, my project had two primary objectives before the COVID-19 pandemic. First, assist the collaborative effort within our lab to develop a library of active RdRps and RdRp complexes from prototypic RNA virus families. Completion of this objective will support timely DAA studies in response to unpredictable RNA virus outbreaks. Second, utilize the library of viral polymerases to assess the biochemical efficacy of investigational and clinically relevant broad-spectrum nucleotide analogs. In conjunction with their known antiviral activity *in vitro* or *in vivo*, these findings will elucidate the parameters required of nucleotide analogs to target a spectrum of RNA viruses.

In response to the COVID-19 pandemic my focus shifted towards SARS-CoV-2 and two broad-spectrum nucleotide analogs, RDV-TP and NHC-TP. My previous work on the MERS-CoV RdRp complex facilitated these efforts, exemplifying the utility of our prototypic pathogen approach. Detailed in the first four data chapters of this thesis is work that supported the approval

and authorization RDV and molnupiravir for the treatment of COVID-19, respectively. The latter two data chapters address pandemic preparedness. Here, RDV-TP and GS-646939, a novel 4′-modified nucleotide analog, were characterized against prototypic viral RdRps and RdRp complexes. Together, the data presented in this thesis offer insight into the parameters that drive the potency of these nucleotide analogs to elicit their antiviral effect. These conclusions will help guide the development of the next generation of nucleotide analogs targeting a spectrum of RNA viruses.

### 1.8.1 Data chapter overviews

Chapter 3: The antiviral compound remdesivir potently inhibits RNA-dependent RNA polymerase from Middle East respiratory syndrome coronavirus

Prior to the COVID-19 pandemic, RDV had been shown to inhibit coronavirus replication in cell culture[251]. However, the exact mechanism of inhibition had yet to be demonstrated against a coronavirus RdRp complex. To this end, we expressed the MERS-CoV RdRp complex for the biochemical evaluation of RDV-TP. This required a novel expression strategy for the coronavirus RdRp complex whereby a large polyprotein containing Nsp5, -7, -8, and -12 was expressed in baculovirus-infected insect cells. An active RdRp complex consisting of Nsp7, -8, and -12 is formed following the post-translational cleavage by the protease Nsp5. Key observations include the exceptional incorporation efficiency of RDV-TP and the first mechanism of action against a coronavirus RdRp complex. These findings were published before the WHO officially declared the COVID-19 pandemic.

Chapter 4: Remdesivir is a direct-acting antiviral that inhibits RNA-dependent RNA polymerase from severe acute respiratory syndrome coronavirus 2 with high potency

This chapter includes data that was published approximately one month after the WHO announced the COVID-19 pandemic. At the time vaccines were unavailable, emphasizing the need for antiviral drugs available for immediate use. Our previous studies with the MERS-CoV RdRp complex established a suitable platform to investigate nucleotide analogs against the SARS-CoV-2 RdRp complex. These findings were the first to indicate that RDV-TP as a substrate outperforms

other nucleotide analogs that were under therapeutic consideration and operates as a delayed-chain terminator against coronavirus RdRp complexes.

Chapter 5: Template-dependent inhibition of coronavirus RNA-dependent RNA polymerase by remdesivir reveals a second mechanism of action

Investigating a myriad of SARS-CoV-2 RdRp mutants revealed Ser-861 the residue responsible for delayed-chain termination. Next, RDV-embedded RNA oligos were enzymatically synthesized to evaluate a template-dependent mechanism of action. RNA synthesis opposite RDV-MP confirmed the second mechanism of action. In concert with our previous study, this work presents a complete mechanistic profile for RDV which would ultimately support its approval as a treatment for COVID-19.

Chapter 6: Molnupiravir promotes SARS-CoV-2 mutagenesis via the RNA template

Due to its oral availability and proven preclinical efficacy against SARS-CoV-2, molnupiravir offered an alternative intervention strategy for SARS-CoV-2 infection. Molnupiravir treatment promoted G to A and C to U genomic transitions in SARS-CoV-2[229]. However, the biochemical parameters that facilitate this mutational pattern were unknown. Here, we demonstrate the first mutagenic mechanism for molnupiravir against the SARS-CoV-2 RdRp complex before it received FDA authorization. Essential for these studies was the ability to enzymatically synthesize an RNA template that contained an embedded NHC residue. This allowed us to monitor the base pairing tendencies of NHC-TP and NHC-MP when embedded in the template-strand. Moreover, these findings help to explain the broad-spectrum activity of NHC against other RNA viruses.

Chapter 7: Efficient incorporation and template-dependent polymerase inhibition are major determinants for the broad-spectrum antiviral activity of remdesivir

RDV is a broad-spectrum nucleoside analog that effectively inhibits positive-sense and nonsegmented negative-sense RNA viruses but is ineffective against segmented negative-sense RNA viruses. Therefore, we aimed to provide a concise biochemical study that explained the RDV's spectrum of activity. Employing a panel of viral RdRp and RdRp complexes we show that

efficient incorporation is a prerequisite for antiviral activity. Moreover, the primer-strand mechanism of RDV was heterogeneous, while the template-dependent mechanism described previously for SARS-CoV-2 was universal.

Chapter 8: Mechanism and spectrum of inhibition of a 4′-cyano modified nucleotide analog against diverse RNA polymerases of prototypic respiratory RNA viruses

Like RDV, GS-7682 is a cyano-modified adenosine analog, however, the modification is located at the 4′-position rather than the 1′-position. GS-7682 demonstrated antiviral activity against several respiratory RNA viruses including HRV and RSV, but it lacked activity against SARS-CoV-2 and influenza. Here, we biochemically investigated the triphosphate form of GS-7682 against the RdRp of prototypic respiratory RNA viruses, RDV-TP served as a benchmark. In agreement with the previous study, efficient incorporation remained a key determinant of antiviral activity. Unlike the 1′-cyano modification, the 4′-modification evokes immediate chain-termination across all RdRp investigated an effect likely due to inhibition of RdRp translocation. This work illustrates the efficacy of novel nucleoside analog that could be instrumental to address future outbreaks or pandemics.

# Chapter 2: Materials and Methods

This chapter contains content from the following sources, republished with permission.

- Gordon CJ[#], Tchesnokov EP[#], Feng JY, Porter DP, Götte M. The antiviral compound remdesivir potently inhibits RNA-dependent RNA polymerase from Middle East respiratory syndrome coronavirus. J Biol Chem. 2020; 295:4773-4779. © the authors.
- Gordon CJ[#], Tchesnokov EP[#], Woolner E, Perry JK, Feng JY, Porter DP, Götte M. Remdesivir is a direct-acting antiviral that inhibits RNA-dependent RNA polymerase from severe acute respiratory syndrome coronavirus 2 with high potency. J Biol Chem. 2020; 295:6785-6797. © the authors.
- Tchesnokov EP[#], Gordon CJ[#], Woolner E, Kocincova D, Perry JK, Feng JY, Porter DP, Götte M. Template-dependent inhibition of coronavirus RNA-dependent RNA polymerase by remdesivir reveals a second mechanism of action. J Biol Chem. 2020; 295:16156-16165. © the authors.
- Gordon CJ, Tchesnokov EP, Schinazi RF, and Götte M. Molnupiravir promotes SARS-CoV-2 mutagenesis via the RNA template. J Biol Chem. 2021; 297:100770. © the authors.
- Gordon CJ[#], Lee HW[#], Tchesnokov EP[#], Perry JK, Feng JY, Bilello JP, Porter DP, and Götte M. Efficient incorporation and template-dependent polymerase inhibition are major determinants for the broad-spectrum antiviral activity of remdesivir. J Biol Chem. 2022; 298:6785-6797. © the authors.
- Gordon CJ, Walker SM, Tchesnokov EP, Kocincova D, Pitts J, Siegel D, Perry JK, Feng JY, Bilello JP, and Götte M. Mechanism and spectrum of inhibition of a 4′-cyano modified nucleotide analog against diverse RNA polymerases of prototypic respiratory RNA viruses. J Biol Chem. 2024; 300:107514. © the authors.

[#]Authors contributed equally to this work; contributions are outlined in subsequent data chapters.

*Dr. Egor Tchesnokov, Dr. Dana Kocincova, and Emma Woolner assisted in the expression and purification of viral RdRp and RdRp complexes.

## 2.1 Nucleic Acids and Chemicals

Synthetic RNA primers and templates were 5′-phosphorylated and purchased from Dharmacon (Lafayette, CO, USA). NTPs were purchased from GE Healthcare (Mississauga, ON, Canada). [α-$^{32}$P]-NTP was purchased from PerkinElmer (Revvity, Waltham, MA,USA). Modified nucleotide analogs investigated in this thesis are included in Table 2.1.

Table 2.1 Modified Nucleotide analogs

| Chapter | Nucleotide Analog | Company / Source | Location |
|---|---|---|---|
| 3/4 | Ara-ATP | TriLink Biotechnologies | San Diego, CA, USA |
| 4 | 2′deoxy-2′fluoro-CTP | TriLink Biotechnologies | San Diego, CA, USA |
| 4 | Ribavirin-TP | Jena Bioscience | Jena, Germany |
| 4 | Favipiravir-TP | Toronto Research Chemicals | North York, ON, Canada |
| 3 / 4 | 2′-CMe-ATP | Gilead Sciences, Inc. | Foster City, CA, USA |
| 4 | Sofosbuvir-TP | Gilead Sciences, Inc. | Foster City, CA, USA |
| 3/4/5/7/8 | RDV-TP (GS-443902) | Gilead Sciences, Inc. | Foster City, CA, USA |
| 6 | NHC-TP | MedChem Express | Monmouth Junction, NJ, USA |
| | | Dr. R.F. Schinazi | Emory University, GA, USA |
| 8 | 3′deoxy UTP | TriLink Biotechnologies | San Diego, CA, USA |
| 8 | GS-646939 | Gilead Sciences, Inc. | Foster City, CA, USA |
| 8 | 2′O-methyl UTP | TriLink Biotechnologies | San Diego, CA, USA |
| 8 | 2-thio UTP | TriLink Biotechnologies | San Diego, CA, USA |
| 8 | 2′deoxy UTP | MedChem Express | Monmouth Junction, NJ, USA |
| 8 | EFdA-TP | MedChem Express | Monmouth Junction, NJ, USA |

## 2.2 Protein expression and purification

### 2.2.1 Baculovirus expression of viral RdRp and RdRp complexes

Different expression strategies were implemented for the various RNA polymerases included in this thesis (Table 2.2). For RdRp and RdRp complexes expressed in insect cells (Sf9, Invitrogen, Burlington, ON, Canada), a pFastBac-1 (Invitrogen, Burlington, ON, Canada) plasmid with the codon-optimized synthetic DNA sequences (GenScript, Piscataway, NJ, USA) was used as the starting material. Using published protocols[331, 332], the MultiBac (Geneva Biotech, Indianapolis, IN, USA) system for protein expression in insect cells was employed for the *Coronaviridae* RdRp complex; HCV (*Flaviviridae*) NS5B; *Pneumo*-, *Paramyxo*-, and *Filoviridae* L/P (VP35 in case of filoviruses) complexes; *Arena*-, *Nairoviridae* L protein; and influenza B (FluB) heterotrimeric complex. The human mitochondrial DNA-dependent RNA polymerase (h-mtRNAP) was also expressed in insect cells.

The expression of RdRp complexes relied on post-translational cleavage or the utilization of a dual promoter. For coronavirus RdRp complexes, the coding portion of 1ab polyproteins containing only nsp5, nsp7, nsp8, and nsp12 were used as starting material for protein expression. The polyprotein is post-translationally cleaved by the nsp5 protease at its original cleavage sites. RSV, HMPV, NiV, EBOV L/P complexes, and FluB heterotrimeric complex were expressed from the same promoter to yield a single polyprotein, which is cleaved by the co-expressed tobacco etch virus (TEV) protease at engineered cleavage sites. This approach was previously reported for the expression of influenza virus RdRp heterotrimeric complex[79, 80]. HPIV-3 and PIV-5 were cloned into the pFastBac Dual vector (Invitrogen, Burlington, ON, Canada); L and P were under the control of the polyhedrin and p10 promoter, respectively. This approach was previously reported for the expression of the PIV-5 L/P complex[72].

### 2.2.2 Bacterial expression of viral RdRp

Dr. Dana Kocincova performed the expression and purification of EV-71 and HRV-16 RdRp. The pET-15b (Novagen) plasmid with codon-optimized synthetic DNA sequences (GenScript, Piscataway, NJ, USA) coding for the RdRp of EV-71 and HRV-16 was expressed in *Escherichia coli* BL21 cells.

Table 2.2 RNA Polymerase Expression Strategies

| Polymerase | Accession Number | Expression System | Construct | M.W. (kDa)[a] | Extinction Coefficient ($M^{-1}$ $cm^{-1}$)[a] |
|---|---|---|---|---|---|
| SARS-CoV | AAP33696.1 | BEVS[b] | nsp5-↓[c]nsp7-↓8xHis-nsp8-↓**nsp12**[d]↓ | 161 | 184280 |
| SARS-CoV-2 | QHD43415.1 | | | 161 | 181300 |
| MERS-CoV | YP_009047202.1 | | | 161 | 196770 |
| HRV-16 | AAA69862.1 | *E. coli* | 8xHis-**3D$^{pol}$** | 50 | 61770 |
| EV-71 | BAJ49823.1 | | | 50 | 72770 |
| HCV[e] | CAB46677.1 | BEVS | 8xHis-**NS5B**$^{\Delta 21}$ | 65 | 83770 |
| RSV | P:AAB59853 L:AAA84898 | BEVS | TEV-↓8xHis-P-↓**L**-Strep | 282 | 309880 |
| HMPV | P:AAQ67693 L:AAQ67700 | | | 267 | 277780 |
| HPIV-3 | P:NP_067149.1 L:NP_067153.2 | BEVS | $^{p10}$P-$^{pPH}$**L**-8xHis | 323 | 358920 |
| PIV-5 | P:AFE48445.1 L:AFE48451.1 | | | 298 | 322130 |
| NiV | P:AEZ01385 L:AEZ01390 | BEVS | TEV-↓8xHis-P-↓**L**-Strep | 336 | 317440 |
| EBOV | VP35:AKG65095 L:AKG65102 | BEVS | TEV-8xHis-VP35-↓**L** | 289 | 310100 |
| LASV | AIT17397 | BEVS | Strep-8xHis-**L** | 255 | 243180 |
| CCHFV | AIE16126 | | Strep-8xHis-**L** | 450 | 352500 |
| FluB | PA:AAU94844 PB1:AAU94857 PB2:AAU94870 | BEVS | TEV-↓8xHis-↓PA-↓**PB1**-↓PB2-Strep | 263 | 278810 |
| h-mtRNAP | NP_005026.3 | BEVS | Strep-8xHis-**RNAP** | 137 | 139230 |

[a] Molecular weight and extinction coefficient is an approximation and calculated according to the subunit composition of the replication complex (e.g. coronavirus replication complex accounts for the ratio 1:2:1 of Nsp7:Nsp8:Nsp12 as observed structurally). The protease is not included in the calculation.

[b] Baculovirus expression vector system

[c] Down arrow represents the cleavage site acted on by that constructs respective protease (underlined).

[d] Bolded domains indicate where the RdRp motifs responsible for catalyzing RNA synthesis are contained.

[e] HCV NS5B expression construct coded for residues 2420-3010 minus the 21 C-terminus residues.

### 2.2.3 Purification of RdRp and RdRp complexes

All RdRp and RdRp complexes in this thesis, except FluB heterotrimeric complex, were purified using the Ni-NTA affinity-chromatography based on their respective eight-histidine tag according to the manufacturer's specifications (Thermo Scientific, Rockford, IL, USA). Enzymes underwent the same general purification scheme; however, different buffers were employed according to "Cytosolic" or "Total" lysis (Table 2.3). Insect cell or *E. coli* pellets resuspended in lysis buffer were subjected to homogenization or sonication, respectively. For "Cytosolic" lysis, pellets from 1L culture were centrifuged at 1000 x g for 25 minutes at 4˚C, supernatant was removed, solid NaCl was added to 1000 mM and centrifuged again at 30000 x g for 15 minutes at 4˚C. Conversely, "Total" lysis underwent a single centrifugation step, 30000 x g for 30 minutes at 4˚C. The resulting supernatant was aliquoted on two or four 0.5 mL Ni-NTA columns and allowed to rotate for 1 hour at 4˚C. The columns were subsequently washed with 30 to 40 column volumes (CV) of a wash buffer (Table 2.3). Proteins were sequentially eluted at increasing imidazole concentrations (50, 100, 200, and 400 mM).

FluB heterotrimeric complex was purified as previously described[80] using strep-tag affinity chromatography according to the manufacturer's specifications (IBA, Goettingen, Germany). Following "Cytosolic" lysis, the supernatant was treated with 1000 mM NaCl and ~0.6% (w/v) polyethyleneimine (PEI) before undergoing the second centrifugation step at 30000 x g for 15 minutes at 4˚C. The resulting supernatant was aliquoted on two 0.5 mL strep-tactin matrix columns, and bound proteins were eluted using a desthiobiotin-containing proprietary solution to the Elution buffer (Table 2.3).

Protein purity and composition was examined by SDS-PAGE migration followed by staining with Coomassie brilliant blue G-250. Purified protein preparations for immediate use were adjusted with glycerol to 40% and stored at -20˚C. For long-term storage, purified protein preparations remained in 10% glycerol and stored at -80˚C. Protein concentration was determined by measuring absorbance at 280 nm using their respective extinction coefficients. The identity of all purified enzymes was confirmed by mass spectrometry analysis (Dr. Jack Moore, Alberta Proteomics and Mass Spectrometry, Edmonton, Canada).

Table 2.3 Purification buffers

| Reagent | Cytosolic | Total | Wash | Elution[a] |
|---|---|---|---|---|
| Tris-HCl (pH 8.0), mM | 100 | 100 | 100 | 100 |
| KCl, mM | 100 | - | - | - |
| NaCl, mM | 1000[b] | 1000 | 1000 | 150 |
| TCEP | 5 | 5 | 5 | 5 |
| Tween-20, % | 0.1 | 1 | 0.01 | 0.01 |
| Glycerol, % | 10 | 10 | 10 | 10 |
| Sucrose, mM | 250 | - | - | - |
| Imidazole, mM | 25 | 25 | 25 | 50 to 400[c] |
| Protease Inhibitor[d] | 1 | 1 | - | - |

[a] For strep-tag affinity chromatography, a desthiobiotin-containing solution was added to an elution buffer free of NaCl and imidazole before eluting protein.
[b] Solid NaCl (1000 mM final concentration) was added to the collected supernatant following the initial centrifugation at 1000 x g at 4°C.
[c] For Ni-NTA affinity-chromatography, different elution buffers were prepared containing 50, 100, 200, and 400 mM imidazole.
[d] cOmplete™ ULTRA EDTA Free Protease Inhibitor tablet (Roche, Cat: 05892791001).

### 2.2.4 RdRp and RdRp complex mutants

For each RdRp and RdRp complex, active-site mutants were expressed and purified as described above. In this case, the metal-coordinating aspartate residues required for catalysis were mutated to asparagine. Abrogation of RNA synthesis by these enzymes confirms that RNA synthesis activity mediated by the wild-type RdRp or RdRp complex is due to the catalytic active site. SARS-CoV-2 nsp12 mutants (S861A, S861G, S861P, and V557L) investigated in Chapter 5 were expressed and purified as described above.

## 2.3 RNA synthesis assays

The synthetic 5′-monophosphorylated RNA oligonucleotide templates used in this thesis are outlined in Table 2.4 **(**the portion of the template which is complimentary to the 4-nt primer is underlined). All RNA oligonucleotide templates were designed such that the radiolabeled nucleotide was incorporated immediately following the 4-nt primer at position 5 (opposite the bolded templating nucleotide) thereby labelling RNA synthesis products at a single nucleotide

resolution. The reaction mixture for RNA synthesis assay (final concentrations after mixing), contained the purified viral RdRp, Tris–HCl (pH 8, 25 mM), RNA primer (200 μM), RNA template (2 μM, except for FluB RdRp reactions where optimal RNA template concentration was 0.5 μM), [α-$^{32}$P]-NTP (0.1 μM), and various nucleotide concentrations were prepared on ice and incubated at 30°C for 5 to 10 minutes. RNA synthesis was initiated by the addition of 5 mM $MgCl_2$, except for SARS-CoV-2 and MERS-CoV RdRp, which required 1.25 mM $MgCl_2$. The duration of reactions varied between 10 and 30 minutes. All reactions were stopped by the addition of equal volume formamide/EDTA (50mM). The reaction products were incubated at 95°C for 5 minutes and then resolved by 20% UREA-PAGE, and the [α-$^{32}$P] generated signal was stored and scanned using Typhoon phosphorimager (Cytiva, Vancouver, BC, Canada). The data were analyzed using GraphPad Prism 7.0 to determine the Michaelis-Menten constants $V_{max}$ and $K_m$, standard deviation, and standard error associated with the fit (GraphPad Software, Inc; San Diego, CA, USA). Standard deviation quantifies the variability within a sample, standard error associated with the fit represents the variability of data points around the line-of-best-fit. Percent error was calculated by dividing the standard deviation by the square root of the number of values in the dataset.

Table 2.4 Synthetic 5′-monophosphorylated RNA oligos and RNA synthesis assays.

| Template | Chapter | Assay |
|---|---|---|
| 3′ UGCG**C**UUGUUUAUUp ′5 | 3 / 4 | Pattern of inhibition |
| 3′ UGCG**C**UAGAAAAAAp ′5 | 3 / 4 / 5 / 7 / 8 | Single Nucleotide Incorporation<br>Pattern of inhibition |
| | 3 | Competition (full-length product) |
| | 6 | Single Nucleotide Incorporation |
| | 8 | Competition (Incorporation)<br>Nucleotide Incorporation “i+1” |
| 3′ UGCG**C**UAGAGAGAGAGAGAGAGAGAGp ′5 | 4 | Pattern of inhibition |
| 3′ UGCG**C**GUAAAAAAAp ′5 | 4 | Single Nucleotide Incorporation |
| | 6 | Pattern of Inhibition |
| 3′ UGCG**G**UACUUUAUUp ′5 | 4 | Single Nucleotide Incorporation |
| 3′ UGCG**G**AUCUUUAUUp ′5 | 4 / 6 | Single Nucleotide Incorporation |
| 3′ UGCG**C**UUGUUUUUUUUUUUUUUUUp ′5 | 4 | Competition (full-length product) |
| 3′ UGCG**C**AGAUAAAAAAAAp ′5 | 5 | Pattern of Inhibition |
| 3′ UGCG**C**GUUUUUUUUp ′5 | 6 | Single Nucleotide Incorporation |
| 3′ UGCG**C**UUUUUUUUUp ′5 | 6 | |
| 3′ UGCG**A**CUUUUUUUUp ′5 | 6 | |
| 3′ UGCG**C**UUGUUUUUUUUUUUUUUUUp ′5 | 4 / 5 | Competition (full-length product) |
| 3′ UGCG**C**UAGAGAGAGAGAGAGAGAGAGp ′5 | 4 | Pattern of Inhibition |
| 3′ UGCG**C**UAGUUUUUUUUUUUUUUUUp ′5 | 6 | Competition (full-length product) |
| 3′ UGCG**C**UAGUUUAUUp ′5 | 7 / 8 | Single Nucleotide Incorporation<br>Pattern of Inhibition |
| 3′ UGCG**C**UUUUUAUUGUUGUUUp ′5[a] | 5 / 7 | Template-dependent Inhibition |
| 3′ UGCG**C**UUUUURUUGUUGUUUp ′5[a] | 5 / 7 | |
| 3′ UGAG**G**UUUUUCUUGUUGUUUp ′5[a] | 6 | |
| 3′ UGAG**G**UUUUUNUUGUUGUUUp ′5[a] | 6 | |
| 3′ UGCG**C**UUUUURAAAAAAAAAp ′5 | 8 | |
| 3′ UGCG**C**UUUUUG$_{646}$AAAAAAAAAp ′5 | 8 | |
| 3′ TGCG**C**TAGTTT[b] | 8 | Single Nucleotide Incorporation |

[a] Template was enzymatically synthesized by T7 DNA-dependent RNA polymerase, protocol described in section 2.3.4.

[b] DNA template used to monitor single nucleotide incorporation by h-mtRNAP.

### 2.3.1 Single nucleotide incorporation assay

The concentrations of various viral RdRp proteins and protein complexes were selected such that incorporation of [α-$^{32}$P]-NTP was linear. The range of NTP and NTP analog concentrations used to determine selectivity values were optimized so minimal misincorporations at subsequent positions were observed.

Data from single nucleotide incorporation assays were used to determine the preference for the natural nucleotide over the nucleotide analog. The selectivity value is calculated as a ratio of the incorporation efficiencies of the natural nucleotide over the nucleotide analogue. The efficiency of nucleotide incorporation is determined by the ratio of Michaelis–Menten constants $V_{max}$ over $K_m$. The substrate for nucleotide incorporation is a 5-nt primer generated by the incorporation of [α-$^{32}$P]-NTP into a 4-nt primer. The formation of the 5-nt primer is linear at a given time point; however, its precise concentration is unknown. Hence, the product generated in the reaction is measured by quantifying the signal corresponding to the 6-nt primer product and dividing it by the total signal in the reaction (5-nt primer and 6-nt primer). This defines the product fraction. The product fraction is commonly multiplied by the total substrate concentration to determine the molar units of the $V_{max}$, which is here not possible as explained above. Therefore, the unit of $V_{max}$ is reported as product fraction over time. The selectivity value is unitless as it is the ratio of two $V_{max}/K_m$ measurements with the same units.

### 2.3.2 Nucleotide incorporation at "i+1" assay

Like single nucleotide incorporation, inhibition at position "i+1" was determined by quantifying the signal corresponding to the 7-nt primer product and dividing it by the total signal in the lane (5-nt primer, 6-nt primer, and 7-nt primer). 5-nt, 6-nt, and 7-nt primer correspond to [α-$^{32}$P]-GTP, ATP or ATP-analog, and UTP incorporation, respectively.

### 2.3.3 RdRp-catalyzed RNA extension assays

For reactions involving primer- or template-embedded nucleotide analogs, viral enzyme concentrations were optimized to promote full-length product RNA synthesis. For pattern of inhibition experiments, the nucleotide analog and its natural counterpart provided to support incorporation at position 6 ("i") were investigated in parallel. The next nucleotides required to

synthesize full-template length product were supplemented to the reaction at increasing concentrations. Direct competition between a nucleotide analog and its natural counterpart was investigated at the level of full-length product synthesized or at the level of single nucleotide incorporation. The former was monitored at constant concentration [α-$^{32}$P]-GTP, ATP, CTP, and UTP and increasing RDV-TP concentration. Competitive single nucleotide incorporation required a constant concentration of ATP or RDV-TP and increasing concentrations of GS-646939. Template-dependent inhibition was investigated by first enzymatically synthesizing an RNA template containing the embedded analog (described below). RNA synthesis was then monitored opposite an embedded analog.

### 2.3.4 Production of a model RNA template with an embedded RDV or NHC residue

Our initial tests revealed that T7 RNA polymerase (Thermo Scientific, Rockford, IL, USA) readily accepted short RNA/DNA primer/templates for RNA synthesis and was capable of incorporating RDV-TP or NHC-TP at high concentrations of 100 μM followed by a full template-length RNA synthesis. The following DNA template (Dharmacon, Lafayette, CO, USA) was used as the starting material: 3′-AAACAACAA**T**AAAAAGCGCA-5′ or 3′-AAACAACAA**G**AAAAACCTCA-5′ to generate an RDV or NHC embedded RNA template, respectively. The underlined portion indicates the region which is complementary to the 5′-monoposphorylated RNA primer: 5′-pUUUGUUGUU. The template residue "**T**" and "**G**" indicate the site of the RDV-TP and NHC-TP incorporation into the RNA primer, respectively. Therefore, the fully extended primer will contain an embedded remdesivir (**R**) or NHC (**N**) and may serve as a 20-nt RNA template for the RNA synthesis by the RdRp: 5′-pUUUGUUGUU**R**UUUUUCGCGU-3′ and 5′-pUUUGUUGUU**N**UUUUUGGAGU-3′, where underlined portion is complementary to the RNA primer 5′-pACGC or 5′-pACUC, respectively. Note that this RNA primer can only anneal to a fully synthesized 20-nt RNA template. The T7 RNA polymerase reaction mixtures contained 30 units of the polymerase, 200 μM RNA primer, 100 μM DNA template, and 100 μM NTP mixture in a 25 mM Tris-HCl buffer (pH 8). Reactions were started with 5 mM $MgCl_2$, incubated at 37°C for 90 min, boiled for 10 min, and incubated with 2 units of TURBO™ DNase (Thermo Fisher Scientific) at 37°C for 30 min. TURBO™ DNase is a recombinantly engineered endonuclease with increased affinity for DNA to improve removal of DNA contaminants compared to wildtype DNase I. The reaction mixtures were then

extracted with phenol/chlorophorm (premixed with isoamyl alcohol 25:24:1; BioShop, Burlington, ON, Canada) and buffer-exchanged consecutively three times using the size-exclusion chromatography Bio-Rad p6 spin columns (Bio-Rad Laboratories).

## Chapter 3: The antiviral compound remdesivir potently inhibits RNA-dependent RNA polymerase from Middle East respiratory syndrome coronavirus

This chapter contains content from the following source, republished with permission:

- Gordon CJ[#], Tchesnokov EP[#], Feng JY, Porter DP, Götte M. The antiviral compound remdesivir potently inhibits RNA-dependent RNA polymerase from Middle East respiratory syndrome coronavirus. J Biol Chem. 2020; 295:4773-4779. © the authors.

Author Contributions

C. J. G., E. P. T., and M. G. formal analysis; C. J. G., E. P. T., and M. G. investigation; C. J. G., E. P. T., and M. G. methodology; E. P. T. and M. G. data curation; E. P. T. software; E. P. T. and M. G. validation; E. P. T. and M. G. visualization; E. P. T., J. Y. F., D.P.P., and M. G. writing-review and editing; M. G. conceptualization; M. G. resources; M. G. supervision; M. G. funding acquisition; M. G. writing-original draft; M. G. project administration.

[#]Authors contributed equally to this work.

*Experiments performed by other authors have been identified in figure legends.

Funding

This study was supported by Canadian Institutes of Health Research Grant 159507 (to M.G.) and a grant from the Alberta Ministry of Economic Development, Trade and Tourism by the Major Innovation Fund Program for the AMR–One Health Consortium (to M.G.). M.G. has previously received funding from Gilead Sciences in support for the study of EBOV RdRp inhibition by RDV.

## 3.1 Introduction

The emergence of a novel coronavirus, named severe acute respiratory syndrome coronavirus 2 (SARS-CoV-2, formerly 2019-nCoV), initiated a global effort to identify effective treatments focusing on agents with demonstrated antiviral activity against SARS-CoV, Middle East respiratory syndrome (MERS-CoV) or related positive-sense RNA viruses. Although currently there are no approved antiviral drugs for the treatment of human coronavirus infections available, preclinical data with the nucleotide analogue remdesivir (RDV) are promising, and human safety data are available[254]. This compound shows a broad spectrum of antiviral activities against several RNA viruses[241, 257, 333], including SARS-CoV and MERS-CoV [251]. RDV was originally developed for the treatment of Ebola virus disease (EVD)[241]. Cell-culture and animal studies revealed potent antiviral activities against filoviruses, including the Ebola virus (EBOV)[333]. Subsequent studies have shown that RDV is also active against coronaviruses with divergent RNA-dependent RNA polymerases (RdRps)[251, 334]. However, biochemical data that support these findings and provide a possible mechanism of action are not available.

The triphosphate form of RDV (RDV-TP) was shown to inhibit the RdRp of respiratory syncytial virus[333], Nipah virus and EBOV[267, 335], which are all nonsegmented negative-sense RNA viruses. Active Ebola RdRp contains the viral L protein in complex with viral protein 35[336, 337]. Viral protein 35 is the functional counterpart of the P protein of respiratory syncytial virus and Nipah[335, 338, 339]. Previously, we generated recombinant Ebola RdRp for the study of nucleotide analogue inhibitors[267]. Enzyme kinetics show that RDV-TP is able to compete with its natural counterpart ATP for incorporation. The selectivity of ATP over the inhibitor is ~ 4-fold. Once incorporated at position i, the compound causes inhibition of RNA synthesis predominantly at position i+5. Delayed chain termination is therefore a plausible mechanism of action.

Progress has also been made in characterizing the SARS-CoV RdRp complex[340-342]. Biochemical data suggest that the active complex is composed of at least three viral non-structural proteins nsp7, nsp8 and nsp12. The RNA polymerase nsp12 alone displays low processivity. Synthesis of longer reaction products require the additional presence of nsp7 and nsp8. Although a heterotrimer was not stable, nsp7 and nsp8 can be linked together to form a complex with nsp12[342]. Here we developed a novel expression system for the MERS-CoV RdRp complex and

studied the mechanism of action of remdesivir. Co-expression of the MERS nsp5 protease with nsp7, nsp8 and nsp12 in insect cells yielded a stable complex composed of nsp8 and nsp12. We demonstrate that this complex is active on model primer/template substrates that adequately mimic the elongation state. Most importantly, selectivity measurements determined here under the inherent limitations of the steady-state conditions revealed that incorporation of the inhibitor is more efficient than its natural counterpart, and delayed chain termination is observed at position i+3.

## 3.2 Results

### 3.2.1 Expression of MERS-CoV RdRp complex

The Baculovirus expression system has recently been used to produce recombinant nsp12 from SARS-CoV[340]. For SARS-CoV, an active RdRp complex was reconstituted with purified nsp7 and nsp8, with and without a linker, expressed in Escherichia coli[340, 342]. Here, we employed an alternative approach whereby MERS nsp5, nsp7, nsp8 and nsp12 were co-expressed in insect cells as a part a polyprotein (NCBI: YP_009047202.1). The polyprotein was post-translationally cleaved by the nsp5 protease at its original cleavage sites (Fig. 3.1*A*). We also expressed a MERS-CoV RdRp complex in which the catalytic residues within the conserved motif C (SDD) of nsp12 were mutated (SNN) to generate an inactive RdRp (Fig. 3.1*B*)[343]. Nickel-nitrilotriacetic acid affinity chromatography via the N-terminal eight-histidine tag of the nsp8 protein resulted in a MERS-CoV RdRp complex containing nsp8 (~23 kDa) and nsp12 (~110 kDa) (Fig. 3.1*C*). Mass spectroscopy confirmed the presence of nsp8 and nsp12, while there was no evidence for the presence of nsp7.

The WT MERS-CoV RdRp complex was tested for RNA synthesis on short model primer/template substrates mimicking a random elongation complex during RNA synthesis. We recently used the same model substrates for the study of other RdRp enzymes (Fig. 3.1*D*)[267, 337]. The 4nt-primer/14-mer templates are designed such that [α-$^{32}$P]GTP is the first incorporated nucleotide, which labels the RNA products. Reactions containing the MERS-CoV RdRp complex, primer/template and various combinations of NTPs were initiated by the addition of $Mg^{2+}$ ions. In the presence [α-$^{32}$P]GTP alone the expected 5-mer product is formed. Addition of specific combinations of NTPs generated defined reaction products: [α-$^{32}$P]GTP and ATP yielded a 7-mer

(Fig. 3.1*D*, *left side of the gel*) or a 6-mer product (Fig. 3.1*D*, *right side of the gel*), depending on the template sequence. Similarly, in the presence of [α-$^{32}$P]GTP, ATP and CTP (or UTP) the 4-mer primer is extended to yield an 11-mer or a 7-mer depending on the template sequence. Addition of all four NTPs resulted in a 14-mer full-length product. Reactions with the SNN mutant enzyme did not show RNA product formation. The lane [α-$^{32}$P]GTP only illustrates the background signal associated with the [α-$^{32}$P]GTP preparation in the absence of enzyme. This data confirms that MERS-CoV nsp12 exhibits the observed RdRp activity. It has recently reported that SARS-CoV nsp8 displays RNA primase activity that yields short (~ 6-mer) reaction products[342, 344]. However, structural data are inconsistent with the formation of a primase active site in SARS-CoV nsp8[340], and our data do not provide any evidence for primase activity in MERS-CoV nsp8.

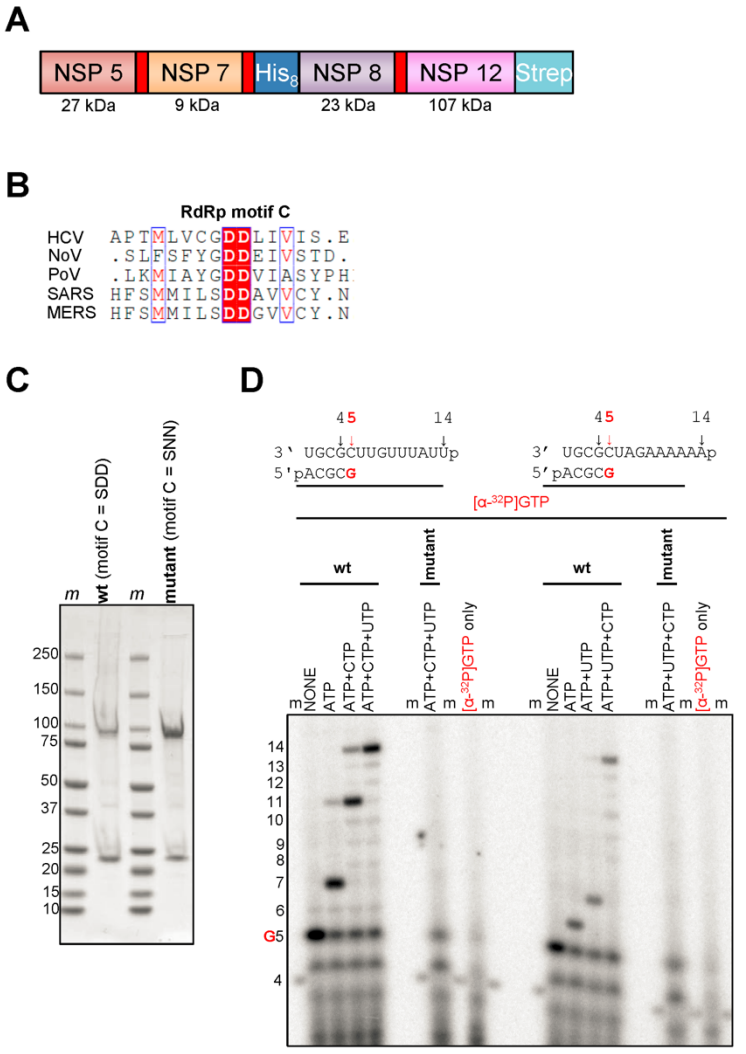


**Figure 3.1. Expression, purification and characterization of the MERS RdRp complex**. ***A***, The construct contains non-structural proteins nsp5, nsp7, nsp8 and nsp12. Red rectangles indicate original nsp5 protease cleavage sites. $His_8$ and Strep indicate the location of histidine- and strep-tags, respectively. ***B***, A snapshot of a sequence alignment (T-Coffee) of representative RdRp enzymes from positive-sense RNA genome viruses illustrating sequence conservation within RdRp motif C. ***C***, SDS PAGE migration pattern of the purified enzyme preparations stained with Coomassie Brilliant Blue G-250 dye. Proteins migrating at ~100 and ~25 kDa contain nsp12 and nsp8, respectively. *D*, RNA synthesis on a short model primer/template substrate. Template and primer were both phosphorylated (p) at their 5'-ends. G indicates incorporation of the radiolabeled nucleotide opposite template position 5. RNA synthesis was monitored with the purified MERS RdRp complex wt (motif C = SDD) and active site mutant (motif C = SNN) in the presence of NTP combinations designed to generate specific products. Lane m illustrates the migration pattern of the radiolabeled 4 nucleotide-long primer.

*EPT contributed panel **B** to this figure.

### 3.2.2 Inhibition of EBOV RdRp and MERS-CoV RdRp with RDV

For EBOV RdRp, it has been challenging to identify a sequence with a single site of incorporation for the RDV. Hence, we devised two different RNA templates that allow multiple and single incorporations (Fig. 3.2*A*). These sequences were used to compare the inhibitory effects of RDV on EBOV RdRp and MERS RdRp. For EBOV RdRp, we observed delayed chain-termination at position i+5 as previously described (Fig. 3.2*B*)[267]. However, the template that provides a single site of RDV-TP incorporation also shows reductions in full-length RNA synthesis. In contrast, the MERS RdRp complex yields the full-length RNA product with both sequences. The inhibition patterns with RDV-TP differ markedly from our results with EBOV RdRp. RNA synthesis is arrested at positions i+3 and i+4 with a template that provides multiple sites of incorporation of the inhibitor, and the full-length product is only seen as a faint band. The template that allows only a single incorporation event yields RNA synthesis arrest at position i+3 and an increased amount of the full-length product. Hence, the mechanism of inhibition is likely delayed chain-termination for both EBOV RdRp and MERS RdRp although the specific patterns show subtle differences. In the absence of inhibitor, RNA synthesis and full-length product formation is generally more efficient with MERS-CoV RdRp. This could also help to explain that a small amount of full-length product is still seen with this enzyme in the presence of inhibitor.

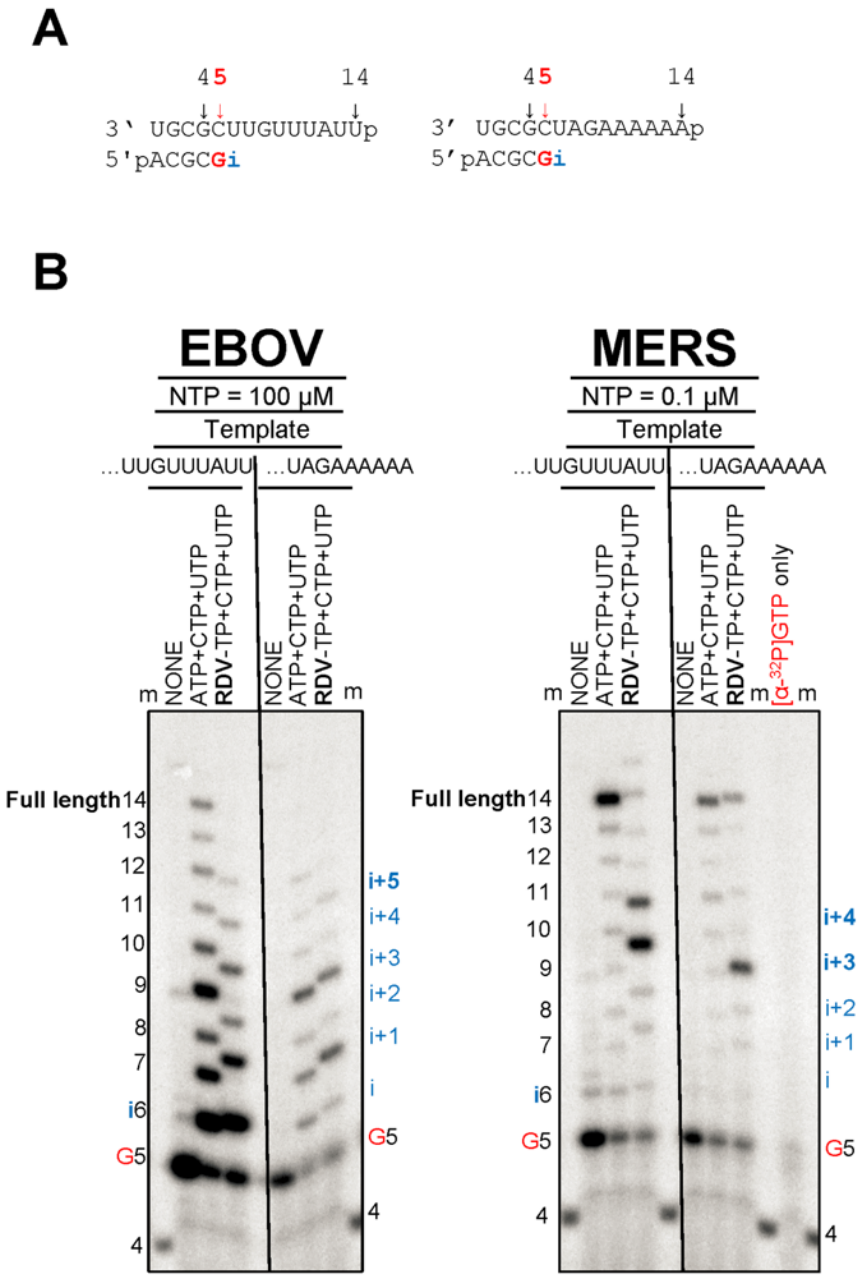


**Figure 3.2. Patterns of inhibition of RNA synthesis with remdesivir-TP (RDV-TP).** ***A***, RNA primer/template substrates used to test multiple (left) or single (right) incorporations of RDV-TP. G indicates incorporation of the radiolabeled nucleotide opposite template position 5. i indicates incorporation site for the first (left) or the only (right) RDV-TP. Full length indicates the full-template length products of RNA synthesis. ***B***, RDV-TP incorporation was monitored with purified EBOV and MERS RdRp complexes in the presence of indicated combinations of NTPs and RDV-TP.

*EPT contributed the EBOV RdRp data in panel **B** of this figure.

### 3.2.3 Competitive inhibition of RNA synthesis by RDV-TP

To study whether RDV-TP is able to compete with its natural counterpart ATP, we monitored RNA synthesis at a fixed concentration of NTPs (0.02 μM) and increasing concentrations of RDV-TP (Fig. 3.3*A*, *top panel*). Increasing concentrations of RDV-TP caused a reduction of the 14-mer product caused by increases in RNA synthesis arrest at position i+3. Formation of the full-length 14-mer product is not evident at RDV-TP concentrations higher than 0.041 μM. Quantification of the data revealed an $IC_{50}$ for RDV-TP of 0.032 μM under these conditions (Fig. 3.3*B*). This value is only 1.5-fold higher than the ATP concentration, which points to an efficient use of the inhibitor. Increasing concentrations of ATP caused a corresponding increase in $IC_{50}$ values for RDV-TP (Fig. 3.3*C*), which shows that RDV-TP is a competitive inhibitor.

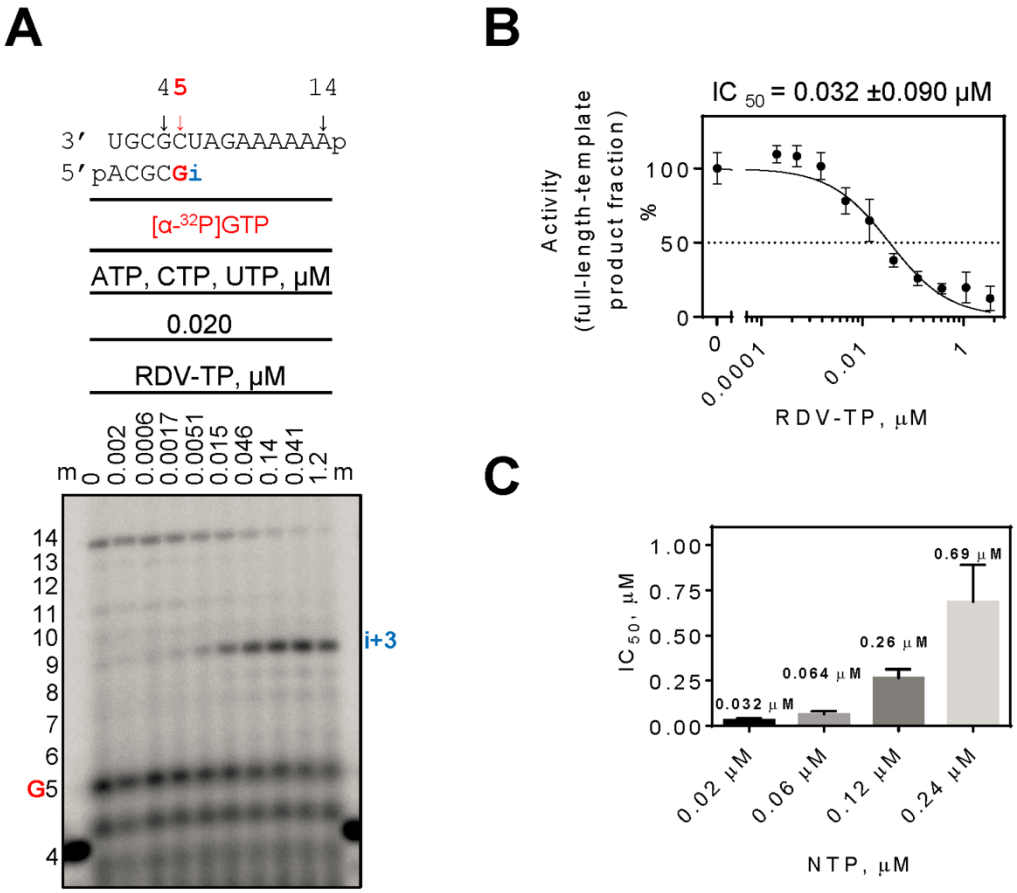


**Figure 3.3. Competition between RDV-TP and ATP**. ***A***, The RNA primer/template substrate used in this assay is shown above the gel. G indicates incorporation of the radiolabeled nucleotide opposite template position 5. Position i allows incorporation of ATP or RDV-TP. RNA synthesis was monitored with purified MERS RdRp complex in the presence of 0.02 μM ATP, CTP and UTP mix and increasing concentrations of RDV-TP as indicated. ***B***, Graphic representation and $IC_{50}$ determination fitting of quantified data from panel A. Error bars represent standard deviation of the data within four independent experiments. ***C***, Graphic representation of the relationship between $IC_{50}$ values for RDV-TP measured at different NTP concentrations. Average $IC_{50}$ values for RDV-TP are shown above the corresponding bars. Error bars represent standard deviation of the data within at least three independent experiments.

### 3.2.4 Selectivity measurements of ATP-analogs

To translate our previous findings into quantitative terms, we determined Michaelis-Menten parameters $V_{max}$ and $K_m$ and calculated the efficiency $V_{max}/K_m$ of nucleotide incorporation for ATP, RDV-TP, and two other nucleotide analogue inhibitors for comparative purpose: ara-ATP and 2′CM-ATP (Fig. 3.4). ATP, or the ATP analogue, was added at increasing concentrations

and the reactions were stopped after 20 min following the addition of $Mg^{2+}$. This approach allowed us to determine the selectivity for nucleotide incorporation, defined as $V_{max}/K_m$ (ATP) over $V_{max}/K_m$ (nucleotide analogue) (Table 3.1). The observed differences in the efficiency of nucleotide analogue substrate utilization are driven solely by differences in the respective $K_m$ values. The data show an unexpectedly low selectivity value for RDV-TP (0.35-fold), whereas ara-ATP (749-fold) and 2′CM-ATP (165-fold) are both associated with high selectivity values. The selectivity value for RDV-TP below 1 suggests that incorporation of the inhibitor is more efficient as compared to the natural substrate. Commonly, the nucleotide analogue is less efficiently incorporated, as seen with ara-ATP and 2′CM-ATP.

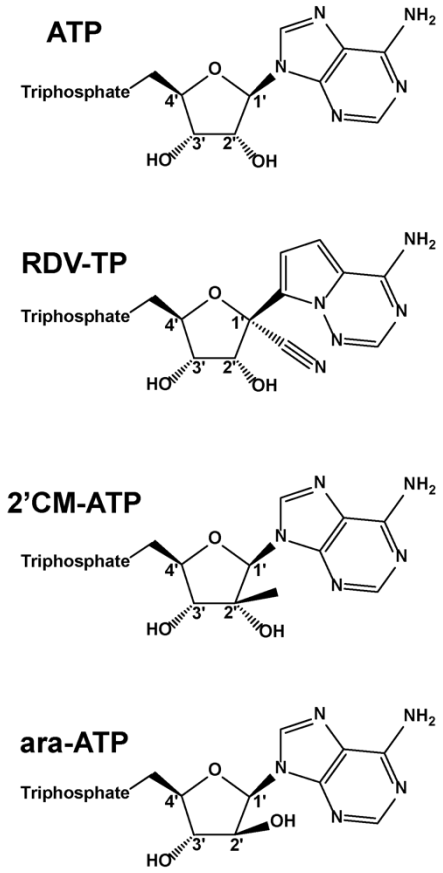


**Figure 3.4. Chemical structures of ATP and ATP-analogs.**

Table 3.1 MERS RdRp complex selectivity values for ATP analogs.

| | ATP | RDV-TP | ara-ATP | 2′CM-ATP |
|---|---|---|---|---|
| | n = 7 | n = 6 | n = 5 | n = 5 |
| $V_{max}$[a] (product fraction) | 0.47[b] | 0.50 | 0.48 | 0.47 |
| ± | 0.011[c] | 0.012 | 0.019 | 0.021 |
| % error[d] | 2 | 2 | 4 | 4 |
| $K_m$[e] (μM) | 0.017 | 0.0063 | 13 | 2.8 |
| ± | 0.0019 | 0.00069 | 1.7 | 0.53 |
| % error | 11 | 11 | 13 | 19 |
| $V_{max}/K_m$ | 28 | 79 | 0.037 | 0.17 |
| **Selectivity[f] (fold)** | **1[g]** | **0.35** | **749** | **165** |

[a] $V_{max}$ is a Michaelis–Menten parameter reflecting the maximal velocity of nucleotide incorporation.
[b] All reported values have been calculated on the basis of a 9-data point experiment repeated indicated number of times (n).
[c] Standard error associated with the fit.
[d] Percent error.
[e] $K_m$ is a Michaelis–Menten parameter reflecting the concentration of the nucleotide substrate at which the velocity of nucleotide incorporation is half of $V_{max}$.
[f] Selectivity of a viral RNA polymerase for a nucleotide substrate analogue is calculated as the ratio of the $V_{max}/K_m$ values for NTP and NTP analogue, respectively.
[g] Reference.

### 3.3 Discussion

Broad spectrum antivirals or compounds with demonstrated activity against SARS-CoV or MERS-CoV are now considered for the treatment of infection caused by the novel coronavirus SARS-CoV-2. The nucleotide analog RDV has been tested in a randomized, controlled trial for Ebola virus disease[345]. Although two other investigational therapies were more efficacious than RDV, an antiviral effect has been demonstrated. This compound also shows a broad spectrum of antiviral activities against coronaviruses *in vitro* and in animal models[253, 254, 334, 346]. Moreover, screening of a compound library of Food and Drug Administration-approved drugs revealed that the human immunodeficiency virus type 1 (HIV-1) protease inhibitor lopinavir is active against MERS-CoV[347]. This drug is currently tested in a clinical trial for the treatment of MERS-CoV in combination with interferon-β and ritonavir[348], which is used for pharmacological boosting. A recent study compared the efficacy of the combination of lopinavir/ritonavir/interferon-β with

RDV in cell culture and showed that RDV was significantly more active against MERS-CoV[254]. Here we focused on the biochemical evaluation of RDV to provide a better understanding of its broad spectrum of antiviral activities and the underlying mechanism of action.

*In vitro* selection experiments with the coronavirus model murine hepatitis virus (MHV)[251] resulted in two variants with resistance-conferring mutations in nsp12. This data provides strong evidence to show that RdRp is the target for RDV. Our biochemical data corroborate that the RNA polymerase of MERS-CoV is indeed the drug target. We demonstrate that MERS nsp8 and nsp12 form an active, binary complex. RDV-TP is utilized as a substrate and competes with its natural counterpart ATP. Natural nucleotide pools are commonly more efficiently incorporated when compared with nucleotide analogs. However, in this case, we observe that incorporation of the nucleotide analogue is significantly more efficient.

Once added into the growing RNA chain, the inhibitor does not cause immediate chain-termination. The presence of the 3′-hydroxyl group allows the addition of three more nucleotides until RNA synthesis is arrested at position i+3. A fraction of the extended primer overcomes this arrest, which can lead to full-length product formation. Full-length product formation is considerably reduced when the inhibitor is added at consecutive sites. The efficient rate of RDV-TP incorporation may translate in multiple incorporation events *in vivo*, and this could add to the overall potency of the drug. It is important to note that other parameters including the intracellular concentration of the triphosphate form of the inhibitor need to be considered as well.

The different inhibition patterns observed with EBOV RdRp and MERS-CoV RdRp point to subtle differences in the mechanism of action. Delayed chain termination could be based on inhibitor-induced structural changes of the newly synthesized double-stranded RNA that at some point prevent a productive alignment of primer and incoming nucleotide, e.g. through primer/template repositioning[268], or backtracking mechanisms[164]. Enzyme-specific interactions with the extended primer may likewise affect the continued extension of the primer, which helps to explain variations in the site of RNA synthesis arrest.

An open question that warrants further investigation is the role of the 3′-5′ exonuclease (nsp14) in susceptibility to RDV. It has previously been reported that nucleotide analogue inhibitors can be excised by the viral exonuclease[341]. A murine hepatitis virus mutant lacking the 3′-5′ exonuclease activity was shown to be more sensitive to RDV[251]. However, given its high potency in cell-based assays, RDV seems to be protected from excision at least to a certain degree. This protection could be provided by the additional three nucleotide following the inhibitor. In contrast, classic chain terminators would be readily accessible for excision. Taken together, this study provides a likely mechanism of action for RDV against coronaviruses. The novel strategy for the expression of MERS-CoV RdRp helps to guide the design of equivalent constructs of related viruses, including SARS-CoV-2.

## Chapter 4: Remdesivir is a direct-acting antiviral that inhibits RNA-dependent RNA polymerase from severe acute respiratory syndrome coronavirus 2 with high potency

This chapter contains content from the following source, republished with permission:

- Gordon CJ[#], Tchesnokov EP[#], Woolner E, Perry JK, Feng JY, Porter DP, Götte M. Remdesivir is a direct-acting antiviral that inhibits RNA-dependent RNA polymerase from severe acute respiratory syndrome coronavirus 2 with high potency. J Biol Chem. 2020; 295:6785-6797. © the authors.

Author contributions

C. J. G., E. P. T., and M. G. data curation; C. J. G., E. P. T., J. K. P., and M. G. software; C. J. G., E. P. T., and M. G. formal analysis; C. J. G., E. P. T., and M. G. validation; C. J. G., E. P. T., E. W., J. K. P., and M. G. investigation; C. J. G., E. P.T., and M. G. visualization; C. J. G., E. P. T., E. W., J. K. P., and M. G. methodology; E. P. T. and M. G. conceptualization; E. P. T. and M. G. writing-original draft; E. P. T., J. K. P., J. Y. F., D. P. P., and M. G. writing-review and editing; M. G. resources; M. G. supervision; M. G. funding acquisition; M. G. project administration.

[#] These authors contributed equally to this work.

* Experiments performed by other authors have been identified in figure legends.

Funding

This study was supported by Canadian Institutes of Health Research (CIHR) Grant 170343, Gilead Sciences, and the Alberta Ministry of Economic Development, Trade, and Tourism Major Innovation Fund Program for the AMR–One Health Consortium (to M. G.). M. G. has previously received funding from Gilead Sciences in support of the study of EBOV RdRp inhibition by RDV.

## 4.1 Introduction

Severe acute respiratory syndrome coronavirus 2 (SARS-CoV-2) is a positive-sense RNA virus and the causative agent of coronavirus disease 2019 (COVID-19)[3, 349]. The initial outbreak in December 2019 in Wuhan, China, was declared a pandemic by the World Health Organization on March 10, 2020[350]. Antiviral treatments are urgently needed to relieve the burden on healthcare systems worldwide. Effective therapeutics are expected to reduce mortality and hospitalizations. In the absence of a vaccine, antiviral therapeutics could also be utilized prophylactically to protect vulnerable populations, including those who are frequently exposed to the virus. Despite the earlier outbreaks of SARS in 2003 and Middle East respiratory syndrome (MERS) in 2012, coronavirus-specific antivirals have yet to advance into clinical trials. At this point, the focus is on compounds with a demonstrated broad spectrum of antiviral activities and on drugs developed for other therapeutic purposes with evidence of acting also against coronaviruses. Several of these compounds are currently being assessed in randomized controlled clinical trials, including remdesivir (RDV, formerly GS-5734)[351].

RDV is a phosphoramidate prodrug of a 1′-cyano-substituted nucleotide analogue[241]. Its triphosphate form (RDV-TP) resembles ATP and is used as a substrate of several viral RNA-dependent RNA polymerase (RdRp) enzymes or complexes[251, 267, 333, 335]. The compound has shown broad-spectrum *in vitro* and *in vivo* antiviral activity against nonsegmented negative-sense RNA viruses of the *Filoviridae* (e.g. Ebola virus (EBOV))[241, 333] and *Paramyxoviridae* (e.g. Nipah virus (NiV)) families[257, 335, 352], as well as *in vitro* activity against viruses in the *Pneumoviridae* (e.g. respiratory syncytial virus (RSV)) family[257]. Antiviral activity against a broad spectrum of coronaviruses including SARS-CoV and MERS-CoV was subsequently demonstrated both *in vitro* and in animal models[251, 253, 254, 334, 346]. No *in vitro* inhibition was reported for several segmented negative-sense RNA viruses of the *Arenaviridae* family (e.g. Lassa virus (LASV)) and the *Bunyavirals* order (formerly the family *Bunyaviridae*, e.g. Crimean Congo Hemorrhagic Fever Virus)[257]. RDV was also recently tested in a randomized controlled trial during the 2019 Ebola outbreak in the Democratic Republic of the Congo[345]. Although two antibody-based treatments showed superior efficacy, mortality in the RDV arm was lower than the overall mortality rate of the outbreak, and human safety data are now available[345]. Inhibition of MERS-CoV replication

and therapeutic efficacy of RDV was also demonstrated in mouse and rhesus macaque models[254, 346].

Progress has been made in elucidating the mechanism of action of RDV-TP. RDV-TP competes with ATP for incorporation by the EBOV RdRp complex composed of the L protein and VP35[267]. Steady-state kinetics reveal that incorporation of ATP is slightly more efficient compared to RDV-TP. In contrast to classic chain terminators, inhibition is not seen immediately following the incorporated RDV-TP, and the existence of a 3′-OH group allows the nucleophilic attack on the next incoming nucleotide. Studies with EBOV RdRp, RSV RdRp, and NiV RdRp have indicated that RNA synthesis is terminated after a few more nucleotide incorporation events [267, 335]. RDV-TP incorporation at position i commonly yields delayed chain-termination between position i+3 and i+5. We have recently expressed and purified an active complex composed of MERS-CoV non-structural proteins nsp8 and nsp12[353]. With the limitations of steady-state kinetic measurements, we showed that incorporation of RDV-TP is more efficient than ATP and delayed chain termination is observed specifically at position i+3. Potential inhibitory effects of RDV-TP on SARS-CoV RdRp or on SARS-CoV-2 RdRp have not been studied. Active SARS-CoV RdRp was shown to form a complex composed of nsp7, nsp8 and nsp12, whereby nsp7 and nsp8 were connected with a linker[342]. Structures of complexes with the three subunits were recently determined using cryo-EM[340].

Here, we expressed SARS-CoV and SARS-CoV-2 RdRp complexes in insect cells and monitored RNA synthesis on short model primer/templates during elongation. We demonstrate that RDV-TP inhibits SARS-CoV RdRp and SARS-CoV-2 RdRp with the same potency and mechanism of action. The ability to efficiently compete with the natural counterpart ATP is a favorable property of RDV-TP. We have tested in the same context several other nucleotide analogs and commonly observe that incorporation of the natural nucleotide is considerably preferred. Favorable selectivity for the RDV-TP over ATP and delayed chain termination at position i+3 are key elements of a refined mechanism of inhibition observed with SARS-CoV, MERS-CoV, and SARS-CoV-2 RdRp complexes.

## 4.2 Results

### 4.2.1 Expression of SARS-CoV and SARS-CoV-2 RdRp complexes

We have recently generated recombinant MERS-CoV RdRp from a bacmid containing nsp5, -7, -8, and -12[353]. Expression of this construct in insect cells resulted in the nsp5-7-8-12 polyprotein processed by the nsp5 protease. Nickel-nitrilotriacetic acid affinity chromatography yielded an active binary nsp8/12 RdRp complex. We therefore expressed SARS-CoV and SARS-CoV-2 RdRp from bacmids containing the equivalent nsp5, -7, -8, and -12 sequences. This approach yielded binary complexes with nsp8 and nsp12, as previously described for MERS-CoV[353]. We also expressed mutant enzymes with amino acid substitutions in the conserved motif C of nsp12 (SDD to SNN) to inactivate the catalytic site (. 4.1*A*). WT and mutant enzymes were tested for RNA synthesis on short model primer/templates mimicking a random elongation complex. Incorporation of a radiolabeled nucleotide allows gel-based detection of reaction products. Whereas WT SARS-CoV and SARS-CoV-2 RdRp complexes were able to synthesize RNA from a 4-mer primer and a 14-mer template, the corresponding active-site mutants showed no template-base-specific nucleotide incorporation (Fig. 4.1*B*). These data confirm that RNA synthesis activity is mediated by nsp12.

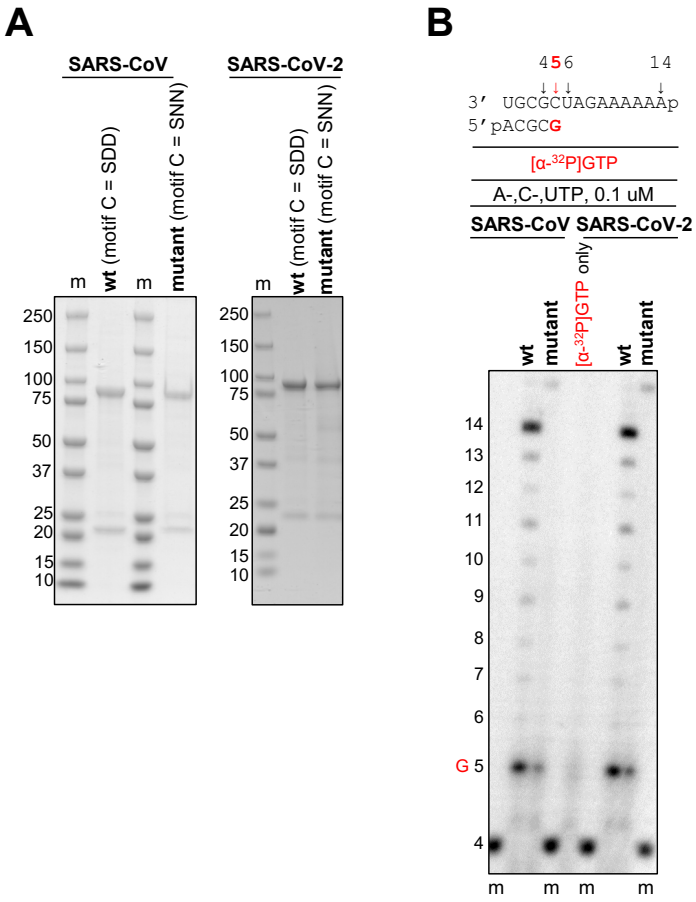


**Figure 4.1. Expression, purification, and characterization of the SARS-CoV and SARS-CoV-2 RdRp complexes.** ***A***, SDS-PAGE migration pattern of the purified enzyme preparations stained with Coomassie Brilliant Blue G-250 dye. Bands migrating at ~100 kDa and ~25 kDa contain nsp12 and nsp8, respectively. ***B***, RNA synthesis on a short model primer/template substrate. Template and primer were both phosphorylated (p) at their 5′-ends. A radiolabeled 4-mer primer serves as a marker (m). G indicates incorporation of the radiolabeled nucleotide opposite template position 5. RNA synthesis was monitored with the purified RdRp complexes representing WT (wt, motif C = SDD) and the active-site mutant (motif C = SNN).

### 4.2.2 Selectivity measurements of RDV-TP with related and distant RdRp enzymes

The ratio of Michaelis-Menten steady-state kinetic parameters $V_{max}/K_m$ for a single incorporation of a natural nucleotide over a nucleotide analogue defines the selectivity. With the limitations of a steady-state approach, a selectivity value lower than 1 suggests the analogue is incorporated more efficiently than the natural NTP. Conversely, a selectivity value higher than 1 suggests the analogue is incorporated less efficiently than the natural NTP. This approach enables comparisons of data with different enzymes and different nucleotide analogs. This approach does not provide distinct information on inhibitor binding, catalysis, or enzyme dissociation from its

nucleic acid substrate. To measure selectivity for RDV-TP incorporation we determined the steady-state kinetic parameters for single nucleotide incorporations in comparison with ATP (Table 4.1, Appendix A, Fig. A1). Previously, we reported a selectivity value of 0.35 for RDV-TP incorporation with MERS-CoV RdRp[353]. SARS-CoV and SARS-CoV-2 also showed low values in a similar range (0.32 and 0.28, respectively). For EBOV, RSV and LASV enzymes we measured higher values (4.0, 2.7, and 20, respectively). Since the RNA template used to measure selectivity in this study differs from the sequence previously used to study inhibition of EBOV and RSV RdRp[267], we repeated these experiments with EBOV and the current RNA template. The observed selectivity value of 4 is in good agreement with our previous measurement of 3.8[267]. LASV RdRp showed the highest selectivity value for RDV-TP of 20-fold, which provides evidence for target specificity. The combined results suggest that the ability of RDV-TP to compete with ATP is most pronounced with the coronavirus RdRp complexes.

Table 4.1. Selectivity values for Remdesivir (RDV-TP) with related and distant RdRp enzymes.

| | **ATP** | | | | **RDV-TP** | | | |
|---|---|---|---|---|---|---|---|---|
| | **$V_{max}$**[a] (product fraction) | **$K_m$**[b] (μM) | **$\frac{V_{max}}{K_m}$** | | **$V_{max}$** (product fraction) | **$K_m$** (μM) | **$\frac{V_{max}}{K_m}$** | **Selectivity**[c] (fold) |
| **MERS-CoV**[d] | n=7 | | | | n = 6 | | | **0.35** |
| | 0.47 | 0.017 | 28 | | 0.50 | 0.0063 | 79 | |
| ±[e] | 0.011 | 0.0019 | | | 0.012 | 0.0006 | | |
| % error[f] | 2 | 11 | | | 2 | 11 | | |
| | | | | | | | | |
| **SARS-CoV** | n = 4[g] | | | | n = 3 | | | **0.32** |
| | 0.73 | 0.03 | 25 | | 0.70 | 0.010 | 68 | |
| ± | 0.017 | 0.003 | 6.3 | | 0.015 | 0.0008 | 5.4 | 0.026 |
| % error | 6 | 23 | 25 | | 11 | 3 | 8 | 8 |
| | | | | | | | | |
| **SARS-CoV-2** | n = 8 | | | | n = 3 | | | **0.28** |
| | 0.75 | 0.03 | 23 | | 0.74 | 0.0089 | 84 | |
| ± | 0.019 | 0.003 | 4.4 | | 0.023 | 0.0010 | 14.3 | 0.045 |
| % error | 10 | 22 | 20 | | 4 | 18 | 17 | 16 |
| | | | | | | | | |
| **EBOV** | n=3 | | | | n=3 | | | **4.0** |
| | 0.80 | 0.72 | 1.1 | | 0.70 | 2.5 | 0.28 | |
| ± | 0.048 | 0.21 | 0.065 | | 0.047 | 0.76 | 0.048 | 0.49 |
| % error | 4 | 6 | 6 | | 2 | 16 | 17 | 12 |
| | | | | | | | | |
| **RSV**[h] | n=3 | | | | n=3 | | | **2.7** |
| | 0.76 | 0.17 | 4.5 | | 0.82 | 0.50 | 1.6 | |
| ± | 0.022 | 0.023 | | | 0.027 | 0.089 | | |
| % error | 3 | 14 | | | 3 | 18 | | |
| | | | | | | | | |
| **LASV** | n = 3 | | | | n=3 | | | **20** |
| | 0.57 | 0.11 | 5.6 | | 0.35 | 1.3 | 0.29 | |
| ± | 0.032 | 0.020 | 0.96 | | 0.016 | 0.18 | 0.059 | 4.7 |
| % error | 2 | 18 | 17 | | 40 | 53 | 20 | 24 |

[a] $V_{max}$ is a Michaelis–Menten parameter reflecting the maximal velocity of nucleotide incorporation.
[b] $K_m$ is a Michaelis–Menten parameter reflecting the concentration of the nucleotide substrate at which the velocity of nucleotide incorporation is half of $V_{max}$.
[c] Selectivity of a viral RNA polymerase for a nucleotide substrate analogue is calculated as the ratio of the $V_{max}/K_m$ values for NTP and NTP analogue, respectively.
[d] Gordon et al., 2020
[e] Standard deviation of the average.
[f] Percent error.

[g] All reported values have been calculated on the basis of a 9-data point experiment repeated indicated number of times (n).
[h] Tchesnokov et al., 2019
*EPT performed EBOV and LASV selectivity experiments.

### 4.2.3 Selectivity of other nucleotide analogs against SARS-CoV-2 RdRp

We determined selectivity values for various other nucleotide analogue inhibitors to provide a limited structure-activity relationship analysis with focus on SARS-CoV-2 RdRp (Fig. 4.2). Selectivity for dATP, which lacks the 2′α-hydroxyl group, 2′-C-methylated compounds, and the broad-spectrum antivirals favipiravir and ribavirin were included in these studies (Table 4.2). A high selectivity value of ~950-fold was measured for dATP, which shows that the enzyme efficiently discriminates against dNTPs as one would expect for an RNA polymerase. Similarly, the 2′β-hydroxyl in ara-ATP also translates in a high selectivity value (>1000-fold). 2′C-Me-ATP contains a 2′β-methyl group, which shows a value of ~170. 2′d-2′fluoro-CTP has been shown to exhibit antiviral activity against several RNA viruses[354-357]. The selectivity value of 25 is relatively low compared to the aforementioned compounds and suggest that the 2′α-fluoro is largely tolerated by the enzyme. Sofosbuvir (SOF) is a uridine analogue that is approved for the treatment of hepatitis C virus (HCV) infection. The drug inhibits HCV RdRp [303]. It contains a fluoro-group at the 2′α-position and a methyl group at the 2′β-position. Here we measured a high selectivity value (~1000-fold), which suggests that the 2′β-position may be the primary constraint for nucleotide incorporation by SARS-CoV-2 RdRp. The active triphosphate forms of favipiravir and ribavirin serve as substrates for several RdRp enzymes and mimic ATP and GTP[129, 154, 195, 358-360] . To compare efficiency of incorporation with RDV-TP, we measured selectivity values for incorporation opposite template uridine. High values of ~500 and >>1000, respectively, indicate that effective competition of these compounds with ATP is unlikely.

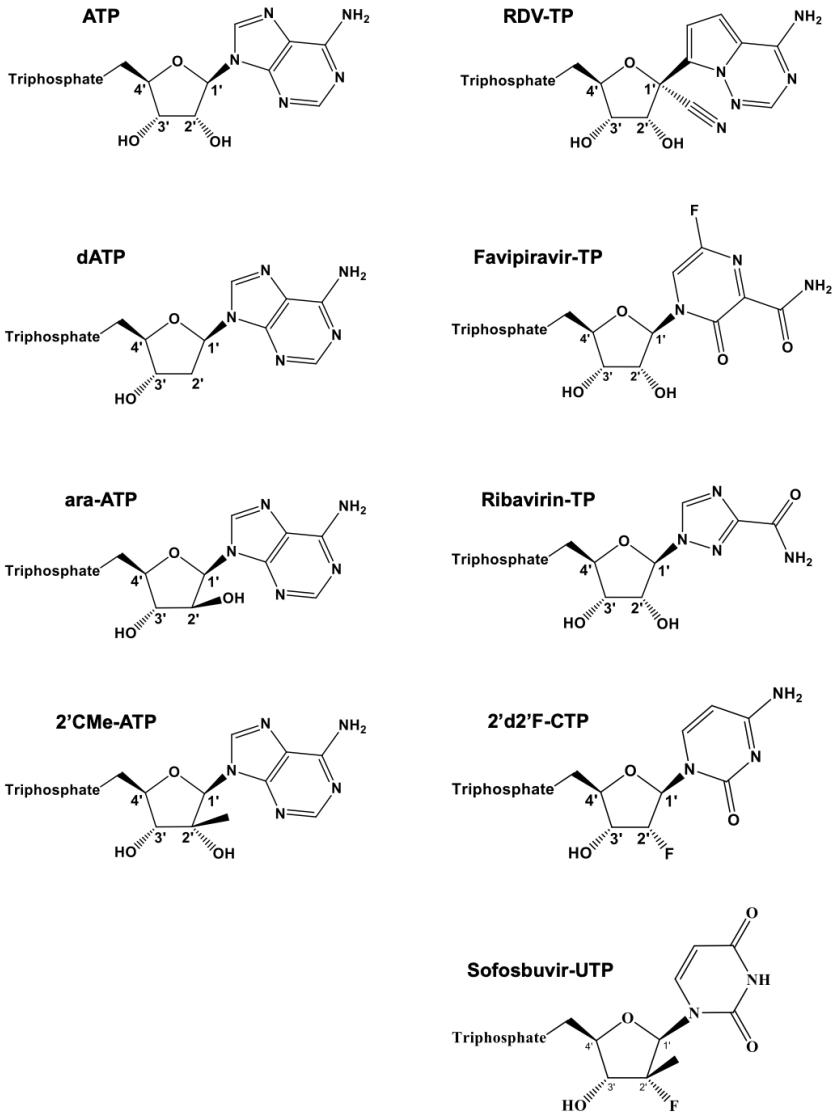


**Figure 4.2. Chemical structures of ATP, and ATP, CTP, and UTP nucleotide analogs.**

Table 4.2 Selectivity values for A-, C-, and UTP analogs against SARS-CoV-2 RdRp

| | $V_{max}$[a] (product fraction) | $K_m$[b] (μM) | $\frac{V_{max}}{K_m}$ | Selectivity[c] (fold) |
|---|---|---|---|---|
| **ATP[d] (n = 8[e])** | 0.75 | **0.03** | 23 | **Reference** |
| ±[f] | 0.019 | 0.004 | 4.4 | |
| % error[g] | 10 | 22 | 20 | |
| **2′CMe-ATP** (n = 3) | 0.84 | **6.4** | 0.13 | **173** |
| ± | 0.013 | 0.37 | 0.007 | 8.9 |
| % error | 1 | 5 | 5 | 5 |
| **dATP** (n = 3) | 0.63 | **27** | 0.02 | **975** |
| ± | 0.021 | 2.41 | 0.04 | 169 |
| % error | 11 | 28 | 16 | 17 |
| **ara-ATP** (n = 3) | 0.56 | **33** | 0.02 | **1329** |
| ± | 0.031 | 4.06 | 0.01 | 371 |
| % error | 15 | 39 | 30 | 28 |
| **ATP[h] (n = 3)** | 0.63 | **0.04** | 14 | **Reference** |
| ± | 0.019 | 0.006 | 1.3 | |
| % error | 3 | 12 | 9 | |
| **Favipiravir-TP** (n = 3) (as ATP-analogue) | 0.52 | **21** | 0.03 | **570** |
| ± | 0.031 | 3.9 | 0.02 | 230 |
| % error | 7 | 41 | 52 | 40 |
| **Ribavirin** (n = 3) (as ATP-analogue) | n.a.[i] | **>>100** | n.a. | **>>1000** |
| ± | | | | |
| % error | | | | |
| **CTP (n = 3)** | 0.72 | **0.001** | 1022 | **Reference** |
| ± | 0.023 | $8.8 \times 10^{-5}$ | 177 | |
| % error | 1 | 18 | 17 | |
| **2′d 2′ fluoro-CTP** (n = 3) | 0.60 | **0.02** | 37 | **29** |
| ± | 0.036 | 0.003 | 8.5 | 7.6 |
| % error | 17 | 36 | 23 | 26 |
| **UTP (n = 3)** | 0.75 | **0.02** | 39 | **Reference** |
| ± | 0.021 | 0.003 | 9.3 | |
| % error | 4 | 22 | 24 | |
| **SOF-TP** (n = 3) | 0.77 | **21** | 0.04 | **1056** |
| ± | 0.030 | 2.3 | 0.01 | 212 |
| % error | 6 | 22 | 22 | 20 |

[a] $V_{max}$ is a Michaelis–Menten parameter reflecting the maximal velocity of nucleotide incorporation.

[b] $K_m$ is a Michaelis–Menten parameter reflecting the concentration of the nucleotide substrate at

which the velocity of nucleotide incorporation is half of $V_{max.}$
[c] Selectivity of a viral RNA polymerase for a nucleotide substrate analogue is calculated as the ratio of the $V_{max}/K_m$ values for NTP and NTP analogue, respectively.
[d] These experiments were conducted on RNA template compatible with [α-$^{32}$P]GTP.
[e] All reported values have been calculated on the basis of a 9-data point experiment repeated indicated number of times (n).
[f] Standard deviation of the average.
[g] Percent error.
[h] These experiments were conducted on RNA template compatible with [α-$^{32}$P]CTP.
[i] n.a., not available.

### 4.2.4 Structural model of nucleotide binding by SARS-CoV-2 RdRp

To provide plausible explanations for our experimental measurements, we generated a model of an elongating SARS-CoV-2 RdRp complex (Fig. 4.3). This model is based on the cryo-electron microscopy structure of the apo SARS-CoV-2 RdRp complex composed of nsp7, nsp8, nsp12[340]. The active site is similar to other enzymes, for which ternary structures have been determined by X-ray crystallography, including HCV RdRp (Fig. 4.3*A*), norovirus, and poliovirus RdRp[116, 303, 361]. The catalytic metal ions in SARS-CoV-2 nsp12 are coordinated by a trio of aspartates, Asp-618, Asp-760, and Asp-761, and the substrate β-phosphate is stabilized by Arg-555. Converting Asp-760 and Asp-761 into Asn-760 and Asn-761 rendered the enzyme inactive (Fig. 4.1). Of particular note, the residues Asp-623, Ser-682, and Asn-691 involved in 2′-OH recognition of the incoming nucleotide are conserved. However, while HCV, norovirus, and poliovirus RdRps use these serine and asparagine residues to coordinate the 2′-OH during incorporation, nsp12 appears to rely on an additional threonine residue (Thr-680) not present in the others enzymes (Fig. 4.3*B*). This interaction has the effect of pulling the substrate deeper into the pocket. The lower positioning of the NTP in the active site is also seen in the interaction of the 3′-OH with the protein. In HCV RdRp, 3′-OH forms a hydrogen bond to the Asp-225 backbone NH, whereas in the coronaviruses, the model instead suggests that the β-phosphate coordinates to the analogous Asp-623 NH. As a consequence of this repositioning of the substrate, the activity of various inhibitors across the coronaviruses is expected to diverge from that seen with other polymerases. The preference for 2′-OH > 2′d2′F >> 2′deoxy is evident from the nature of the polar residues coordinating that position and is similar to the other enzymes. In contrast, SOF-TP and 2′-CMe-ATP have increased clashes between the 2′β-Me and Asp-623 and Ser-682 (Fig. 4.3*C*). This is partially relieved by a conformational change in Ser-682, but overall, the poorer incorporation efficiencies of the 2′β-Me substituted inhibitors is likely due to these putative steric

clashes. In contrast, RDV-TP (Fig. 4.3*D*) is recognized at the 2′-OH in a manner similar to ATP, and the 1′-CN modification is well-positioned in a pocket formed between Thr-687 and Ala-688. The high efficiency of incorporation reported here is consistent with this model.

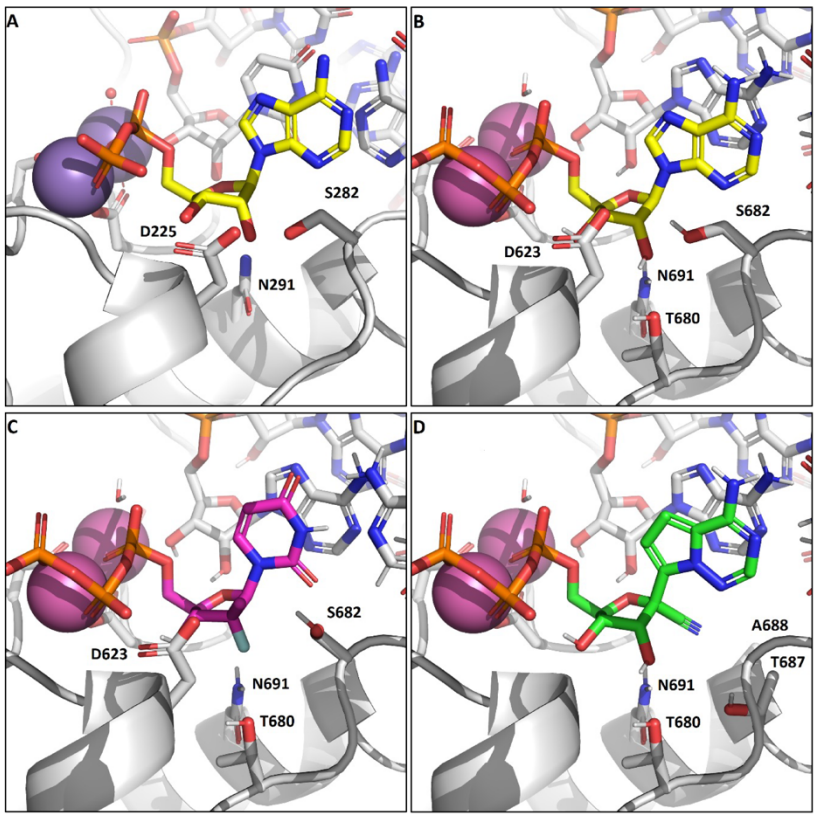


**Figure 4.3. X-ray structure of HCV RdRp with an incoming nonhydrolyzable ADP substrate (PDB entry 4WTD)**. The 2′-OH of the substrate is recognized by the trio of residues, Asp-225, Ser-282, and Asn-291, with hydrogen bonds formed to Ser-282 and Asn-291 in this preincorporation state. B, model of SARS-CoV-2 nsp12 with incoming ATP. In addition to the analogous Asp/Ser/Asn residues, Thr-680 is positioned to alter the hydrogen-bonding network and effectively pull the substrate lower into the pocket relative to NS5B. C, model of SARS-CoV-2 with SOF-TP. The greater occlusion of the 2′ position due to Asp-623 and Ser-682 makes 2′β-methyl substitution less effective than with NS5B. D, model of SARS-CoV-2 with remdesivir-TP. The remdesivir 1′CN sits in a pocket formed by residues Thr-687 and Ala-688. Residues Asp-623 and Ser-682 (not shown) adopt the same conformations as with ATP.

*JKP contributed this figure.

### 4.2.5 Patterns of inhibition of RNA synthesis by RDV-TP

The incorporation of a nucleotide analogue into the growing RNA chain does not necessarily translate into inhibition. To determine the patterns of inhibition of RNA synthesis, we devised two RNA templates that contain single or multiple sites of incorporation (template

uridines) (Fig. 4.4*A*). These sequences were used to compare the inhibitory effects of RDV-TP against MERS-CoV, SARS-CoV, SARS-CoV-2 and LASV RdRp. The latter enzyme showed a significantly higher selectivity value for RDV-TP (Table 4.1) and RDV does not show antiviral activity against LASV[257]. For CoV RdRp complexes with templates allowing multiple incorporations, we observe termination of RNA synthesis at positions i+3 and i+4. A faint band representing the full-length product suggests low levels of read-through (Fig. 4.4*B*). On a template that allows only a single RDV-TP incorporation, termination is seen solely at position i+3. Full-length product formation is generally more pronounced under these conditions, following the order MERS-CoV RdRp > SARS-CoV RdRp > SARS-CoV-2 RdRp. For LASV RdRp, RNA synthesis patterns in the presence or absence of the nucleotide analogue are very similar. Chain termination or delayed chain termination is not evident. To further investigate the possibility of long-range effect of RDV-TP incorporation, we used a 26-mer RNA template and did not observe any change in the pattern of RNA synthesis (Appendix A, Fig. A2*A*). Hence, LASV L protein is likely not inhibited by RDV-TP.

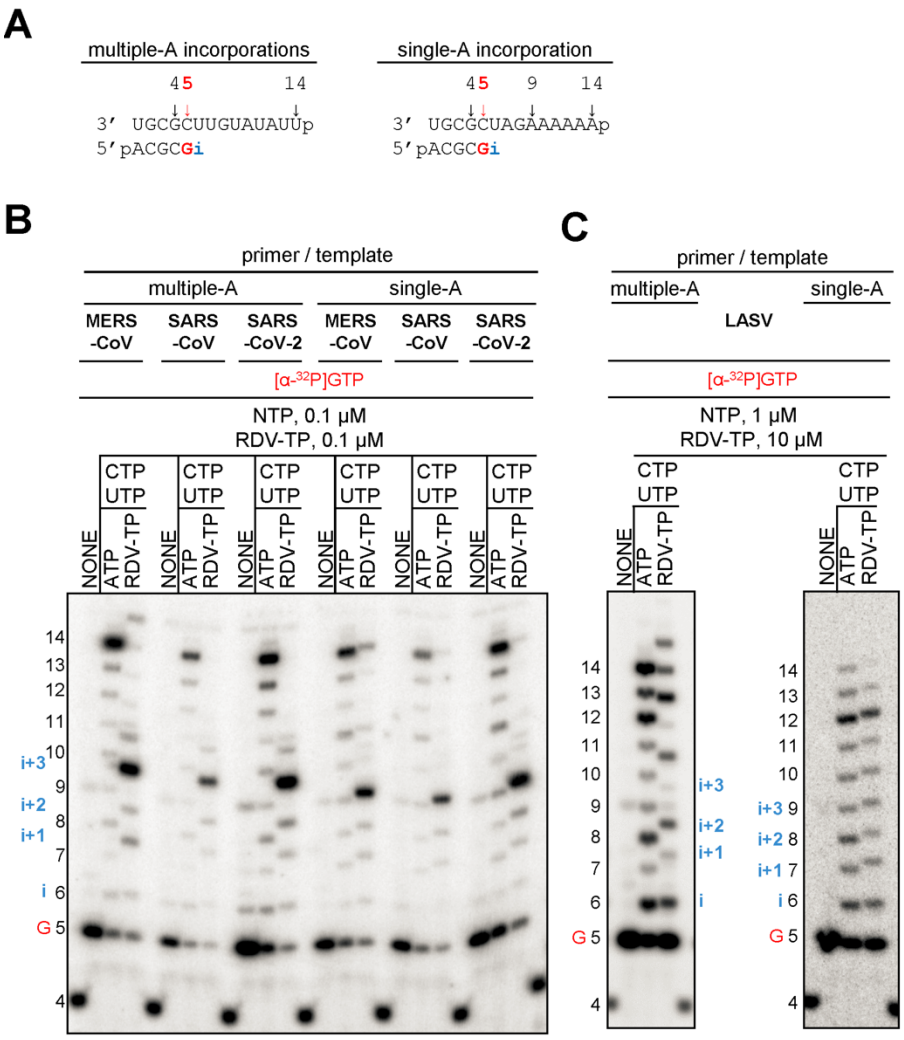


**Figure 4.4. Patterns of inhibition of RNA synthesis with RDV-TP.** ***A***, RNA primer/template substrates used to test multiple (*left*) or single (*right*) incorporations of RDV-TP. G indicates incorporation of the radiolabeled nucleotide opposite template position 5. RDV-TP incorporation is indicated by i. RDV-TP incorporation was monitored with purified CoV RdRp complexes (***B***) and LASV L protein (***C***) in the presence of the indicated combinations of NTPs and RDV-TP.

*EPT contributed panel **C** to this figure.

Examination of the structural model suggests the primer with the incorporated RDV can translocate without obstruction to position i+1 (Fig. 4.5, *A* and *B*). Similarly, no obstructions can be discerned at the i+2 (Fig. 4.5*C*) or i+3 (Fig. 4.5*D*). This would allow the incorporation of three subsequent nucleotides, in agreement with our experimental data. However, at position i+4 (Fig. 4.5, *E* and *F*), a steric clash is seen between the 1′-CN substituent of RDV and residue Ser-861. The serine O is only 1.7 Å from the 1′-CN N. The short distance is expected to lead to a significant distortion of the positioning of the RNA, hampering translocation to the i+4 position.

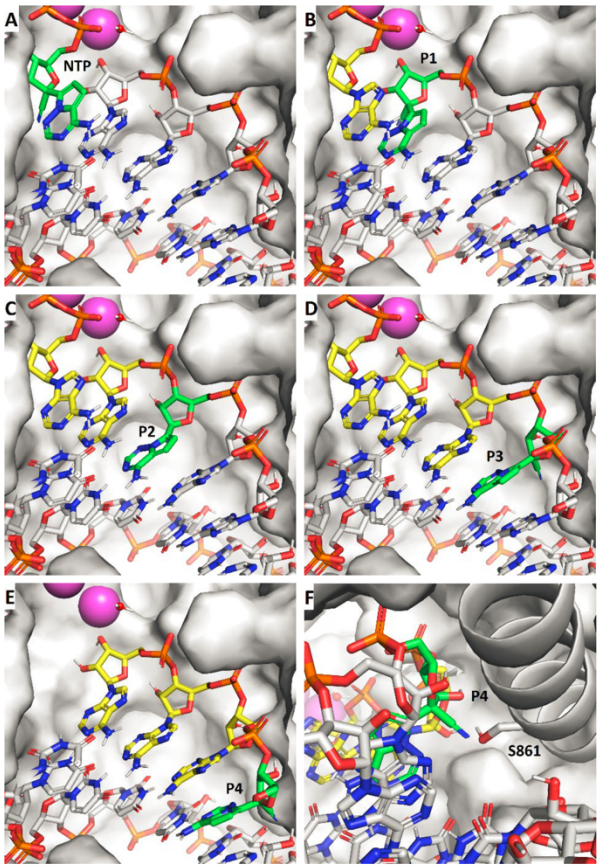


**Figure 4.5. A steric clash between the incorporated RDV and Ser-861 prevents enzyme translocation at i+3**. ***A–D***, the primer with the incorporated RDV (*green*) translocates without obstruction from the substrate position i through i+3, allowing incorporation of three subsequent nucleotides (yellow). *E*, at i4, the 1-CN moiety of RDV encounters a steric clash with Ser-861 of nsp12. F, this clash likely prevents the enzyme from advancing into i+4.

*JKP contributed this figure.

### 4.2.6 Overcoming of the delayed chain termination by incorporated RDV

Read-through at a site of delayed chain temination may reduce the inhibitory effect of RDV-TP. We therefore tested whether termination of RNA synthesis could be overcome with time or with increasing concentrations of nucleotide pools (Fig. 4.6). In the presence of equivalent concentrations of RDV-TP and UTP (0.1 μM), which is the next nucleotide to be incorporated following the RDV-TP incorporation site and also following the site of delayed chain termination, the full-length product formation is negligible. The signal for delayed chain termination is not alleviated with time, which provides more evidence for a bona fide termination site and not enzyme pausing. (Fig. 4.6*A*, *left*). In contrast, full-length product formation is time-dependent when ATP

replaces RDV-TP in the reaction mixture (Fig. 4.6*A*, *middle*). As expected, the ommision of both ATP and RDV-TP prevents RNA synthesis beyond product 5 thus controlling for C:U and U:U misincorporations under the present reaction conditions (Fig. 4.6*A*, *right*). However, delayed chain termination can be overcome with higher NTP concentrations. In the presence of increasing concentrations of UTP, the signal at i+3 decreases concomitantly with an increase in the full-length product. UTP concentrations that are ~100-fold higher than RDV-TP can cause significant reductions in delayed chain termination (Fig. 4.6*B*).

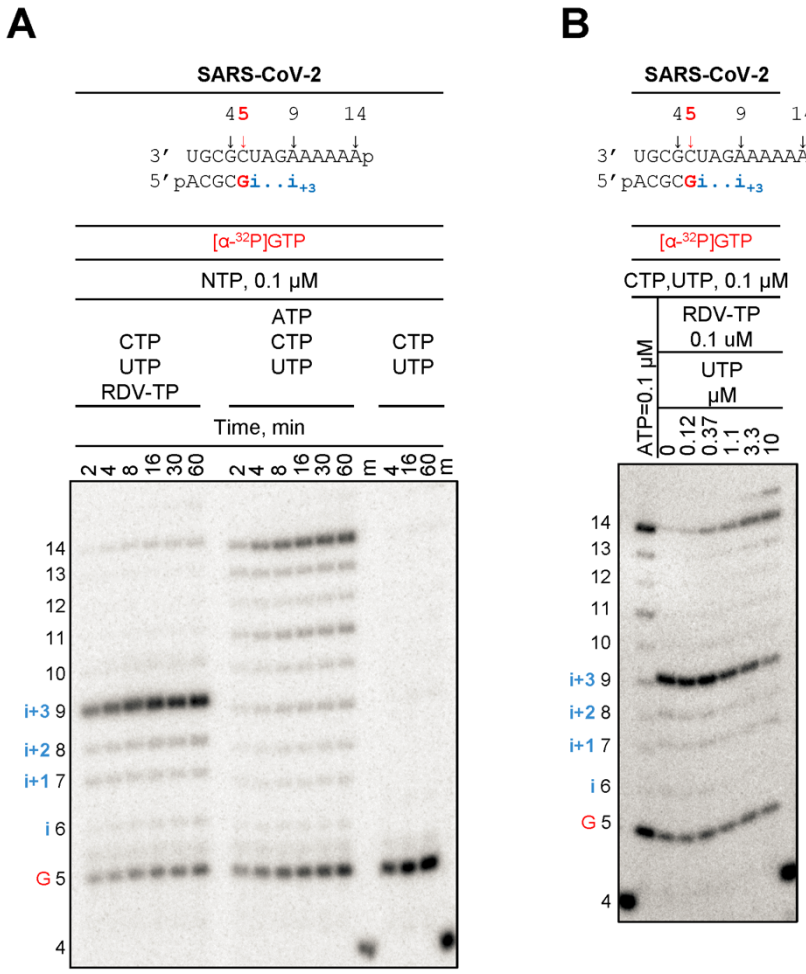


**Figure 4.6. Overcoming of delayed chain termination**. The RNA primer/template substrate used in this assay is shown above the gels. G indicates incorporation of the radiolabeled nucleotide opposite template position 5. Position i allows incorporation of ATP or RDV-TP. RNA synthesis was monitored with purified SARS-CoV-2 RdRp complex in the presence of indicated concentrations of NTP mixtures. ***A***, time dependence of delayed chain termination. ***B***, overcoming delayed chain termination with increasing concentrations of UTP.

*EPT Contributed to this figure.

## 4.3 Discussion

RDV is an investigational nucleotide analogue with a broad spectrum of antiviral activities against several RNA viruses, including filoviruses and coronaviruses[241, 253, 257, 333, 334, 346]. Studies in mice and rhesus macaques have helped to assess the therapeutic potential of this drug against EBOV, SARS-CoV and MERS-CoV[253, 254, 333, 346]. Antiviral activity of RDV has also been demonstrated against SARS-CoV-2 in cell culture[186], while data from animal models and clinical trials are pending. Moreover, it remains to be seen whether the mechanism of inhibition described for EBOV RdRp and MERS RdRp is also relevant for SARS-CoV-2. Here, we expressed and purified active SARS-CoV-2 RdRp to study RNA synthesis and its inhibition by RDV-TP. Based on our biochemical data, we propose a unifying, refined mechanism of inhibition of SARS-CoV, MERS-CoV, and SARS-CoV-2 (Fig. 4.7).

Co-expression of SARS-CoV-2 nsp5, nsp7, nsp8, and nsp12 in insect cells yields an active RdRp complex composed of nsp8 and nsp12. The same data were obtained with MERS-CoV and SARS-CoV. RNA synthesis was monitored on short primer/templates that mimic the elongation stage (Fig. 4.7, *stage 1*). We initially compared efficiency of incorporation of RDV-TP with its natural counterpart ATP (Fig. 4.7, *stage 2*). A steady-state kinetic approach was employed to translate our findings into quantitative terms and to facilitate comparisons among the various enzymes and compounds tested. Efficiency of incorporation of the natural nucleotide over the nucleotide analogue defines selectivity. For RDV-TP, we measured selectivity values of ~ 0.3 with SARS-CoV, SARS-CoV-2 and previously also with MERS-CoV RdRp. SARS-CoV and SARS-CoV-2 both belong to the betacoronaviruses of the B lineage and the nsp 12 amino acid sequences of the two viruses are 96% identical. In contrast, MERS-CoV belongs to the betacoronaviruses of the C lineage and is only 71% identical with SARS-CoV-2. Despite greater sequence variations, RdRp motifs that play important roles in substrate binding and catalysis are highly conserved among the three coronaviruses (Appendix A, Fig. A3). Hence, interactions with nucleotide analogue inhibitors are expected to be similar and our selectivity data provide experimental evidence for this notion. Whereas the active sites of EBOV and RSV enzymes still share a number of key residues within the classic polymerase motifs, LASV RdRp shows substantial differences when these motifs are compared with EBOV and RSV and also with SARS-CoV, SARS-CoV-2, and MERS-CoV (Appendix A, Fig. A3).

We have evaluated several other nucleotide analogs using the same protocol with focus on SARS-CoV-2 RdRp (Fig.4.2, Table 4.2). The selectivity of ATP over dATP is ~1000, which shows that the enzyme effectively discriminates against deoxyribonucleotides that are substrates for DNA polymerases. Similar results were obtained with the broad spectrum antivirals favipiravir and ribavirin[358-360]. These compounds show high selectivity values of ~500 and ~10,000 in favor of ATP. Compounds with modifications at the 2'β-position are also associated with high selectivity values in favor of the natural nucleotide. SOF-TP and 2'-CMe-ATP show selectivity value of ~1000 and ~170 in favor of UTP and ATP, respectively. Selectivity of ATP over ara-ATP is likewise high (~1000). A homology model of SARS-CoV-2 points to a putative steric clash of 2'β-modifications with residues Asp-623 and Ser-682. With the limitations of a steady-state approach, we are unable to ascribe differences in selectivity measurements solely to inhibitor binding; however, while the model is not based on structural data of SARS-CoV-2 RdRp it provides a plausible explanation for our experimental observations.

RDV-TP is a non-obligate chain terminator, which contains a 3′-hydroxyl group that may still form a phosphodiester bond with the next incoming nucleotide. Indeed, as demonstrated for RdRp enzymes from RSV, EBOV, NiV and MERS, delayed chain termination provides a likely mechanism of action[267, 333, 335, 353]. For all three coronavirus RdRp complexes, we observe a specific termination site at position i+3 (Fig. 4.7, *stage 3*). The structural reasons for the precise termination event remain to be elucidated; however, the underlying mechanism is likely to be common to all three coronaviruses if we consider the identical patterns of inhibition. At i+4, our model predicts a steric clash between the 1'-CN substituent of the incorporated RDV and residue Ser-861. This model is consistent with the observed termination at i+3 and the inability of the enzyme to translocate a single position further downstream to accommodate the next nucleotide. Sequences extracted from Genebank™ reveal that this serine residue is conserved across all alpha-, beta-, and deltacoronaviruses.

Termination of RNA synthesis can be overcome by higher concentrations of the natural nucleotide pools (Fig. 4.7, *stage 4*). NTP concentrations can reach low millimolar concentrations[362, 363]. The intracellular concentration of RDV-TP can vary between low and high micromolar concentrations in relevant cell cultures[253, 333], and high ratios of NTP/RDV-TP are likely detrimental to inhibition. However, the efficient incorporation of RDV-TP into the growing

RNA chain may also provide a mechanism that counteracts reduced termination in the presence of high NTP concentrations. Our data confirm that consecutive and/or multiple sites of incorporation of RDV-TP increase termination and in turn inhibition; however, the efficiency of this effect remains to be determined (Appendix A, Fig. A2*B*). Another factor that can reduce the potency of nucleotide analogs is the 3'-5' exonuclease activity of nsp14[55, 251, 341, 364]. This enzyme displays proofreading activity in conjunction with nsp10[55, 341, 365]. In this context, we have recently proposed that the additional three nucleotides that follow the incorporated RDV may provide protection from excision[268, 353]. Future studies that take into account rates of nucleotide incorporation, rates of excision of multiple nucleotides, and the likelihood of RDV-TP reincorporation will be required to address this problem.

Several independent examples point to a significant correlation between the efficiency of selective incorporation of a given nucleotide analogue and the corresponding antiviral effect measured in cell culture. Half-maximal effective concentrations ($EC_{50}$) of RDV against coronaviruses and filoviruses are in the submicromolar range, which is unusually low for a compound with a broad spectrum of antiviral activity[253, 257, 333, 334, 366]. High potency in cell culture correlates with highly effective incorporation of RDV-TP with EBOV RdRp and, even more so, with the three coronavirus enzymes. Conversely, RDV shows a weak antiviral effect against LASV[257], and our biochemical data revealed low rates of incorporation by LASV RdRp. In this context it is also important to note that our previous measurements with human mitochondrial RNA polymerase revealed high selectivity of ATP over RDV-TP [267], which is consistent with low levels of cytotoxicity of RDV[253, 333]. Favipiravir-TP and ribavirin-TP are also less well incorporated by SARS-CoV-2 RdRp. This is also evident with a template that offers multiple incorporation sites (Appendix A, Fig. A2*B*). In cell culture, these inhibitors often show $EC_{50}$ values in the higher micromolar range depending on the nature of the RNA virus[169, 358, 366]. High concentrations of favipiravir and ribavirin were also required to reduce infection with SARS-CoV-2 ($EC_{50}$ = 109.50 μM and $EC_{50}$ = 61.88 μM, respectively)[186]. Moreover, ribavirin does not seem to provide clinical benefits in the context of SARS-CoV and MERS-CoV infection [366], 2'-CMe-ATP is not utilized as a substrate by EBOV RdRp and 2'-C-methylated compounds show no significant antiviral effects in mini-genome replicons of EBOV[367]. Equivalent studies are not yet available for coronaviruses; however, the high selectivity for the natural nucleotides over SOF-TP and 2'-CMe-ATP would not predict a potent antiviral effect.

In conclusion, the combined data provide evidence for a unifying mechanism of inhibition of RDV-TP against coronavirus RdRp. Favorable selectivity for the nucleotide analogue over its natural counterpart ATP and delayed chain-termination at position i+3 are key elements of inhibition observed with SARS-CoV, MERS-CoV, and SARS-CoV-2 RdRp complexes. The availability of human safety data along with the antiviral studies in cell culture and in animal models, as well as a clear mechanism of action provide a large body of evidence to justify the ongoing clinical trials with RDV for the treatment of COVID-19[186, 253, 254, 257, 333, 334, 345, 346, 353]. The refined biochemical mechanism described in this study characterizes RDV as a direct-acting antiviral (DAA). This term was previously introduced to describe newer classes of HCV drugs that target a specific process in the viral life cycle[368], as opposed to older treatments with interferon and ribavirin that have been associated with multiple possible mechanisms[369]. Compounds that are currently considered as potential treatments for COVID-19 include approved drugs for other conditions, repurposed drugs, and inhibitors with a broad-spectrum of antiviral activities. Research into underlying mechanisms is needed to classify any of these compounds as a DAA.

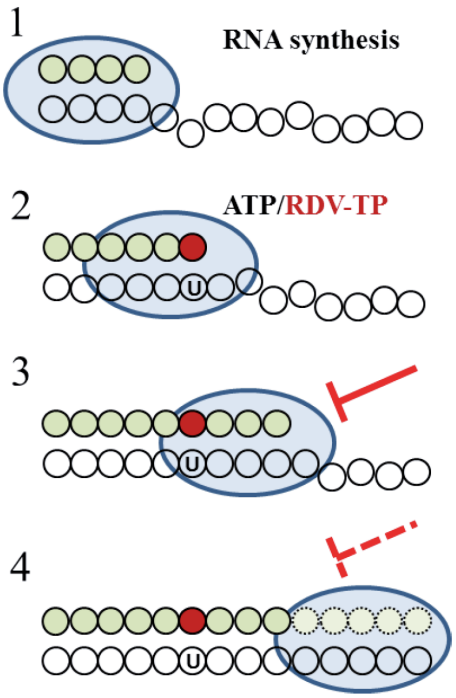


**Figure 4.7. Mechanism of inhibition of CoV RdRp by RDV-TP**. *1*, the priming strand is shown with *green circles, colorless circles* represent residues of the template, and the *blue oval* represents the active CoV RdRp complex. This is a *schematic representation* of a random elongation complex. The footprint of the RdRp on its primer/template is unknown. *2*, competition of RDV-TP with its natural counterpart ATP opposite template uridine (*U*). The incorporated nucleotide analog is illustrated by the *red circle*. *3*, RNA synthesis is terminated after the addition of three or more nucleotides, which is referred to as delayed chain termination. *4*, delayed chain termination can be overcome by ratios of NTP/RDV-TP.

# Chapter 5: Template-dependent inhibition of coronavirus RNA-dependent RNA polymerase by remdesivir reveals a second mechanism of action

This chapter contains content from the following source, republished with permission:

- Tchesnokov EP[#], Gordon CJ[#], Woolner E, Kocincova D, Perry JK, Feng JY, Porter DP, Götte M. Template-dependent inhibition of coronavirus RNA-dependent RNA polymerase by remdesivir reveals a second mechanism of action. J Biol Chem. 2020; 295:16156-16165. © the authors.

Author contributions

E. P. T., C. J. G., J. K. P., and M. G. software; E. P. T. and M. G. formal analysis; E. P. T. and M. G. supervision; E. P. T. and M. G. validation; E. P. T., C. J. G., E. W., D. K., and J. K. P. investigation; E. P. T. and M. G. visualization; E. P. T., C. J. G., E. W., D. K., and J. K. P. methodology; E. P. T., C. J. G., J. K. P., J. Y. F., D. P. P., and M. G. writing-review and editing; J. K. P., J. Y. F., D. P. P., and M. G. resources; M. G. conceptualization; M. G. data curation; M. G. funding acquisition; M. G. writing-original draft; M. G. project administration.

[#] These authors contributed equally to this work.

* Experiments performed by other authors have been identified in figure legends.

Funding

This study was supported by Canadian Institutes of Health Research (CIHR) Grant 170343, Gilead Sciences, and the Alberta Ministry of Economic Development, Trade, and Tourism Major Innovation Fund Program for the AMR–One Health Consortium (to M. G.). M. G. has previously received funding from Gilead Sciences in support of the study of EBOV RdRp inhibition by RDV.

## 5.1 Introduction

The US FDA has recently issued an emergency use authorization (EUA) for the investigational drug remdesivir (RDV) to treat infection with severe acute respiratory syndrome coronavirus 2 (SARS-CoV-2)[370]. The EUA was largely based on a randomized clinical trial that showed a significant reduction in the time of recovery of hospitalized individuals diagnosed with coronavirus disease 2019 (COVID-19)[371]. RDV is a nucleotide analogue prodrug that was designed to target the RNA-dependent RNA polymerase (RdRp) of RNA viruses[241, 257]. The triphosphate form of RDV (RDV-TP) is an analog of the natural adenosine triphosphate (ATP) with 1′-C-nucleoside bond and a 1′-cyano-substitution. RDV has shown a broad-spectrum of antiviral activity in cell culture and animal models against negative-sense RNA viruses of the *Filoviridae* [e.g. Ebola virus (EBOV)] and *Paramyxoviridae* [e.g. Nipah virus (NiV) and measles virus (MV) as well as *in vitro* activity against viruses in the *Pneumoviridae* [e.g. respiratory syncytial virus (RSV)] family[241, 257, 333, 335, 352]. Antiviral activity against positive-sense RNA viruses, including flaviviruses and coronaviruses, was also demonstrated in various systems[251-253, 334, 372]. Several previous studies have demonstrated prophylactic and therapeutic efficacy in animal models of SARS-CoV, Middle East respiratory syndrome (MERS)-CoV and SARS-CoV-2[252, 372].

Low 50% effective concentrations ($EC_{50}$) and a high barrier to the development of resistance were observed in cell cultures [251]. $EC_{50}$ values in the lower nanomolar range have been measured for each of these three viruses, depending on the cell-type-specific metabolism of RDV-TP [252]. *In vitro* selection experiments with the mouse hepatitis virus (MHV) revealed two mutations in the RdRp enzyme that confer low-level resistance to RDV[251]. F476L and V553L were shown to cause 2.4-fold resistance and 5.0-fold resistance, respectively. The F476L+V553L double mutant showed 5.5-fold resistance to RDV. The equivalent mutations F480L and V557L introduced together in SARS-CoV were also shown to confer low-level (6.0-fold) resistance to the drug [251]. Resistance data for SARS-CoV-2 are pending.

Despite progress, there are gaps in our understanding of the mechanism of action of RDV. A key element of a refined mechanism of action is based on high rates of incorporation of RDV-TP, which translates in efficient competition with its natural counterpart ATP [49, 50]. However, the existence of a 3′-OH group allows further nucleotide incorporation events to occur and inhibition

of RNA synthesis is not immediately evident. Biochemical experiments with various recombinant RdRp complexes from both minus-sense and plus-sense RNA viruses show delayed chain-termination[49, 50, 333, 335]. RdRp complexes of SARS-CoV, MERS-CoV and SARS-CoV-2 stop RNA synthesis after position i+3, i.e. three nucleotides following incorporation of RDV-TP at position i[49, 50]. This pattern is identical with the three RdRp complexes, which points to a common mechanism of inhibition. Modeling studies suggested that a steric clash between the side chain of the conserved Ser-861 and the 1′-CN group of the incorporated RDV prevent translocation, which means that the nucleotide binding site at position i+4 is still occupied with the 3′-end of the primer[49]. Another important observation is that RNA synthesis arrest can be overcome with higher concentrations of natural nucleotide pools[49]. Increasing NTP concentrations gradually reduces termination efficiency and favors read-through to yield the full-length RNA product. Efficient read-through is seen at concentrations as low as 10 μM. Intracellular NTP concentrations are in the high μM and low mM range[362, 363], which suggests that read-through reactions likely occur under biologically relevant conditions. It is therefore conceivable that the primer strand, and by extension the entire negative-sense copy of the genome, contains several RDV residues. Although the CoV exonuclease (ExoN) exhibits 3′-5′ proofreading activity[55, 251, 341, 365], access to internal RDV residues is expected to be compromised. This scenario raises the question whether RDV residues embedded in the template strand may also cause inhibition during synthesis of the second RNA strand, i.e. during transcription or viral genome synthesis.

To address this question, we have devised a method that allows synthesis of small RNA model templates with RDV-TP incorporated at a single strategic position. RNA synthesis with recombinant SARS-CoV-2 RdRp shows that incorporation of UTP opposite RDV as well as the following nucleotide incorporation are compromised. Similar to earlier observations with the primer strand, this inhibition can be overcome with increasing NTP concentrations, although the threshold is here much higher. This effect is partially reversed with a known resistance-conferring mutation that can affect the positioning of the template strand. Based on this data, we propose a comprehensive mechanism of action of RDV that involves both the primer strand and the template.

## 5.2 Results

### 5.2.1 Effects of mutations at position Ser-861 on delayed chain termination

Several recent structural and biochemical studies have demonstrated that that the active SARS-CoV-2 RdRp complex is composed of the three non-structural proteins nsp7, nsp8 and nsp12[41, 46, 340, 342, 373]. Reconstitution of separately expressed proteins commonly yields complexes with stoichiometry of 1:1:2 for the nsp12 (RdRp) and the other components nsp7 and nsp8, respectively. We utilized constructs that co-express the viral protease nsp5 together with nsp7, nsp8 and nsp12 in insect cells [49, 50]. Active complexes were captured via the histidine-tagged nsp8, and binary complexes composed of nsp8 and nsp12 were identified with Coomassie staining. Here we show that overloading of the gel with the soluble protein sample also visualizes nsp7 (Appendix B, Fig. B1). Using the same construct design, we generated complexes with mutations at position Ser-861 in nsp12 that are expected to affect efficiency of delayed chain-termination with RDV-TP. The steric clash hypothesis predicts that smaller side chains will reduce delayed chain-termination and larger side chains will increase inhibition, provided that substitutions do not impede regular NTP incorporations.

We compared RNA synthesis of the wild type SARS-CoV-2 RdRp complex with S861G, S861A and S861P mutants (Fig. 5.1). Reactions were monitored on a 17-mer RNA template that contains a single site of incorporation for RDV-TP at position 9 or i (Fig. 5.1*A*). The wild-type enzyme shows delayed chain-termination at position 12 (i+3) (Fig. 5.1*A*), which is illustrated by more than 95% reduction in the full template length-to-(i+3) product ratio in the presence of RDV-TP as compared to the full template length-to-p12 product ratio in the presence of ATP (Fig. 5.1*B*). Termination efficiency is gradually reduced by increasing the concentration of the next incoming nucleotide (UTP), as previously reported[49]. 50% read-through is seen at UTP concentrations of ~ 0.3 μM, 90% read-through is seen with ~3 μM, and inhibition is abolished with ~ 30 μM (Fig. 5.1*C*). Delayed chain-termination is not observed with the S861G mutant. These findings are consistent with the removal of a steric clash when serine is replaced with glycine. Full-length product formation is already seen to near completion at UTP concentrations of ~ 1 μM (Fig. 5.1*A*). The S861A mutation shows only subtle reductions in delayed chain-termination (Fig. 5.1, *A* and *B*), which is in agreement with a previous report by Wang and colleagues [373]. We further show that

the bulkier side chain of S861P shows subtle increases in UTP concentrations required to overcome delayed chain-termination (Fig. 5.1, *A* and *C*).

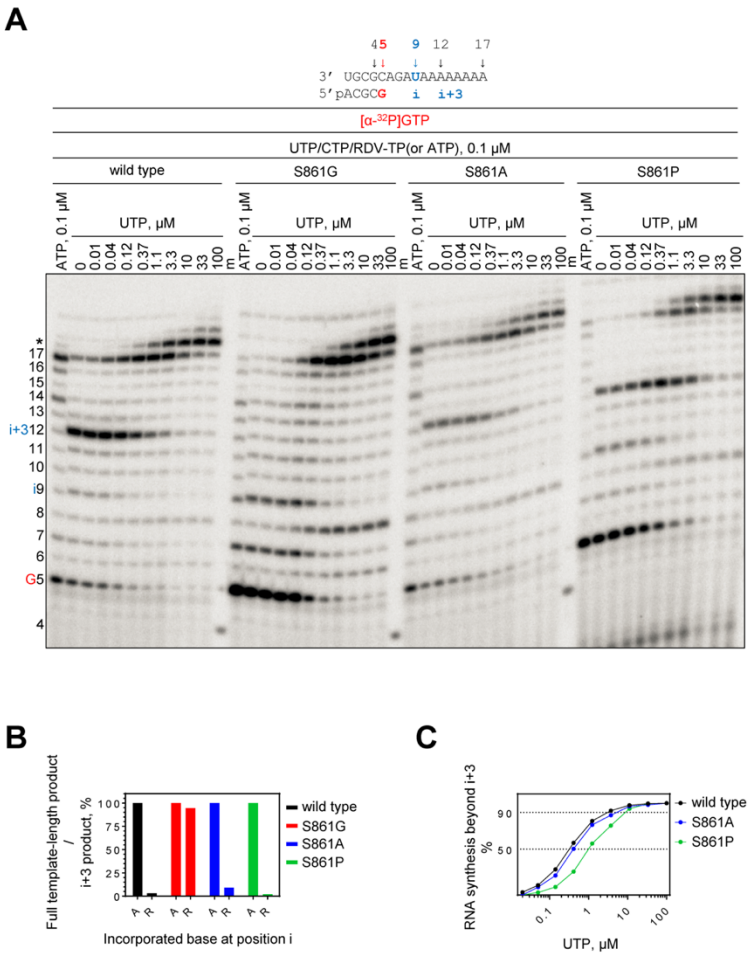


**Figure 5.1. RNA synthesis catalyzed by SARS-CoV-2 RdRp wild-type, S861G, S861A, and S861P mutant complexes on an RNA template containing single "U" for RDV-TP incorporation**. ***A***, RNA primer/template supporting incorporation of RDV-TP at position 9 (i = 9) is shown on top. i+3 illustrates delayed chain termination at position 12. G5 indicates incorporation of [α-$^{32}$P]-GTP at position 5. RNA synthesis was catalyzed by CoV-SARS-2 RdRp wild-type and mutant complexes in the presence of RNA primer/template, $MgCl_2$ and indicated concentrations of NTP and RDV-TP for 30 minutes. Reactions loaded in lanes "ATP, 0.1 μM" contained only UTP/CTP/ATP at 0.1 μM; reactions loaded in the remaining lanes contained UTP/CTP/RDV-TP, each at 0.1 μM, supplemented with indicated concentrations of UTP. "4" indicates the migration pattern of 5′-$^{32}$P-labeled 4-nt primer used here as a size marker. Asterisk indicates slippage due to the polyA context of the template. ***B***, Graphic representation of the effect of delayed chain-termination at i+3 on full template-length RNA synthesis. The fold-ratio of full-length product 17 to delayed chain-termination at i+3 when RDV-TP is present in the reaction (in the absence of supplemental UTP). This value was normalized to the corresponding ratio when ATP was present in the reaction. Normalized values were plotted versus incorporated nucleotide at position i. ***C***, Graphic representation of products of RNA synthesis beyond position i+3 plotted as a function of UTP concentration.

### 5.2.2 RDV inhibits RNA synthesis when embedded in the template

The high efficiency of read-through with increasing NTP concentrations suggests that the newly synthesized copy of the RNA genome contains several RDV residues. This raises the question whether RDV may also inhibit RNA synthesis when present in the template (Fig. 5.2). The challenge to synthesize sufficient amounts of RNAs with embedded RDV residues using RdRp is the need for strand separation. Hence, we developed a protocol to generate single-stranded RNAs using T7 RNA polymerase along a DNA template that can be selectively degraded (Materials and Methods, **2.3.4**). We synthesized two 20-mer model RNAs that contain either adenosine (Template A) or RDV (Template R) at the same strategic position 11 (Appendix B, Fig. B2).

A 4-mer primer was used to initiate RNA synthesis with SARS-CoV-2 RdRp in the presence of [α-$^{32}$P]GTP (Fig. 5.2*A*). With Template A, a cocktail of minimal concentrations of 0.1 μM CTP and UTP, and 1 μM ATP yields predominantly the full-length, 20-mer RNA product (Fig. 5.2*B*). Increasing the concentration of UTP shows no significant increases in RNA synthesis. With Template R, we observe an intermediate product at position 10 at the same base concentrations of CTP, UTP and ATP (Fig. 5.2*B*). These findings demonstrate that 0.1 μM UTP is not sufficient for incorporation opposite RDV, which is a marked difference to results obtained with Template A. Increasing concentrations of UTP can overcome the inhibitory effects and we observe an accumulation of product at position 11, which points to a second site of inhibition immediately after the template-embedded RDV. A similar effect is seen with increasing the concentration of UTP and CTP that is required later at position 14. Increases only in CTP did not yield significant amounts of product at position 11, suggesting that incorporation of CTP opposite RDV is negligible. Higher concentrations of UTP and ATP or UTP, ATP and CTP gradually reduced the inhibitory effects and increased the yield of full-length product. Overall inhibition is driven by the accumulation of products at positions 10 and 11. Together these findings show that a single RDV residue in the template inhibits efficiency of incorporation of the complementary UTP and the adjacent NTP (ATP in this particular sequence context). NTP concentrations required to overcome these obstacles are higher than observed with delayed chain-termination (Fig. 5.2*C*).

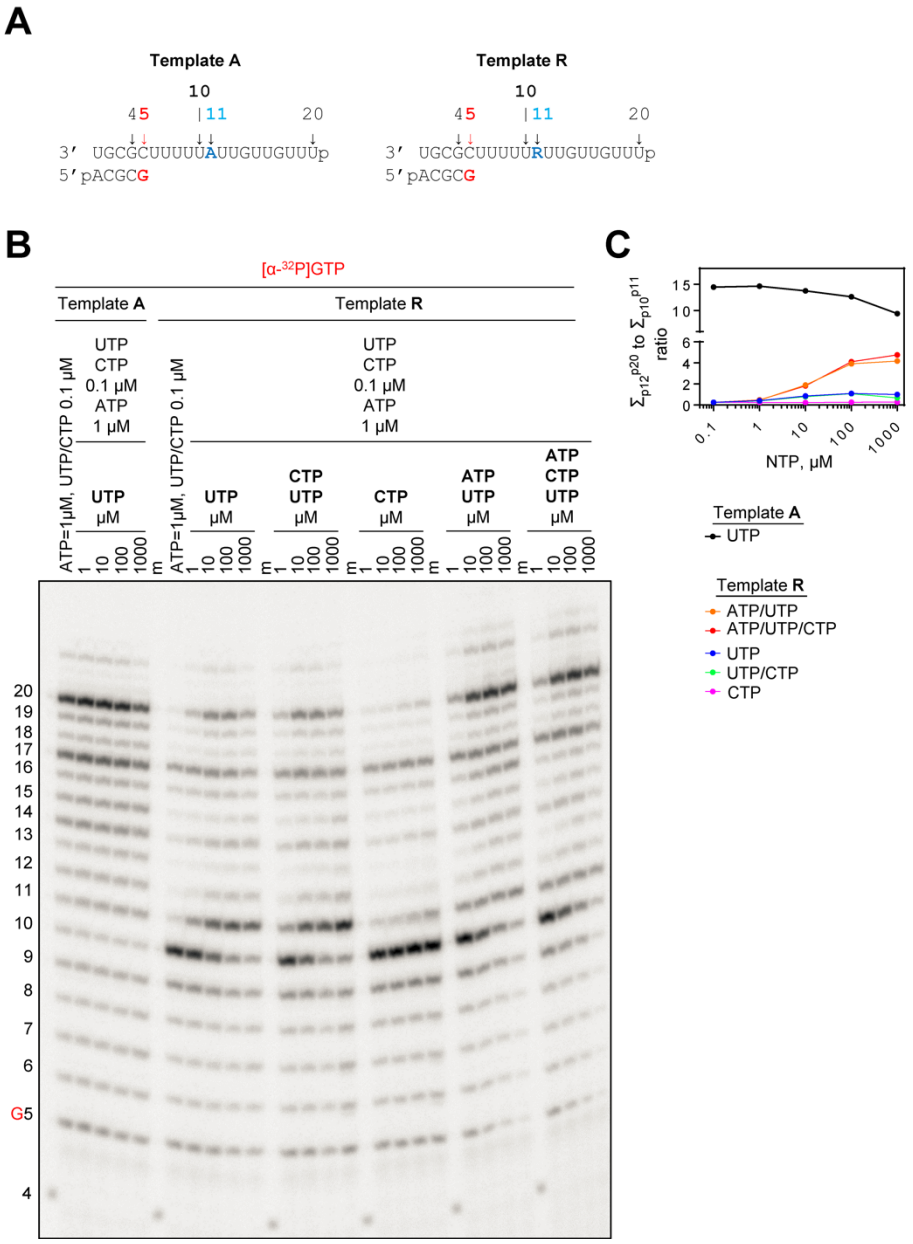


**Figure 5.2. RNA synthesis catalyzed by SARS-CoV-2 RdRp using a template with a single RDV residue at position 11**. ***A***, RNA primer/template with template-embedded RDV (*Template R*) at position 11; the corresponding primer/template (*Template A*) with adenosine at this position is shown on the left. G5 indicates the incorporation of [α-$^{32}$P]-GTP opposite template position 5. ***B***, Migration pattern of the products of RNA synthesis catalyzed by CoV-SARS-2 RdRp wild-type complex in the presence of RNA primer/templates shown in panel A, $MgCl_2$ and indicated concentrations of NTP cocktails after incubation for 30 minutes. "4" indicates the migration pattern of 5′-$^{32}$P-labeled 4-nt primer used here as a size marker. ***C***, Graphic representation of the fold-ratio of the sum of products 12 through 20 to the sum of products 10 and 11.

*EPT contributed panel **C** to this figure.

### 5.2.3 The V557L mutation in nsp12 counteracts the inhibitory effects of RDV in the template

We next asked whether such template-dependent inhibition provides a biologically relevant mechanism of action of RDV. To address this question we attempted to study possible neutralizing effects of known resistance conferring mutations. In nsp12, two amino acid substitutions have been associated with low-level resistance to RDV[251]. The effect of F480L is subtle and structural data do not suggest a direct effect on RNA synthesis. In contrast, the hydrophobic side chain of Val-557 is located close to the template opposite the incoming nucleotide[252]. Hence, a mutation at this position could conceivably affect nucleotide incorporation. We therefore expressed and purified the V557L mutant and studied its potential effect on the concentration of UTP required to overcome the obstacle imposed by the complementary RDV (Fig. 5.3). We compared WT RdRp with the V557L mutant. Increasing the concentrations of UTP gradually from 0.1 μM to 100 μM showed the following effects (Fig. 5.3*A*). The primary observation is that the UTP concentration required to overcome inhibition at position 10 and to generate the product at position 11 is lower with the Val-557 mutant (0.7 versus 4 μM for 50% incorporation, and 10 versus 50 μM for 90% incorporation of UTP by V557L and WT, respectively) (Fig. 5.3*B*). The associated steady-state kinetic parameters show that UTP incorporation is ~5-fold more efficient with the mutant enzyme (Appendix B, Table B1). The effect of V557L is specific to incorporation of UTP opposite RDV. Incorporation of the next nucleotide (ATP) is not significantly affected by the V557L mutant enzyme (Appendix B, Figure B3 and Table B1).

However, the increase in efficiency of UTP usage with the V557L mutant does not translate in increases in the amount of the full-length product (Fig. 5.3*A*). These findings suggest that regular nucleotide incorporations might be compromised, which is not unusual of enzymes that contain resistance-conferring mutations. Steady-state kinetic parameters show that the efficiency of ATP incorporation is ~3-fold reduced with the mutant enzyme (Appendix B, Table B2). However, it is important to note that the selectivity [$V_{max}/K_m$ (ATP) / $V_{max}/K_m$ (RDV-TP)] is almost identical for V557L and the wild-type enzyme. Thus, V557L does not show a resistance phenotype at the level of incorporation of RDV-TP. Moreover, V557L is also not significantly different from the wild-type in assays monitoring delayed chain-termination with either a single or multiple sites of incorporation for RDV-TP (Appendix B, Fig. B4). The collective data provide evidence to show

that the effect of V557L is specific to RDV embedded in the template, which in turn suggests that this type of inhibition is biologically relevant. Moreover, the S861G mutant specifically reduces delayed chain-termination and does not affect template-dependent inhibition of RNA synthesis (Appendix B, Fig. B5). However, this mutation is here newly described and it remains to be seen whether the corresponding virus is viable and may affect drug susceptibility.

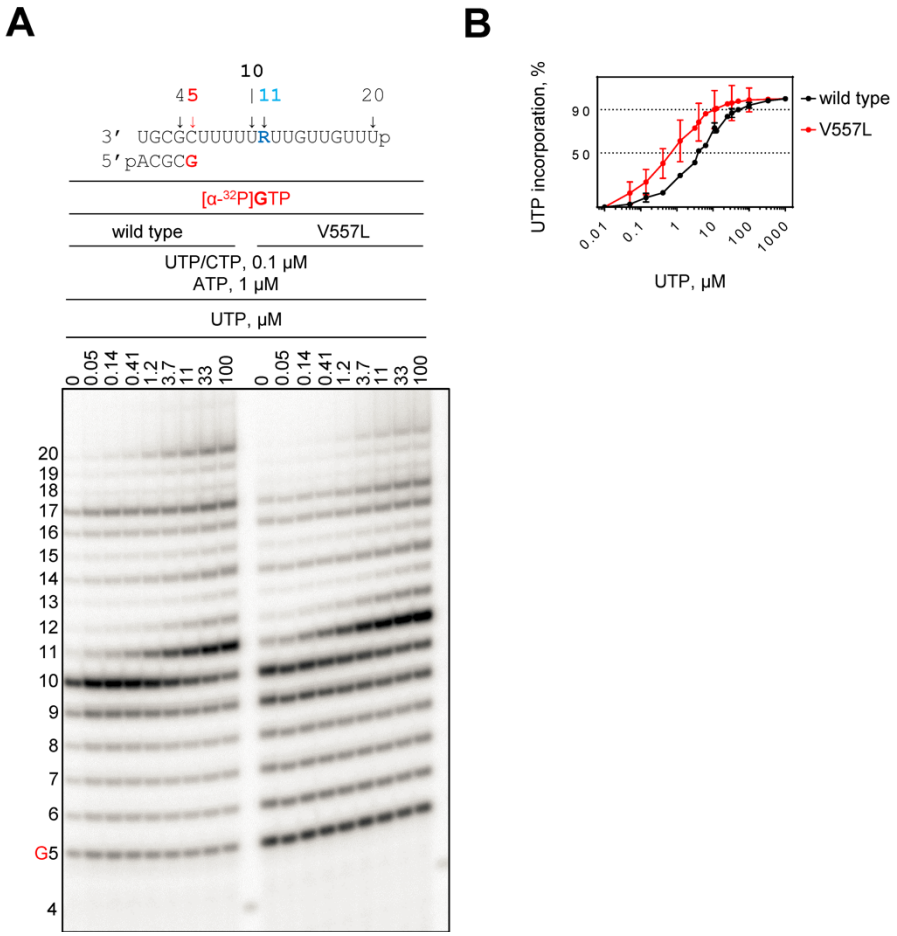


**Figure 5.3. RNA synthesis catalyzed by SARS-CoV-2 RdRp wild-type and the V557L mutant complex on Template R**. ***A***, RNA primer/template with template-embedded RDV at position 11 is shown on top. G5 indicates the incorporation of [α-$^{32}$P]-GTP opposite template position 5. Below the primer/template sequence is the migration pattern of the products of RNA synthesis catalyzed by SARS-CoV-2 RdRp complexes in the presence of RNA primer/template, $MgCl_2$, indicated concentrations of NTP cocktail supplemented with indicated concentrations of UTP after 30 minutes. "4" indicates the migration pattern of 5′-$^{32}$P-labeled 4-nt primer used here as a size marker. ***B***, Graphic representation of the percent UTP incorporation opposite RDV plotted as a function of UTP concentration.

*EPT contributed to this figure.

### 5.2.4 Modeling shows template RDV is significantly perturbed relative to A

Building on our previous models of the pre-incorporation state of the replicating SARS-CoV-2 nsp7/nsp8/nsp12 complex [49, 252], we found that RDV, when serving as template for the incoming UTP, is not properly positioned (Fig. 5.4). In the absence of any relaxation relative to the reference A-containing template, the 1′-CN has a significant clash with the backbone carbonyl of residue Ala-558. Allowing for minimization of RDV and the template overhang, the clash can be relieved, but base pairing between RDV and UTP is compromised. As a result, RDV functions as a poor template for the incoming NTP. Furthermore, translocation to the next template position may involve additional clashes, particularly between the 1′-CN and residue Thr-687. This model therefore provides a plausible explanation for data shown in Figure 2. However, the structural reasons for V557L resistance remain elusive and a fuller dynamic examination or structural data may be required.

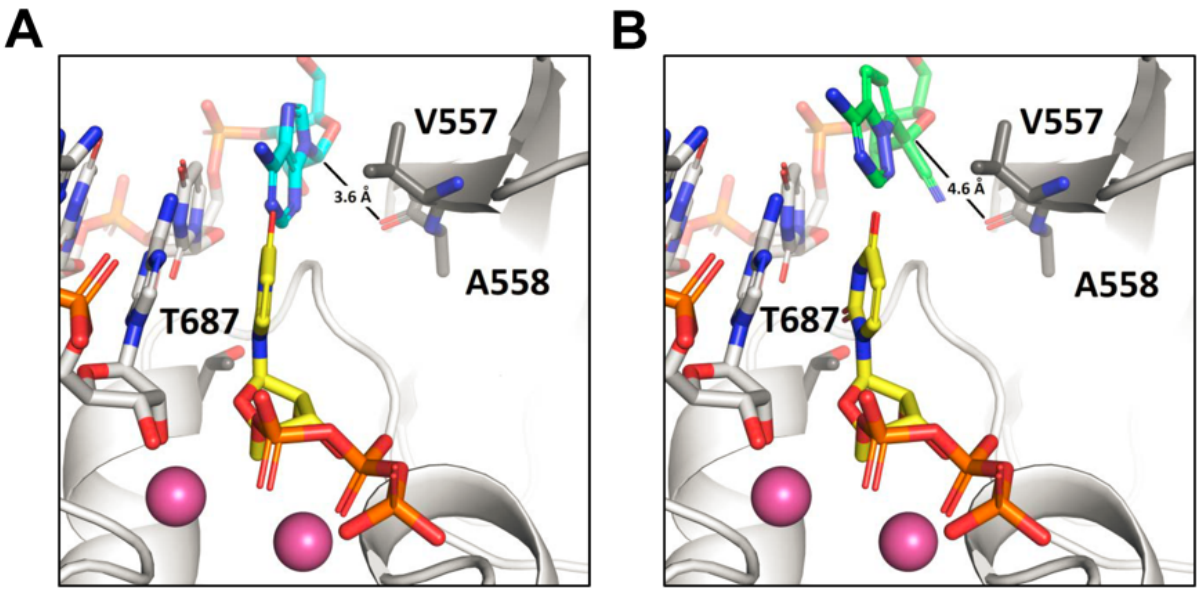


**Figure 5.4. Structural model of UTP incorporation with (*A*) adenosine (*cyan*) serving as the template base and (*B*) RDV (*green*) serving as the template base**. With respect to the optimal position seen with adenosine, RDV is significantly perturbed, shifting by ~1 Å, due to a clash between its 1′-CN and the protein backbone at residue Ala-558.

*JKP contributed this figure.

## 5.3 Discussion

The investigational nucleotide analogue prodrug RDV is a direct-acting antiviral that has been approved in several countries for the treatment of COVID-19 patients[374]. Previously, we initiated studies on the mechanism of action of RDV and demonstrated that RDV-TP is efficiently incorporated into the growing RNA chain by recombinant SARS-CoV-2 RdRp[49]. Inhibition of RNA synthesis is delayed and observed at position i+3, i.e. three residues downstream of the site of incorporation. However, higher concentrations of NTP pools can reduce the efficiency of delayed chain-termination, concomitantly enhancing read-through and full-length product formation[49, 50]. Efficient read-through may therefore yield a complete copy of the positive-sense RNA genome with embedded RDV residues. This negative-sense RNA is then utilized as a template for viral genome synthesis and the generation of RNA transcripts. It is currently unknown whether RDV exhibits inhibitory effects when present in the template. Using a biochemical approach, we have addressed this question directly and propose a model of the mechanism of action of RDV against SARS-CoV-2 RdRp that involves both RNA strands (Fig. 5.5).

The mechanism of inhibition during synthesis of the first RNA strand is adapted from our previous study[49]. In this model, RNA synthesis by SARS-CoV-2 RdRp is reduced to the polymerase, the primer strand and the template. The complex interactions between nsp7, nsp8, nsp12, RNA and other viral factors that are implicated in replication and transcription are not considered (*stage 1*). As RNA synthesis proceeds, RDV-TP competes with its natural counterpart ATP for incorporation opposite template U at a random position "i" (*stage 2*). Steady-state kinetics suggests that the efficiency of incorporation is three times higher with RDV-TP[49, 50], which is unusually efficient for a nucleotide analogue inhibitor. The presence of a 3′-hydroxyl group allows a nucleophilic attack on the next incoming nucleotide and no significant inhibition is seen at position i+1. Three additional nucleotides are incorporated before RNA synthesis is arrested at position i+3 (*stage 3*). Inhibitors of this type are commonly referred to as "delayed chain terminators", in contrast to obligate or classic chain terminators that lack the 3′-hydroxyl group and prevent further nucleotide additions at i+1[268]. Modeling suggested that a steric clash between the side chain of Ser-861 and the 1′-CN group of RDV blocks translocation of the RdRp complex into position i+4. This hypothesis was supported by experiments with the S861A mutant that

showed subtle reductions in efficiency of delayed chain-termination[43]. Here we demonstrate that the smaller S861G eliminates termination.

At this stage it is important to note that the steric clash does not represent an unsurmountable obstacle. Delayed chain termination is gradually reduced when increasing the concentration of the next incoming nucleotide. This effect is also shown here even with the bulkier S861P substitution. The reduction in termination efficiency coincides with an increase in read-through monitored as full-length RNA product synthesis. A possible explanation is that the increased NTP concentration shifts the translocational equilibrium from i+3 (pre-translocation) to i+4 (post-translocation), which liberates the nucleotide binding site. For HIV type 1 (HIV-1) reverse transcriptase (RT), we developed site-specific footprinting techniques that demonstrated such nucleotide-dependent translocation[305]. Seifert and colleagues recently applied a single molecule approach, based on magnetic tweezers, to study the function of SARS-CoV-2 RdRp and its inhibition with nucleotide analogs[375]. The authors found that the incorporated RDV causes enzyme pausing at high NTP concentrations, whereas termination was not observed. The full-length products seen in this study are equivalent to read-through events and full-length product formation seen in our experiments. It is therefore tempting to predict that the S861G mutant will eliminate or reduce pausing. Each of the aforementioned studies provide evidence to suggest that synthesis of the first RNA strand may continue to completion especially in the presence of high concentrations of NTPs. We determined that NTP concentrations as low as 10 μM cause ~90% read-through.

The 3′-5′ proofreading ExoN activity of the replication complex plays another important role in the generation of RNA strands with embedded RDV residues. ExoN(-) MHV shows a ~ 5-fold increase in RDV susceptibility; however, potent inhibition was still seen with an intact ExoN [251]. This partial protection from 3′-5′ proofreading may therefore preserve RDV residues in complete copies of the first RNA strand (*stage 5*). This assumption provides the basis for a template-dependent inhibition mechanism. Here we show that incorporation of UTP at position i opposite RDV is indeed compromised. UTP concentrations of ~50 μM are required to bypass this obstacle (*stage 6*). This concentration is significantly lowered with the V557L mutant, which provides a mechanism for drug resistance[251]. Val-557 is located in close proximity to the

incorporated RDV. It is therefore conceivable that the V557L facilitates incorporation of UTP through repositioning of the template strand. The effect of V557L is specifically seen when RDV is present in the template. WT and V557L mutant do not show significant differences regarding selective incorporation of RDV-TP or delayed chain termination.

The link between the newly discovered template-dependent inhibition and a resistance-conferring mutation suggests that this mechanism is biologically relevant. However, it is important to note that neither V557L nor F480L or any other RDV resistance associated mutations in SARS-CoV-2 have been reported at this point. The selection of the structural equivalent V553L MHV required a high number of passages and RNA levels in the presence of drug are still lower than RNA levels in the absence of drug[251]. These results indicate a high barrier to the development of resistance, which is likely due to a fitness deficit associated with this mutation. In agreement with these observations, we demonstrate the V557L in SARS-CoV-2 RdRp diminishes efficiency of regular nucleotide incorporations and neutralizes its advantageous effects on UTP incorporation opposite RDV. Hence, the barrier to the selection of V557L might be even higher for SARS-CoV-2. Moreover, incorporation of the adjacent NTP, immediately downstream of the newly added UTP is likewise inhibited and the effect of V557L is less pronounced at this position (*stage 7*). NTP concentrations required to overcome this obstacle exceed 100 µM and rescue of RNA synthesis remains incomplete even at higher NTP concentrations (*stage 8*). Finally, we note that template-dependent inhibition mechanisms have also been demonstrated with other nucleotide analogue inhibitors[154, 164, 268, 269].

In conclusion, RDV can inhibit RNA synthesis by SARS-CoV-2 RdRp when incorporated in the primer strand and when present in the template strand. The two distinct modes of inhibition can be linked to interactions between the 1′-CN group of the nucleotide analogue and conserved residues in nsp12. The side chain of Ser-861 causes a steric clash with the incorporated RDV and inhibition is seen at position i+3. The backbone of Ala-558 causes steric problems when UTP is incorporated opposite RDV in the template and inhibition is seen at positions i and i+1. The neighboring resistance-associated mutation V557L counteracts this effect. The challenge is to determine which mechanism is dominant. Delayed chain-termination is solely seen at low concentrations of NTPs; however, the highly efficient use of RDV-TP can lead to multiple

incorporation events, e.g. along polyU-tracts, that can amplify inhibition (Appendix B, Fig. B4). This effect has been demonstrated with various RdRp complexes[49, 267, 333, 335]. Template-dependent inhibition can be observed at higher NTP concentrations, but this mechanism relies on a certain degree of protection from proofreading that retains RDV in copies of the viral genome. Biochemical approaches do often not capture the complexity of antiviral effects in a cellular environment. It is therefore important to continue to monitor the emergence of resistance in attempts to link specific amino acid substitutions to specific inhibition pathways. This work helps to guide drug development efforts and the design of future structural or kinetic studies that address these problems.

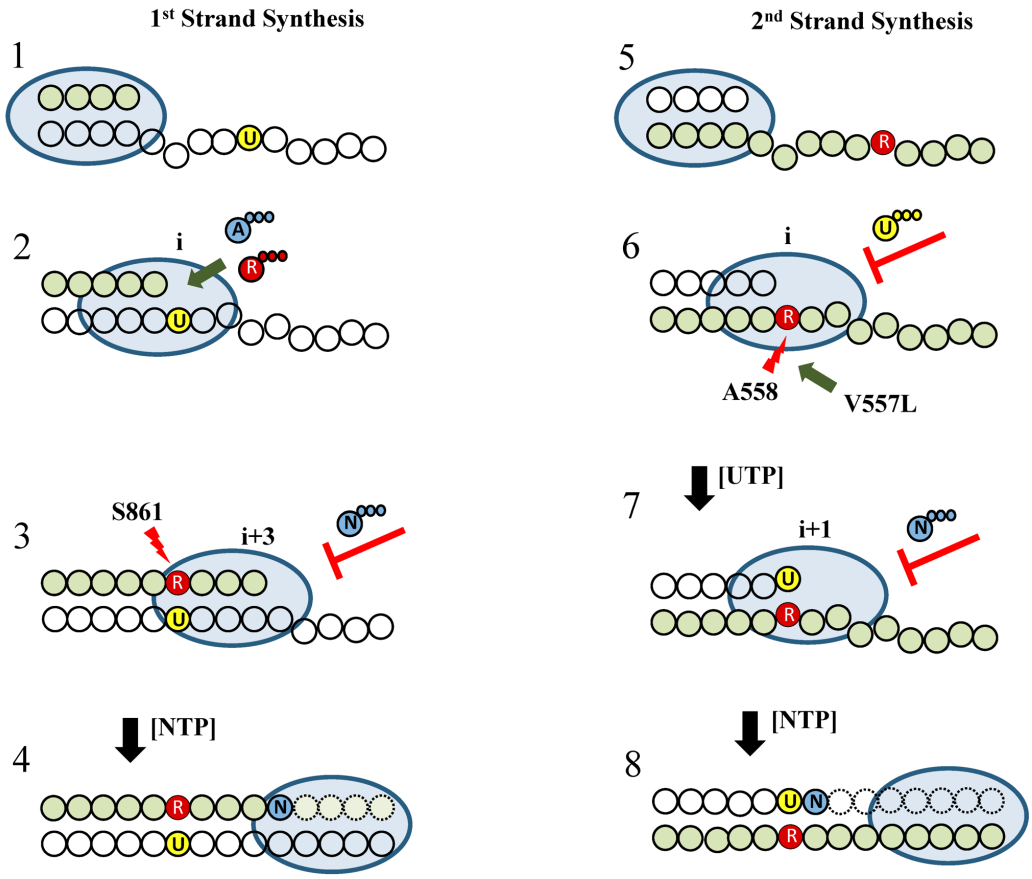


**Figure 5.5. Model of the mechanism of action of RDV against SARS-CoV-2 RdRp**. *Left*, a model for inhibition during synthesis of the first RNA strand is adapted from our previous study[49]. The priming strand is shown with green circles, colorless circles represent residues of the template, and the light blue oval represents the RdRp complex (*stage 1*). RDV-TP (R, *red*) competes with ATP (A, *blue*) for incorporation opposite template U labeled yellow (*stage 2*). RNA synthesis is terminated after the addition of three more nucleotides. This effect is referred to as "delayed chain-termination" as a result of a steric clash between Ser-861 (*red arrow*) and the 1′-CN group of the incorporated RDV (*stage 3*). Higher concentrations of NTP can overcome this effect and read-through facilitates formation of full-length RNA products (*stage 4*). This mechanism retains RDV residues in the primer strand that is later used as a template (*stage 5*). Incorporation of UTP opposite RDV is compromised due to a steric clash between Ala-558 (*red arrow*) and RDV's 1′-CN group (*stage 6*). Higher concentrations of the next nucleotide can overcome inhibition. This concentration is further reduced with the resistance-associated Val-557 mutant enzyme (green arrow). NTP incorporation at the adjacent position is likewise inhibited (*stage 7*). This obstacle is also partially overcome with higher NTP concentrations (*stage 8*).

## Chapter 6: Molnupiravir promotes SARS-CoV-2 mutagenesis via the RNA template

This chapter contains content from the following source, republished with permission:

- Gordon CJ, Tchesnokov EP, Schinazi RF, and Götte M. Molnupiravir promotes SARS-CoV-2 mutagenesis via the RNA template. J Biol Chem. 2021; 297:100770. © the authors.

Author contributions

M. G., C. J. G., and E. P. T. conceptualization; C. J. G., E. P. T., and R. F. S. methodology; E. P. T. software; M. G., C. J. G., and E. P. T. validation; M. G., C. J. G. and E. P. T. formal analysis; C. J. G. and E. P. T. investigation; M. G. and R. F. S. resources; M. G., C. J. G. and E. P. T. data curation; M. G. and E. P. T. writing-original draft; M. G., C. J. G., E. P. T. and R. F. S. writing-review and editing; M. G., C. J. G., and E. P. T. visualization; M. G. supervision; M. G. project administration; M. G. funding acquisition.

*Experiments performed by other authors have been identified in figure legends.

Funding

This study was supported by grants to M. G. from the Canadian Institutes of Health Research (CIHR, grant number 170343), and from the Alberta Ministry of Economic Development, Trade and Tourism by the Major Innovation Fund Program for the AMR – One Health Consortium.

## 6.1 Introduction

The discovery and development of potent antiviral drugs for the treatment of infection with severe acute respiratory syndrome coronavirus 2 (SARS-CoV-2) remains challenging. The virus can cause severe forms of coronavirus disease 2019 (COVID-19) that require hospitalization. Remdesivir (RDV) targets the viral RNA-dependent RNA polymerase (RdRp) and is currently the only antiviral agent approved by the US Food and Drug Administration[49, 376]. Antibody therapies were granted emergency use authorization for the treatment of outpatients who are at high risk for progressing to severe disease and/or hospitalization[377]. Both RDV and antibody therapies are intravenously administered, which limits their utility especially for outpatient use. Oral drugs that can be used much earlier in the disease are under investigation and molnupiravir (MK-4482/EIDD-2801) is perhaps the most advanced candidate compound in this category[378]. Molnupiravir is a prodrug of β-D-$N^4$-hydroxycytidine (NHC, EIDD-1931). It is intracellularly metabolized to its triphosphate form (NHC-TP) that can serve as substrate for RNA polymerases[222, 223]. NHC shows a broad spectrum of antiviral activities against several positive- and negative-sense RNA viruses[222, 223, 227, 379-382]. More recent studies focused on the development of molnupiravir for the treatment of infection with influenza and coronaviruses[113, 229, 383-385].

NHC potently inhibits MERS-CoV, SARS-CoV and SARS-CoV-2 with $EC_{50}$ values in the submicromolar range, depending on the specific cell type[229]. Molnupiravir was also shown to inhibit SARS-CoV-2 replication in humanized mice[229, 385]. Treatment 24 hours after exposure to the virus was more efficient than treatment 48 hours after virus exposure, and treatment before virus exposure shows the strongest antiviral effects. The large body of preclinical data justified human clinical trials that are presently ongoing although there are concerns about its mammalian cell mutagenic potential[222, 227, 386-389]. Molnupiravir was evaluated in a phase 1 clinical study in healthy volunteers, which demonstrated good tolerability and no apparent signs of adverse events after a short duration of treatment and follow-up[390]. Knowledge on the mechanism of action is largely derived from cell culture studies. Unlike RDV that inhibits RNA synthesis, molnupiravir seems to act as a mutagen[113, 223, 229, 382]. Exposure to NHC increases G to A and C to U transition mutations in MHV, MERS-CoV, and SARS-CoV-2[229, 382]. Increases in mutation frequencies will ultimately yield non-functional genomes, which explains the antiviral effect. Other broad-spectrum antiviral agents, such as ribavirin or favipiravir have also been characterized as

mutagenic nucleoside analogs although the potency of these compounds is generally low with $EC_{50}$ values in the higher micromolar range[45, 129, 157]. The proofreading exonuclease of coronaviruses can excise incorporated nucleotide analogs and diminish the inhibitory effects[159, 160], but recent data have shown that NHC is resistant to this proofreading activity[382]. However, it is currently not known how the interaction between the drug and RdRp determines drug potency and the nature of the observed mutations.

Herein, we employed a biochemical approach to study the mechanism of action of molnupiravir. We expressed and purified the RdRp complex with non-structural proteins nsp7, nsp8 and nsp12, and studied the efficiency of incorporation of NHC-TP in relation to natural NTP pools. NHC-TP is preferentially incorporated as a C-analogue. When the monophosphate (NHC-MP) is embedded in the template, it base pairs with either GTP or ATP. While the incorporation of GTP causes subtle inhibition of RNA synthesis, mismatch extension with the incorporated ATP is not inhibited and leads to transition mutations. The collective data presented in this study provide a model that explains the antiviral effects of molnupiravir and NHC.

## 6.2 Results

### 6.2.1 Selective Incorporation of NHC-TP by SARS-CoV-2 RdRp

Biochemical data on NHC-TP as a substrate for RNA polymerases are scarce[237]. It has been shown that the respiratory syncytial virus RdRp complex accepts NHC-TP as a substrate for incorporation opposite template G. The incorporated NHC-MP does not act as a chain terminator in this case[223]. Human mitochondrial DNA-dependent RNA polymerase (h-mtRNAP) can use NHC-TP as C- or U-analogue[237]. Inhibitory effects following incorporation have not been reported. Here we measured steady-state-kinetic parameters for incorporation of NHC-TP by SARS-CoV-2 RdRp (Fig. 6.1). We have employed the same biochemical approach for RDV-TP, other nucleotides and other RdRp complexes, which facilitates comparisons[49, 50, 267, 325, 337, 391]. RNA synthesis was monitored with a short model primer/template after addition of a single radio-labeled [α-$^{32}$P]NTP (Fig. 6.1*A*). The preference for a natural nucleotide over the analogue is calculated as a ratio of their incorporation efficiencies. The efficiency of incorporation of the natural nucleotide over the efficiency of incorporation of the analogue provides a selectivity value. SARS-CoV-2 RdRp shows a 30-fold preference for CTP over NHC-TP (Fig. 6.1*B*). Selectivity

values follow the order GTP (12,841) > ATP (424) > UTP (171) > CTP (30), which shows that all NTPs are more efficiently incorporated than the NHC-TP. The data suggest that competition with CTP is most efficient.

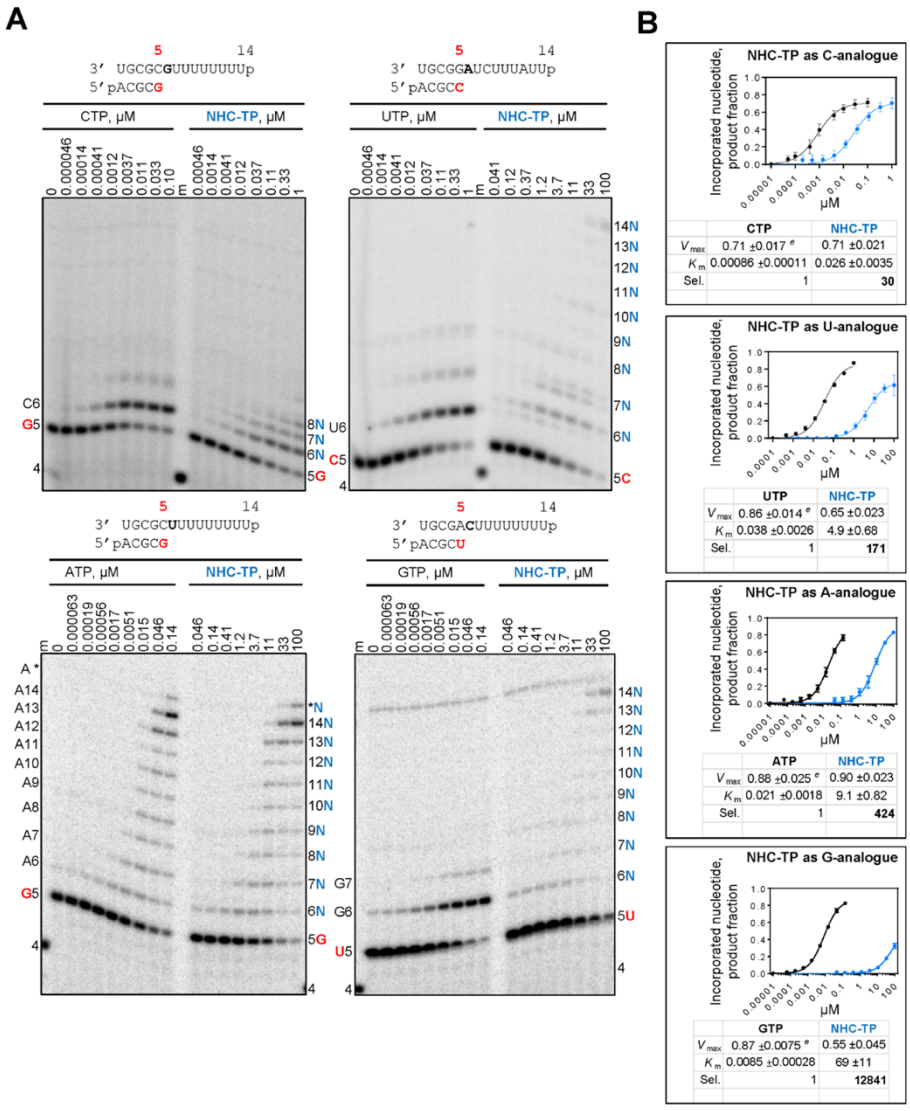


**Figure 6.1. Efficiency of NHC-TP incorporation**. ***A***, migration pattern of the products of RNA synthesis catalyzed by SARS-CoV-2 RNA-dependent RNA polymerase along the RNA primer/templates as shown above the panels. The sequences support incorporation of NHC-monophosphate as either a C-, U-, A-, or G-analogue at position 6. G, U, or C indicates incorporation of [α-$^{32}$P]G-, [α-$^{32}$P]U-, or [α-$^{32}$P]CTP at position 5 (red). N indicates incorporation of NHC-monophosphate. Asterisk indicates terminal transferase activity. A 5′-$^{32}$P-labeled 4-nt primer (4) serves as a size marker (m). ***B***, graphical representation of the data shown in A. Fitting the data points to Michaelis–Menten function and the calculation of the selectivity values. Sel., selectivity for a nucleotide substrate analogue is calculated as the ratio of the $V_{max}/K_m$ values for NTP over NTP analogue. Error bars illustrate standard deviation of the data. ±, standard error of the fit. All reported values have been calculated on the basis of an 8-data point experiment repeated at least three times.

### 6.2.2 Extension of incorporated NHC-MP

We next monitored RNA synthesis following incorporation of NHC-MP opposite template G at position 6 (Fig. 6.2). The same concentrations of CTP and NHC-TP generate different incorporation patterns at position 6. For CTP, most of the primer is converted to yield the 6-nt product with minimal formation of larger products. Incorporation of CTP opposite subsequent other bases would lead to mismatch formation and is negligible under these conditions. For NHC-TP, the both a 6-nt product and a 7-nt product are formed, which points to a certain degree of ambiguous base pairing. Since both products are formed in the absence of ATP and UTP (lane 0), the 7-nt product illustrates NHC misincorporation as a U-analog opposite AMP in the template. In the presence of increasing concentrations of ATP and UTP that allow full-length product formation, the primer is almost completely extended regardless of whether CMP or NHC-MP was incorporated (Fig. 6.2, *left* CTP and NHC-TP panels). This shows that the incorporated NHC-MP is efficiently extended. Higher concentrations of ATP and UTP reduce mismatch formations and generate similar levels of full template-length products (Fig. 6.2, *right* CTP and NHC-TP panels). Moreover, similar levels of terminal transferase activity are also seen at high concentrations of ATP and UTP regardless of whether CMP or NHC-MP are being extended from a 6-nt product[392].

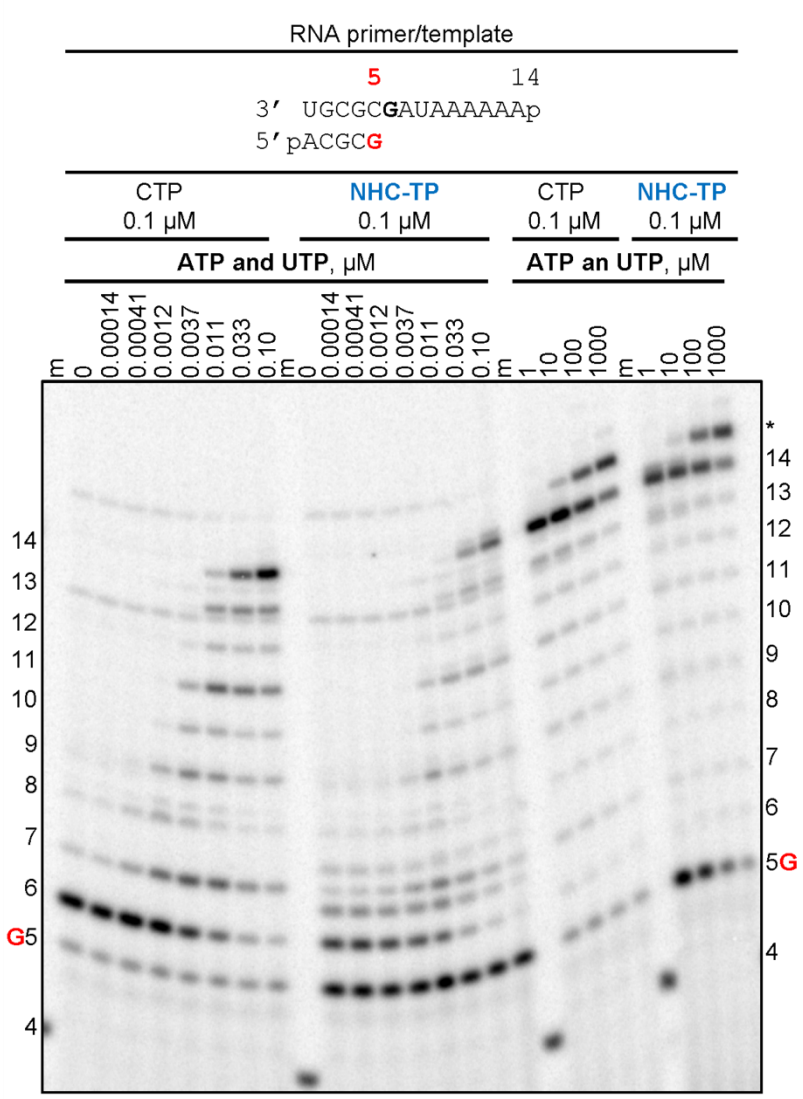


**Figure 6.2. SARS-CoV-2 RNA-dependent RNA polymerase–catalyzed RNA synthesis following incorporation of NHC-monophosphate**. Migration pattern of the products of RNA synthesis catalyzed by SARS-CoV-2 RdRp complex along the RNA primer/template as shown at the top of the panel. RNA primer/template supports a single incorporation event of CMP or NHC-monophosphate as a C-analogue at position 6. G indicates incorporation of [α-$^{32}$P]-GTP at position 5. A 5′-$^{32}$P-labeled 4-nt primer (4) serves as a size marker (m). Asterisk indicates products of the terminal transferase activity.

### 6.2.3 RNA synthesis using NHC-MP embedded in the template

In the absence of significant RNA synthesis inhibition, the copy of the viral genome is likely synthesized in full length and contains embedded NHC-MP residues. Hence, efficiency and fidelity of RNA synthesis may be affected at a later stage when this strand is utilized as a template. To address this question, we have synthesized an RNA template with a single NHC-MP using T7

RNA polymerase (Appendix C, Fig. C1). For comparative purpose, we generated two model RNAs with either a single CMP (Template "C") or a single NHC-MP (Template "N") at position 11. To test whether an incorporated NHC-MP still acts as a C-analogue when present in the template we monitored RNA synthesis in the presence of increasing concentrations of GTP (Fig. 6.3). Incorporation of GTP opposite CMP (Template "C") is very efficient even at concentrations as low as 0.015 μM. In contrast, the incorporation of GTP opposite NHC-MP is less efficient and concentrations of 0.41 μM (or 27-fold higher) GTP are required to completely convert 10-nt product to 11-nt product. Note that, even though RNA synthesis past 11-nt product along template "C" is not very efficient; the full-length products are formed concomitantly with GTP incorporation at position 11. Hence, the full-length product formation depends solely on ATP concentration which is kept here low at 0.030 μM in order to reduce misincorporations. Another caveat is that concentrations of GTP above 4 μM results in U:G misincorporation on both templates (Fig. 6.3, asterisks). Full-length product formation along template "N" is less evident than with template "C", suggesting that overall RNA synthesis might be inhibited. The accumulation of 11-nt product points to a specific site of inhibition.

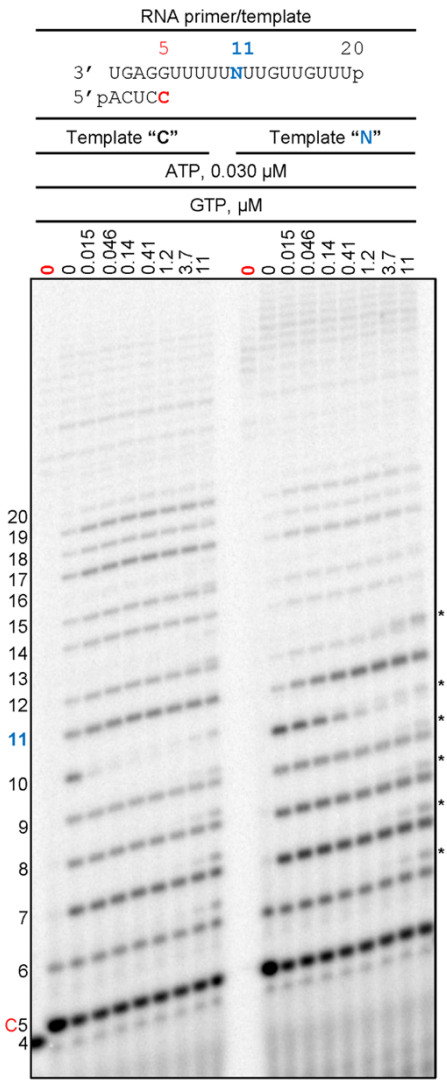


**Figure 6.3. RNA synthesis with NHC-MP in the template strand.** Migration pattern of the reaction products catalyzed by SARS-CoV-2 RNA-dependent RNA polymerase. The template contains an embedded NHC-MP at position 11 (Template "N") or CMP (Template "C"). Reactions with [α-$^{32}$P]-CTP as the only NTP are indicated by "0" in red. Figure notations are as in Figure 6.1. Asterisks indicate products of GTP misincorporation opposite U in the template.

*EPT contributed this figure.

To avoid the confounding effect of nucleotide misincorporations, we monitored RNA synthesis also in the presence of the other required NTPs. For template N, increasing concomitantly the concentrations of GTP and ATP yields transiently an 11-nt product that is almost completely converted into full-length product at NTP concentrations as low as 10 μM (Fig. 6.4, panel "ATP and GTP"). The intermediate 11-nt product is not seen with template "C", which shows specific inhibition by NHC-MP in the template. The 11-nt product is also not seen when increasing the concentration of ATP in the absence of GTP (Fig. 6.4, panel "ATP"), which demonstrates that incorporation of GTP opposite NHC-MP is the cause for inhibition. Thus, while both GTP and ATP can be incorporated opposite NHC-MP with similar efficiencies, only GTP causes a subtle inhibitory effect that can be overcome by increasing NTP concentrations. We have also shown that neither CTP nor UTP are incorporated opposite NHC-MP (Appendix C, Fig. C2). Taken together, NHC-MP embedded in the template shows ambiguous base-pairing with GTP and ATP. At the level of incorporation, NHC-TP shows a preference for template G.

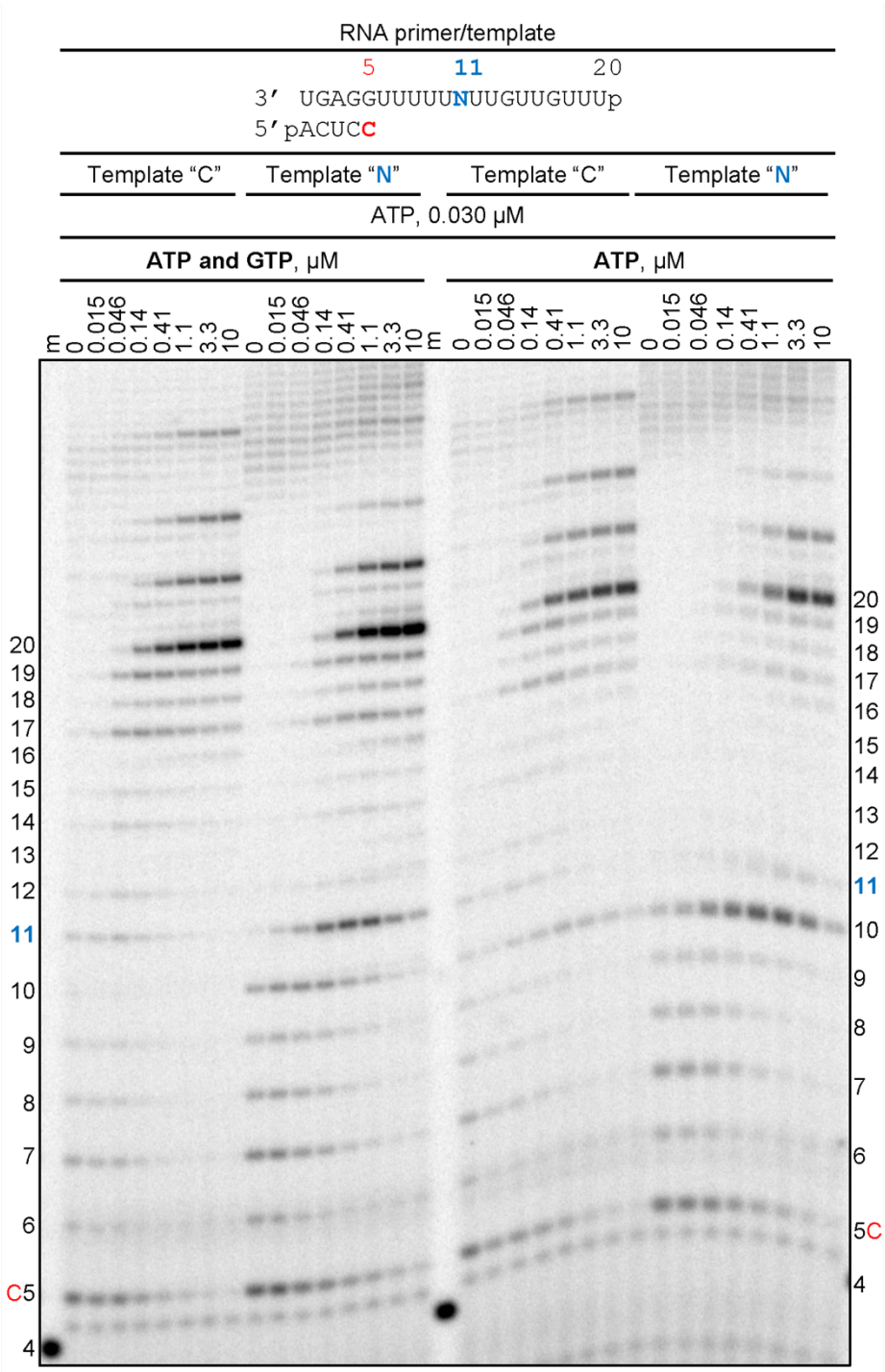


**Figure 6.4. Mechanism of template-dependent inhibition of SARS-CoV-2 RNA-dependent RNA polymerase complex**. Figure notations are as in Figure 6.2. Signal accumulation at position 11 illustrates inhibition of nucleotide incorporation right after template-embedded β-D-$N^4$-hydroxycytidine 5′-monophosphate, which can be overcome with increasing concentrations of NTP.

## 6.3 Discussion

The broad-spectrum antiviral agent molnupiravir, a prodrug of NHC, is currently being evaluated in advanced clinical trials for the treatment of SARS-CoV-2 infections[390]. The drug is orally bioavailable and can be given to outpatients early in the disease with the potential to reduce hospitalizations. Preclinical data in cell culture revealed a dose-dependent increase in G to A and C to U transition mutations that correlated with increases in antiviral effects against coronaviruses[229, 382]. Molnupiravir is therefore classified as a mutagenic nucleotide analog. Here we studied the underlying biochemical mechanisms with the purified RdRp complex of SARS-CoV-2. Based on our data, we developed a model that describes effects on both efficiency and fidelity of RNA synthesis (Fig. 6.5).

Steady-state kinetic measurements demonstrated that NHC-TP acts predominantly as a C-analogue and is preferentially incorporated opposite template G (Fig. 6.5*A*, *step 1*). Selective incorporation, defined as efficiency of incorporation of CTP over efficiency of incorporation of NHC-TP, is relatively low with a value of 30. By comparison, the selectivity value of RDV-TP is below one, suggesting that RDV-TP is more efficiently incorporated than its natural counterpart ATP[49, 50]. However, earlier studies have shown that NHC, in contrast to RDV, is resistant to the coronavirus-associated proofreading exonuclease activity[382]. For hepatitis C virus RdRp, the selectivity value of the 5′-triphosphate metabolite of sofosbuvir is also relatively low (45-fold), but in the absence of a proofreading activity, sofosbuvir is an efficient inhibitor of HCV replication[287]. Thus, the limited opportunities for incorporation of NHC-TP may still have an impact on efficiency and fidelity of viral genome replication.

When NHC-MP is present in the template, base pairing is more ambiguous and both the incoming GTP or ATP are accepted with no significant preference (Fig. 6.5*A*, *step 1*). Like other mutagenic nucleotides, NHC-TP likely exists in different tautomeric forms that affect base pairing[128]. The hydroxylamine form acts like C and enables base pairing with G, whereas the oxime form (C=NOH) acts like U and allows base pairing with A (Fig. 6.5*B*). Our data suggest that the NHC-TP substrate exists predominantly in its hydroxylamine form and acts like CTP; however, when present as NHC-MP in the template, both tautomeric forms seem to co-exist and act like CTP or UTP, favoring incorporation of GTP and ATP, respectively.

Incorporation of GTP opposite NHC-MP inhibits incorporation of the next incoming nucleotide. Increasing NTP concentrations to 10 μM can overcome this obstacle (Fig. 6.5*C*, *steps 3* and *4*). This inhibitory effect on RNA synthesis is not observed with ATP (Fig. 6.5*C*, *steps 3′* and *4′*). Instead, incorporation of ATP yields a G to A transition mutation via G:NHC-TP and NHC-MP:A base pairing or short G:NHC:A (Fig. 6.5*D*). C to U transitions are realized if the positive sense viral RNA contains a C via C:G:NHC:A:U. Thus, the preference for the G:NHC:A pattern is necessary and sufficient to explain the higher frequencies of G to A and C to U transition mutations in the presence of molnupiravir or NHC. The same mechanism may also apply to influenza virus that shows the same transition mutations in the presence of the drug, but not to respiratory syncytial virus that shows a different pattern[113, 223]. However, biochemical data are generally lacking, and it will be important to study potential differences among various viral and cellular polymerases that utilize NHC-TP as substrate. In the present study, we have shown that the incorporated NHC-MP can either inhibit RNA synthesis in G:NHC:G, or act as a mutagen in G:NHC:A. The mutagenic effect seems to be dominant given that increasing NTP concentrations can overcome G:NHC:G inhibition at relatively low concentrations of GTP. In addition, considering that intracellular concentration of ATP are several-fold higher than that of GTP[362], the G:NHC:A pairing may also be favored in a cellular environment.

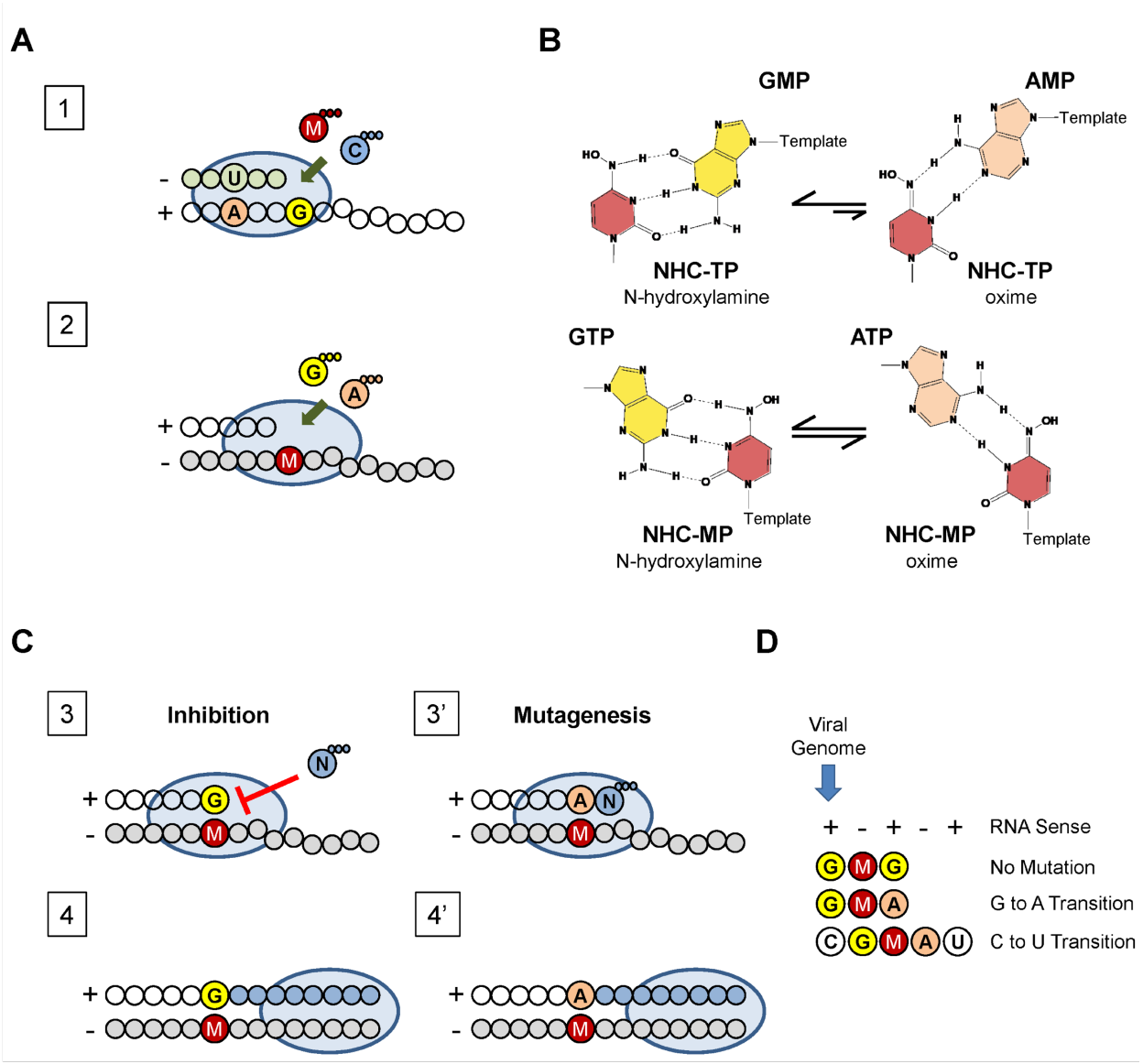


**Figure 6.5. Mutagenesis model of NHC against SARS-CoV-2**. ***A***, schematic representation of SARS-CoV-2 RNA-dependent RNA polymerase (*oval*)-mediated nucleotide incorporation into RNA primer (*gray circles*)/template (*white circles*). Plus and minus signs indicate RNA sense. Letters A, C, G, and U refer to natural nucleotide bases. Letter M refers to molnupiravir. Three small circles refer to a triphosphate moiety of the NTP. ***B***, alternative base pairing of NHC base moiety is supported by its tautomerization. The N-hydroxylamine form is dominant when NHC-TP is the substrate, whereas both the N-hydroxylamine and the oxime form are available when NHC-MP is embedded in the template. ***C***, mechanism of viral inhibition and mutagenesis by template-embedded NHC-MP. Blue circles illustrate NTP incorporation past NHC-MP in the template. ***D***, summary of NHC-mediated inhibitory and mutagenic effects on viral replication.

*MG contributed to this figure.

## Chapter 7: Efficient incorporation and template-dependent polymerase inhibition are major determinants for the broad-spectrum antiviral activity of remdesivir

This chapter contains content from the following source, republished with permission:

- Gordon CJ[#], Lee HW[#], Tchesnokov EP[#], Perry JK, Feng JY, Bilello JP, Porter DP, and Götte M. Efficient incorporation and template-dependent polymerase inhibition are major determinants for the broad-spectrum antiviral activity of remdesivir. J Biol Chem. 2022; 298:6785-6797. © the authors.

Author Contributions

C. J. G., H. W. L., E. P. T., and J. K. P. investigation; C. J. G. and H. W. L. validation; C. J. G., H. W. L., E. P. T., J. K. P., and M. G. formal analysis; C. J. G., H. W. L., E. P. T., and J. K. P. visualization; C. J. G., H. W. L., E. P. T., and M. G. writing–original draft; J. K. P., J. Y. F., J. P. B., D. P. P., and M. G. writing–review and editing; J. Y. F., J. P. B., and D. P. P. resources; M. G. conceptualization; M. G. methodology; M. G. supervision; M. G. funding acquisition.

[#] These authors contributed equally to this work.

* Experiments performed by other authors have been identified in figure legends.

Funding

This study was supported by grants to M. G. from the Canadian Institutes of Health Research (CIHR, grant number 170343) and from the Alberta Ministry of Jobs, Economy and Innovation by the Major Innovation Fund Program for the AMR – One Health Consortium. M. G. received funding from Gilead Sciences in support for studies on the mechanism of action of remdesivir.

## 7.1 Introduction

The coronavirus disease 2019 (COVID-19) caused by severe acute respiratory syndrome coronavirus 2 (SARS-CoV-2) revealed the importance of broad-spectrum antivirals as the first line of defense in a pandemic[3, 393]. Vaccines that effectively protect against severe COVID-19 were developed in less than a year after the World Health Organization (WHO) declared a pandemic in March 2020[394-397]. Antibody therapies, directed specifically against SARS-CoV-2, were also developed in a relatively short time and the first antiviral drug approved for the treatment of COVID-19 was the nucleotide analog prodrug remdesivir (RDV)[398]. Its broad spectrum of antiviral activity was described in earlier pre-clinical studies[251, 253, 254, 257, 267, 333-335, 352, 372]. RDV is a 1′-cyano modified C-adenosine monophosphate prodrug that targets the RNA-dependent RNA polymerase (RdRp) of a diverse panel of RNA viruses, including coronaviruses[240, 241, 251, 252, 257]. In 2019, prior to the COVID-19 pandemic, RDV was tested in a randomized clinical phase 3 trial for the treatment of Ebola virus disease[242]. Although the clinical efficacy of RDV against Ebola virus disease is inferior to two antibody therapies, its human safety data became available and this enabled RDV compassionate use in January 2020 to treat COVID-19 patients[399].

Clinical studies of RDV for the treatment of COVID-19 have shown a shortened time to recovery with an unclear effect on mortality[400, 401]. RDV is intravenously administered and is therefore limited to patients under supervised medical care. In general, oral antiviral drugs would allow earlier initiation of treatment in a broader patient population which may reduce the risk of progression to more severe disease outcomes, not only in the context of infection with coronaviruses but potentially for the treatment of other viral infections. The development of oral broad-spectrum antiviral drugs is therefore critical to public health and pandemic preparedness. Successful efforts in this field require a better understanding of biochemical mechanisms that translate to antiviral activity. RDV shows antiviral activity against human positive-sense RNA viruses including members of *Coronaviridae* (SARS-CoV, Middle Eastern respiratory syndrome, MERS-CoV, and SARS-CoV-2)[251, 252] and the *Flaviviridae* (HCV)[240], as well as nonsegmented negative-sense RNA viruses including members of the *Filoviridae* (Zaire ebolavirus [Ebola virus, EBOV]), *Pneumoviridae* (respiratory syncytial virus [RSV]), and *Paramyxoviridae* (Nipah virus [NiV])[257]. However, antiviral activity against segmented negative-sense RNA viruses is less pronounced or not significant, as shown with members of the *Arenaviridae* (Lassa virus [LASV]),

the *Orthomyxoviridae* (influenza [Flu] virus), and *Nairoviridae* (Crimean-Congo hemorrhagic fever virus [CCHFV])[240, 257].

Here, we expressed and purified representative RdRp enzymes or complexes associated with these different families of RNA viruses and studied biochemical mechanisms of RDV-mediated inhibition of RNA synthesis to better understand the molecular requirements for antiviral effects. Previous studies with purified SARS-CoV, MERS-CoV and SARS-CoV-2 RdRp complexes have shown that the triphosphate form of RDV (RDV-TP) is 2-3 times more efficiently incorporated than its natural counterpart ATP[43, 49, 50, 261]. Inhibition is not seen immediately downstream of the site of RDV-monophosphate (MP) incorporation "i", it is rather seen at position "i+3" following the addition of three more nucleotides[49, 50]. This pattern is consistent with the definition of "delayed chain-terminators" that inhibit nucleotide incorporation events distant from the site of incorporation [402, 403]. Per definition, "termination" is not necessarily absolute and may be overcome with longer reaction times or increasing NTP concentrations[267, 268, 335, 402-407]. For Ebola RdRp, it has been shown that delayed chain-termination with RDV-TP is in fact absolute at position i+5[267]. For SARS-CoV-2 RdRp, it has been demonstrated that higher NTP concentrations can overcome inhibition at "i+3"[43, 49, 198, 263, 266, 408]. Others have therefore used a different terminology and refer to "delayed translocation"[263], “delayed chain extension”[263], “delayed stalling"[266], “delayed intervention"[264], or enzyme "pausing"[43, 198, 264, 409]. “Pausing” has also been observed on long templates that better mimic the RNA genome[198]. Most importantly, continuation of RNA synthesis would yield newly synthesized RNA strands with embedded RDV-MP residues and these RNAs will later serve as templates. We have recently shown that incorporation of UTP opposite the complementary RDV-MP provides a second opportunity for inhibition[265]. We now demonstrate that this template-dependent inhibition of RNA synthesis is observed across a diverse panel of viral polymerases. However, efficient incorporation of RDV-TP is a prerequisite for downstream inhibition of RNA synthesis and its translation into antiviral activity.

## 7.2 Results

### 7.2.1 Selective Incorporation of RDV-TP

To address the differences seen in the antiviral activity of RDV against a diverse spectrum of virus families, we compared the efficiency and pattern of inhibition of recombinant RdRp enzymes or enzyme complexes representing members of relevant families of viruses, and for which antiviral activity data were available (Table 7.1). Partial biochemical data were available for SARS-CoV, MERS-CoV, SARS-CoV-2, EBOV, and RSV RdRp complexes. Here, we included polymerases from HCV and NiV that are also sensitive to RDV, LASV that is less sensitive to RDV, and influenza B (FluB) and CCHFV that are not sensitive to RDV in antiviral assays. RNA synthesis was monitored with short primer/templates mimicking random elongation complexes as previously described[49, 50, 265, 267, 391]. We first determined the steady-state kinetic parameters for RDV-TP incorporation for each RdRp and normalized the values to the rates of incorporation of ATP. The enzyme concentration is the same in both cases and therefore cancels out during the normalization. The ratio of efficiency of single incorporations of ATP over RDV-TP defines the selectivity, which is a unitless parameter that facilitates comparisons between enzymes. Selectivity is less than 1, if incorporation of the analog is more efficient than incorporation of its natural counterpart.

Table 7.1 Selective incorporation of RDV-TP and antiviral activity against selected RNA viruses

| **Sense** | **Family** (*-viridae*) | **Virus** | Incorporation in biochemical assays | Antiviral activity in cell culture | |
|---|---|---|---|---|---|
| | | | ATP/GS-441524-TP | GS-441524[b] | Remdesivir[b] |
| | | | **Selectivity**[a] | **$EC_{50}$** | **$EC_{50}$** |
| Positive ssRNA | *Corona-* | **SARS-CoV** | 0.32[c] | 0.18[d] | 0.069[d] |
| | | **SARS-CoV-2** | 0.28[c] | 0.28 - 1.65[e]<br>0.869[f] | 0.47 – 1.09[e]<br>0.115[f] |
| | | **MERS-CoV** | 0.35[i] | 0.86[d] | 0.074[d] |
| | *Flavi-* | **HCV** | 0.93 | 4.1[g] | 0.085[g] |
| Non-segmented negative ssRNA | *Filo-* | **EBOV** | 4.0[c] | 1.0 – 3.1[h] | 0.003 – 0.021[h] |
| | *Pneumo-* | **RSV** | 2.7[j] | 0.63[h] | 0.021[h] |
| | *Paramyxo-* | **NiV** | 1.6 | 0.49 – 2.2[h] | 0.029 – 0.047[h] |
| Segmented negative ssRNA | *Arena-* | **LASV** | 20[c] | No Inhibition[h] | 4.5[h] |
| | *Nairo-* | **CCHFV** | 41 | No Inhibition[h] | No Inhibition[h] |
| | *Orthomyxo-* | **FluB** | 68 | | |
| | | **FluA** | | 27.9[g] | |

[a] Selectivity of each viral RNA polymerase for RDV-TP is calculated as the ratio of the $V_{max}/K_m$ values for ATP and RDV-TP, respectively.
[b] Reported antiviral effects of RDV measured in cell culture.
[c] Data from Gordon et al., 2020[49]
[d] Data from Agostini et al., 2018[251]
[e] Data from Pruijssers et al., 2020[252]

[f] Data from Xie et al., 2020[157]
[g] Data from Cho et al., 2012[240]
[h] Data from Lo et al., 2017[257]
[i] Data from Gordon et al., 2020[50]
[j] Data from Tchesnokov et al., 2020[267]
*HWL contributed the NiV selectivity data.
*EPT contributed the CCHFV and FluB selectivity data.

Previous data have shown that RdRp complexes of coronaviruses SARS-CoV, MERS-CoV, and SARS-CoV-2 produce an RDV-TP selectivity value of less than 1 (~0.3) (Table 7.1). The selectivity value obtained in our previous studies on SARS-CoV-2 RdRp using a steady-state approach is comparable with the value obtained in pre-steady-state assays that used much higher concentrations of ATP and RDV-TP[49, 261]. Effective inhibitory concentrations ($EC_{50}$) measured in cell-based assays demonstrate potent antiviral activity of RDV across virus families. $EC_{50}$ values for RDV or its parent nucleoside (GS-441524) are in the submicromolar range. Here we demonstrate that HCV RdRp incorporates RDV-TP with a low selectivity value (0.93) (Table 7.1 and Appendix D, Table D1), indicating that both RDV-TP and ATP are used with similar efficiency at the ATP and RDV-TP concentrations used in our study. The published $EC_{50}$ values between ~0.08 μM for RDV and ~4 μM for GS-441524 are also indicative of efficient antiviral activity although the prodrug has greater activity. A similar range of $EC_{50}$ values is observed with RDV against the nonsegmented negative-sense RNA viruses EBOV (0.003-0.021 μM), RSV (0.021 μM), and NiV (0.029-0.047 μM). The selectivity values are between 1.6 and 4, which are slightly higher when compared with our measurements for polymerases from the positive-sense RNA viruses. Conversely, RDV does not show significant antiviral activity against segmented RNA viruses CCHFV and FluB, and the $EC_{50}$ value for LASV is relatively high (~4.5 mM for RDV). Corresponding $EC_{50}$ values have not been reported for GS-441524. In each of these cases, we also measured high selectivity values for RDV-TP incorporation, which are 20, 41, and 68, for LASV, CCHFV, and FluB, respectively. Thus, the combined results revealed a correlation between antiviral activity as measured in cell-based assays and efficient rates of incorporation of RDV-TP as measured in enzymatic assays. However, the incorporation of a nucleotide analogue does not necessarily translate into inhibition of RNA synthesis. The overarching remaining question is whether a uniform mechanism of action may help explain the broad spectrum of antiviral activities associated with RDV.

### 7.2.2 Inhibition of RNA synthesis catalyzed by HCV RdRp

Previous biochemical and structural studies with SARS-CoV-2 RdRp have shown that the incorporated RDV-MP at position "i" causes inhibition of nucleotide incorporation at position "i+3" due to a steric clash between the 1′-cyano group and the hydroxyl group of the conserved Ser-861[43, 49, 263-266]. We further demonstrated that a Ser-861-Gly mutation eliminated this blockage[265]. A structural comparison of SARS-CoV-2 and HCV identified Gly-410 of the HCV RdRp as the residue corresponding to Ser-861 in SARS-CoV-2 RdRp (Appendix D, Fig. D1). A similar mechanism of inhibition is therefore not expected with HCV RdRp. For SARS-CoV-2, the extent of inhibition at position 9, or "i+3" depends crucially on the concentration of the nucleotide substrate at position "i+4". Low NTP concentrations favor inhibition, whereas high NTP concentrations override inhibition due to enhanced enzyme translocation. To monitor inhibition caused by RDV-TP, we utilized RNA templates with single sites of incorporation for RDV-TP and gradually increased the concentrations of the next NTP substrates (Fig. 7.1*A*). Incorporation of RDV-TP by SARS-CoV-2 RdRp resulted in inhibition of nucleotide incorporation at position 9 (i+3) (Fig. 7.1*B*). For HCV RdRp, subtle inhibition of RNA synthesis was observed at the point of incorporation (position 6, or i) and no inhibition at position 9, or "i+3" (Fig. 7.1*C*). Inhibition at position "i" is however easily overcome with low concentrations of the following NTP substrates. 50% read-through beyond the point of inhibition required a 10-fold greater nucleotide concentration for SARS-CoV-2 to overcome the inhibition at i+3 as compared to HCV (Fig. 7.1*D*).

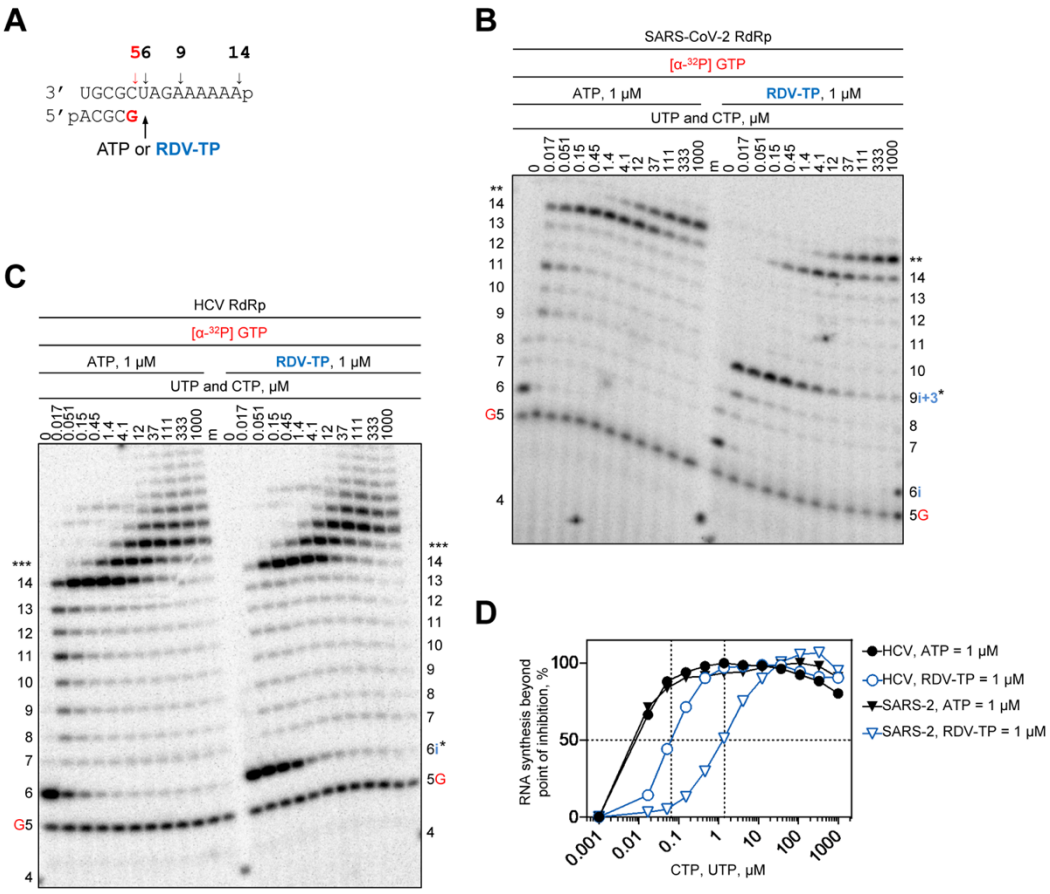


**Figure 7.1. SARS-CoV-2 or HCV RdRp-catalyzed RNA synthesis and inhibition patterns following a single incorporation of RDV-MP as a function of nucleotide concentration**. ***A***, RNA primer/template supporting a single incorporation event of AMP or RDV-MP at position 6. G indicates incorporation of [α-$^{32}$P]-GTP at position 5. ***B***, Migration pattern of the products of RNA synthesis catalyzed by SARS-CoV-2 RdRp. A 5′-$^{32}$P-labeled 4-nt primer (4) serves as a size marker. The asterisk indicates the point at which RNA synthesis is inhibited (position 9 or "i+3"). Two asterisks indicate slippage products that are likely sequence-dependent. ***C***, Reactions with HCV RdRp, inhibition of RNA synthesis occurs at the site of RDV-MP (position 6 or "i"). Three asterisks indicate increased slippage, likely sequence- and nucleotide-dependent. ***D***, Graphical representation of RNA synthesis beyond the point of RDV-TP induced inhibition for SARS-CoV-2 RdRp ("i+3") and HCV RdRp ("i").

To study whether repeated incorporations of RDV-TP could increase overall inhibition, we utilized a template with longer stretch of uridines (Fig. 7.2*A*). RNA synthesis by SARS-CoV-2 and HCV RdRp was monitored under competitive conditions in which we utilized a constant concentration of ATP and increasing concentrations of RDV-TP. RNA synthesis by SARS-CoV-2 RdRp was inhibited at ratios of RDV-TP over ATP as low as 0.1 and as high as 25 (Fig. 7.2*B*, *left*). An apparent rescue of RNA synthesis is seen at higher ratios of inhibitor over the natural

nucleotide. This observation results from efficient RDV-TP incorporation by the SARS-CoV-2 RdRp that overrides inhibition; however, these high ratios of RDV-TP over ATP are unlikely relevant in a cellular environment. The possibility for multiple incorporations of RDV-TP by HCV RdRp did not show any significant RNA synthesis inhibition at the level of the full template-length product. However, as seen in Figure 7.1C (right) the inhibitory effect at the site of RDV incorporation is more pronounced with higher RDV concentrations because the concentrations of the ATP and NTPs for subsequent incorporations are kept constant and are therefore not sufficient to overcome the inhibitory effect (Fig. 7.2*B*, *right*). These results demonstrate that while SARS-CoV-2 and HCV RdRp both incorporate RDV-TP with high efficiency, significant inhibition of primer extension reactions at the level of the full template-length product is solely seen with SARS-CoV-2 RdRp. While RDV-mediated inhibition of RNA synthesis three nucleotides downstream of an incorporated RDV-MP may therefore contribute to the observed antiviral effects in coronaviruses, the antiviral effect of RDV against HCV is likely based on a different mechanism.

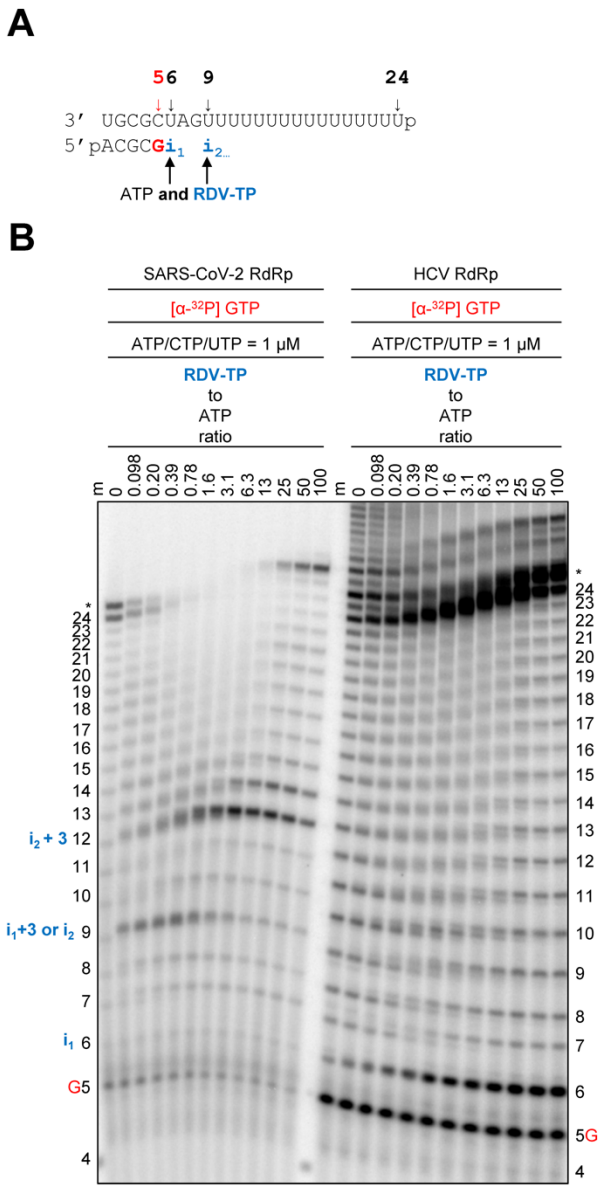


**Figure 7.2. SARS-CoV-2 or HCV RdRp-catalyzed RNA synthesis following multiple incorporations of RDV-MP as a function of RDV-TP concentration in the presence of a constant NTP concentration**. ***A***, RNA primer/template supporting multiple incorporation events of ATP or RDV-TP. ***B***, Migration pattern of the products of RNA synthesis catalyzed by SARS-CoV-2 RdRp (left), First and second incorporation of RDV-TP occurs at position 6 ("i") and 9 ("$i_2$"), respectively, with inhibition appearing at position 9 ("i+3") and 12 ("$i_2$+3"). Migration pattern of HCV RdRp (right), minor product accumulation occurs at position 6, but inhibition of RNA synthesis resulting in full template length product is not evident. The asterisk likely indicates reactions products due to slippage events.

### 7.2.3 Template-dependent inhibition of HCV RNA synthesis

High rates of incorporation of RDV-TP along with mechanisms that overcome inhibition provide conditions that allow synthesis of full-length RNA copies. These copies are modified with multiple RDV-MP residues that could affect RNA synthesis when used as templates. For SARS-CoV-2 RdRp, the RDV-MP in the template causes inhibition of the incorporation of complementary UTP and the following NTP. A similar mechanism is also considered for HCV RdRp (Fig. 7.3). We used RNA templates with a single RDV-MP incorporated at position 11. Both SARS-CoV-2 and HCV RdRp show inhibition at position 10 prior to the site of UTP incorporation. Increasing UTP concentration diminishes inhibition in both cases. HCV RdRp also requires a lower concentration of UTP to overcome this obstacle. While inhibition of SARS-CoV-2 RdRp is also seen at the adjacent position that requires ATP incorporation, inhibition of HCV is confined to position 10. As a result of these two effects, overall inhibition of RNA synthesis is more pronounced for SARS-CoV-2 RdRp. Increasing both UTP and ATP concentrations yielded more full-length product, indicating that this obstacle is eventually overcome as well (Appendix D, Fig. D2). For both SARS-CoV-2 and HCV RdRp, template-dependent inhibition is more pronounced than the inhibitory effects in primer extension reactions.

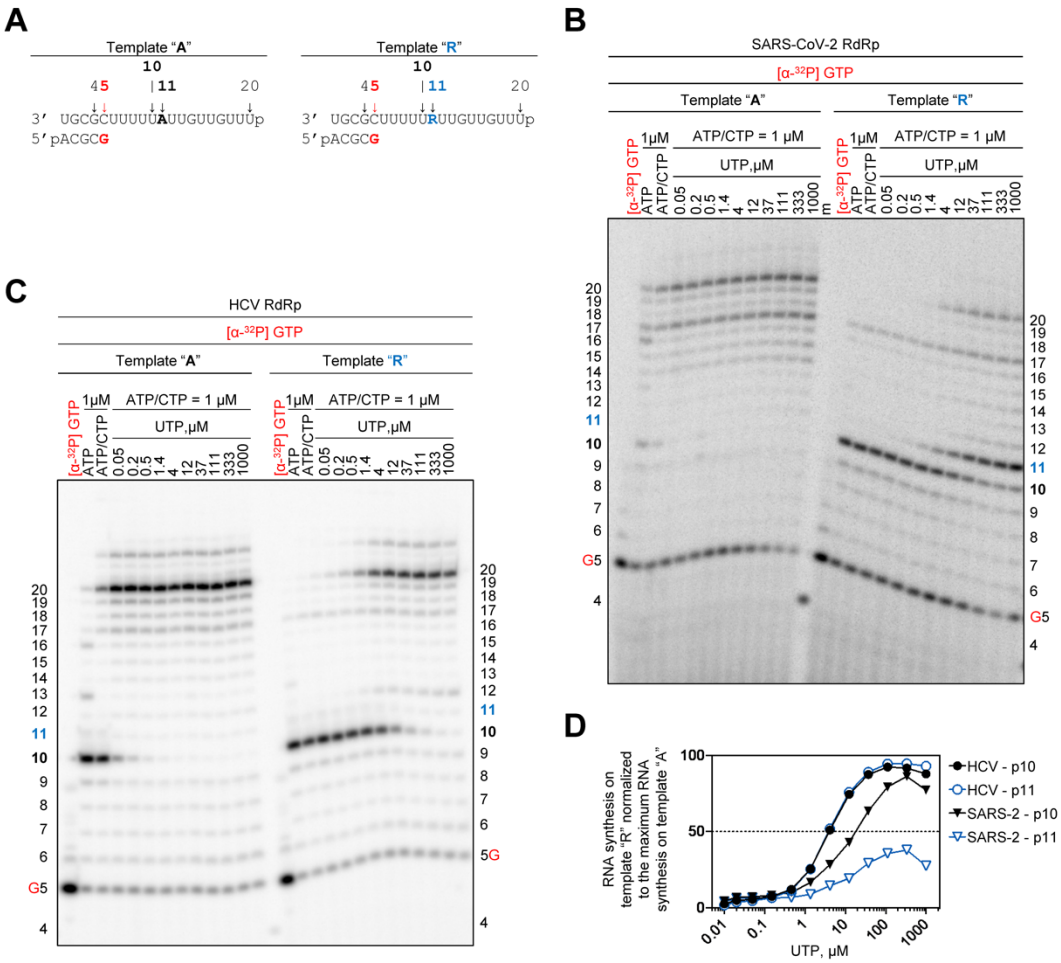


**Figure 7.3. Template-dependent inhibition of SARS-CoV-2 and HCV RdRp by an embedded RDV-MP**. ***A***, RNA primer/template with an embedded AMP (Template "A", *left*) and RDV-MP (Template "R", *right*) at position 11. ***B***, Migration pattern of products of RNA synthesis catalyzed by SARS-CoV-2 RdRp, incorporation of ATP at position 12 is inhibited ***C***, Reactions with HCV RdRp, incorporation of ATP at position 12 is not inhibited. ***D***, Graphical representation of RNA synthesis beyond position 10 and 11 (p10 and p11, respectively) on template "R".

### 7.2.4 Embedded RDV-MP demonstrates a uniform mechanism of inhibition

It has previously been reported that RDV-TP causes "delayed chain-termination" in the context of NiV RdRp[335]. NiV RdRp RNA synthesis was here monitored following a single RDV-TP or ATP incorporation in conjunction with increasing NTP concentrations (Fig. 7.4*A*). However, we were unable to detect significant inhibitory effects under these conditions. Similar patterns of intermediate reaction products were seen after AMP and RDV-MP incorporation. In the absence of significant inhibition, the newly synthesized RNA strand will contain embedded RDV-MP residues. Employing the same approach as above, RNA synthesis inhibition was again seen

opposite RDV-MP at position 11 (Fig. 7.4*B*). Incorporation opposite templated RDV-MP and AMP, respectively, was evaluated with increasing concentrations of UTP. Templated AMP allowed RNA synthesis to proceed to the full-length RNA at a UTP concentration as low as 4 μM. In contrast, a UTP concentration up to 1000 μM was not sufficient to support incorporation opposite RDV-MP, thus halting RNA synthesis at position 10 (Fig. 7.4*B*). Previous work with RSV and EBOV RdRp revealed difficulties in identifying a template that enables the investigation of a single RDV-TP incorporation and generation of full template length product[50, 267]. However, multiple incorporations of RDV-TP can cause "delayed chain-termination" with RSV and EBOV RdRp at position i+5[267, 333]. Here we also examined RNA synthesis opposite the embedded RDV-MP at position 11 of the template (Appendix D, Fig. D3*A*). RSV RdRp-catalyzed RNA synthesis could not proceed beyond the embedded RDV-MP even at the highest NTP concentrations, with most of the product accumulating at position 10 (Appendix D, Fig. D3*B*). The diminished processivity of EBOV RdRp makes it difficult to accurately determine RNA synthesis and its inhibition beyond 10 nucleotides (Appendix D, Fig. D3*C*).

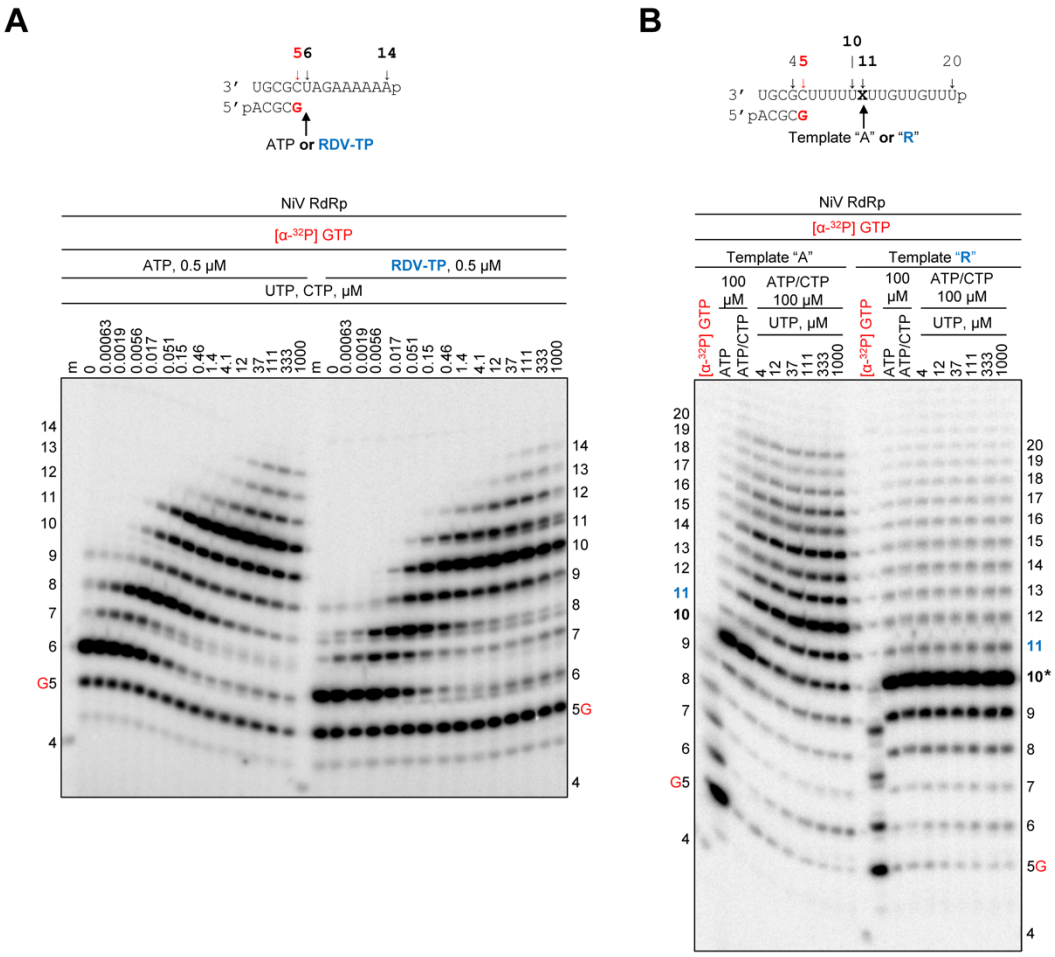


**Figure 7.4. RNA synthesis patterns following AMP and RDV-MP incorporation and template-dependent inhibition of NiV RdRp**. ***A***, RNA primer/template as indicated in Figure 5.1 and migration pattern of products of RNA following the incorporation of AMP or RDV-MP. No inhibition is evident. ***B***, RNA primer/template as indicated in Figure 7.3 and migration pattern of RNA synthesis opposite AMP (*left*) or RDV-MP (*right*). The asterisk at position 10 indicates the point of inhibition as a result of the embedded RDV-MP at position 11.

*HWL and EPT contributed to this figure.

Finally, we studied the inhibitory effects of RDV-TP or RDV-MP against RdRp enzymes from segmented negative-sense RNA viruses. We have previously demonstrated that RDV-TP is also a weak substrate for LASV RdRp, and its incorporation does not cause significant inhibition[49]. Here, we demonstrate that the embedded RDV-MP in the template causes a complete stop of RNA synthesis (Appendix D, Fig. D3D). For FluB RdRp, the presence of RDV-TP also does not mediate significant inhibition of RNA synthesis (Fig. 7.5*A*). Minor differences in the degree of full-length product formed can likely be attributed to the inefficient incorporation of RDV-TP as compared

to ATP. Templates containing AMP and RDV-MP, respectively, demonstrate again that the embedded RDV-MP causes RNA synthesis arrest at position 10 (Fig. 7.5*B*). A very similar pattern is seen with CCHFV RdRp (Appendix D, Fig. D4). No significant inhibition by RDV-TP in primer extensions, and strong inhibition or even termination when RDV-MP is embedded in the template. However, inhibition translates to antiviral effects only if the rate of incorporation of RDV-TP is sufficiently high, which is unlikely the case for LASV, FluB, and CCHFV RdRp.

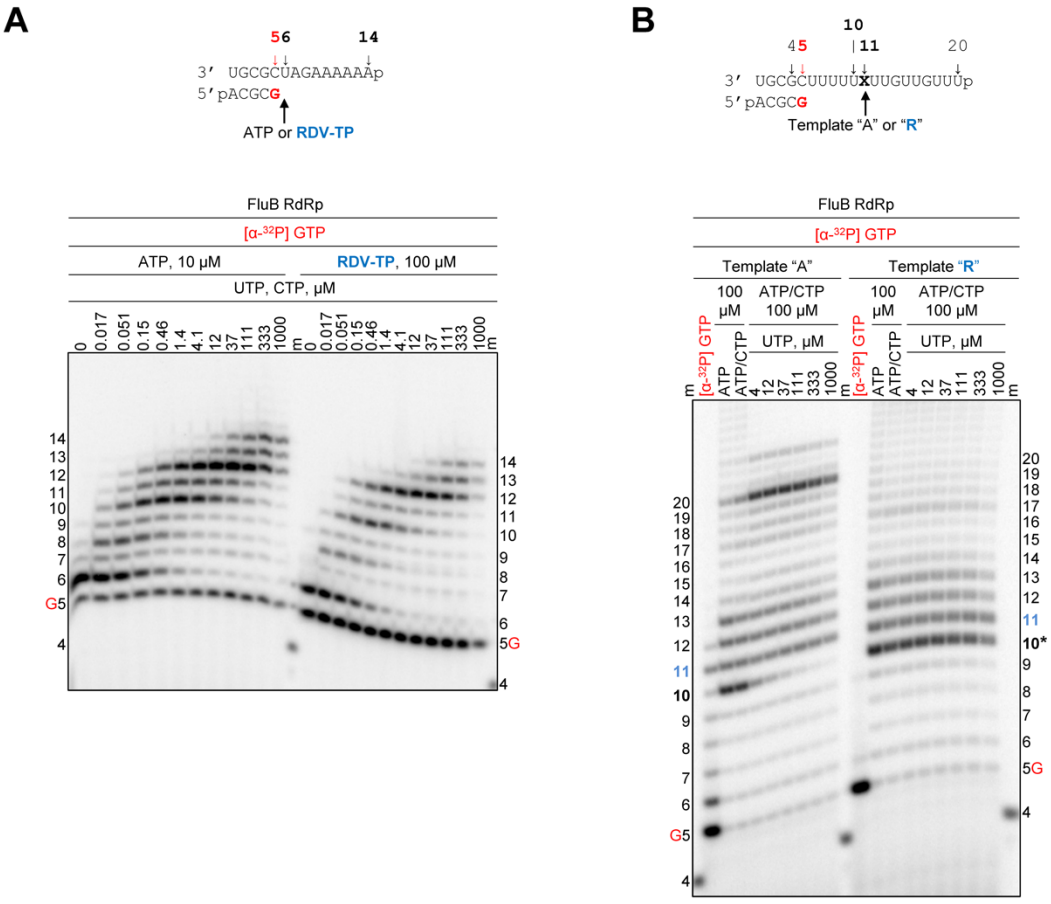


**Figure 7.5. RNA synthesis patterns following AMP and RDV-MP incorporation and template-dependent inhibition of FluB RdRp**. ***A***, RNA primer/template as indicated in Figure 6.1 and migration pattern of RNA products following the incorporation of AMP or RDV-MP. No inhibition is evident. ***B***, RNA primer/template as indicated in Figure 7.3 and migration pattern of RNA synthesis opposite AMP (left) or RDV-MP (right). The asterisk at position 10 indicates the point of inhibition as a result of the embedded RDV-MP at position 11.

*EPT contributed this figure.

## 7.3 Discussion

We compared the inhibitory effects of RDV-TP against a panel of viral RNA polymerases that represent diverse families of RNA viruses. The goal was to identify correlations between antiviral effects as previously measured in cell-based assays and the mechanism of inhibition.

Members of the positive-sense *Coronaviridae* (SARS-CoV-2) and *Flaviviridae* (HCV) families, as well as the nonsegmented negative-sense *Pneumoviridae* (RSV), *Filoviridae* (EBOV) and *Paramyxoviridae* (NiV) families are sensitive to RDV treatment, while members of the segmented negative-sense *Arenaviridae* (LASV), *Orthomyxoviridae* (FluB), and *Nairoviridae* (CCHFV) families are not sensitive to the drug[240, 251, 252, 257]. We expressed the corresponding RdRp enzymes or enzyme complexes and studied: (i) selective incorporation of the nucleotide substrate RDV-TP, (ii) the effect of the incorporated RDV-MP on primer extensions, and (iii) the effect of the template-embedded RDV-MP on UTP incorporation.

Efficient selective incorporation of RDV-TP, calculated as ratio of efficiency of incorporation of ATP over RDV-TP, is seen with SARS-CoV-2 (0.3), HCV (0.9), EBOV (4.0), NiV (1.6), and RSV enzymes (2.7). In contrast, much higher selectivity values for LASV (20), CCHFV (41), and FluB (68) enzymes suggest poor RDV-TP substrate usage. The ability of a nucleotide analogue inhibitor to be incorporated by viral RdRp enzymes is largely dependent on variations in the residues that define the nucleotide-binding site[44]. The overall structure of the active site is well conserved across a wide array of viruses and is commonly defined by a set of motifs[98]. Of these, motifs A, B, and C form important interactions with the incoming NTP.

From available ternary structures of SARS-CoV-2, HCV, and FluB RdRp, primer/template and incoming NTP, we developed models of how RDV-TP binds in its pre-incorporated state as compared to ATP (Fig. 7.6). Consistent with our biochemical findings, SARS-CoV-2 and HCV RdRp enzymes show similar active sites for favorable binding of RDV-TP with virtually no distortion in position or alteration in how the ribose is recognized as compared to ATP. Moreover, the 1′-pocket is polar and therefore conducive to accommodating the 1′-cyano group of RDV-TP. In contrast, for FluB RdRp, polar residues at the active site appear to be too far to interact directly with the ribose portion of the NTP, as in SARS-CoV-2 and HCV. A WaterMap analysis predicted the presence of a water molecule in the nucleotide binding site that facilitates recognition of the

ribose 2′OH[410, 411]. However, the location of this water molecule overlaps with the location of the 1′-cyano group and would be necessarily displaced. A sequence alignment of FluB, LASV and CCHFV enzymes suggests similarities, which may explain the poor incorporation of RDV-TP by these polymerases. Structures of EBOV, NiV, CCHFV RdRp enzymes are not available, and structures of RSV and LASV RdRp lack the RNA substrate, which is a limitation of our modeling approach[1].

[1] Since the publication of this study the structures have become available for EBOV[66], RSV[69], and LASV[90].

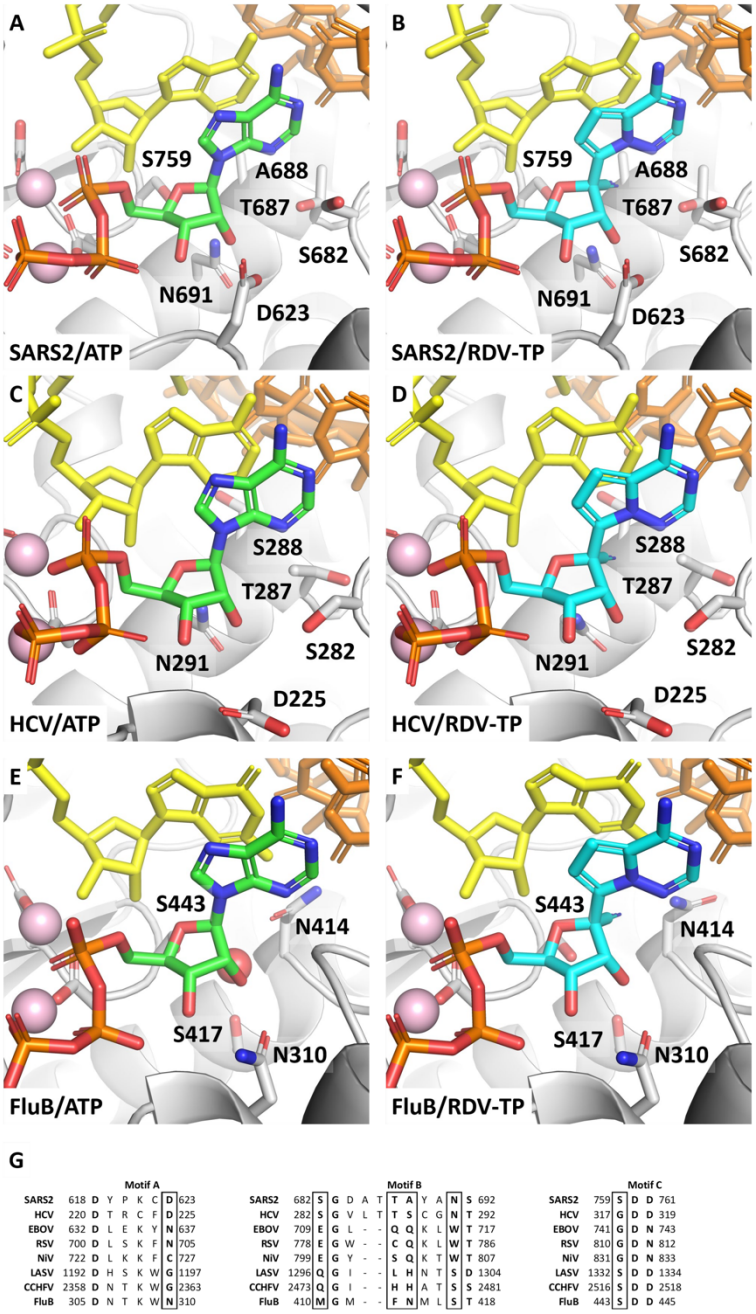


**Figure 7.6. Models of ATP and RDV-TP in their pre-incorporation states for SARS-CoV-2 (*A* and *B*), HCV (*C* and *D*) and FluB (*E* and *F*) RdRps**. RDV-TP is seen to be a good substrate for SARS-CoV-2 and HCV, showing little difference in binding position relative to ATP. However, RDV-TP displaces a water molecule critical to recognition of the ribose 2′OH in FluB, compromising its binding affinity. G, A comparison of the key motifs that make up the polymerase active site suggests LASV and CCHFV may recognize the NTP in a manner more similar to FluB, while EBOV and RSV likely recognize the NTP by a different set of interactions.

*JKP contributed this figure.

Incorporation of a nucleotide analog at position "i" does not necessarily translate in inhibition of RNA synthesis. Structural evidence for inhibition at position "i+3" has been provided for SARS-CoV-2 RdRp[43, 44, 263, 266]. The conserved Ser-861 clashes with the 1′-cyano group of the incorporated RDV-MP and diminishes enzyme translocation. However, NTP concentrations > 10 μM are often sufficient to overcome the inhibition[43, 49, 263, 265, 266, 408]. Interestingly, a very similar pattern is seen in the context of enterovirus A71 (EV-A71) RdRp and may be ascribed to the equivalent Ser-417[264]. No significant inhibition was observed with HCV or dengue virus type 2 RdRp, both of which lack a structurally equivalent residue. Here, we have shown a subtle inhibitory effect at position "i" with HCV RdRp. RSV and EBOV RdRp show inhibition at position i+5[267]; however, the structural reasons for these patterns remains elusive. Overall, this analysis suggests that the inhibitory effect in primer extension reactions is heterogeneous and generally weak. In contrast, the template-dependent inhibition of RNA synthesis seems to provide a uniform mechanism that shows strong inhibition of UTP incorporation opposite RDV-MP.

The template nucleotide that base pairs with the incoming nucleotide substrate is positioned through conserved interactions with residues in motif F (Fig. 7.7). As seen in ternary structures of SARS-CoV-2, HCV and FluB RdRp, the template base interacts with a bulky hydrophobic residue, while the ribose interacts with a second residue of varying character. These residues are separated by one additional residue, which is turned away from the template. In the case of SARS-CoV-2, the base moiety contacts Val-557 while the ribose interacts with Gly-559. For HCV, similar interactions are seen with Ile-160 and Tyr-162, while for FluB, the equivalent interactions are with Ile-241 and Thr-243. A sequence alignment suggests that this sub-motif is conserved across all enzymes included in this study (Fig. 7.7). From the available structures, we have generated molecular models with template incorporated RDV-MP positioned for UTP incorporation. In each case, the template RDV-MP 1′-cyano would be positioned between these two motif F residues, leading to a clash with the backbone carbonyl of the middle residue. In SARS-CoV-2, the 1′-cyano is positioned too close to the carbonyl of Ala-558[265]. Similarly, the 1′-cyano appears too close to the carbonyl of Ala-242 in FluB as well. The hydrophobic nature of this area is likewise not conducive to placement of the polar cyano group and may also drive a shift in the position of template RDV. It is conceivable that this unfavorable environment is sufficient to prevent UTP binding or its proper alignment for incorporation. While these details can vary across polymerases,

a proposed uniform model is shown schematically in Figure 7.8. With fewer constraints on the single stranded 5′ template overhang, RDV-MP is likely to be translocated to the active site without obstruction (Stages 1 and 2). The formation of a polymerase-competent complex with the incoming UTP is however constrained due to the putative steric problem between the 1′-cyano group of RDV-MP and motif F (Stage 3). Additional steric problems may also arise with the first translocation subsequent to UTP incorporation, but once past this point, further translocation does not appear to be impeded (Stage 4).

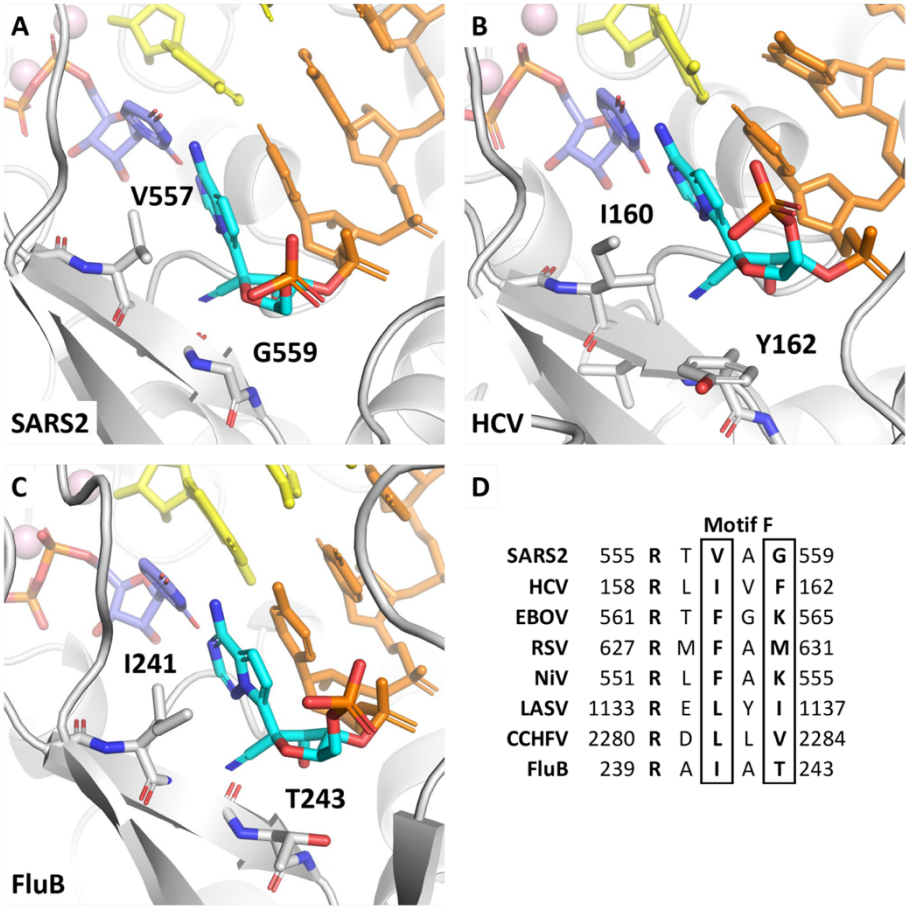


**Figure 7.7. Template-dependent inhibition by RDV for SARS-CoV-2 (*A*), HCV (*B*), and FluB (*C*) RdRps**. The 1′-CN of template incorporated RDV-MP is positioned between two typically hydrophobic residues, pushing against the backbone of the intermediate residue. **D**, As the overall structure of Motif F is widely conserved, if not the exact sequence, this represents a uniform mechanism of inhibition across a diverse set of polymerases.

*JKP contributed this figure.

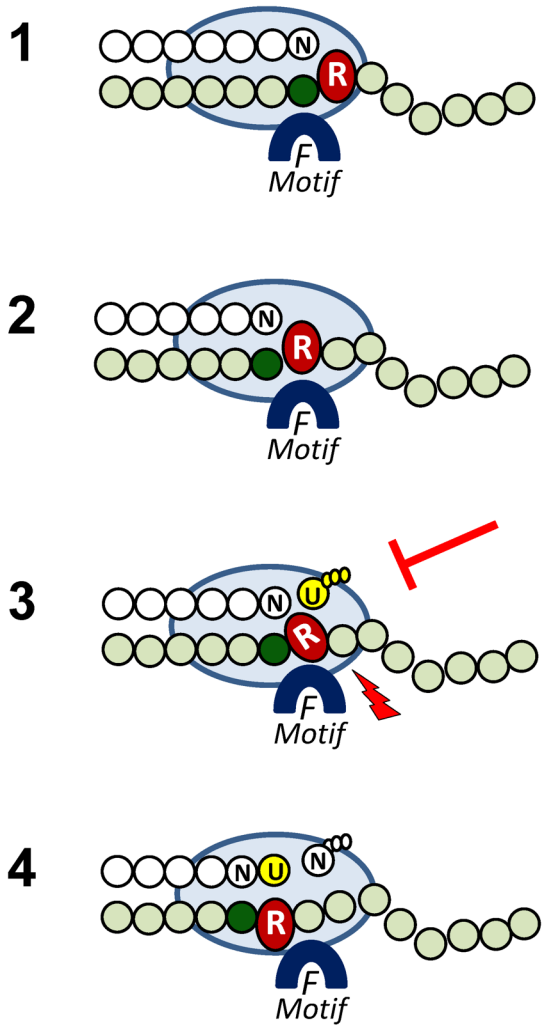


**Figure 7.8. A uniform model of the mechanism of action of RDV**. (*Stage 1*) The priming strand is shown with white circles, green circles represent residues of the template, the light blue oval represents RdRp, the dark blue semi-circle represents motif F, the red oval (R) represents RDV-MP with its 1′-cyano group, and the dark green circle represents the templating nucleotide that precedes RDV-MP. The complex is here shown immediately after nucleotide (N) incorporation. (*Stages 2* and *3*). Molecular modeling predicts a steric clash between the 1′-cyano group and motif F. The magnitude of the clash (*red arrow*) is a function of the sequence variation in motif F across the various viral RdRp and will determine the extent of UTP (*yellow*) incorporation. For HCV and SARS-CoV-2 RdRp, higher UTP concentrations can overcome inhibition. For SARS-CoV-2 RdRp, another obstacle arises at the level of the subsequent nucleotide incorporation (*white*) that is observed in our biochemical assays (*Stage 4*).

*MG contributed this figure.

Taken together, the combined results of this biochemical study and previously reported cell-based data suggest a strong correlation between the antiviral effect of RDV, or its nucleoside parent, and effective use of RDV-TP as substrate. The high selectivity of RDV-TP over ATP is a prerequisite for any downstream inhibitory effect. The patterns of inhibition of primer extension reactions can differ substantially depending on the nature of the polymerase. However, inhibition is usually inefficient at higher NTP concentrations. These are conditions that facilitate polymerase translocation and continuation of RNA synthesis. For coronaviruses, weak inhibition during synthesis of the first RNA strand might even be desired, so as to evade the intrinsic proofreading activity associated with the replication complex. A uniform mechanism of action is provided by the template-dependent inhibition of RNA synthesis opposite the embedded RDV-MP. Inhibition of incorporation of an incoming UTP base-pairing with RDV-MP is likely due to steric conflicts between the 1′-cyano group of RDV-MP and conserved residues of motif F. This inhibitory effect is seen with each of the diverse RdRp enzymes used in this study, including polymerases from the segmented negative-sense RNA viruses that are not sensitive to RDV. In these cases, the selective use of RDV-TP as substrate was poor. Thus, future drug development efforts that aim at a broader spectrum of antiviral activities should focus on improving rates of incorporation while still capitalizing on the inhibitory effects of a bulky 1′-modification.

# Chapter 8: Mechanism and spectrum of inhibition of a 4′-cyano modified nucleotide analog against diverse RNA polymerases of prototypic respiratory RNA viruses

This chapter contains content from the following source, republished with permission:

- Gordon CJ, Walker SM, Tchesnokov EP, Kocincova D, Pitts J, Siegel D, Perry JK, Feng JY, Bilello JP, and Götte M. Mechanism and spectrum of inhibition of a 4′-cyano modified nucleotide analog against diverse RNA polymerases of prototypic respiratory RNA viruses. J Biol Chem. 2024; 300:107514. © the authors.

Author Contributions

CJG, SMW, EPT, DK, and JKP investigation; CJG, SMW, and EPT validation; CJG, SMW, EPT, JKP, and MG formal analysis; CJG, SMW, EPT, and JKP visualization; CJG and MG writing–original draft; CJG, SMW, EPT, DK, JP, DSS, JKP, JYF, JPB, and MG. writing–review and editing; JYF, JPB, and MG resources; CJG data curation; MG conceptualization; CJG, SMW, EPT, JKP, and MG methodology; MG supervision; MG project administration; MG funding acquisition.

* Experiments performed by other authors have been identified in figure legends.

- HRV-16 and EV-71 RdRp were expressed and purified by DK

Funding

This study was supported by grants to M. G. from the Canadian Institutes of Health Research (CIHR) under the funding reference number 170343, Gilead Sciences Inc, the Alberta Ministry of Technology and Innovation through SPP-ARC (Striving for Pandemic Preparedness-The Alberta Research Consortium) and by the National Institute of Allergy and Infectious Diseases of the National Institutes of Health under Award Number U19AI171292. C. J. G. is supported by a grant from the CIHR under the funding reference number 181545.

## 8.1 Introduction

Respiratory RNA viruses represent a substantial public health burden worldwide. Facile transmission from person to person can cause outbreaks, epidemics, or pandemics. Severe acute respiratory syndrome coronavirus-2 (SARS-CoV-2), the causative agent of coronavirus disease 2019 (COVID-19), is a most recent example. Other prominent examples include members of the *Coronaviridae* such as SARS-CoV and Middle East respiratory syndrome coronavirus (MERS-CoV); the *Picornaviridae*, e.g. human rhinovirus (HRV); the *Pneumoviridae*, e.g. respiratory syncytial virus (RSV); the *Paramyxoviridae*, e.g. human parainfluenza viruses (HPIV); and influenza viruses of the *Orthomyxoviridae* family. Infection with these pathogens is associated with diverse disease outcomes, from asymptomatic or mild sequelae to viral bronchiolitis and pneumonia. High rates of hospitalizations and mortality from viral respiratory infections are of particular concern in children, older adults, and those with chronic airway inflammatory diseases, such as asthma[6, 412-416].

The development of effective medical countermeasures is challenging due to the diverse nature of the aforementioned viruses that cover positive-sense RNA viruses (coronaviruses and picornaviruses), non-segmented negative-sense RNA viruses (pneumoviruses and paramyxoviruses) and segmented negative-sense RNA viruses (orthomyxoviruses). A common target for pharmaceutical intervention strategies is the viral RNA-dependent RNA polymerase (RdRp), which is required for viral genome replication. Although the structural details of these enzymes differ across virus families and to a lesser degree from virus species to species, the active site is relatively conserved to accommodate nucleoside 5′-triphosphate (NTP) substrates. The development of antiviral nucleoside or nucleotide analogs is therefore a logical strategy to identify therapeutics with potential for broad-spectrum antiviral activity. Once incorporated into the growing RNA chain, the nucleotide analog can cause inhibition of RNA synthesis. The detailed mechanism of action depends on both the nature of the inhibitor and the nature of the polymerase.

Remdesivir (RDV) is a 1′-cyano modified C-adenosine monophosphate prodrug (Fig. 8.1*A*) derived from the parent nucleoside GS-441524 (Fig. 8.1*B*)[241]. RDV was the first antiviral drug to receive approval from the US Food and Drug Administration (FDA) for the treatment of COVID-19[244]. *In vitro*, RDV and GS-441524 exhibit broad-spectrum antiviral activity against

respiratory viruses, including coronaviruses (SARS-CoV-2, SARS-CoV, and MERS-CoV)[157, 251-254], picornaviruses (HRV-16, enterovirus D68 [EV-D68])[256, 259], pneumoviruses (RSV, human metapneumovirus [HMPV]) [257, 258], and human paramyxoviruses (HPIV)[240, 257]. Antiviral activity is not observed against several segmented negative-sense RNA viruses, including Lassa virus (LASV), Crimean-Congo hemorrhagic fever virus (CCHFV), and influenza viruses[240, 257, 259]. The 5′ ester prodrug of GS-441524, obeldesivir (ODV) (Fig. 8.1*C*), is metabolized pre-systemically to GS-441524 and subsequently to GS-443902, and therefore shares the same antiviral profile as RDV and its parent nucleoside [247]. ODV was recently evaluated in phase 3 clinical trials for COVID-19 and was efficacious against filoviruses in a post-exposure prophylaxis non-human primate model[250].

Key biochemical attributes of RDV and GS-441524 that enable potent inhibition of the SARS-CoV-2 RdRp complex have been identified. Their active 5′-triphosphate metabolite, herein referred to as GS-443902 (Fig. 8.1*D*), outcompetes its natural counterpart adenosine triphosphate (ATP) 2- to 3-fold[40, 50, 261]. Incorporation into the growing RNA chain at position "i" results in delayed chain-termination at position "i+3". A steric clash between the 1′-cyano group of GS-443902 and the conserved Ser-861 in the RdRp causes inhibition of primer extension [49, 265]. Higher NTP concentrations can overcome delayed-chain termination at position "i+3", potentially yielding complete copies of the viral genome with embedded GS-443902 residues[49, 198, 263-266]. When used as templates, incorporation of the complementary UTP is likewise inhibited. This template-dependent inhibition is more effective, but higher NTP concentrations can overcome this obstacle as well [265].

Here we compare the 1′-cyano modified C-adenosine with a newly discovered 4′-cyano modified C-adenosine. Derived from the nucleoside GS-646089 (Fig. 8.1*E*), the monophosphate prodrug GS-7682 is associated with a broad-spectrum of antiviral activities[417]. Viruses that belong to the *Picorna*- and *Pneumoviridae* families were most sensitive to GS-7682 treatment in cell culture. The 50% effective concentration ($EC_{50}$) of GS-7682 was less than 100 nM against several picornaviruses, including HRV-16[417]. Further, GS-7682 was potent against HMPV and RSV with $EC_{50}$ values of 210 ± 50 and 3-46 nM (various assays), respectively. However, GS-7682 demonstrated limited antiviral activity against corona- and orthomyxoviruses[417]. In this study, we

compared the biochemical properties of the active 5′-trisphosphate form of GS-7682, referred to as GS-646939 (Fig. 1*F*), with GS-443902 against an array of RdRp enzymes representing multiple families of respiratory viruses. Highly efficient rates of GS-646939 incorporation are seen with picornaviruses HRV-16 and EV-71 RdRp and, to a lesser extent, with pneumoviruses RSV and HMPV RdRp. In contrast to GS-443902, inhibition with GS-646939 is based on immediate chain-termination at position "i". Overall, the biochemical evaluation of the two nucleotide analogs against their targets provides mechanistic detail for the observed antiviral effects.

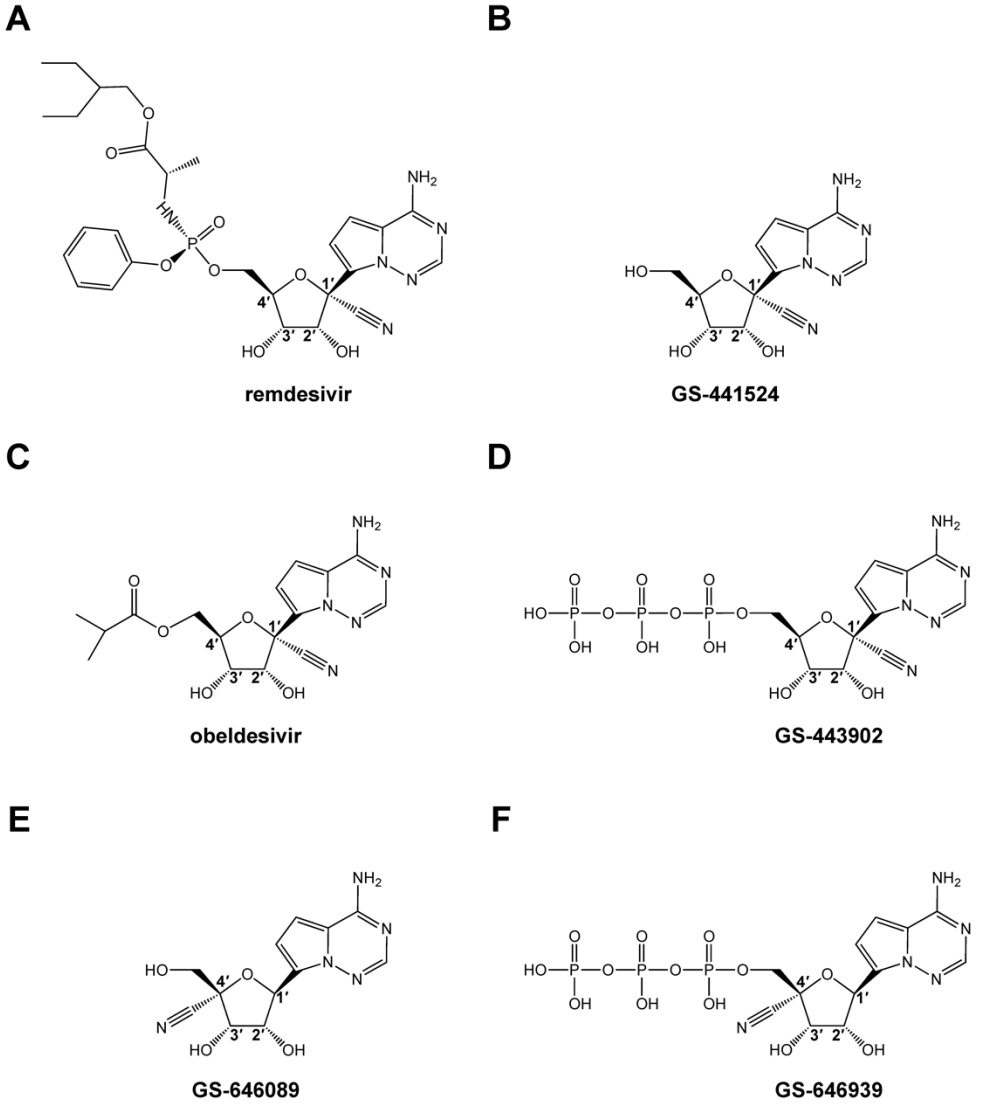


**Figure 8.1. Chemical structures of remdesivir (*A*), GS-441524 (*B*), obeldesivir (*C*), GS-443902 (*D*), GS-646089 (*E*), and GS-646939 (*F*).**

## 8.2 Results

### 8.2.1 Experimental strategy

The main objective of this study was to elucidate the mechanism of action of GS-646939 using purified RdRp enzymes from prototypic respiratory RNA viruses of the *Coronaviridae*, *Picornaviridae*, *Pneumoviridae*, *Paramyxoviridae* and *Orthomyxoviridae* (Table 8.1). The prototypic pathogen approach is based on research efforts with selected viruses that represent specific families[2]. To strengthen this approach, we expressed the RdRp from two prototypic species within each of the five families mentioned above. SARS-CoV-2 and MERS-CoV were selected to represent coronaviruses, HRV-16 and EV-71 for picornaviruses, RSV and HMPV for pneumoviruses, and HPIV-3 and PIV-5 for paramyxoviruses. Orthomyxoviruses were represented by influenza B virus. The RdRp from Lassa virus (LASV) a segmented negative-sense RNA virus (like influenza) which belongs to the *Arenaviridae* family, was also evaluated. Human mitochondrial RNA polymerase (h-mtRNAP) was utilized to assess potential off-target effects. The comprehensive approach was designed to identify common biochemical properties that are associated with broad-spectrum antiviral activity. Active RdRp enzymes used in this study exist either as monomers, dimers or multimeric complexes (Table 8.1). The coronaviruses SARS-CoV-2 and MERS-CoV form complexes with non-structural protein 12 (Nsp12), which contains the RdRp active site, and essential cofactors Nsp7 and Nsp8[40-42]. Picornavirus RdRps from HRV-16 and EV-71, also referred to as $3D^{pol}$, are monomeric and do not require additional cofactors[10, 11]. The replication complex of the pneumoviruses RSV and HMPV, as well as paramyxoviruses HPIV-3 and PIV-5, consists of the large (L) protein, containing the RdRp active site, and a phosphoprotein (P)[67, 70]. PIV-5, or canine parainfluenza virus, was included because the structure of the RdRp complex is available[72] (Table 8.1). While this manuscript was under review, the structure of the HPIV-3 polymerase complex was also reported [71]. Influenza viruses assemble a heterotrimeric complex composed of PA (cap-snatching endonuclease subunit), PB1 (RdRp subunit), and PB2 (cap-binding subunit) [82]. The LASV L protein is a dynamic monomer functionally similar to the trimeric influenza replication complex, possessing an N-terminus endonuclease, RdRp core, and C-terminus cap-binding domain[90]. Finally, h-mtRNAP is a single subunit enzyme responsible for the transcription of the mitochondrial genome[418]. In this study, we combined enzymatic assays with structural modeling to provide insight into the requirements for

nucleotide incorporation and inhibition of RNA synthesis, respectively, with GS-443902 serving as a benchmark.

Table 8.1: Expression of RNA polymerases

| Sense | Family (*-virdae*) | Virus | Expression System | Construct | Composition | M.W. (kDa)[a] | PDB |
|---|---|---|---|---|---|---|---|
| Positive ssRNA | *Corona-* | SARS-CoV-2 | BEVS[b] | nsp5-↓[c]nsp7-↓8xHis-nsp8-↓**nsp12**[d]↓ | Tetramer | 165 | 7UO4[e] |
| | | MERS-CoV | | nsp5-↓nsp7-↓8xHis-nsp8-↓**nsp12**-Strep | Tetramer | 165 | n/a |
| | *Picorna-* | HRV-16 | *E. coli* | 8xHis-**3D$^{pol}$** | Monomer | 50 | 4K50 |
| | | EV-71 | | | | 50 | 3N6L |
| Non-segmented negative ssRNA | *Pneumo-* | RSV | BEVS | TEV-↓8xHis-P-↓**L**-Strep | Dimer | 282 | 6PZK |
| | | HMPV | | TEV-↓8xHis-P-↓Strep-**L** | | 267 | 6U5O |
| | *Paramyxo-* | HPIV-3[f] | BEVS | $^{p10}$P-$^{pPH}$**L**-8xHis | Dimer | 323 | 8KDB |
| | | PIV-5[f] | | | | 298 | 6V85 |
| Segmented negative ssRNA | *Orthomyxo-* | FluB | BEVS | TEV-↓8xHis-↓PA-↓**PB1**-↓PB2-Strep | Trimer | 263 | 6QCV |
| | *Arena-* | LASV | BEVS | Strep-8xHis-**L** | Monomer | 257 | 7OJN |
| Human DNA-dependent RNA polymerase | | h-mtRNAP | BEVS | Strep-8xHis-**RNAP** | Monomer | 138 | 4BOC |

[a] Molecular weight is an approximation and calculated according to the subunit composition of the replication complex (e.g. coronavirus replication complex accounts for the ratio 1:2:1 of Nsp7:Nsp8:Nsp12 as observed structurally). The protease is not included in the calculation.
[b] Baculovirus expression vector system
[c] Down arrow represents the cleavage site acted on by that constructs respective protease (underlined).
[d] Bolded domains indicate where the RdRp motifs responsible for catalyzing RNA synthesis are contained.
[e] Ternary structure of the SARS-CoV-2 replication complex with GS-443902 in the active site as reported by Malone et al.[40]
[f] Cloned into pFastBac-DUAL vector employing the p10 and polyhedrin (PH) promoter as reported by Abdella at el.[72]

### 8.2.2 Selective incorporation of GS-443902 and GS-646939 by representative RdRp enzymes

We compared nucleotide incorporation efficiency of the 1′-cyano GS-443902 (Table 8.2, *column 4*) with the 4′-cyano GS-646939 (Table 8.2, *column 5*) modified NTP. Enzyme reactions were monitored in gel-based assays using model primer/templates (Appendix E, Fig. E1)[49, 130, 260,

[267, 273]. Steady-state kinetic parameters $V_{max}/K_m$ for ATP incorporation over $V_{max}/K_m$ for the nucleotide analog provide a measure of the efficiency of nucleotide incorporation in relation to its natural counterpart (Appendix E, Tables E1 and E2). The numerical value is unitless and defines the selectivity for a given nucleotide analog. Selectivity values below 1 indicate that the nucleotide analog is more efficiently incorporated than ATP. Previous studies revealed selectivity values of ~0.3 for GS-443902 incorporation by RdRp complexes of coronaviruses SARS-CoV-2, SARS-CoV, and MERS-CoV (Table 8.2, *column 4*)[49, 50, 260, 265]. HRV-16 and EV-71 RdRp show selectivity values around 1 for GS-443902, indicating that picornavirus enzymes incorporate this nucleotide analog and ATP with similar efficiency. RdRp complexes of pneumoviruses RSV and HMPV show higher selectivity values of 2.7 and 6.7, respectively, signifying a preference for the natural ATP nucleotide. A similar observation was made with paramyxovirus enzyme complexes of HPIV-3 (7.2) and PIV-5 (8.3). Incorporation of GS-443902 by influenza B and LASV RdRp is even more limited, with selectivity values of 68 and 20, respectively. GS-443902 incorporation by h-mtRNAP is highly inefficient, with a selectivity value of ~500 [267].

GS-646939 shows incorporation selectivity values of approximately 1.2-1.4 for SARS-CoV-2 and MERS-CoV RdRp (Table 8.2, *column 5*). For HRV-16 and EV-71 RdRp, GS-646939 selectivity values are as low as 0.018, markedly exceeding the incorporation efficiency of the 1′-cyano GS-443902 by up to ~50-fold. RSV and HMPV RdRp show selectivity values of ~1.5 for GS-646939, a slight improvement over GS-443902. Incorporation by HPIV-3 and PIV-5 RdRp show comparable selectivity values between 5 and 10 for both nucleotide analogs. Similar to GS-443902, GS-646939 served as a poor substrate for influenza B and LASV RdRp, generating selectivity values greater than 200. Likewise, h-mtRNAP demonstrated poor incorporation efficiency of GS-646939 with a selectivity value of ~1500. Overall, GS-646939 and GS-443902 follow similar trends. The exception is the preference for GS-646939 by picornavirus RdRp and a predilection for GS-443902 by coronavirus RdRp.

Table 8.2: Selective incorporation of GS-443902 and GS-646939, by selected RdRp enzymes

| | | | GS-443902 | GS-646939 |
|---|---|---|---|---|
| RNA Sense | Family (*-viridae*) | Virus | Selectivity[a] (fold) | Selectivity[b] (fold) |
| Positive ssRNA | *Corona-* | **SARS-CoV-2** | **0.30[1]** | **1.37** |
| | | **SARS-CoV** | **0.34[1]** | **N.R.[c]** |
| | | **MERS-CoV** | **0.35[1]** | **1.17** |
| | *Picorna-* | **HRV-16** | **1.03** | **0.018** |
| | | **EV-71** | **0.93** | **0.051** |
| Nonsegemented negative ssRNA | *Pneumo-* | **RSV** | **2.73[2]** | **1.58** |
| | | **HMPV** | **6.71** | **1.73** |
| | *Paramyxo-* | **HPIV-3** | **7.20** | **10.3** |
| | | **PIV-5** | **8.31** | **5.05** |
| Segmented Negative ssRNA | *Orthomyxo-* | **FluB** | **68[1]** | **2288** |
| | *Arena-* | **LASV** | **20[1]** | **225** |
| Human DNA-dependent RNA polymerase | | **h-mtRNAP** | **503[2]** | **1538** |

[a] Selectivity of a viral RNA polymerase for a GS-443902 is calculated as the ratio of the $V_{max}/K_m$ values for ATP and GS-443902 analog, respectively.
[b] Selectivity of a viral RNA polymerase for a GS-646939 is calculated as the ratio of the $V_{max}/K_m$ values for ATP and GS-646939 analog, respectively.
[c] Not reported.
[1] Data from Gordon et al. [260]
[2] Data from Tchesnokov et al. [267]
*HPIV-3 and HPIV-5 selectivity values were generated by SMW

The exceptional substrate utilization of GS-646939 by HRV-16 and EV-71 RdRp suggests that the nucleotide analog can outcompete its natural counterpart ATP. To address this question directly, we simultaneously added ATP and GS-646939 to the reaction and monitored incorporation of the corresponding monophosphate (MP) formed (Fig. 8.2). AMP ("$i_1$") and GS-646939 ("$i_2$") terminated primers could be distinguished from one another due to the difference in migration pattern (Fig. 8.2*A*). The concentration of GS-646939 required to match 50% ATP incorporation is defined as the matching concentration ($MC_{50}$). As expected for a competitive

inhibitor, the $MC_{50}$ value increased with increasing concentrations of the competing ATP (Fig. 8.2*B*). The ratio of the $MC_{50}$ value over the ATP concentration provides the competition index (Fig. 8.2*C*). The lower the value, the better the competitive advantage for incorporation of a given nucleotide. The average competition index values for GS-646939 were 0.04 and 0.07 for HRV-16 and EV-71 RdRp, respectively (Fig. 8.2*D*). These data suggest that, under competitive conditions, the picornavirus RdRp enzymes use GS-646939 ~14- to 25-fold more efficiently than ATP. Furthermore, both picornavirus enzymes demonstrated a greater than 30-fold preference for GS-646939 over GS-443902 under competitive conditions (Appendix E, Fig. E2). Together, the competitive incorporation data corroborate the selectivity measurements.

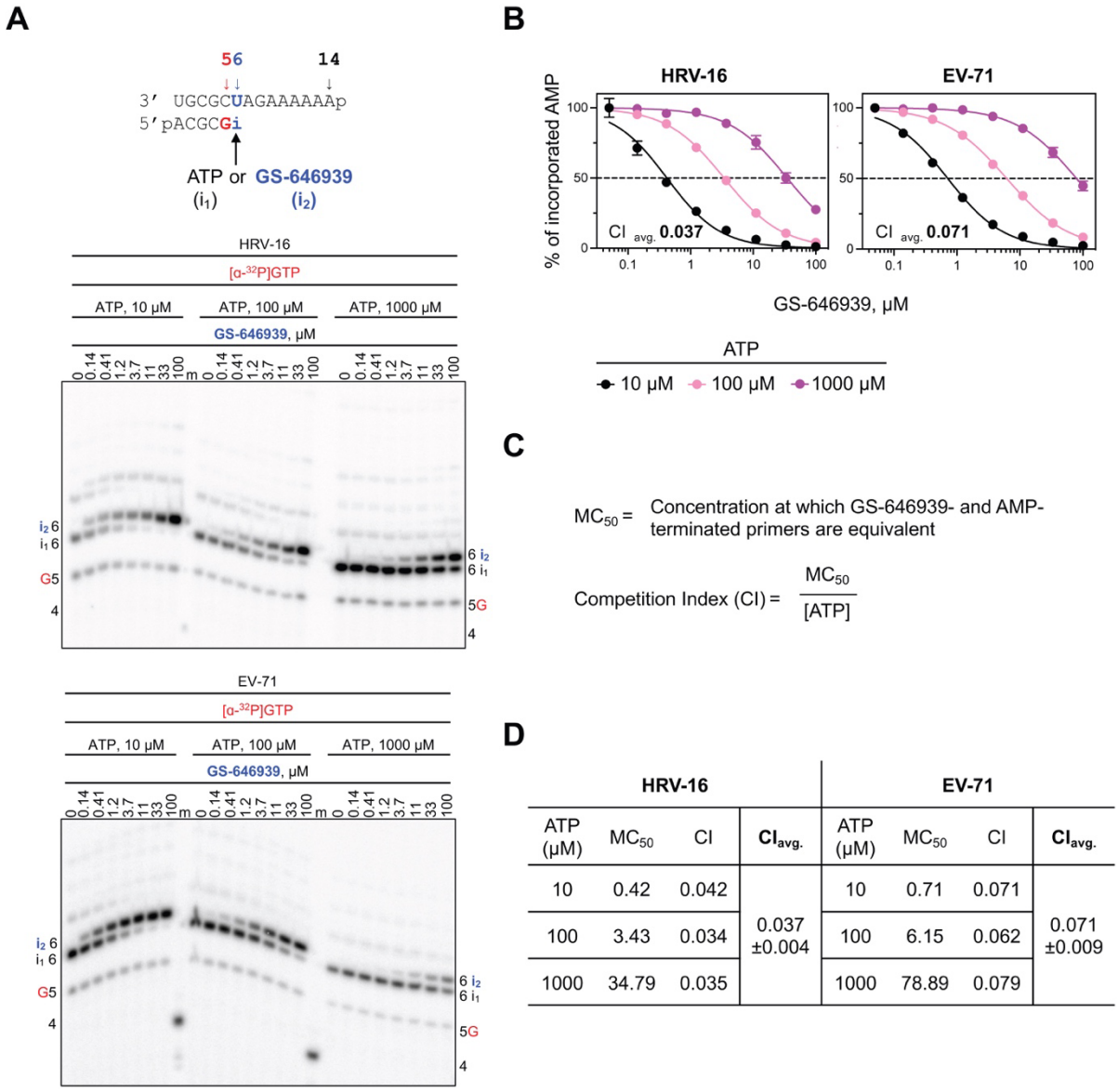


| HRV-16 | | | | EV-71 | | | |
|---|---|---|---|---|---|---|---|
| ATP (μM) | $MC_{50}$ | CI | $CI_{avg.}$ | ATP (μM) | $MC_{50}$ | CI | $CI_{avg.}$ |
| 10 | 0.42 | 0.042 | 0.037 ±0.004 | 10 | 0.71 | 0.071 | 0.071 ±0.009 |
| 100 | 3.43 | 0.034 | | 100 | 6.15 | 0.062 | |
| 1000 | 34.79 | 0.035 | | 1000 | 78.89 | 0.079 | |

**Figure 8.2. Incorporation of GS-646939 under competitive conditions by HRV-16 and EV-71 RdRp**. ***A***, RNA primer/template (*top*) supporting a single incorporation of ATP ("$i_1$") or GS-646939 ("$i_2$") at position 6. G indicates incorporation of [α-$^{32}$P]-GTP at position 5. Migration pattern of RNA synthesis products catalyzed by HRV-16 (*middle*) and EV-71 RdRp (*bottom*). Product formation resulting in AMP- or GS-646939-terminated primers was compared across increasing GS-646939 concentrations at ATP concentrations of 10, 100, and 1000 μM. A 5′-$^{32}$P-labeled 4-nt primer serves as a size marker. ***B***, Graphical representation of AMP-terminated primers (%) at increasing GS-646939 concentrations as shown in A. Independent 8-data point experiments were performed at least three times (n=3) and error bars represent standard error associated with the fit. ***C***, The $MC_{50}$ value is defined as the concentration at which GS-646939 matches ATP for incorporation at position 6. The competition index (CI) is the ratio of the $MC_{50}$ value to the ATP concentration present in the reaction. ***D***, CI values determined for HRV-16 and EV-71 RdRp and the CI average ($CI_{avg}$) and standard deviation (±) across all ATP concentrations.

### 8.2.3 Structural models of incorporation

Based on existing x-ray and cryo-EM structures[10, 40, 67, 72, 82, 90, 418], we generated models of the pre-incorporated states of ATP, GS-443902, and GS-646939 for representative RdRp enzymes investigated in this study (Table 8.1). The active site of viral RdRps is generally characterized by a set of motifs with highly conserved residues involved in substrate binding and catalysis [419]. However, subtle variations in the active site landscape seem to govern the specificity of inhibitor incorporation. For HRV-16, EV-71, SARS-CoV-2, MERS-CoV, RSV, HMPV, PIV-5 and HPIV-3, both the 1′-cyano of GS-443902 and the 4′-cyano of GS-646939 are tolerated to varying degrees. As previously described, the 1′-cyano of GS-443902 is particularly well positioned in the coronavirus active site, occupying a uniquely polar pocket defined by Thr-687, Asn-691 and Ser-759 in SARS-CoV-2 [40], and similarly for MERS-CoV. For GS-646939, the 4′-cyano appears to have a favorable interaction with Asn-296 of HRV-16 (Fig. 8.3*A*). The Motif C residue Gly-326 in HRV-16 allows for maximum flexibility in the 4′ pocket, in contrast to the similar SARS-CoV-2 and MERS-CoV pocket, in which the corresponding residue is a serine (Fig. 8.3*B*). For RSV (Fig. 8.3*C*) and HMPV, PIV-5 (Fig. 8.3*D*) and HPIV-3, the 4′-cyano fits nicely in the pocket, but doesn't appear to convey any advantage.

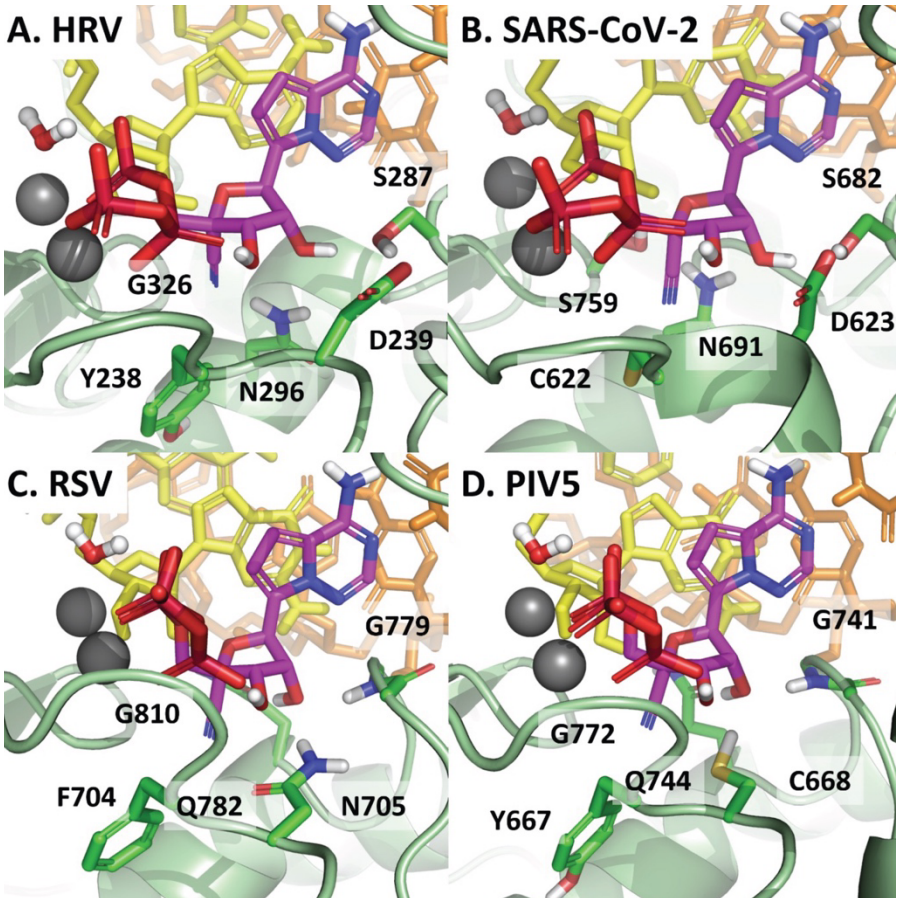


**Figure 8.3. Selectivity is largely driven by the nature of the 4′ pocket and the specifics of how the 2′-OH is recognized by the polymerase**. GS-646939 is shown in magenta. HRV (***A***) and SARS-CoV-2 (***B***) have a similar overall active site structure, differing primarily at Gly-326/Ser-759 and Tyr-238/Cys-622. While somewhat different from HRV and SARS-CoV-2, RSV (***C***) and PIV5 (***D***) also have a similar overall structure, differing primarily at Phe-704/Tyr-667 and Asn-705/Cys-668. In each case, the 4′-cyano of GS-646939 is at least tolerated. The interaction between the 4′-cyano and Asn-296 in HRV appears to be particularly ideal and is likely responsible for the inhibitor's increased affinity compared to ATP.

*JKP contributed this figure.

For LASV and FluB, both the 1′-cyano of GS-443902 and 4′-cyano of GS-646939 disrupt a water-mediated hydrogen bond network, which is essential for recognition of the substrate 2′-OH (Appendix E, Fig. E3*A* and E3*B*). For GS-646939, the water molecule is likely completely displaced, with no means to compensate for the loss in hydrogen bonding at 2′. Compounding the issue, both LASV and FluB have a bulky tryptophan residue forming the floor of the 4′ pocket. The comparable residue in the polymerases for which GS-646939 has demonstrably greater activity is typically a tyrosine, phenylalanine, or another smaller residue. This provides a degree

more flexibility to accommodate the 4′-cyano. In the case of h-mtRNAP, Motif B is fundamentally different from viral RdRps (Appendix E, Fig. E3*C*). With respect to GS-443902, the 1′ pocket is clearly occluded by His-1125, while for GS-646939, the 4′ pocket is occluded by a salt bridge formed from Arg-802 and Asp-1128. In both cases, incorporation of the inhibitor should be significantly compromised.

### 8.2.4 Inhibition of RNA primer extension reactions

Incorporation of the nucleotide analog into the growing RNA chain is a prerequisite for any potential inhibitory effect. Notably, GS-443902 and GS-646939 possess a 3′-hydroxyl group, classifying them as non-obligate chain-terminators. The presence of a 3′-hydroxyl group may allow for the nucleophilic attack on the incoming nucleotide and its subsequent incorporation. Previous biochemical and structural studies of SARS-CoV-2 have established that incorporation of GS-443902 at position "i" results in delayed-chain termination at position "i+3" [49, 265, 266]. This mechanism can be attributed to a steric clash between the 1′-cyano group and the hydroxyl group of the conserved Ser-861. A structural comparison between Nsp12 of SARS-CoV-2 and the $3D^{pol}$ of HRV-16 and EV-71 revealed that the picornaviruses share an analogous serine (Fig. 8.4*A*) [264]. RNA synthesis following GS-443902 incorporation by SARS-CoV-2, EV-71, and HRV-16 RdRp at position "i" generated the same intermediate product at position "i+3" (Fig. 8.4*B*). As reported for SARS-CoV-2 RdRp, the inhibitory effect was favoured at low nucleotide concentrations and could be overcome with increasing concentrations of the nucleotide substrate at position "i+4" [49, 265].

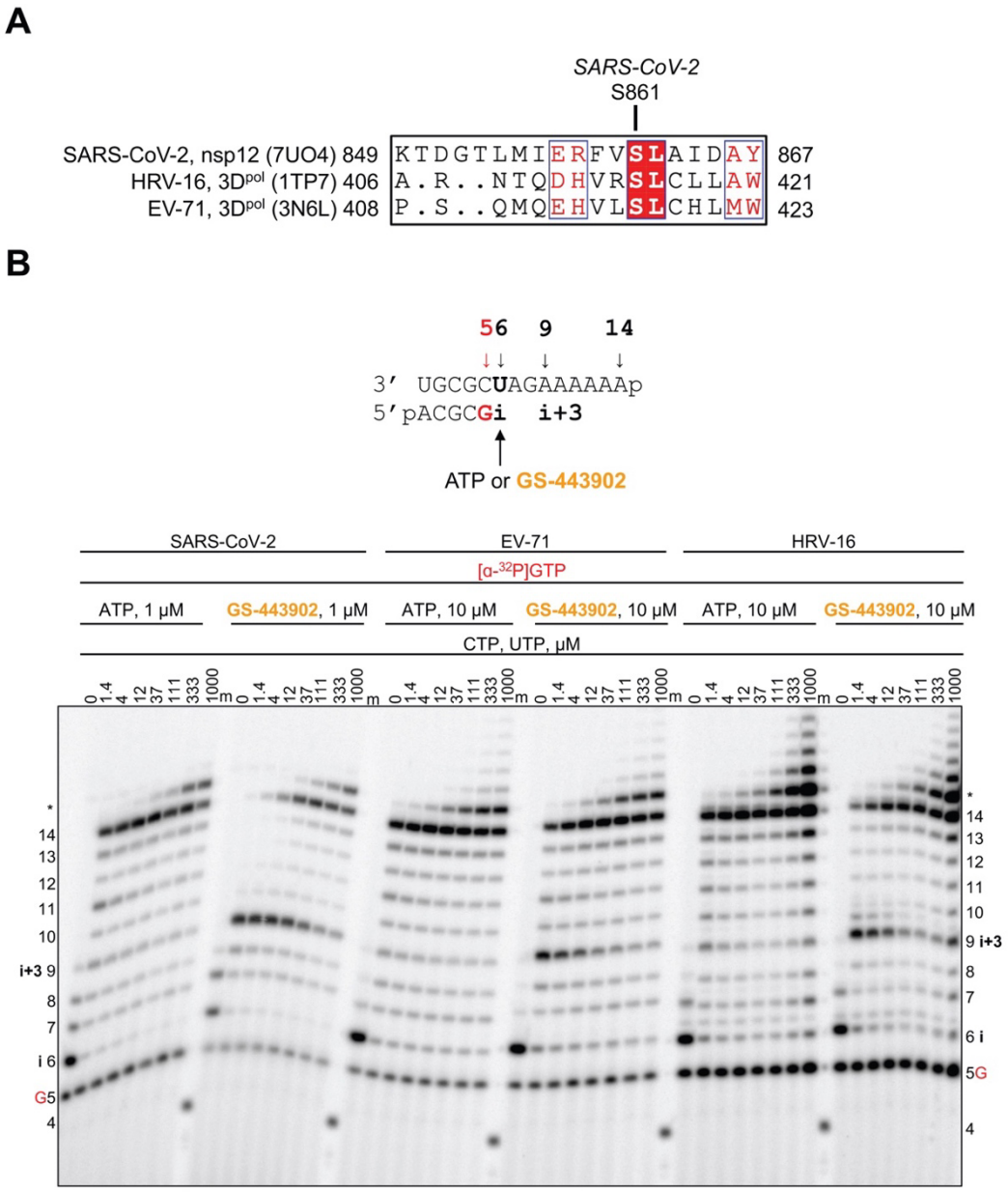


**Figure 8.4. SARS-CoV-2, EV-71, and HRV-16 RdRp-catalyzed RNA synthesis pattern of inhibition following a single incorporation of ATP or GS-443902 as a function of nucleotide concentration**. ***A***, Sequence alignment based on a 3D structural overlay of SARS-CoV-2 Nsp12 (PDB:7UO4), HRV-16 3D$^{pol}$ (PDB:1TP7), and EV-71 3D$^{pol}$ (PDB:3N6L) composed using ESPript 3.0 [102]. Ser-861 (SARS-CoV-2 numbering) is conserved in HRV-16 and EV-71 RdRp. ***B***, RNA primer/template supporting a single incorporation of ATP or GS-443902 at position 6 (*top*). G indicates incorporation of [α-$^{32}$P]-GTP at position 5. Extension following the incorporation of ATP and GS-443902 at position 6 ("i") at increasing CTP and UTP concentrations catalyzed by SARS-CoV-2, EV-71, and HRV-16 RdRp (*bottom*). Following GS-443902, an intermediate product forms at position 9 ("i+3"), which is overcome at elevated CTP and UTP concentrations. A 5′-$^{32}$P-labeled 4-nt primer serves as a size marker. Product formation at and above the asterisk indicates RNA products that are likely a result of sequence-dependent slippage events.

Employing the same approach as above, we show that GS-646939 inhibited HRV-16 and EV-71 RdRp-mediated RNA synthesis at the site of incorporation (Fig. 8.5). While GS-443902 incorporation promotes delayed chain-termination, GS-646939 causes immediate chain-termination. Inhibition by GS-646939 is overcome with increasing NTP concentration following the incorporated analog. A similar pattern was observed for SARS-CoV-2 and MERS-CoV RdRp (Appendix E, Fig. E4). GS-443902 inhibits other RdRp enzymes likewise via delayed chain-termination. However, the patterns are more heterogeneous, with variations in the position of inhibition; the structural reasons have yet to be determined[267]. In contrast, GS-646939 incorporation by RSV and HMPV RdRp resulted in immediate chain-termination (Appendix E, Fig. E5), which was nearly absolute and could not be overcome to a discernable extent with increased NTP concentrations. Inhibition of HPIV-3 and PIV-5 RdRp with GS-646939 shows a similar immediate chain-termination pattern (Appendix E, Fig. E6).

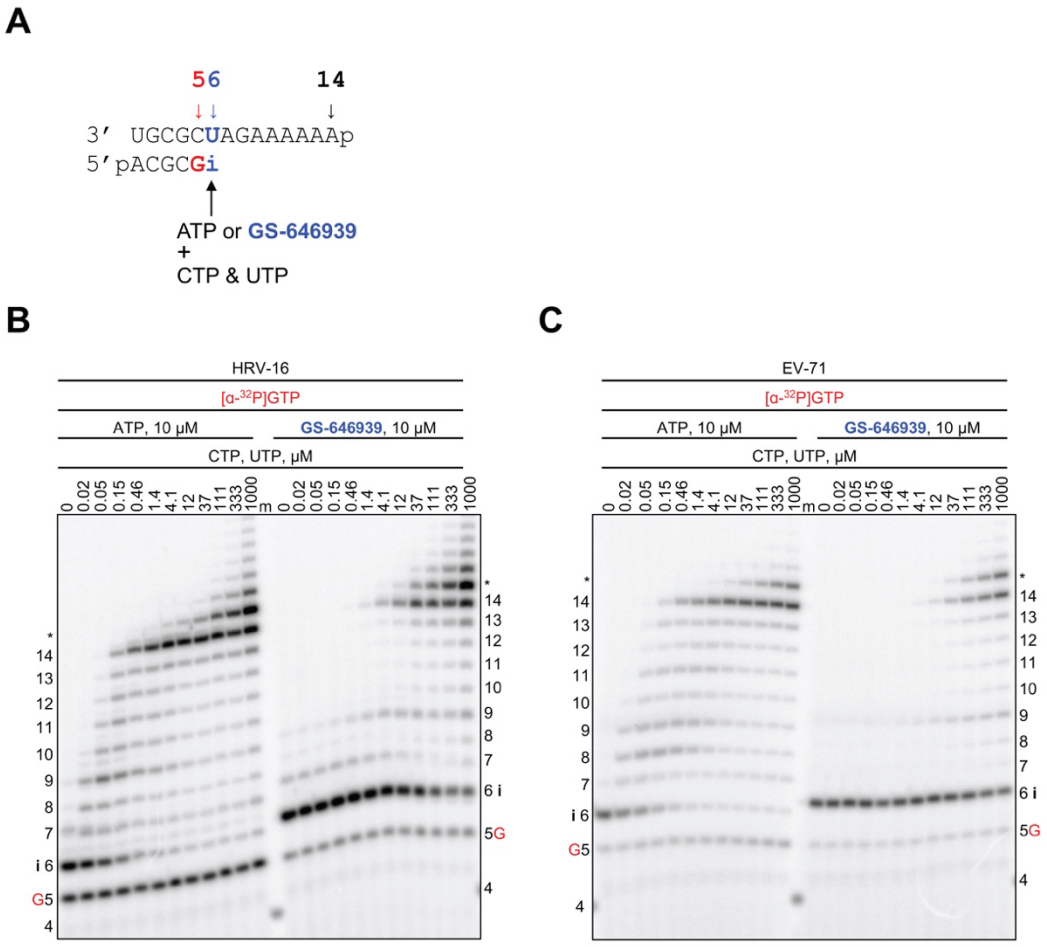


**Figure 8.5. HRV-16 or EV-71 RdRp-catalyzed RNA synthesis and pattern of inhibition following a single incorporation of ATP or GS-646939 as a function of nucleotide concentration**. ***A***, RNA primer/template supporting RNA synthesis and a single incorporation of ATP or GS-646939 at position 6 ("i"). G indicates incorporation of [α-$^{32}$P]-GTP at position 5. ***B***, Migration pattern of RNA products resulting from HRV-16 RdRp-catalyzed RNA extension of AMP (left) of GS-646939 (right) at increasing concentrations of CTP and UTP. A 5′-$^{32}$P-labeled 4-nt primer serves as a size marker. Product formation at and beyond the asterisk indicates RNA products that are likely a result of sequence-dependent slippage events. ***C***, RNA synthesis products catalyzed by EV-71 RdRp. Incomplete inhibition of RNA synthesis occurs at the site of GS-646939 incorporation ("i"), full template-length product is generated at elevated nucleotide concentrations.

To quantify the inhibitory effect of GS-443902 and GS-646939 on subsequent nucleotide incorporation, we generated AMP-, GS-443902-, and GS-646939-terminated primers and measured kinetic parameters of the natural UTP substrate incorporation at position "i+1" (Fig. 8.6 and Appendix E, Table E3). For all RdRp enzymes, compared to AMP-terminated primers, the extension of GS-646939-terminated primers required a marked increase in UTP concentration. Conversely, GS-443902-terminated primers promoted subtle inhibition of UTP incorporation for HRV-16, EV-71, RSV, and HMPV RdRp. For SARS-CoV-2, MERS-CoV, HPIV-3, and PIV-5 RdRp, equivalent or improved utilization of the GS-443902-terminated primer was observed.

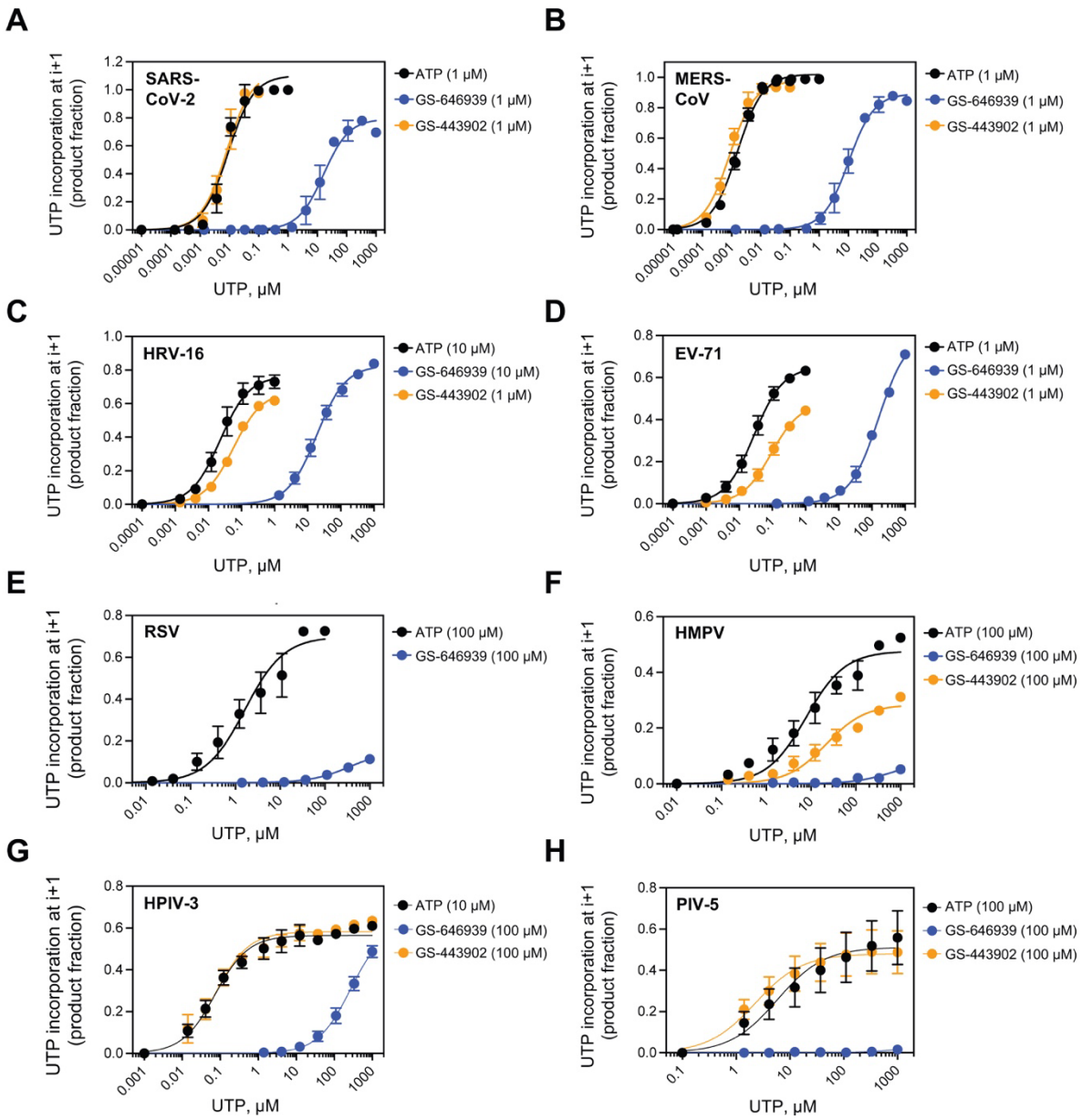


**Figure 8.6. GS-646939 inhibits subsequent nucleotide incorporation**. UTP incorporation at position "i+1" was monitored at increasing concentrations immediately following ATP (*black*), GS-443902 (*orange*), or GS-646939 (*blue*) incorporation at position "i". Concentrations of ATP, GS-443902, and GS-646939 supplemented to the reaction are shown in brackets. Viral RdRp enzymes investigated include SARS-CoV-2 (***A***), MERS-CoV (***B***), HRV-16 (***C***), EV-71 (***D***), RSV (***E***), HMPV (**F**), HPIV-3 (***G***), and PIV-5 (***H***). The product fraction was calculated as the total signal above position "i" divided by total signal in the lane. Independent 8-data point experiments were performed 3 times (n=3) and error bars represent standard error associated with the fit.

*HPIV-3 and HPIV-5 inhibition data were generated by SMW

### 8.2.5 Structural rationale for chain-termination

An analysis of the trajectory of the incorporated GS-646939 during translocation from the "i" substrate position to the "i+1" primer position may help to provide a better understanding of the requirements for chain-termination. For all the RdRps studied here, the 4′-cyano moiety of the inhibitor must pass through a set of Motif C residues, which coordinate the two catalytic metals (Fig. 8.7). The obstacle presented by these residues is largely independent of the specific sidechains and instead derives from the protein backbone itself. For HRV (Fig. 8.7*A*) and SARS-CoV-2 (Fig. 8.7*B*), this clash is moderate. But for RSV (Fig. 8.7*C*) and PIV5 (Fig. 8.7*D*), the clash appears to be severe, significantly impairing proper positioning of the primer. If translocation is indeed compromised, one would expect diminished NTP incorporation independent of the nature of the incoming nucleotide. Like GS-646939, 4′-ethynyl-2-fluoro-2′-deoxyadenosine (EFdA) possesses a bulky 4′-modification and was shown to block translocation of human immunodeficiency virus type 1 reverse transcriptase (HIV-1 RT) [406, 420, 421]. Therefore, we used EFdA as a benchmark. For HRV-16 RdRp, GS-646939- and EFdA-terminated primers generally reduce NTP incorporation of all nucleotides tested (Appendix D, Fig. D7). High concentrations of UTP and 2-thio-UTP are required to obtain the "i+1" product, while 3′deoxy UTP, 2′O-methyl UTP, and 2′deoxy UTP are not incorporated. In contrast, AMP- and GS-443902-terminated primers do not cause immediate chain-termination and instead enable the incorporation of each of these nucleotide analogs to a similar extent.

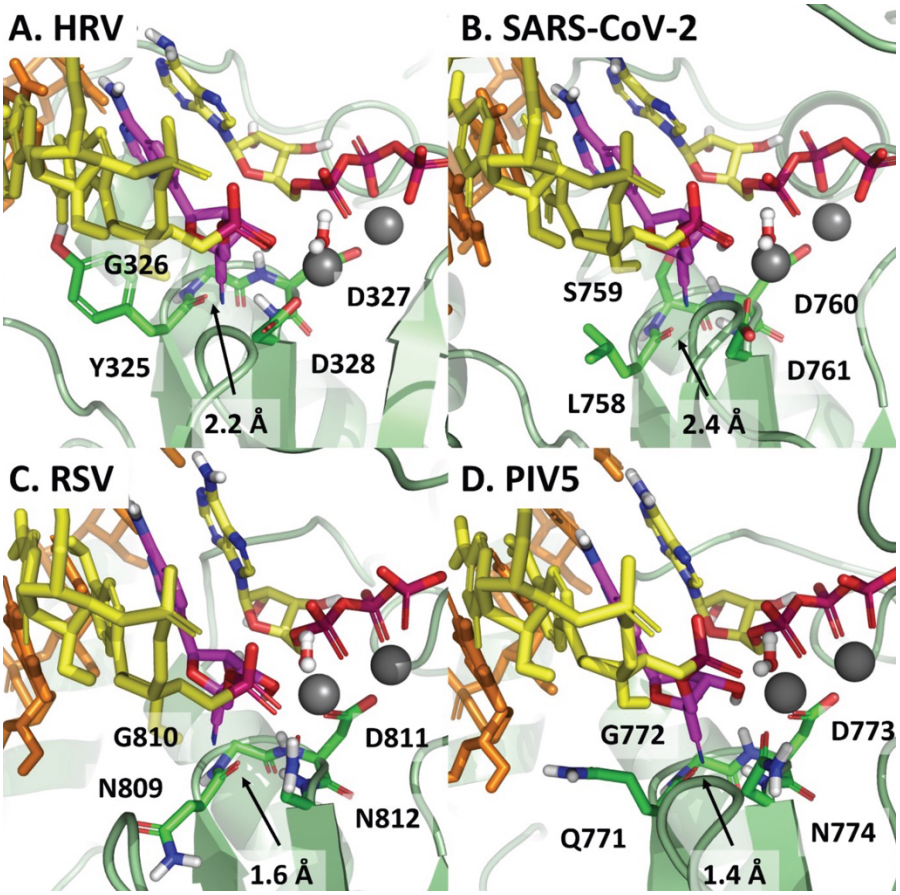


**Figure 8.7. Models of incorporated GS-646939 translocated to the "i+1" position for HRV (*A*), SARS-CoV-2 (*B*), RSV (*C*), and PIV-5 (*D*)**. Structures are not optimized but serve as a guide to clashes that impair further incorporation. Following incorporation, translocation of the RNA to position the inhibitor in the first primer position is hindered by residues of Motif C which coordinate the catalytic metals. For HRV, Cα of Gly-326 and NH of Asp-327 present a translocation obstacle to the 4′-cyano of the incorporated inhibitor. A similar impediment to translocation exists for the other RdRps. Assuming translocation occurs, C=O of Tyr-325 presents a significant steric clash which would perturb proper primer positioning. This clash appears to be more significant in RSV and PIV5.

*JKP contributed this figure.

### 8.2.6 Significance of template-dependent inhibition by GS-646939

For SARS-CoV-2 RdRp, it has been demonstrated that higher NTP concentrations can overcome GS-443902-induced delayed chain-termination or pausing[49, 50, 198, 265]. This in turn may lead to full-length products containing embedded nucleotide analogs. When used as a template, UTP incorporation opposite the complementary GS-443902 is diminished. This unified template-dependent inhibition mechanism for GS-443902 has been described for several viral RdRps [265]. Here, we designed RNA templates to monitor UTP incorporation opposite a template-embedded

GS-443902 or GS-646939 residue, respectively (Fig. 8.8*A*). For the HRV-16 RdRp, submicromolar UTP concentration was sufficient to generate full-template length product on Template "A" that contains the natural nucleotide (Fig. 8.8*B*). Comparatively, on Template "GS-443902" and "GS-646939", inhibition opposite the embedded analog could be rescued by increasing UTP concentrations ~8- and 2-fold, respectively (Fig. 8.8*C*). Similarly, EV-71 RdRp-catalyzed UTP incorporation was inhibited to a greater extent across GS-443902 (~16-fold) than GS-646939 (~9-fold) (Appendix E, Fig. E8). For SARS-CoV-2 and MERS-CoV RdRp, RNA synthesis opposite GS-646939 generates multiple intermediate products, indicative of an inhibitory effect (Appendix E, Fig. E9). To conclude, GS-443902 and GS-646939 cause inhibition in primer extension reactions when embedded in the template. While the template-dependent mechanism seems to be the dominant mode of inhibition of RdRp enzymes by GS-443902, GS-646939 acts primarily as a chain-terminator.

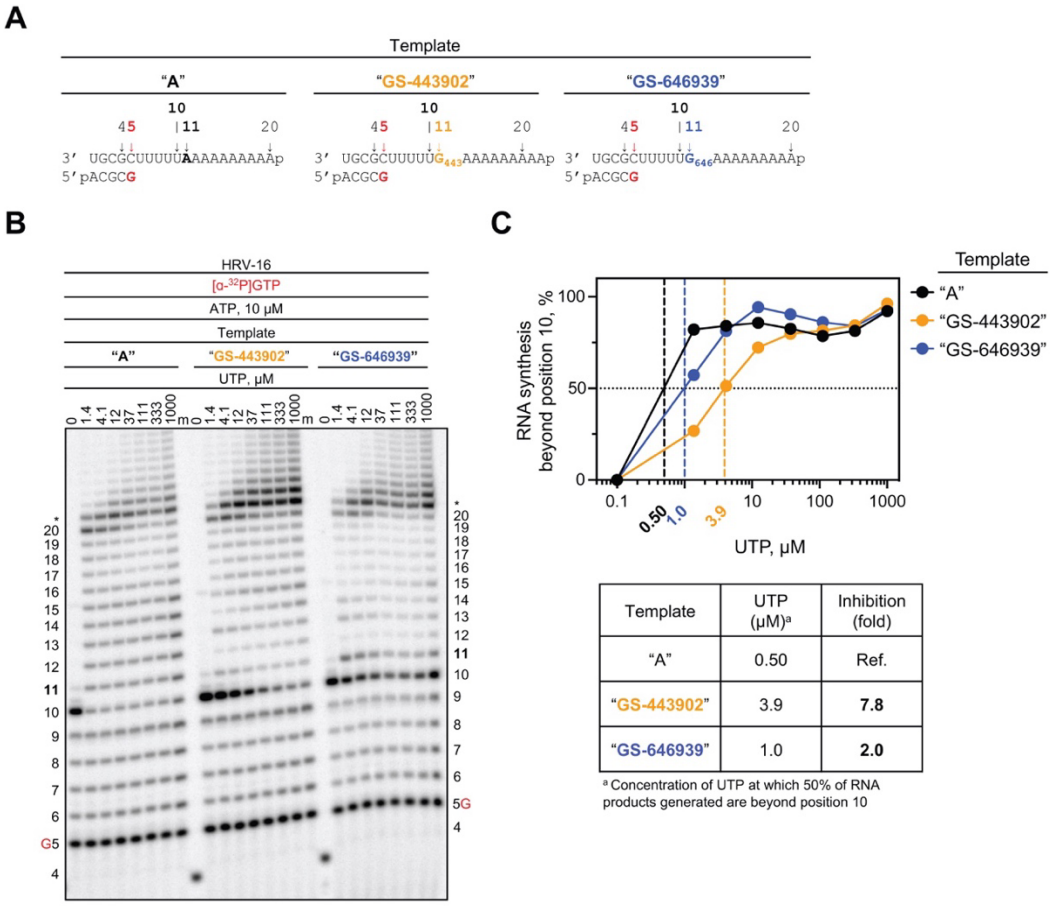


**Figure 8.8. RNA synthesis catalyzed by HRV-16 RdRp using a template with a single GS-443902 or GS-646939 residue embedded in the template at position 11**. ***A***, RNA primer/template with an embedded GS-443902 (Template "GS-443902", middle) or GS-646939 (Template "GS-646939", *right*); the corresponding primer/template with adenosine (Template A) at this position is shown on the left. G5 indicates incorporation of [α-$^{32}$P]-GTP at position 5. ***B***, Migration pattern of the products of RNA synthesis catalyzed by HRV-16 RdRp. $MgCl_2$, [α-$^{32}$P]-GTP, and ATP provided to the reaction to support RNA synthesis up to position 10. Increasing concentrations of UTP were supplemented to the reactions to monitor incorporation opposite a templated adenosine, GS-443902, or GS-646939 at position 11, and templated adenosines from position 12 to 20. Compared to Template A, intermediate products form at position 10 on Template "GS-443902" and "GS-646939", indicating template-dependent inhibition. Product formation at and beyond the asterisk indicates RNA products that are likely a result of sequence-dependent slippage events. A 5′-$^{32}$P-labeled 4-nt primer serves as a size marker. ***C***, Quantification of B (*top*) where the sum of RNA products generated beyond position 10 was divided by the total signal in the lane and normalized as a percentage, fold-inhibition resulting from an embedded GS-443902 or GS-646939 (*bottom*). To account for template-dependent differences in activity, product fraction was normalized as a percentage to product fraction observed at 1000 μM UTP for that template.

## 8.3 Discussion

The availability of effective antivirals for treating infections with respiratory RNA viruses is limited. Nucleotide analog RdRp inhibitors have the potential to act broadly against diverse RNA viruses, which is of particular importance in outbreak situations with emerging pathogens. Mutagenic nucleotides such as ribavirin, favipiravir, or molnupiravir provide prominent examples in this regard[113, 129, 223, 226, 232, 422]. These compounds are base-modified, which can cause lethal mutagenesis when the active triphosphate metabolite is used as a substrate[130, 224]. Classic nucleotide analogs with modifications in the sugar moiety commonly inhibit RNA synthesis. Here, we studied the mechanism of action of the GS-646939 nucleotide triphosphate metabolite of the newly discovered GS-7682 4′-cyano modified C-adenosine nucleotide phosphoramidate analog. Inhibition of RNA synthesis was evaluated against an array of purified recombinant RdRp enzymes representing medically relevant respiratory RNA viruses. The broadly acting 1′-cyano modified C-adenosine nucleotide triphosphate analog GS-443902 was included in this study for comparative purpose. Despite a certain degree of overlap in the spectrum of antiviral activities, the results of this study demonstrate distinct mechanisms of action for GS-443902 and GS-646939. While GS-443902 inhibits RNA synthesis predominantly when embedded in the template strand, GS-646939 causes chain-termination at the site of incorporation.

For RNA polymerases evaluated in this and our previous studies, the data reveal a decrease in selectivity for GS-443902 in the order of SARS-CoV-2, SARS-CoV, MERS-CoV > HRV-16, EV-71 > RSV, HMPV > HPIV-3, PIV-5 > LASV > influenza B ≫ h-mtRNAP. GS-443902 is a better substrate for the SARS-CoV-2 RdRp complex than its natural counterpart ATP[49, 261]. Cryo-EM structures of the enzyme complex with bound RNA and a pre-incorporated GS-443902 revealed a hydrophilic pocket composed of Nsp12 Thr-687, Asn-691, and Ser-759 that accommodates the 1′-cyano group[40]. Of note, the S759A mutation was shown to confer resistance to GS-5734, due to a 5- to 10-fold increase in discrimination against GS-443902 [40, 273]. Thus, biochemical and structural data align with *in vitro* selection experiments in explaining the selectivity for GS-443902 over ATP.

The preference for selective incorporation of GS-646939 follows the order: HRV-16 and EV-71 > SARS-CoV-2 and MERS-CoV ≈ RSV and HMPV > HPIV-3 and PIV-5 ≫ LASV ≫

influenza B = h-mtRNAP. For HRV-16 and EV-71 RdRp, GS-646939 is used ~20-50 fold more efficiently as a substrate than ATP. To the best of our knowledge, this is the most favourable selectivity ever reported for the incorporation of a nucleotide analog by viral polymerases. Modeling of the pre-incorporated GS-646939 indicates that the 4′-cyano is tolerated by each of the aforementioned polymerases with the exception of LASV, influenza B and h-mtRNAP. With respect to HRV-16 and EV-71 RdRp, the particular combination of residues that form both the 2′-OH recognition motif and the 4′ pocket allow for a favorable interaction between the 4′-cyano and Asn-296 in HRV. In the case of LASV and influenza B, both the 1′-cyano of GS-443902 and the 4′-cyano of GS-646939 disrupt a water-mediated hydrogen bonding network which serves to recognize the ribose 2′-OH. The active site of h-mtRNAP is dissimilar to any of the viral RdRps, with predicted clashes for both 1′-cyano and 4′-cyano substitutions.

GS-443902-mediated inhibition of primer extension reactions is generally heterogeneous[260]. The position and extent of inhibition depend upon the nature of the polymerase, and the underlying structural determinants have not yet been investigated for RSV and other RdRps. For the SARS-CoV-2 RdRp complex, delayed chain-termination and backtracking have been associated with the incorporation of GS-443902[49, 198]. Although structural evidence for backtracking has been reported[204], it is currently not known whether these events can be linked to each other and whether GS-443902 triggers similar effects also on other viral polymerases. In contrast, all viral RNA polymerases tested towards this end inhibit the incorporation of UTP opposite an embedded GS-443902 in the template. This inhibition may not necessarily translate into significant antiviral effects because the incorporation of GS-443902 may be inefficient in some cases, as it is for LASV and influenza viruses[260]. For GS-646939, the unifying mechanism of action is chain-termination. The extent of inhibition depends on the NTP concentration that can overcome blockages. Chain-termination with HRV-16 and EV-71 RdRp is indeed not absolute, and higher NTP concentrations allow the continuation of RNA synthesis. However, the high selectivity for GS-646939 over ATP seems sufficient to cause potent antiviral effects. Chain-termination with SARS-CoV-2 and MERS-CoV is also overcome with higher NTP concentrations, but a limited antiviral effect in cellular assays may be explained by the presence of a viral exonuclease, which can remove the incorporated inhibitor and allow synthesis to continue[286]. For

RSV and HMPV, chain-termination is nearly absolute and lower nucleotide analog incorporation rates are therefore still sufficient for potent antiviral effects.

The antiviral effects and biochemical properties of several other nucleotide analogs with bulky 4′-modifications have been reported, and chain-termination is the dominant mechanism of action[238, 291, 325-327, 421, 423-425]. Prodrugs of 4′-azidocytidine (balapiravir) and 4′-chloromethyl-2′-deoxy-2′-fluoro-cytidine (lumicitabine) were developed for the treatment of HCV and RSV infection, respectively. EFdA was developed for the treatment of HIV-1 infection. EFdA-TP is efficiently incorporated by HIV-1 RT, and structural data provide strong evidence to show that chain-termination is based on compromised enzyme translocation [406, 420, 421]. A hydrophobic pocket accommodates the 4′-ethynyl moiety, which facilitates binding of EFdA-TP and stabilizes the complex after incorporating the nucleotide analog. The favourable interactions in the pre-translocated state and unfavourable interactions in the post-translocated state essentially block RT translocation and further incorporation events. Our structural models of RdRp enzymes considered in this study point to a similar mechanism with GS-646939. In contrast, 4′-fluorouridine was shown to cause delayed chain-termination against RSV RdRp [327]. This data suggests that the relatively small 4′-fluoro modification does not interfere with translocation at the point of incorporation.

In conclusion, 1′-cyano and 4′-cyano modified nucleotide analogs inhibit diverse RdRp enzymes of respiratory RNA viruses via different mechanisms. Enzymes of the *Coronaviridae* (SARS-CoV-2 and MERS-CoV) and the *Pneumoviridae* (RSV and HMPV), are effectively targeted by the 1′-cyano modified C-adenosine GS-443902. Selective incorporation, various blockages during primer extension, and efficient template-dependent inhibition provide biochemical explanations for the observed antiviral activity [49, 50, 265]. RdRps of the *Picornaviridae* (HRV-16 and EV-71) and *Pneumoviridae* (RSV and HMPV) are effectively targeted by the 4′-cyano modified C-adenosine GS-646939. Selective incorporation and efficient chain-termination were identified here as important parameters that correlate with potent antiviral activity in cell culture. The described inhibitory effects were observed with two prototypic polymerases of the *Coronaviridae*, the *Pneumoviridae* and the *Picornaviridae*; hence, the data provide confidence

that the 1′-cyano and 4′-cyano modified nucleotides can be considered broadly to target emerging viruses that belong to these families.

Chapter 9: Concluding remarks and future directions

## 9.1 General summary and contributions to the COVID-19 pandemic

The aim of this dissertation was to investigate broad-spectrum nucleotide analogs, namely RDV-TP, NHC-TP, and GS-646989, and determine the biochemical parameters that facilitate their antiviral effect. Central to this goal was the successful expansion of our viral RdRp library that offers coverage across important RNA virus families. Collectively, the data reported in this thesis supported COVID-19 pandemic rapid response efforts and demonstrate the utility of the prototypic pathogen approach to improve our preparedness for future pandemics (Fig. 9.1). Finally, this work offers strategies that will support the study of the next generation of nucleotide analogs against the RdRp from prototypic RNA viruses.

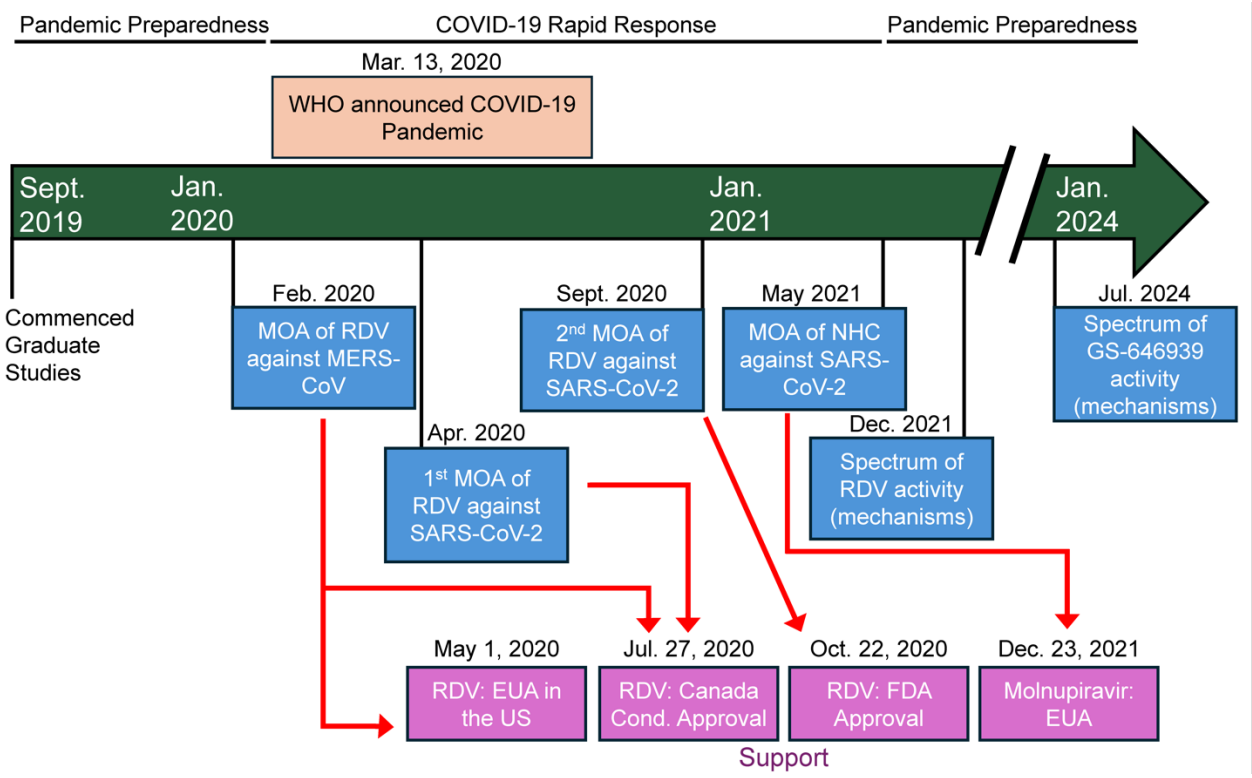


**Figure 9.1. Timeline of publications that contributed to COVID-19 rapid response efforts and pandemic preparedness**. Publications (*blue boxes*) included in this dissertation that detail the mechanism of action (MOA) of RDV and molnupiravir against coronavirus RdRp supported their approval or emergency use authorization (EUA) for the treatment of COVID-19, respectively. Pandemic preparedness is addressed by the spectrum of activity studies for RDV and GS-646939 (*right*) against a panel of viral RdRp.

### 9.1.1 Supporting the approval of RDV and molnupiravir for the treatment of COVID-19

The initial investigation of MERS-CoV RdRp complex offered a novel expression strategy for coronavirus RdRp complexes and provided a springboard into pandemic rapid response efforts. The following studies directed towards SARS-CoV-2 focused on RDV-TP, and other nucleotide analogs that were also under therapeutic consideration at the time (i.e. ribavirin, favipiravir, and sofosbuvir). These results would be the first to indicate that RDV-TP is a superior substrate compared to other nucleotide analogs. Subsequent preclinical and clinical data would corroborate these findings. RDV-TP inhibits RNA synthesis via two mechanisms downstream from the site of incorporation. This is a key attribute that likely helps RDV-TP evade excision by the proofreading ExoN. Ultimately, this work supported the approval of RDV as the first available antiviral therapy for people infected with SARS-CoV-2 and would be included in the FDA factsheet for healthcare providers under "mechanism of action". In contrast, the antiviral activity of molnupiravir is not reliant on chain termination but rather promiscuous base pairing. Disclosed in these studies is biochemical mechanism of action for molnupiravir that facilitate its observed mutagenic effects. These findings helped support the EUA authorization of molnupiravir by the FDA for the treatment of COVID-19. Together, this portion of my thesis presents the first mechanistic evaluation of RDV-TP and NHC-TP against SARS-CoV-2 RdRp complex, which offer valuable insight towards the parameters required for anti-coronavirus activity.

### 9.1.2 Evaluating broad-spectrum nucleoside analogs to address pandemic preparedness efforts

Broad-spectrum nucleoside analogs offer a logical and efficient solution to address pandemic preparedness efforts. The final studies included in this thesis detail a collaborative effort by our group investigating a 1′-cyano (RDV-TP) and 4′-cyano (GS-646939) modified nucleotide against several prototypic viral RdRp. At a biochemical level, these projects demonstrate successful nucleotide analogs must efficiently compete with its natural counterpart for incorporation by the viral RdRp. As a substrate, bulky 1′- or 4′-modifications are most suitable to target positive- and nonsegmented negative-sense RNA viruses. Conversely, these modifications are not viable options to target segmented negative RNA viruses and alternative substitutions should be considered. As summarized in figure 9.2, the 1′-cyano modification elicits a uniform and more potent mechanism of inhibition when acting as the templating base. Whereas the 4′-

cyano modification promotes immediate chain termination. The different mechanistic behavior between these cyano-modified nucleotide analogs will aid the development of future nucleotide analogs targeting a spectrum of RNA viruses.

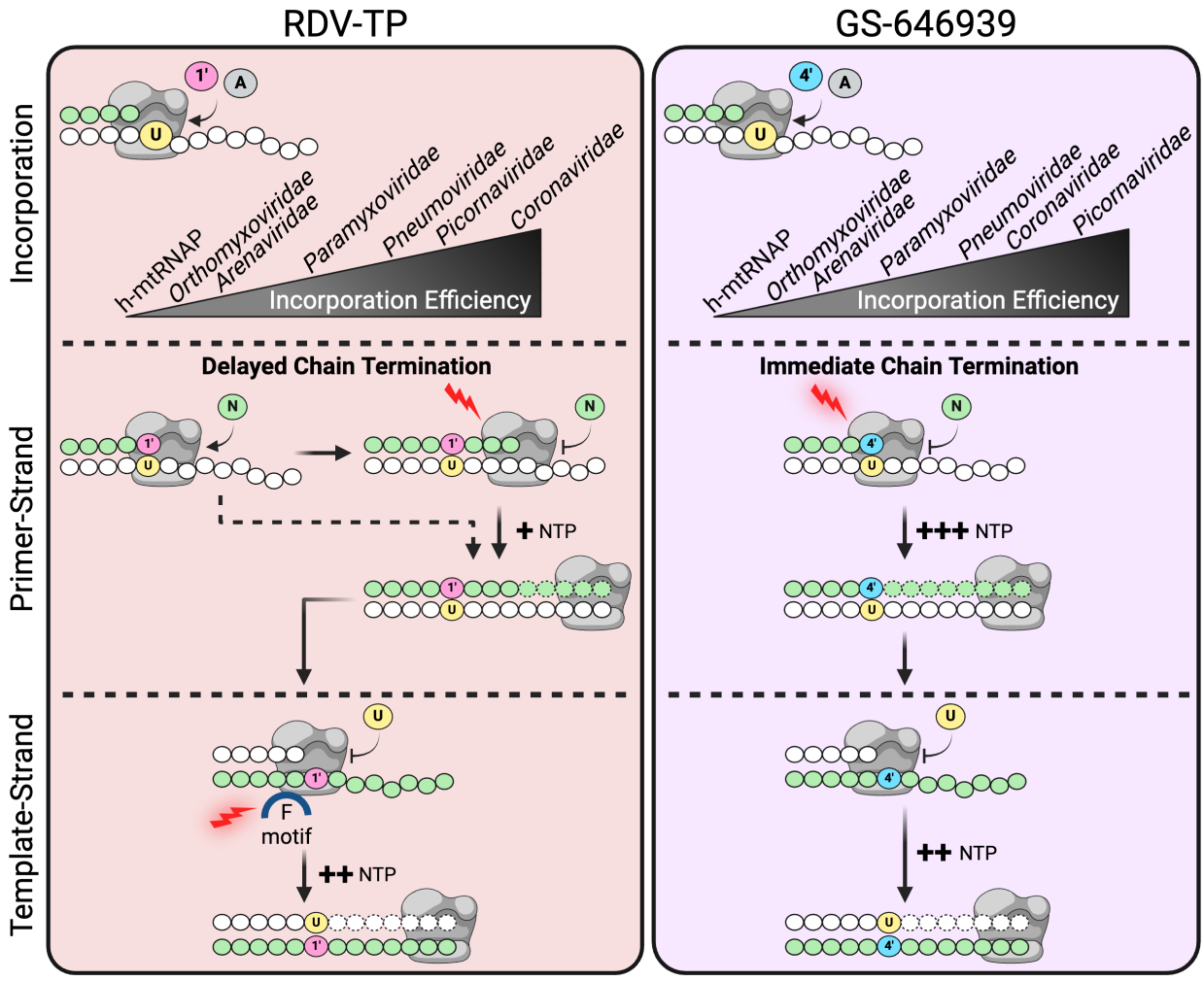


**Figure 9.2. Summary of the mechanism of action for RDV-TP (left) and GS-646939 (right)**. *Top*, RDV-TP (*pink circle*) and GS-646939 (*blue circle*) compete with ATP (*grey circle*) for incorporation by the viral polymerase (*grey*) into the elongating primer strand (*green circles*). Middle, during primer strand elongation RDV-TP inhibitory effects are more heterogenous and inhibition can be easily overcome with increased subsequent nucleotide concentration. Whereas GS-646939 acts uniformly as an immediate chain terminator requiring much greater subsequent nucleotide concentration to overcome inhibition. Bottom, when embedded in the template strand both RDV-MP and GS-646939-MP provoke an inhibitory effect. These data suggest that the primary mechanism of action for RDV-TP and GS-646939 are template-dependent inhibition and immediate chain termination, respectively.

To conclude, RNA viruses from the *Picorna*-, *Paramyxo*-, *Filo*-, *Bunya*-, and *Orthomyxoviridae* families pose a significant threat to human health due to their epidemic potential and absence of effective medical countermeasures. This thesis presents the first mechanistic studies of 1′- or 4′-cyano-modified nucleotide analogs against several important RNA virus families. I provide a biochemical rationale supporting the development of these modified nucleoside analog prodrugs for preparedness against future picorna- and paramyxo-, and filovirus outbreaks. Conversely, therapeutic intervention strategies towards orthomyxo- and high-priority bunyaviruses are generally lacking. I have identified the limitations of bulky 1′- or 4′-modified nucleoside analogs and key biochemical parameters that must be improved for enhanced potency. Future preclinical studies should employ a comprehensive approach which addresses DAA development from a prototypic pathogen perspective. The strategies outlined in this thesis provide a foundation for subsequent biochemical studies investigating the next generation of nucleotide analogs targeting priority pathogens.

## 9.2 Future directions

### 9.2.1 Continued nucleoside analog development for improved treatment efficacy

Vaccines remain the gold-standard for reducing viral transmission and instances of severe disease. However, vaccines may not be available at the onset of RNA virus outbreaks and therefore readily available DAAs, such as nucleoside analogs, are needed to mitigate early spread. Still, a nucleoside analog is only as effective as its prodrug formulation. When considering acute viral infection, the optimal prodrug would be orally available to allow for treatment early in disease progression. Remdesivir requires intravenous administration, and as a result is limited to hospitalized patients whose disease may have advanced beyond the therapeutic window. Indeed, remdesivir treatment was more efficacious in an outpatient setting at reducing severe disease progression[426]. Oral availability can also broaden prodrug utility to include post-exposure prophylaxis. Baloxavir, although not a polymerase inhibitor, is an orally available DAA approved for the treatment of influenza and is highly effective as a post-exposure prophylactic[427, 428]. Unfortunately, increased exposure to an antiviral monotherapy, will likely introduce drug resistance into a viral population. Indeed, resistance was detected following a single dose treatment of baloxavir[427]. Therefore, clinical resistance to nucleoside analog prodrugs must be monitored. Identifying resistance-conferring mutations will not only provide greater insight into the

mechanism of action but also guide the development of the next generation of antivirals. Exemplified by antiretroviral therapy (ART) for HIV-positive patients, multi-drug treatment regimens offer an effective strategy to combat resistance[429]. Taken together, there remains a need for additional medical countermeasures, ideally ones that are orally available and can work in tandem with already approved DAAs.

### 9.2.2 SARS-CoV-2 3′ to 5′ proofreading exoribonuclease

The characterization of RDV-TP, NHC-TP, and GS-646939 against the SARS-CoV-2 RdRp complex is not entirely complete. A key variable missing from these studies is their ability to evade recognition by the 3′ to 5′ proofreading ExoN. Based on previous coronavirus ExoN-deficient studies, one would anticipate that RDV-TP is somewhat susceptible to excision[251], while NHC-TP may be resistant[226]. Preliminary data generated in our lab, as well as data published by others, have established a system to monitor coronavirus ExoN activity[270, 321]. To thoroughly divulge ExoN susceptibility, these studies would require investigating the interplay between the RdRp complex and the ExoN, a relationship that remains unresolved[270, 321]. Work by Chinthapatla and colleagues found that stable RdRp complex association with the terminal basepair, regardless of its composition, blocked ExoN access[270]. This observation highlights an additional confounding variable the helicase (Nsp13), which has been associated with backtracking as a mechanism to partition RNA duplex allowing ExoN access to the single-stranded RNA 3′-terminus[204, 205]. Therefore, a logical approach to ExoN susceptibility would require an assay that can first evaluate the relationship between SARS-CoV-2 RdRp complex (Nsp7, -8, -12) and Nsp13.

Protein-protein interactions facilitate Nsp7, -8, -12, and -13 complex formation[204-206], and the addition of Nsp12 enhances Nsp13 unwinding activity[430, 431]. Recent work has demonstrated ultraviolet (UV)-induced cross-linking as viable technique to monitor RdRp backtracking[204]. Here, the authors rely on an already incorporated 4-thiouridine that, when released from the RNA duplex due to helicase unwinding, can crosslink with the replication complex. Studies have yet to achieve an assay that is capable of monitoring RNA synthesis and backtracking activity by a Nsp7, -8, -12, and -13 complex. It is assumed that backtracking is initiated by RdRp complex stalling, therefore RdRp pre-translocation may be necessary to engage Nsp13. Supplementing increased NTP concentration can shift the RdRp to post-translocation, which in turn, should prevent Nsp13-mediated backtracking activity.

A major hurdle to this investigation is the NTPase activity of Nsp13 which would inherently sequester available NTP substrate away from the RdRp active site preventing RNA catalysis. A potential solution to this would be the use of nonhydrolyzable nucleotide diphosphate (NDP) substrates which cannot support Nsp13 helicase activity[432] but can be incorporated by the RdRp active site, albeit less efficiently than their NTP counterpart[433]. Taken together, it is feasible that complex backtracking and RNA synthesis can be monitored in the absence or presence of NTP/NDP substrate, respectively. By extension, the hypothesis that backtracking enables ExoN access to the single-stranded RNA 3′-terminus promoting excision could then be investigated. The inclusion of RDV-TP, NHC-TP, or GS-646939 in these studies would provide additional biochemical parameters that determine their antiviral activity against SARS-CoV-2.

GS-646939 is efficiently incorporated by the SARS-CoV-2 RdRp complex, but the prodrug demonstrates limited antiviral activity in cell culture. This is likely because it acts as an immediate chain terminator, a mechanism that in theory should promote ExoN excision. Assuming GS-646939 is efficiently excised by the ExoN, an interesting follow-up study would include replacing the non-bridging oxygen of the 5′-α-phosphate with a sulfur atom. This strategy proved to be successful for limiting the ExoN excision[270, 321], therefore it may improve antiviral activity against SARS-CoV-2.

### 9.2.3 GS-646939 as a translocation inhibitor

In Chapter 7 we conclude GS-646939 likely prevents translocation to inhibit RNA synthesis. This was based on structural similarity to EFdA-TP (an established translocation inhibitor), modeling, and subsequent incorporation of modified nucleotides. To further elucidate how GS-646939 may affect translocation, future work should include structural and biochemical experimentation with picornavirus $3D^{pol}$. In both cases a stable elongation complex must be established, this will require optimization which is likely to be different for structural and biochemical studies. As demonstrated previously for EFdA-TP against HIV-1 RT[421], this study would require capturing structural intermediates before and after incorporation of GS-646989. One technique that proved successful to trap a pre-incorporation SARS-CoV-2 structure was the incorporation of 3′-deoxy nucleotide prior to the analog[40]. The greatest barrier to these structural

studies may be resources, this could be overcome through collaboration or implementation of the new Cryo-EM facility on campus.

Biochemically, potential phosphorolytic excision of GS-646939 would be an interesting pursuit that pairs nicely with structural studies. Techniques evaluating this mechanism have been described in detail for 2′-modified nucleotide analogs against HCV. This investigation would require reaction conditions that allow for a stable elongation complex to form with a labelled RNA substrate. We have generated preliminary data to support this approach, however it has not been demonstrated for all available viral RdRp. If phosphorolytic excision is achieved, next steps would include demonstrating the rescue of RNA synthesis following GS-646939 removal from the nascent primer strand. Naturally, completion of these objectives would facilitate the investigation of other nucleotide analogs, specifically RDV-TP. Together, this work would provide valuable information regarding the efficacy of structurally related analogs (1′- versus 4′-cyano) and support development of the next generation of nucleotide analogs.

### 9.2.4 GS-646939 resistance

Resistance to GS-7682, the prodrug of GS-646939, has yet to be observed in the literature. Considering the highly efficient rates of incorporation and inhibition of RNA synthesis via immediate chain termination. Anticipated mechanisms of resistance could include reduced incorporation efficiency or phosphorolytic excision of GS-646939. Three key residues in motif B of RSV, when mutated, reduced the incorporation efficiency of 2′-F,4′-$ClCH_2$ CTP, another bulky 4′-modified nucleotide analog. Until resistance is discovered, future work should evaluate GS-646939 against the analogous mutations in picornavirus $3D^{pol}$. This investigation could be extended to other nucleotide analogs to assess potential cross-resistance or hypersusceptibility. A mechanism of HIV-1 RT resistance to AZT is phosphorolytic excision where ATP is the acting pyrophosphate donor. Although this resistant mechanism has not been described for an RNA virus, the pyrophosphorolysis assay described above would enable the investigation of phosphorolytic excision as a potential mechanism of resistance.

### 9.2.5 4′-fluoro modified nucleotide analogs

As exemplified by 4′-Fl U, less bulky 4′-modified nucleotide analogs present an exciting opportunity to target a diverse spectrum of RNA viruses. 4′-Fl UTP can act as a substrate for SARS-CoV-2, RSV, and influenza RdRp[327, 329]. However, the mechanism of action is convoluted and likely dependent on the nature of the RdRp. Using the same strategy shown in Chapters 6 and 7, future work should consider a comprehensive biochemical study of diverse viral RdRp against a less bulky 4′-modified nucleotide analog. RNA synthesis following a single 4′-Fl UMP can proceed uninterrupted[330], therefore this study would require the investigation of a template-dependent mechanism. To this end, our T7 RNA oligo synthesis platform will prove to be instrumental.

Nucleotide analogs that effectively target segmented negative-sense RNA virus RdRp (e.g. influenza) remain a challenge. 4′-Fl U, given its activity against influenza, should act as a guide for additional structure-activity relationship studies. Previous nucleotide analogs that effectively target influenza RdRp have low specificity, therefore, candidate nucleotide analogs should be evaluated against h-mtRNAP for insight into potential toxicities.

Literature Cited


1. Organization, W. H. Targeting research on diseases of greatest epidemic and pandemic threat. https://www.who.int/teams/blueprint/who-r-and-d-blueprint-for-epidemics.
2. Cassetti, M. C.; Pierson, T. C.; Patterson, L. J.; Bok, K.; DeRocco, A. J.; Deschamps, A. M.; Graham, B. S.; Erbelding, E. J.; Fauci, A. S., Prototype Pathogen Approach for Vaccine and Monoclonal Antibody Development: A Critical Component of the NIAID Plan for Pandemic Preparedness. *J Infect Dis* **2023,** *227* (12), 1433-1441.
3. Lu, R.; Zhao, X.; Li, J.; Niu, P.; Yang, B.; Wu, H.; Wang, W.; Song, H.; Huang, B.; Zhu, N.; Bi, Y.; Ma, X.; Zhan, F.; Wang, L.; Hu, T.; Zhou, H.; Hu, Z.; Zhou, W.; Zhao, L.; Chen, J.; Meng, Y.; Wang, J.; Lin, Y.; Yuan, J.; Xie, Z.; Ma, J.; Liu, W. J.; Wang, D.; Xu, W.; Holmes, E. C.; Gao, G. F.; Wu, G.; Chen, W.; Shi, W.; Tan, W., Genomic characterisation and epidemiology of 2019 novel coronavirus: implications for virus origins and receptor binding. *Lancet* **2020,** *395* (10224), 565-574.
4. Zhu, N.; Zhang, D.; Wang, W.; Li, X.; Yang, B.; Song, J.; Zhao, X.; Huang, B.; Shi, W.; Lu, R.; Niu, P.; Zhan, F.; Ma, X.; Wang, D.; Xu, W.; Wu, G.; Gao, G. F.; Tan, W., A Novel Coronavirus from Patients with Pneumonia in China, 2019. *New England Journal of Medicine* **2020,** *382* (8), 727-733.
5. Falsey, A. R.; McElhaney, J. E.; Beran, J.; van Essen, G. A.; Duval, X.; Esen, M.; Galtier, F.; Gervais, P.; Hwang, S. J.; Kremsner, P.; Launay, O.; Leroux-Roels, G.; McNeil, S. A.; Nowakowski, A.; Richardus, J. H.; Ruiz-Palacios, G.; St Rose, S.; Devaster, J. M.; Oostvogels, L.; Durviaux, S.; Taylor, S., Respiratory syncytial virus and other respiratory viral infections in older adults with moderate to severe influenza-like illness. *J Infect Dis* **2014,** *209* (12), 1873-81.
6. Li, Y.; Wang, X.; Blau, D. M.; Caballero, M. T.; Feikin, D. R.; Gill, C. J.; Madhi, S. A.; Omer, S. B.; Simoes, E. A. F.; Campbell, H.; Pariente, A. B.; Bardach, D.; Bassat, Q.; Casalegno, J. S.; Chakhunashvili, G.; Crawford, N.; Danilenko, D.; Do, L. A. H.; Echavarria, M.; Gentile, A.; Gordon, A.; Heikkinen, T.; Huang, Q. S.; Jullien, S.; Krishnan, A.; Lopez, E. L.; Markic, J.; Mira-Iglesias, A.; Moore, H. C.; Moyes, J.; Mwananyanda, L.; Nokes, D. J.; Noordeen, F.; Obodai, E.; Palani, N.; Romero, C.; Salimi, V.; Satav, A.; Seo, E.; Shchomak, Z.; Singleton, R.; Stolyarov, K.; Stoszek, S. K.; von Gottberg, A.; Wurzel, D.; Yoshida, L. M.; Yung, C. F.; Zar, H. J.; Respiratory Virus Global Epidemiology, N.; Nair, H.; investigators, R., Global, regional, and national disease burden estimates of acute lower respiratory infections due to respiratory syncytial virus in children younger than 5 years in 2019: a systematic analysis. *Lancet* **2022,** *399* (10340), 2047-2064.
7. Letunic, I.; Bork, P., Interactive Tree of Life (iTOL) v6: recent updates to the phylogenetic tree display and annotation tool. *Nucleic Acids Res* **2024**.
8. De Clercq, E.; Li, G., Approved Antiviral Drugs over the Past 50 Years. *Clin Microbiol Rev* **2016,** *29* (3), 695-747.
9. Seley-Radtke, K. L.; Thames, J. E.; Waters, C. D., 3rd, Broad spectrum antiviral nucleosides-Our best hope for the future. *Annu Rep Med Chem* **2021,** *57*, 109-132.
10. Gong, P.; Kortus, M. G.; Nix, J. C.; Davis, R. E.; Peersen, O. B., Structures of coxsackievirus, rhinovirus, and poliovirus polymerase elongation complexes solved by engineering RNA mediated crystal contacts. *PloS one* **2013,** *8* (5), e60272.
11. Wu, Y.; Lou, Z.; Miao, Y.; Yu, Y.; Dong, H.; Peng, W.; Bartlam, M.; Li, X.; Rao, Z., Structures of EV71 RNA-dependent RNA polymerase in complex with substrate and analogue

provide a drug target against the hand-foot-and-mouth disease pandemic in China. *Protein Cell* **2010,** *1* (5), 491-500.
12. Ferrer-Orta, C.; Ferrero, D.; Verdaguer, N., RNA-Dependent RNA Polymerases of Picornaviruses: From the Structure to Regulatory Mechanisms. *Viruses* **2015,** *7* (8), 4438-60.
13. Peersen, O. B., Picornaviral polymerase structure, function, and fidelity modulation. *Virus research* **2017,** *234*, 4-20.
14. Hansen, J. L.; Long, A. M.; Schultz, S. C., Structure of the RNA-dependent RNA polymerase of poliovirus. *Structure* **1997,** *5* (8), 1109-22.
15. Ago, H.; Adachi, T.; Yoshida, A.; Yamamoto, M.; Habuka, N.; Yatsunami, K.; Miyano, M., Crystal structure of the RNA-dependent RNA polymerase of hepatitis C virus. *Structure* **1999,** *7* (11), 1417-26.
16. Bressanelli, S.; Tomei, L.; Roussel, A.; Incitti, I.; Vitale, R. L.; Mathieu, M.; De Francesco, R.; Rey, F. A., Crystal structure of the RNA-dependent RNA polymerase of hepatitis C virus. *Proceedings of the National Academy of Sciences of the United States of America* **1999,** *96* (23), 13034-9.
17. Lesburg, C. A.; Cable, M. B.; Ferrari, E.; Hong, Z.; Mannarino, A. F.; Weber, P. C., Crystal structure of the RNA-dependent RNA polymerase from hepatitis C virus reveals a fully encircled active site. *Nat Struct Biol* **1999,** *6* (10), 937-43.
18. Jia, H.; Gong, P., A Structure-Function Diversity Survey of the RNA-Dependent RNA Polymerases From the Positive-Strand RNA Viruses. *Front Microbiol* **2019,** *10*, 1945.
19. Ferrari, E.; Wright-Minogue, J.; Fang, J. W.; Baroudy, B. M.; Lau, J. Y.; Hong, Z., Characterization of soluble hepatitis C virus RNA-dependent RNA polymerase expressed in Escherichia coli. *J Virol* **1999,** *73* (2), 1649-54.
20. Yamashita, T.; Kaneko, S.; Shirota, Y.; Qin, W.; Nomura, T.; Kobayashi, K.; Murakami, S., RNA-dependent RNA polymerase activity of the soluble recombinant hepatitis C virus NS5B protein truncated at the C-terminal region. *The Journal of biological chemistry* **1998,** *273* (25), 15479-86.
21. Keating, G. M., Sofosbuvir: a review of its use in patients with chronic hepatitis C. *Drugs* **2014,** *74* (10), 1127-46.
22. Gilead Sciences Inc. Sovaldi™ (sofosbuvir) tablets, for oral use: US prescribing information. https://www.gilead.com/-/media/files/pdfs/medicines/liver-disease/sovaldi/sovaldi_patient_pi.pdf.
23. Pierson, T. C.; Diamond, M. S., The continued threat of emerging flaviviruses. *Nat Microbiol* **2020,** *5* (6), 796-812.
24. Potisopon, S.; Priet, S.; Collet, A.; Decroly, E.; Canard, B.; Selisko, B., The methyltransferase domain of dengue virus protein NS5 ensures efficient RNA synthesis initiation and elongation by the polymerase domain. *Nucleic Acids Res* **2014,** *42* (18), 11642-56.
25. Latour, D. R.; Jekle, A.; Javanbakht, H.; Henningsen, R.; Gee, P.; Lee, I.; Tran, P.; Ren, S.; Kutach, A. K.; Harris, S. F.; Wang, S. M.; Lok, S. J.; Shaw, D.; Li, J.; Heilek, G.; Klumpp, K.; Swinney, D. C.; Deval, J., Biochemical characterization of the inhibition of the dengue virus RNA polymerase by beta-d-2'-ethynyl-7-deaza-adenosine triphosphate. *Antiviral research* **2010,** *87* (2), 213-22.
26. Ackermann, M.; Padmanabhan, R., De novo synthesis of RNA by the dengue virus RNA-dependent RNA polymerase exhibits temperature dependence at the initiation but not elongation phase. *The Journal of biological chemistry* **2001,** *276* (43), 39926-37.

27. Guyatt, K. J.; Westaway, E. G.; Khromykh, A. A., Expression and purification of enzymatically active recombinant RNA-dependent RNA polymerase (NS5) of the flavivirus Kunjin. *J Virol Methods* **2001,** *92* (1), 37-44.
28. Jin, Z.; Deval, J.; Johnson, K. A.; Swinney, D. C., Characterization of the elongation complex of dengue virus RNA polymerase: assembly, kinetics of nucleotide incorporation, and fidelity. *The Journal of biological chemistry* **2011,** *286* (3), 2067-77.
29. Potisopon, S.; Ferron, F.; Fattorini, V.; Selisko, B.; Canard, B., Substrate selectivity of Dengue and Zika virus NS5 polymerase towards 2'-modified nucleotide analogues. *Antiviral research* **2017,** *140*, 25-36.
30. Wu, J.; Lu, G.; Zhang, B.; Gong, P., Perturbation in the conserved methyltransferase-polymerase interface of flavivirus NS5 differentially affects polymerase initiation and elongation. *J Virol* **2015,** *89* (1), 249-61.
31. Selisko, B.; Papageorgiou, N.; Ferron, F.; Canard, B., Structural and Functional Basis of the Fidelity of Nucleotide Selection by Flavivirus RNA-Dependent RNA Polymerases. *Viruses* **2018,** *10* (2).
32. Stern, D. F.; Kennedy, S. I., Coronavirus multiplication strategy. I. Identification and characterization of virus-specified RNA. *J Virol* **1980,** *34* (3), 665-74.
33. Gorbalenya, A. E.; Enjuanes, L.; Ziebuhr, J.; Snijder, E. J., Nidovirales: evolving the largest RNA virus genome. *Virus research* **2006,** *117* (1), 17-37.
34. Snijder, E. J.; Decroly, E.; Ziebuhr, J., The Nonstructural Proteins Directing Coronavirus RNA Synthesis and Processing. *Adv Virus Res* **2016,** *96*, 59-126.
35. Lehmann, K. C.; Gulyaeva, A.; Zevenhoven-Dobbe, J. C.; Janssen, G. M.; Ruben, M.; Overkleeft, H. S.; van Veelen, P. A.; Samborskiy, D. V.; Kravchenko, A. A.; Leontovich, A. M.; Sidorov, I. A.; Snijder, E. J.; Posthuma, C. C.; Gorbalenya, A. E., Discovery of an essential nucleotidylating activity associated with a newly delineated conserved domain in the RNA polymerase-containing protein of all nidoviruses. *Nucleic Acids Res* **2015,** *43* (17), 8416-34.
36. Slanina, H.; Madhugiri, R.; Bylapudi, G.; Schultheiss, K.; Karl, N.; Gulyaeva, A.; Gorbalenya, A. E.; Linne, U.; Ziebuhr, J., Coronavirus replication-transcription complex: Vital and selective NMPylation of a conserved site in nsp9 by the NiRAN-RdRp subunit. *Proceedings of the National Academy of Sciences of the United States of America* **2021,** *118* (6).
37. Small, G. I.; Fedorova, O.; Olinares, P. D. B.; Chandanani, J.; Banerjee, A.; Choi, Y. J.; Molina, H.; Chait, B. T.; Darst, S. A.; Campbell, E. A., Structural and functional insights into the enzymatic plasticity of the SARS-CoV-2 NiRAN domain. *Mol Cell* **2023,** *83* (21), 3921-3930 e7.
38. Park, G. J.; Osinski, A.; Hernandez, G.; Eitson, J. L.; Majumdar, A.; Tonelli, M.; Henzler-Wildman, K.; Pawlowski, K.; Chen, Z.; Li, Y.; Schoggins, J. W.; Tagliabracci, V. S., The mechanism of RNA capping by SARS-CoV-2. *Nature* **2022,** *609* (7928), 793-800.
39. Yan, L.; Huang, Y.; Ge, J.; Liu, Z.; Lu, P.; Huang, B.; Gao, S.; Wang, J.; Tan, L.; Ye, S.; Yu, F.; Lan, W.; Xu, S.; Zhou, F.; Shi, L.; Guddat, L. W.; Gao, Y.; Rao, Z.; Lou, Z., A mechanism for SARS-CoV-2 RNA capping and its inhibition by nucleotide analog inhibitors. *Cell* **2022,** *185* (23), 4347-4360 e17.
40. Malone, B. F.; Perry, J. K.; Olinares, P. D. B.; Lee, H. W.; Chen, J.; Appleby, T. C.; Feng, J. Y.; Bilello, J. P.; Ng, H.; Sotiris, J.; Ebrahim, M.; Chua, E. Y. D.; Mendez, J. H.; Eng, E. T.; Landick, R.; Gotte, M.; Chait, B. T.; Campbell, E. A.; Darst, S. A., Structural basis for substrate selection by the SARS-CoV-2 replicase. *Nature* **2023,** *614* (7949), 781-787.
41. Hillen, H. S.; Kokic, G.; Farnung, L.; Dienemann, C.; Tegunov, D.; Cramer, P., Structure of replicating SARS-CoV-2 polymerase. *Nature* **2020,** *584* (7819), 154-156.

42. Gao, Y.; Yan, L.; Huang, Y.; Liu, F.; Zhao, Y.; Cao, L.; Wang, T.; Sun, Q.; Ming, Z.; Zhang, L.; Ge, J.; Zheng, L.; Zhang, Y.; Wang, H.; Zhu, Y.; Zhu, C.; Hu, T.; Hua, T.; Zhang, B.; Yang, X.; Li, J.; Yang, H.; Liu, Z.; Xu, W.; Guddat, L. W.; Wang, Q.; Lou, Z.; Rao, Z., Structure of the RNA-dependent RNA polymerase from COVID-19 virus. *Science* **2020,** *368* (6492), 779-782.
43. Wang, Q.; Wu, J.; Wang, H.; Gao, Y.; Liu, Q.; Mu, A.; Ji, W.; Yan, L.; Zhu, Y.; Zhu, C.; Fang, X.; Yang, X.; Huang, Y.; Gao, H.; Liu, F.; Ge, J.; Sun, Q.; Yang, X.; Xu, W.; Liu, Z.; Yang, H.; Lou, Z.; Jiang, B.; Guddat, L. W.; Gong, P.; Rao, Z., Structural Basis for RNA Replication by the SARS-CoV-2 Polymerase. *Cell* **2020,** *182* (2), 417-428 e13.
44. Yin, W.; Mao, C.; Luan, X.; Shen, D. D.; Shen, Q.; Su, H.; Wang, X.; Zhou, F.; Zhao, W.; Gao, M.; Chang, S.; Xie, Y. C.; Tian, G.; Jiang, H. W.; Tao, S. C.; Shen, J.; Jiang, Y.; Jiang, H.; Xu, Y.; Zhang, S.; Zhang, Y.; Xu, H. E., Structural basis for inhibition of the RNA-dependent RNA polymerase from SARS-CoV-2 by remdesivir. *Science* **2020,** *368* (6498), 1499-1504.
45. Shannon, A.; Selisko, B.; Le, N. T.; Huchting, J.; Touret, F.; Piorkowski, G.; Fattorini, V.; Ferron, F.; Decroly, E.; Meier, C.; Coutard, B.; Peersen, O.; Canard, B., Rapid incorporation of Favipiravir by the fast and permissive viral RNA polymerase complex results in SARS-CoV-2 lethal mutagenesis. *Nature communications* **2020,** *11* (1), 4682.
46. Peng, Q.; Peng, R.; Yuan, B.; Zhao, J.; Wang, M.; Wang, X.; Wang, Q.; Sun, Y.; Fan, Z.; Qi, J.; Gao, G. F.; Shi, Y., Structural and Biochemical Characterization of the nsp12-nsp7-nsp8 Core Polymerase Complex from SARS-CoV-2. *Cell reports* **2020,** *31* (11), 107774.
47. Madru, C.; Tekpinar, A. D.; Rosario, S.; Czernecki, D.; Brule, S.; Sauguet, L.; Delarue, M., Fast and efficient purification of SARS-CoV-2 RNA dependent RNA polymerase complex expressed in Escherichia coli. *PloS one* **2021,** *16* (4), e0250610.
48. Dangerfield, T. L.; Huang, N. Z.; Johnson, K. A., Expression and purification of tag-free SARS-CoV-2 RNA-dependent RNA polymerase in Escherichia coli. *STAR Protoc* **2021,** *2* (1), 100357.
49. Gordon, C. J.; Tchesnokov, E. P.; Woolner, E.; Perry, J. K.; Feng, J. Y.; Porter, D. P.; Gotte, M., Remdesivir is a direct-acting antiviral that inhibits RNA-dependent RNA polymerase from severe acute respiratory syndrome coronavirus 2 with high potency. *The Journal of biological chemistry* **2020,** *295* (20), 6785-6797.
50. Gordon, C. J.; Tchesnokov, E. P.; Feng, J. Y.; Porter, D. P.; Gotte, M., The antiviral compound remdesivir potently inhibits RNA-dependent RNA polymerase from Middle East respiratory syndrome coronavirus. *The Journal of biological chemistry* **2020,** *295* (15), 4773-4779.
51. Smith, E. C.; Denison, M. R., Coronaviruses as DNA wannabes: a new model for the regulation of RNA virus replication fidelity. *PLoS pathogens* **2013,** *9* (12), e1003760.
52. Eckerle, L. D.; Lu, X.; Sperry, S. M.; Choi, L.; Denison, M. R., High fidelity of murine hepatitis virus replication is decreased in nsp14 exoribonuclease mutants. *J Virol* **2007,** *81* (22), 12135-44.
53. Eckerle, L. D.; Becker, M. M.; Halpin, R. A.; Li, K.; Venter, E.; Lu, X.; Scherbakova, S.; Graham, R. L.; Baric, R. S.; Stockwell, T. B.; Spiro, D. J.; Denison, M. R., Infidelity of SARS-CoV Nsp14-exonuclease mutant virus replication is revealed by complete genome sequencing. *PLoS pathogens* **2010,** *6* (5), e1000896.
54. Graham, R. L.; Becker, M. M.; Eckerle, L. D.; Bolles, M.; Denison, M. R.; Baric, R. S., A live, impaired-fidelity coronavirus vaccine protects in an aged, immunocompromised mouse model of lethal disease. *Nature medicine* **2012,** *18* (12), 1820-6.

55. Bouvet, M.; Imbert, I.; Subissi, L.; Gluais, L.; Canard, B.; Decroly, E., RNA 3'-end mismatch excision by the severe acute respiratory syndrome coronavirus nonstructural protein nsp10/nsp14 exoribonuclease complex. *Proceedings of the National Academy of Sciences of the United States of America* **2012,** *109* (24), 9372-7.
56. Ma, Y.; Wu, L.; Shaw, N.; Gao, Y.; Wang, J.; Sun, Y.; Lou, Z.; Yan, L.; Zhang, R.; Rao, Z., Structural basis and functional analysis of the SARS coronavirus nsp14-nsp10 complex. *Proceedings of the National Academy of Sciences of the United States of America* **2015,** *112* (30), 9436-41.
57. Liu, C.; Shi, W.; Becker, S. T.; Schatz, D. G.; Liu, B.; Yang, Y., Structural basis of mismatch recognition by a SARS-CoV-2 proofreading enzyme. *Science* **2021,** *373* (6559), 1142-1146.
58. PyMOL Molecular Graphics System, Version 3.0 Schrödinger, LLC.
59. Ogino, T.; Green, T. J., RNA Synthesis and Capping by Non-segmented Negative Strand RNA Viral Polymerases: Lessons From a Prototypic Virus. *Front Microbiol* **2019,** *10*, 1490.
60. Ouizougun-Oubari, M.; Fearns, R., Structures and Mechanisms of Nonsegmented, Negative-Strand RNA Virus Polymerases. *Annu Rev Virol* **2023,** *10* (1), 199-215.
61. Fearns, R.; Plemper, R. K., Polymerases of paramyxoviruses and pneumoviruses. *Virus research* **2017,** *234*, 87-102.
62. Hume, A. J.; Muhlberger, E., Distinct Genome Replication and Transcription Strategies within the Growing Filovirus Family. *J Mol Biol* **2019,** *431* (21), 4290-4320.
63. Whelan, S. P.; Barr, J. N.; Wertz, G. W., Transcription and replication of nonsegmented negative-strand RNA viruses. *Curr Top Microbiol Immunol* **2004,** *283*, 61-119.
64. Noton, S. L.; Fearns, R., Initiation and regulation of paramyxovirus transcription and replication. *Virology* **2015,** *479-480*, 545-54.
65. Rahmeh, A. A.; Morin, B.; Schenk, A. D.; Liang, B.; Heinrich, B. S.; Brusic, V.; Walz, T.; Whelan, S. P., Critical phosphoprotein elements that regulate polymerase architecture and function in vesicular stomatitis virus. *Proceedings of the National Academy of Sciences of the United States of America* **2012,** *109* (36), 14628-33.
66. Yuan, B.; Peng, Q.; Cheng, J.; Wang, M.; Zhong, J.; Qi, J.; Gao, G. F.; Shi, Y., Structure of the Ebola virus polymerase complex. *Nature* **2022,** *610* (7931), 394-401.
67. Gilman, M. S. A.; Liu, C.; Fung, A.; Behera, I.; Jordan, P.; Rigaux, P.; Ysebaert, N.; Tcherniuk, S.; Sourimant, J.; Eleouet, J. F.; Sutto-Ortiz, P.; Decroly, E.; Roymans, D.; Jin, Z.; McLellan, J. S., Structure of the Respiratory Syncytial Virus Polymerase Complex. *Cell* **2019,** *179* (1), 193-204 e14.
68. Cao, D.; Gao, Y.; Roesler, C.; Rice, S.; D'Cunha, P.; Zhuang, L.; Slack, J.; Domke, M.; Antonova, A.; Romanelli, S.; Keating, S.; Forero, G.; Juneja, P.; Liang, B., Cryo-EM structure of the respiratory syncytial virus RNA polymerase. *Nature communications* **2020,** *11* (1), 368.
69. Cao, D.; Gao, Y.; Chen, Z.; Gooneratne, I.; Roesler, C.; Mera, C.; D'Cunha, P.; Antonova, A.; Katta, D.; Romanelli, S.; Wang, Q.; Rice, S.; Lemons, W.; Ramanathan, A.; Liang, B., Structures of the promoter-bound respiratory syncytial virus polymerase. *Nature* **2024,** *625* (7995), 611-617.
70. Pan, J.; Qian, X.; Lattmann, S.; El Sahili, A.; Yeo, T. H.; Jia, H.; Cressey, T.; Ludeke, B.; Noton, S.; Kalocsay, M.; Fearns, R.; Lescar, J., Structure of the human metapneumovirus polymerase phosphoprotein complex. *Nature* **2020,** *577* (7789), 275-279.

71. Xie, J.; Ouizougun-Oubari, M.; Wang, L.; Zhai, G.; Wu, D.; Lin, Z.; Wang, M.; Ludeke, B.; Yan, X.; Nilsson, T.; Gao, L.; Huang, X.; Fearns, R.; Chen, S., Structural basis for dimerization of a paramyxovirus polymerase complex. *Nature communications* **2024,** *15* (1), 3163.
72. Abdella, R.; Aggarwal, M.; Okura, T.; Lamb, R. A.; He, Y., Structure of a paramyxovirus polymerase complex reveals a unique methyltransferase-CTD conformation. *Proc Natl Acad Sci U S A* **2020,** *117* (9), 4931-4941.
73. Liang, B., Structures of the Mononegavirales Polymerases. *J Virol* **2020,** *94* (22).
74. Nishio, M.; Tsurudome, M.; Garcin, D.; Komada, H.; Ito, M.; Le Mercier, P.; Nosaka, T.; Kolakofsky, D., Human parainfluenza virus type 2 L protein regions required for interaction with other viral proteins and mRNA capping. *J Virol* **2011,** *85* (2), 725-32.
75. Feller, J. A.; Smallwood, S.; Horikami, S. M.; Moyer, S. A., Mutations in conserved domains IV and VI of the large (L) subunit of the sendai virus RNA polymerase give a spectrum of defective RNA synthesis phenotypes. *Virology* **2000,** *269* (2), 426-39.
76. Sun, M.; Fuentes, S. M.; Timani, K.; Sun, D.; Murphy, C.; Lin, Y.; August, A.; Teng, M. N.; He, B., Akt plays a critical role in replication of nonsegmented negative-stranded RNA viruses. *J Virol* **2008,** *82* (1), 105-14.
77. Pickar, A.; Xu, P.; Elson, A.; Li, Z.; Zengel, J.; He, B., Roles of serine and threonine residues of mumps virus P protein in viral transcription and replication. *J Virol* **2014,** *88* (8), 4414-22.
78. Cox, R. M.; Plemper, R. K., Design and Execution of In Vitro Polymerase Assays for Measles Virus and Related Mononegaviruses. *Methods Mol Biol* **2024,** *2808*, 19-33.
79. Pflug, A.; Guilligay, D.; Reich, S.; Cusack, S., Structure of influenza A polymerase bound to the viral RNA promoter. *Nature* **2014,** *516* (7531), 355-60.
80. Reich, S.; Guilligay, D.; Pflug, A.; Malet, H.; Berger, I.; Crepin, T.; Hart, D.; Lunardi, T.; Nanao, M.; Ruigrok, R. W.; Cusack, S., Structural insight into cap-snatching and RNA synthesis by influenza polymerase. *Nature* **2014,** *516* (7531), 361-6.
81. Hengrung, N.; El Omari, K.; Serna Martin, I.; Vreede, F. T.; Cusack, S.; Rambo, R. P.; Vonrhein, C.; Bricogne, G.; Stuart, D. I.; Grimes, J. M.; Fodor, E., Crystal structure of the RNA-dependent RNA polymerase from influenza C virus. *Nature* **2015,** *527* (7576), 114-7.
82. Kouba, T.; Drncova, P.; Cusack, S., Structural snapshots of actively transcribing influenza polymerase. *Nat Struct Mol Biol* **2019,** *26* (6), 460-470.
83. Dias, A.; Bouvier, D.; Crepin, T.; McCarthy, A. A.; Hart, D. J.; Baudin, F.; Cusack, S.; Ruigrok, R. W., The cap-snatching endonuclease of influenza virus polymerase resides in the PA subunit. *Nature* **2009,** *458* (7240), 914-8.
84. Wandzik, J. M.; Kouba, T.; Karuppasamy, M.; Pflug, A.; Drncova, P.; Provaznik, J.; Azevedo, N.; Cusack, S., A Structure-Based Model for the Complete Transcription Cycle of Influenza Polymerase. *Cell* **2020,** *181* (4), 877-893 e21.
85. Fodor, E.; Te Velthuis, A. J. W., Structure and Function of the Influenza Virus Transcription and Replication Machinery. *Cold Spring Harb Perspect Med* **2020,** *10* (9).
86. Malet, H.; Williams, H. M.; Cusack, S.; Rosenthal, M., The mechanism of genome replication and transcription in bunyaviruses. *PLoS pathogens* **2023,** *19* (1), e1011060.
87. Ferron, F.; Weber, F.; de la Torre, J. C.; Reguera, J., Transcription and replication mechanisms of Bunyaviridae and Arenaviridae L proteins. *Virus research* **2017,** *234*, 118-134.
88. Te Velthuis, A. J. W.; Grimes, J. M.; Fodor, E., Structural insights into RNA polymerases of negative-sense RNA viruses. *Nat Rev Microbiol* **2021,** *19* (5), 303-318.

89. Olschewski, S.; Cusack, S.; Rosenthal, M., The Cap-Snatching Mechanism of Bunyaviruses. *Trends Microbiol* **2020,** *28* (4), 293-303.
90. Kouba, T.; Vogel, D.; Thorkelsson, S. R.; Quemin, E. R. J.; Williams, H. M.; Milewski, M.; Busch, C.; Gunther, S.; Grunewald, K.; Rosenthal, M.; Cusack, S., Conformational changes in Lassa virus L protein associated with promoter binding and RNA synthesis activity. *Nature communications* **2021,** *12* (1), 7018.
91. Arragain, B.; Durieux Trouilleton, Q.; Baudin, F.; Provaznik, J.; Azevedo, N.; Cusack, S.; Schoehn, G.; Malet, H., Structural snapshots of La Crosse virus polymerase reveal the mechanisms underlying Peribunyaviridae replication and transcription. *Nature communications* **2022,** *13* (1), 902.
92. Williams, H. M.; Thorkelsson, S. R.; Vogel, D.; Milewski, M.; Busch, C.; Cusack, S.; Grünewald, K.; Quemin, Emmanuelle R. J.; Rosenthal, M., Structural insights into viral genome replication by the severe fever with thrombocytopenia syndrome virus L protein. *Nucleic Acids Research* **2023,** *51* (3), 1424-1442.
93. Mirza, M. U.; Vanmeert, M.; Froeyen, M.; Ali, A.; Rafique, S.; Idrees, M., In silico structural elucidation of RNA-dependent RNA polymerase towards the identification of potential Crimean-Congo Hemorrhagic Fever Virus inhibitors. *Scientific reports* **2019,** *9* (1), 6809.
94. Wang, X.; Hu, C.; Ye, W.; Wang, J.; Dong, X.; Xu, J.; Li, X.; Zhang, M.; Lu, H.; Zhang, F.; Wu, W.; Dai, S.; Wang, H. W.; Chen, Z., Structure of Rift Valley Fever Virus RNA-Dependent RNA Polymerase. *J Virol* **2022,** *96* (3), e0171321.
95. Gorbalenya, A. E.; Pringle, F. M.; Zeddam, J. L.; Luke, B. T.; Cameron, C. E.; Kalmakoff, J.; Hanzlik, T. N.; Gordon, K. H.; Ward, V. K., The palm subdomain-based active site is internally permuted in viral RNA-dependent RNA polymerases of an ancient lineage. *J Mol Biol* **2002,** *324* (1), 47-62.
96. Venkataraman, S.; Prasad, B.; Selvarajan, R., RNA Dependent RNA Polymerases: Insights from Structure, Function and Evolution. *Viruses* **2018,** *10* (2).
97. Ng, K. K.; Arnold, J. J.; Cameron, C. E., Structure-function relationships among RNA-dependent RNA polymerases. *Curr Top Microbiol Immunol* **2008,** *320*, 137-56.
98. te Velthuis, A. J., Common and unique features of viral RNA-dependent polymerases. *Cell Mol Life Sci* **2014,** *71* (22), 4403-20.
99. Bruenn, J. A., A structural and primary sequence comparison of the viral RNA-dependent RNA polymerases. *Nucleic Acids Res* **2003,** *31* (7), 1821-9.
100. Thompson, A. A.; Albertini, R. A.; Peersen, O. B., Stabilization of poliovirus polymerase by NTP binding and fingers-thumb interactions. *J Mol Biol* **2007,** *366* (5), 1459-74.
101. Pettersen, E. F.; Goddard, T. D.; Huang, C. C.; Couch, G. S.; Greenblatt, D. M.; Meng, E. C.; Ferrin, T. E., UCSF Chimera--a visualization system for exploratory research and analysis. *J Comput Chem* **2004,** *25* (13), 1605-12.
102. Robert, X.; Gouet, P., Deciphering key features in protein structures with the new ENDscript server. *Nucleic Acids Res* **2014,** *42* (Web Server issue), W320-4.
103. Steitz, T. A., DNA- and RNA-dependent DNA polymerases. *Current Opinion in Structural Biology* **1993,** *3* (1), 31-38.
104. Steitz, T. A., A mechanism for all polymerases. *Nature* **1998,** *391* (6664), 231-2.
105. Castro, C.; Smidansky, E. D.; Arnold, J. J.; Maksimchuk, K. R.; Moustafa, I.; Uchida, A.; Gotte, M.; Konigsberg, W.; Cameron, C. E., Nucleic acid polymerases use a general acid for nucleotidyl transfer. *Nat Struct Mol Biol* **2009,** *16* (2), 212-8.

106. Castro, C.; Smidansky, E.; Maksimchuk, K. R.; Arnold, J. J.; Korneeva, V. S.; Gotte, M.; Konigsberg, W.; Cameron, C. E., Two proton transfers in the transition state for nucleotidyl transfer catalyzed by RNA- and DNA-dependent RNA and DNA polymerases. *Proceedings of the National Academy of Sciences of the United States of America* **2007,** *104* (11), 4267-72.
107. Yang, X.; Smidansky, E. D.; Maksimchuk, K. R.; Lum, D.; Welch, J. L.; Arnold, J. J.; Cameron, C. E.; Boehr, D. D., Motif D of viral RNA-dependent RNA polymerases determines efficiency and fidelity of nucleotide addition. *Structure* **2012,** *20* (9), 1519-27.
108. Liu, X.; Yang, X.; Lee, C. A.; Moustafa, I. M.; Smidansky, E. D.; Lum, D.; Arnold, J. J.; Cameron, C. E.; Boehr, D. D., Vaccine-derived mutation in motif D of poliovirus RNA-dependent RNA polymerase lowers nucleotide incorporation fidelity. *The Journal of biological chemistry* **2013,** *288* (45), 32753-32765.
109. Shi, J.; Perryman, J. M.; Yang, X.; Liu, X.; Musser, D. M.; Boehr, A. K.; Moustafa, I. M.; Arnold, J. J.; Cameron, C. E.; Boehr, D. D., Rational Control of Poliovirus RNA-Dependent RNA Polymerase Fidelity by Modulating Motif-D Loop Conformational Dynamics. *Biochemistry* **2019,** *58* (36), 3735-3743.
110. Ferrer-Orta, C.; Arias, A.; Perez-Luque, R.; Escarmis, C.; Domingo, E.; Verdaguer, N., Sequential structures provide insights into the fidelity of RNA replication. *Proceedings of the National Academy of Sciences of the United States of America* **2007,** *104* (22), 9463-8.
111. Gohara, D. W.; Crotty, S.; Arnold, J. J.; Yoder, J. D.; Andino, R.; Cameron, C. E., Poliovirus RNA-dependent RNA polymerase (3Dpol): structural, biochemical, and biological analysis of conserved structural motifs A and B. *The Journal of biological chemistry* **2000,** *275* (33), 25523-32.
112. Sholders, A. J.; Peersen, O. B., Distinct conformations of a putative translocation element in poliovirus polymerase. *J Mol Biol* **2014,** *426* (7), 1407-19.
113. Toots, M.; Yoon, J. J.; Cox, R. M.; Hart, M.; Sticher, Z. M.; Makhsous, N.; Plesker, R.; Barrena, A. H.; Reddy, P. G.; Mitchell, D. G.; Shean, R. C.; Bluemling, G. R.; Kolykhalov, A. A.; Greninger, A. L.; Natchus, M. G.; Painter, G. R.; Plemper, R. K., Characterization of orally efficacious influenza drug with high resistance barrier in ferrets and human airway epithelia. *Science translational medicine* **2019,** *11* (515).
114. Wang, M.; Li, R.; Shu, B.; Jing, X.; Ye, H. Q.; Gong, P., Stringent control of the RNA-dependent RNA polymerase translocation revealed by multiple intermediate structures. *Nature communications* **2020,** *11* (1), 2605.
115. Jacome, R.; Becerra, A.; Ponce de Leon, S.; Lazcano, A., Structural Analysis of Monomeric RNA-Dependent Polymerases: Evolutionary and Therapeutic Implications. *PloS one* **2015,** *10* (9), e0139001.
116. Gong, P.; Peersen, O. B., Structural basis for active site closure by the poliovirus RNA-dependent RNA polymerase. *Proceedings of the National Academy of Sciences of the United States of America* **2010,** *107* (52), 22505-10.
117. Guajardo, R.; Sousa, R., A model for the mechanism of polymerase translocation. *J Mol Biol* **1997,** *265* (1), 8-19.
118. Abbondanzieri, E. A.; Greenleaf, W. J.; Shaevitz, J. W.; Landick, R.; Block, S. M., Direct observation of base-pair stepping by RNA polymerase. *Nature* **2005,** *438* (7067), 460-5.
119. Kamzeeva, P. N.; Aralov, A. V.; Alferova, V. A.; Korshun, V. A., Recent Advances in Molecular Mechanisms of Nucleoside Antivirals. *Curr Issues Mol Biol* **2023,** *45* (8), 6851-6879.
120. Stein, D. S.; Moore, K. H., Phosphorylation of nucleoside analog antiretrovirals: a review for clinicians. *Pharmacotherapy* **2001,** *21* (1), 11-34.

121. Sacramento, C. Q.; de Melo, G. R.; de Freitas, C. S.; Rocha, N.; Hoelz, L. V.; Miranda, M.; Fintelman-Rodrigues, N.; Marttorelli, A.; Ferreira, A. C.; Barbosa-Lima, G.; Abrantes, J. L.; Vieira, Y. R.; Bastos, M. M.; de Mello Volotao, E.; Nunes, E. P.; Tschoeke, D. A.; Leomil, L.; Loiola, E. C.; Trindade, P.; Rehen, S. K.; Bozza, F. A.; Bozza, P. T.; Boechat, N.; Thompson, F. L.; de Filippis, A. M.; Bruning, K.; Souza, T. M., The clinically approved antiviral drug sofosbuvir inhibits Zika virus replication. *Scientific reports* **2017,** *7*, 40920.
122. Shannon, A.; Canard, B., Kill or corrupt: Mechanisms of action and drug-resistance of nucleotide analogues against SARS-CoV-2. *Antiviral research* **2023,** *210*, 105501.
123. Seley-Radtke, K. L.; Yates, M. K., The evolution of nucleoside analogue antivirals: A review for chemists and non-chemists. Part 1: Early structural modifications to the nucleoside scaffold. *Antiviral research* **2018,** *154*, 66-86.
124. Yates, M. K.; Seley-Radtke, K. L., The evolution of antiviral nucleoside analogues: A review for chemists and non-chemists. Part II: Complex modifications to the nucleoside scaffold. *Antiviral research* **2019,** *162*, 5-21.
125. Smith, E. C., The not-so-infinite malleability of RNA viruses: Viral and cellular determinants of RNA virus mutation rates. *PLoS pathogens* **2017,** *13* (4), e1006254.
126. Tremaglio, C. Z.; Barr, J. N.; Fearns, R., Chapter 2 - Genetic instability of RNA viruses. In *Genome Stability (Second Edition)*, Kovalchuk, I.; Kovalchuk, O., Eds. Academic Press: Boston, 2021; Vol. 26, pp 23-38.
127. Vignuzzi, M.; Stone, J. K.; Arnold, J. J.; Cameron, C. E.; Andino, R., Quasispecies diversity determines pathogenesis through cooperative interactions in a viral population. *Nature* **2006,** *439* (7074), 344-8.
128. Jena, N. R., Role of different tautomers in the base-pairing abilities of some of the vital antiviral drugs used against COVID-19. *Phys Chem Chem Phys* **2020,** *22* (48), 28115-28122.
129. Crotty, S.; Maag, D.; Arnold, J. J.; Zhong, W.; Lau, J. Y.; Hong, Z.; Andino, R.; Cameron, C. E., The broad-spectrum antiviral ribonucleoside ribavirin is an RNA virus mutagen. *Nature medicine* **2000,** *6* (12), 1375-9.
130. Gordon, C. J.; Tchesnokov, E. P.; Schinazi, R. F.; Gotte, M., Molnupiravir promotes SARS-CoV-2 mutagenesis via the RNA template. *The Journal of biological chemistry* **2021,** *297* (1), 100770.
131. Witkowski, J. T.; Robins, R. K.; Sidwell, R. W.; Simon, L. N., Design, synthesis, and broad spectrum antiviral activity of 1- -D-ribofuranosyl-1,2,4-triazole-3-carboxamide and related nucleosides. *Journal of medicinal chemistry* **1972,** *15* (11), 1150-4.
132. Fried, M. W.; Shiffman, M. L.; Reddy, K. R.; Smith, C.; Marinos, G.; Goncales, F. L., Jr.; Haussinger, D.; Diago, M.; Carosi, G.; Dhumeaux, D.; Craxi, A.; Lin, A.; Hoffman, J.; Yu, J., Peginterferon alfa-2a plus ribavirin for chronic hepatitis C virus infection. *The New England journal of medicine* **2002,** *347* (13), 975-82.
133. Hall, C. B.; McBride, J. T.; Walsh, E. E.; Bell, D. M.; Gala, C. L.; Hildreth, S.; Ten Eyck, L. G.; Hall, W. J., Aerosolized ribavirin treatment of infants with respiratory syncytial viral infection. A randomized double-blind study. *The New England journal of medicine* **1983,** *308* (24), 1443-7.
134. Smith, D. W.; Frankel, L. R.; Mathers, L. H.; Tang, A. T.; Ariagno, R. L.; Prober, C. G., A controlled trial of aerosolized ribavirin in infants receiving mechanical ventilation for severe respiratory syncytial virus infection. *The New England journal of medicine* **1991,** *325* (1), 24-9.

135. McCormick, J. B.; King, I. J.; Webb, P. A.; Scribner, C. L.; Craven, R. B.; Johnson, K. M.; Elliott, L. H.; Belmont-Williams, R., Lassa fever. Effective therapy with ribavirin. *The New England journal of medicine* **1986,** *314* (1), 20-6.
136. Sarrazin, C.; Zeuzem, S., Resistance to direct antiviral agents in patients with hepatitis C virus infection. *Gastroenterology* **2010,** *138* (2), 447-62.
137. Turner, T. L.; Kopp, B. T.; Paul, G.; Landgrave, L. C.; Hayes, D., Jr.; Thompson, R., Respiratory syncytial virus: current and emerging treatment options. *Clinicoecon Outcomes Res* **2014,** *6*, 217-25.
138. Simoes, E. A. F.; Bont, L.; Manzoni, P.; Fauroux, B.; Paes, B.; Figueras-Aloy, J.; Checchia, P. A.; Carbonell-Estrany, X., Past, Present and Future Approaches to the Prevention and Treatment of Respiratory Syncytial Virus Infection in Children. *Infect Dis Ther* **2018,** *7* (1), 87-120.
139. Law, B. J.; Wang, E. E.; MacDonald, N.; McDonald, J.; Dobson, S.; Boucher, F.; Langley, J.; Robinson, J.; Mitchell, I.; Stephens, D., Does ribavirin impact on the hospital course of children with respiratory syncytial virus (RSV) infection? An analysis using the pediatric investigators collaborative network on infections in Canada (PICNIC) RSV database. *Pediatrics* **1997,** *99* (3), E7.
140. Eriksson, B.; Helgstrand, E.; Johansson, N. G.; Larsson, A.; Misiorny, A.; Noren, J. O.; Philipson, L.; Stenberg, K.; Stening, G.; Stridh, S.; Oberg, B., Inhibition of influenza virus ribonucleic acid polymerase by ribavirin triphosphate. *Antimicrobial agents and chemotherapy* **1977,** *11* (6), 946-51.
141. Sidwell, R. W.; Huffman, J. H.; Khare, G. P.; Allen, L. B.; Witkowski, J. T.; Robins, R. K., Broad-spectrum antiviral activity of Virazole: 1-beta-D-ribofuranosyl-1,2,4-triazole-3-carboxamide. *Science* **1972,** *177* (4050), 705-6.
142. Beaucourt, S.; Vignuzzi, M., Ribavirin: a drug active against many viruses with multiple effects on virus replication and propagation. Molecular basis of ribavirin resistance. *Current opinion in virology* **2014,** *8*, 10-5.
143. Graci, J. D.; Cameron, C. E., Mechanisms of action of ribavirin against distinct viruses. *Rev Med Virol* **2006,** *16* (1), 37-48.
144. Wyde, P. R., Respiratory syncytial virus (RSV) disease and prospects for its control. *Antiviral research* **1998,** *39* (2), 63-79.
145. Testoni, B.; Levrero, M.; Durantel, D., Mechanism of action of ribavirin in anti-HCV regimens: new insights for an age-old question? *Gut* **2014,** *63* (1), 3-4.
146. Lau, J. Y.; Tam, R. C.; Liang, T. J.; Hong, Z., Mechanism of action of ribavirin in the combination treatment of chronic HCV infection. *Hepatology* **2002,** *35* (5), 1002-9.
147. Streeter, D. G.; Witkowski, J. T.; Khare, G. P.; Sidwell, R. W.; Bauer, R. J.; Robins, R. K.; Simon, L. N., Mechanism of action of 1- -D-ribofuranosyl-1,2,4-triazole-3-carboxamide (Virazole), a new broad-spectrum antiviral agent. *Proceedings of the National Academy of Sciences of the United States of America* **1973,** *70* (4), 1174-8.
148. Bergamini, A.; Cepparulo, M.; Bolacchi, F.; Araco, A.; Tisone, G.; Ombres, D.; Rocchi, G.; Angelico, M., Ribavirin increases mitogen- and antigen-induced expression of CD40L on CD4+ T cells in vivo. *Clin Exp Immunol* **2002,** *130* (2), 293-9.
149. Miller, J. P.; Kigwana, L. J.; Streeter, D. G.; Robins, R. K.; Simon, L. N.; Roboz, J., The relationship between the metabolism of ribavirin and its proposed mechanism of action. *Ann N Y Acad Sci* **1977,** *284*, 211-29.

150. Airaksinen, A.; Pariente, N.; Menendez-Arias, L.; Domingo, E., Curing of foot-and-mouth disease virus from persistently infected cells by ribavirin involves enhanced mutagenesis. *Virology* **2003,** *311* (2), 339-49.
151. Galli, A.; Mens, H.; Gottwein, J. M.; Gerstoft, J.; Bukh, J., Antiviral Effect of Ribavirin against HCV Associated with Increased Frequency of G-to-A and C-to-U Transitions in Infectious Cell Culture Model. *Scientific reports* **2018,** *8* (1), 4619.
152. Moreno, H.; Gallego, I.; Sevilla, N.; de la Torre, J. C.; Domingo, E.; Martin, V., Ribavirin can be mutagenic for arenaviruses. *J Virol* **2011,** *85* (14), 7246-55.
153. Cheung, P. P.; Watson, S. J.; Choy, K. T.; Fun Sia, S.; Wong, D. D.; Poon, L. L.; Kellam, P.; Guan, Y.; Malik Peiris, J. S.; Yen, H. L., Generation and characterization of influenza A viruses with altered polymerase fidelity. *Nature communications* **2014,** *5*, 4794.
154. Maag, D.; Castro, C.; Hong, Z.; Cameron, C. E., Hepatitis C virus RNA-dependent RNA polymerase (NS5B) as a mediator of the antiviral activity of ribavirin. *The Journal of biological chemistry* **2001,** *276* (49), 46094-8.
155. Hofmann, W. P.; Polta, A.; Herrmann, E.; Mihm, U.; Kronenberger, B.; Sonntag, T.; Lohmann, V.; Schonberger, B.; Zeuzem, S.; Sarrazin, C., Mutagenic effect of ribavirin on hepatitis C nonstructural 5B quasispecies in vitro and during antiviral therapy. *Gastroenterology* **2007,** *132* (3), 921-30.
156. Dietz, J.; Schelhorn, S. E.; Fitting, D.; Mihm, U.; Susser, S.; Welker, M. W.; Fuller, C.; Daumer, M.; Teuber, G.; Wedemeyer, H.; Berg, T.; Lengauer, T.; Zeuzem, S.; Herrmann, E.; Sarrazin, C., Deep sequencing reveals mutagenic effects of ribavirin during monotherapy of hepatitis C virus genotype 1-infected patients. *J Virol* **2013,** *87* (11), 6172-81.
157. Xie, X.; Muruato, A. E.; Zhang, X.; Lokugamage, K. G.; Fontes-Garfias, C. R.; Zou, J.; Liu, J.; Ren, P.; Balakrishnan, M.; Cihlar, T.; Tseng, C. K.; Makino, S.; Menachery, V. D.; Bilello, J. P.; Shi, P. Y., A nanoluciferase SARS-CoV-2 for rapid neutralization testing and screening of anti-infective drugs for COVID-19. *Nature communications* **2020,** *11* (1), 5214.
158. Zhou, S.; Hill, C. S.; Sarkar, S.; Tse, L. V.; Woodburn, B. M. D.; Schinazi, R. F.; Sheahan, T. P.; Baric, R. S.; Heise, M. T.; Swanstrom, R., beta-d-N4-hydroxycytidine Inhibits SARS-CoV-2 Through Lethal Mutagenesis But Is Also Mutagenic To Mammalian Cells. *J Infect Dis* **2021,** *224* (3), 415-419.
159. Ferron, F.; Subissi, L.; Silveira De Morais, A. T.; Le, N. T. T.; Sevajol, M.; Gluais, L.; Decroly, E.; Vonrhein, C.; Bricogne, G.; Canard, B.; Imbert, I., Structural and molecular basis of mismatch correction and ribavirin excision from coronavirus RNA. *Proceedings of the National Academy of Sciences of the United States of America* **2018,** *115* (2), E162-E171.
160. Smith, E. C.; Blanc, H.; Surdel, M. C.; Vignuzzi, M.; Denison, M. R., Coronaviruses lacking exoribonuclease activity are susceptible to lethal mutagenesis: evidence for proofreading and potential therapeutics. *PLoS pathogens* **2013,** *9* (8), e1003565.
161. Pfeiffer, J. K.; Kirkegaard, K., A single mutation in poliovirus RNA-dependent RNA polymerase confers resistance to mutagenic nucleotide analogs via increased fidelity. *Proceedings of the National Academy of Sciences of the United States of America* **2003,** *100* (12), 7289-94.
162. Arnold, J. J.; Vignuzzi, M.; Stone, J. K.; Andino, R.; Cameron, C. E., Remote site control of an active site fidelity checkpoint in a viral RNA-dependent RNA polymerase. *The Journal of biological chemistry* **2005,** *280* (27), 25706-16.
163. Sadeghipour, S.; Bek, E. J.; McMinn, P. C., Ribavirin-resistant mutants of human enterovirus 71 express a high replication fidelity phenotype during growth in cell culture. *J Virol* **2013,** *87* (3), 1759-69.

164. Dulin, D.; Arnold, J. J.; van Laar, T.; Oh, H. S.; Lee, C.; Perkins, A. L.; Harki, D. A.; Depken, M.; Cameron, C. E.; Dekker, N. H., Signatures of Nucleotide Analog Incorporation by an RNA-Dependent RNA Polymerase Revealed Using High-Throughput Magnetic Tweezers. *Cell reports* **2017,** *21* (4), 1063-1076.
165. Korboukh, V. K.; Lee, C. A.; Acevedo, A.; Vignuzzi, M.; Xiao, Y.; Arnold, J. J.; Hemperly, S.; Graci, J. D.; August, A.; Andino, R.; Cameron, C. E., RNA virus population diversity, an optimum for maximal fitness and virulence. *The Journal of biological chemistry* **2014,** *289* (43), 29531-44.
166. Pfeiffer, J. K.; Kirkegaard, K., Ribavirin resistance in hepatitis C virus replicon-containing cell lines conferred by changes in the cell line or mutations in the replicon RNA. *J Virol* **2005,** *79* (4), 2346-55.
167. Mori, K.; Hiraoka, O.; Ikeda, M.; Ariumi, Y.; Hiramoto, A.; Wataya, Y.; Kato, N., Adenosine kinase is a key determinant for the anti-HCV activity of ribavirin. *Hepatology* **2013,** *58* (4), 1236-44.
168. Zhou, S.; Liu, R.; Baroudy, B. M.; Malcolm, B. A.; Reyes, G. R., The effect of ribavirin and IMPDH inhibitors on hepatitis C virus subgenomic replicon RNA. *Virology* **2003,** *310* (2), 333-42.
169. Delang, L.; Abdelnabi, R.; Neyts, J., Favipiravir as a potential countermeasure against neglected and emerging RNA viruses. *Antiviral research* **2018,** *153*, 85-94.
170. Julander, J. G.; Shafer, K.; Smee, D. F.; Morrey, J. D.; Furuta, Y., Activity of T-705 in a hamster model of yellow fever virus infection in comparison with that of a chemically related compound, T-1106. *Antimicrobial agents and chemotherapy* **2009,** *53* (1), 202-9.
171. Furuta, Y.; Takahashi, K.; Fukuda, Y.; Kuno, M.; Kamiyama, T.; Kozaki, K.; Nomura, N.; Egawa, H.; Minami, S.; Watanabe, Y.; Narita, H.; Shiraki, K., In vitro and in vivo activities of anti-influenza virus compound T-705. *Antimicrobial agents and chemotherapy* **2002,** *46* (4), 977-81.
172. Sun, L.; Meijer, A.; Froeyen, M.; Zhang, L.; Thibaut, H. J.; Baggen, J.; George, S.; Vernachio, J.; van Kuppeveld, F. J.; Leyssen, P.; Hilgenfeld, R.; Neyts, J.; Delang, L., Antiviral Activity of Broad-Spectrum and Enterovirus-Specific Inhibitors against Clinical Isolates of Enterovirus D68. *Antimicrobial agents and chemotherapy* **2015,** *59* (12), 7782-5.
173. Oestereich, L.; Ludtke, A.; Wurr, S.; Rieger, T.; Munoz-Fontela, C.; Gunther, S., Successful treatment of advanced Ebola virus infection with T-705 (favipiravir) in a small animal model. *Antiviral research* **2014,** *105*, 17-21.
174. Jochmans, D.; van Nieuwkoop, S.; Smits, S. L.; Neyts, J.; Fouchier, R. A.; van den Hoogen, B. G., Antiviral Activity of Favipiravir (T-705) against a Broad Range of Paramyxoviruses In Vitro and against Human Metapneumovirus in Hamsters. *Antimicrobial agents and chemotherapy* **2016,** *60* (8), 4620-9.
175. Oestereich, L.; Rieger, T.; Ludtke, A.; Ruibal, P.; Wurr, S.; Pallasch, E.; Bockholt, S.; Krasemann, S.; Munoz-Fontela, C.; Gunther, S., Efficacy of Favipiravir Alone and in Combination With Ribavirin in a Lethal, Immunocompetent Mouse Model of Lassa Fever. *J Infect Dis* **2016,** *213* (6), 934-8.
176. Tipih, T.; Meade-White, K.; Rao, D.; Bushmaker, T.; Lewis, M.; Shaia, C.; Feldmann, H.; Hawman, D. W., Favipiravir and Ribavirin protect immunocompetent mice from lethal CCHFV infection. *Antiviral research* **2023,** *218*, 105703.
177. Hawman, D. W.; Haddock, E.; Meade-White, K.; Nardone, G.; Feldmann, F.; Hanley, P. W.; Lovaglio, J.; Scott, D.; Komeno, T.; Nakajima, N.; Furuta, Y.; Gowen, B. B.; Feldmann,

H., Efficacy of favipiravir (T-705) against Crimean-Congo hemorrhagic fever virus infection in cynomolgus macaques. *Antiviral research* **2020,** *181*, 104858.
178. Borrego, B.; de Avila, A. I.; Domingo, E.; Brun, A., Lethal Mutagenesis of Rift Valley Fever Virus Induced by Favipiravir. *Antimicrobial agents and chemotherapy* **2019,** *63* (8).
179. Caroline, A. L.; Powell, D. S.; Bethel, L. M.; Oury, T. D.; Reed, D. S.; Hartman, A. L., Broad spectrum antiviral activity of favipiravir (T-705): protection from highly lethal inhalational Rift Valley Fever. *PLoS neglected tropical diseases* **2014,** *8* (4), e2790.
180. Golan, Y.; Campos, J. A. S.; Woolson, R.; Cilla, D.; Hanabergh, R.; Gonzales-Rojas, Y.; Lopez, R.; Finberg, R.; Balboni, A., Favipiravir in Patients With Early Mild-to-moderate Coronavirus Disease 2019 (COVID-19): A Randomized Controlled Trial. *Clin Infect Dis* **2023,** *76* (3), e10-e17.
181. Shah, P. L.; Orton, C. M.; Grinsztejn, B.; Donaldson, G. C.; Crabtree Ramirez, B.; Tonkin, J.; Santos, B. R.; Cardoso, S. W.; Ritchie, A. I.; Conway, F.; Riberio, M. P. D.; Wiseman, D. J.; Tana, A.; Vijayakumar, B.; Caneja, C.; Leaper, C.; Mann, B.; Samson, A.; Bhavsar, P. K.; Boffito, M.; Johnson, M. R.; Pozniak, A.; Pelly, M.; group, P. t., Favipiravir in patients hospitalised with COVID-19 (PIONEER trial): a multicentre, open-label, phase 3, randomised controlled trial of early intervention versus standard care. *Lancet Respir Med* **2023,** *11* (5), 415-424.
182. Luvira, V.; Schilling, W. H. K.; Jittamala, P.; Watson, J. A.; Boyd, S.; Siripoon, T.; Ngamprasertchai, T.; Almeida, P. J.; Ekkapongpisit, M.; Cruz, C.; Callery, J. J.; Singh, S.; Tuntipaiboontana, R.; Kruabkontho, V.; Ngernseng, T.; Tubprasert, J.; Abdad, M. Y.; Keayarsa, S.; Madmanee, W.; Aguiar, R. S.; Santos, F. M.; Hanboonkunupakarn, P.; Hanboonkunupakarn, B.; Poovorawan, K.; Imwong, M.; Taylor, W. R. J.; Chotivanich, V.; Chotivanich, K.; Pukrittayakamee, S.; Dondorp, A. M.; Day, N. P. J.; Teixeira, M. M.; Piyaphanee, W.; Phumratanaprapin, W.; White, N. J.; Group, P. C., Clinical antiviral efficacy of favipiravir in early COVID-19 (PLATCOV): an open-label, randomised, controlled, adaptive platform trial. *BMC Infect Dis* **2024,** *24* (1), 89.
183. AlQahtani, M.; Kumar, N.; Aljawder, D.; Abdulrahman, A.; Mohamed, M. W.; Alnashaba, F.; Fayyad, M. A.; Alshaikh, F.; Alsahaf, F.; Saeed, S.; Almahroos, A.; Abdulrahim, Z.; Otoom, S.; Atkin, S. L., Randomized controlled trial of favipiravir, hydroxychloroquine, and standard care in patients with mild/moderate COVID-19 disease. *Scientific reports* **2022,** *12* (1), 4925.
184. Bosaeed, M.; Alharbi, A.; Mahmoud, E.; Alrehily, S.; Bahlaq, M.; Gaifer, Z.; Alturkistani, H.; Alhagan, K.; Alshahrani, S.; Tolbah, A.; Musattat, A.; Alanazi, M.; Jaha, R.; Sultana, K.; Alqahtani, H.; Al Aamer, K.; Jaser, S.; Alsaedy, A.; Ahmad, A.; Abalkhail, M.; AlJohani, S.; Al Jeraisy, M.; Almaziad, S.; Albaalharith, N.; Alabdulkareem, K.; Alshowair, A.; Alharbi, N. K.; Alrabiah, F.; Alshamrani, M.; Aldibasi, O.; Alaskar, A., Efficacy of favipiravir in adults with mild COVID-19: a randomized, double-blind, multicentre, placebo-controlled clinical trial. *Clin Microbiol Infect* **2022,** *28* (4), 602-608.
185. Jeon, S.; Ko, M.; Lee, J.; Choi, I.; Byun, S. Y.; Park, S.; Shum, D.; Kim, S., Identification of Antiviral Drug Candidates against SARS-CoV-2 from FDA-Approved Drugs. *Antimicrobial agents and chemotherapy* **2020,** *64* (7).
186. Wang, M.; Cao, R.; Zhang, L.; Yang, X.; Liu, J.; Xu, M.; Shi, Z.; Hu, Z.; Zhong, W.; Xiao, G., Remdesivir and chloroquine effectively inhibit the recently emerged novel coronavirus (2019-nCoV) in vitro. *Cell research* **2020,** *30* (3), 269-271.

187. Escribano-Romero, E.; Jimenez de Oya, N.; Domingo, E.; Saiz, J. C., Extinction of West Nile Virus by Favipiravir through Lethal Mutagenesis. *Antimicrobial agents and chemotherapy* **2017,** *61* (11).
188. Arias, A.; Thorne, L.; Goodfellow, I., Favipiravir elicits antiviral mutagenesis during virus replication in vivo. *Elife* **2014,** *3*, e03679.
189. de Avila, A. I.; Gallego, I.; Soria, M. E.; Gregori, J.; Quer, J.; Esteban, J. I.; Rice, C. M.; Domingo, E.; Perales, C., Lethal Mutagenesis of Hepatitis C Virus Induced by Favipiravir. *PloS one* **2016,** *11* (10), e0164691.
190. Baranovich, T.; Wong, S. S.; Armstrong, J.; Marjuki, H.; Webby, R. J.; Webster, R. G.; Govorkova, E. A., T-705 (favipiravir) induces lethal mutagenesis in influenza A H1N1 viruses in vitro. *J Virol* **2013,** *87* (7), 3741-51.
191. Goldhill, D. H.; Langat, P.; Xie, H.; Galiano, M.; Miah, S.; Kellam, P.; Zambon, M.; Lackenby, A.; Barclay, W. S., Determining the Mutation Bias of Favipiravir in Influenza Virus Using Next-Generation Sequencing. *J Virol* **2019,** *93* (2).
192. Guedj, J.; Piorkowski, G.; Jacquot, F.; Madelain, V.; Nguyen, T. H. T.; Rodallec, A.; Gunther, S.; Carbonnelle, C.; Mentre, F.; Raoul, H.; de Lamballerie, X., Antiviral efficacy of favipiravir against Ebola virus: A translational study in cynomolgus macaques. *PLoS Med* **2018,** *15* (3), e1002535.
193. de Avila, A. I.; Moreno, E.; Perales, C.; Domingo, E., Favipiravir can evoke lethal mutagenesis and extinction of foot-and-mouth disease virus. *Virus research* **2017,** *233*, 105-112.
194. Janissen, R.; Woodman, A.; Shengjuler, D.; Vallet, T.; Lee, K. M.; Kuijpers, L.; Moustafa, I. M.; Fitzgerald, F.; Huang, P. N.; Perkins, A. L.; Harki, D. A.; Arnold, J. J.; Solano, B.; Shih, S. R.; Vignuzzi, M.; Cameron, C. E.; Dekker, N. H., Induced intra- and intermolecular template switching as a therapeutic mechanism against RNA viruses. *Mol Cell* **2021,** *81* (21), 4467-4480 e7.
195. Jin, Z.; Smith, L. K.; Rajwanshi, V. K.; Kim, B.; Deval, J., The ambiguous base-pairing and high substrate efficiency of T-705 (Favipiravir) Ribofuranosyl 5'-triphosphate towards influenza A virus polymerase. *PloS one* **2013,** *8* (7), e68347.
196. Naydenova, K.; Muir, K. W.; Wu, L. F.; Zhang, Z.; Coscia, F.; Peet, M. J.; Castro-Hartmann, P.; Qian, P.; Sader, K.; Dent, K.; Kimanius, D.; Sutherland, J. D.; Lowe, J.; Barford, D.; Russo, C. J., Structure of the SARS-CoV-2 RNA-dependent RNA polymerase in the presence of favipiravir-RTP. *Proceedings of the National Academy of Sciences of the United States of America* **2021,** *118* (7).
197. Peng, Q.; Peng, R.; Yuan, B.; Wang, M.; Zhao, J.; Fu, L.; Qi, J.; Shi, Y., Structural Basis of SARS-CoV-2 Polymerase Inhibition by Favipiravir. *Innovation (Camb)* **2021,** *2* (1), 100080.
198. Seifert, M.; Bera, S. C.; van Nies, P.; Kirchdoerfer, R. N.; Shannon, A.; Le, T. T.; Meng, X.; Xia, H.; Wood, J. M.; Harris, L. D.; Papini, F. S.; Arnold, J. J.; Almo, S.; Grove, T. L.; Shi, P. Y.; Xiang, Y.; Canard, B.; Depken, M.; Cameron, C. E.; Dulin, D., Inhibition of SARS-CoV-2 polymerase by nucleotide analogs from a single-molecule perspective. *Elife* **2021,** *10*.
199. Sangawa, H.; Komeno, T.; Nishikawa, H.; Yoshida, A.; Takahashi, K.; Nomura, N.; Furuta, Y., Mechanism of action of T-705 ribosyl triphosphate against influenza virus RNA polymerase. *Antimicrobial agents and chemotherapy* **2013,** *57* (11), 5202-8.
200. Kouba, T.; Dubankova, A.; Drncova, P.; Donati, E.; Vidossich, P.; Speranzini, V.; Pflug, A.; Huchting, J.; Meier, C.; De Vivo, M.; Cusack, S., Direct observation of backtracking

by influenza A and B polymerases upon consecutive incorporation of the nucleoside analog T1106. *Cell reports* **2023,** *42* (1), 111901.
201. Dulin, D.; Vilfan, I. D.; Berghuis, B. A.; Hage, S.; Bamford, D. H.; Poranen, M. M.; Depken, M.; Dekker, N. H., Elongation-Competent Pauses Govern the Fidelity of a Viral RNA-Dependent RNA Polymerase. *Cell reports* **2015,** *10* (6), 983-992.
202. Shaevitz, J. W.; Abbondanzieri, E. A.; Landick, R.; Block, S. M., Backtracking by single RNA polymerase molecules observed at near-base-pair resolution. *Nature* **2003,** *426* (6967), 684-7.
203. Dulin, D.; Vilfan, I. D.; Berghuis, B. A.; Poranen, M. M.; Depken, M.; Dekker, N. H., Backtracking behavior in viral RNA-dependent RNA polymerase provides the basis for a second initiation site. *Nucleic Acids Res* **2015,** *43* (21), 10421-9.
204. Malone, B.; Chen, J.; Wang, Q.; Llewellyn, E.; Choi, Y. J.; Olinares, P. D. B.; Cao, X.; Hernandez, C.; Eng, E. T.; Chait, B. T.; Shaw, D. E.; Landick, R.; Darst, S. A.; Campbell, E. A., Structural basis for backtracking by the SARS-CoV-2 replication-transcription complex. *Proceedings of the National Academy of Sciences of the United States of America* **2021,** *118* (19).
205. Chen, J.; Malone, B.; Llewellyn, E.; Grasso, M.; Shelton, P. M. M.; Olinares, P. D. B.; Maruthi, K.; Eng, E. T.; Vatandaslar, H.; Chait, B. T.; Kapoor, T. M.; Darst, S. A.; Campbell, E. A., Structural Basis for Helicase-Polymerase Coupling in the SARS-CoV-2 Replication-Transcription Complex. *Cell* **2020,** *182* (6), 1560-1573 e13.
206. Chen, J.; Wang, Q.; Malone, B.; Llewellyn, E.; Pechersky, Y.; Maruthi, K.; Eng, E. T.; Perry, J. K.; Campbell, E. A.; Shaw, D. E.; Darst, S. A., Ensemble cryo-EM reveals conformational states of the nsp13 helicase in the SARS-CoV-2 helicase replication-transcription complex. *Nat Struct Mol Biol* **2022,** *29* (3), 250-260.
207. Delang, L.; Segura Guerrero, N.; Tas, A.; Querat, G.; Pastorino, B.; Froeyen, M.; Dallmeier, K.; Jochmans, D.; Herdewijn, P.; Bello, F.; Snijder, E. J.; de Lamballerie, X.; Martina, B.; Neyts, J.; van Hemert, M. J.; Leyssen, P., Mutations in the chikungunya virus non-structural proteins cause resistance to favipiravir (T-705), a broad-spectrum antiviral. *J Antimicrob Chemother* **2014,** *69* (10), 2770-84.
208. Goldhill, D. H.; Te Velthuis, A. J. W.; Fletcher, R. A.; Langat, P.; Zambon, M.; Lackenby, A.; Barclay, W. S., The mechanism of resistance to favipiravir in influenza. *Proceedings of the National Academy of Sciences of the United States of America* **2018,** *115* (45), 11613-11618.
209. Abdelnabi, R.; Morais, A. T. S.; Leyssen, P.; Imbert, I.; Beaucourt, S.; Blanc, H.; Froeyen, M.; Vignuzzi, M.; Canard, B.; Neyts, J.; Delang, L., Understanding the Mechanism of the Broad-Spectrum Antiviral Activity of Favipiravir (T-705): Key Role of the F1 Motif of the Viral Polymerase. *J Virol* **2017,** *91* (12).
210. Gnadig, N. F.; Beaucourt, S.; Campagnola, G.; Borderia, A. V.; Sanz-Ramos, M.; Gong, P.; Blanc, H.; Peersen, O. B.; Vignuzzi, M., Coxsackievirus B3 mutator strains are attenuated in vivo. *Proceedings of the National Academy of Sciences of the United States of America* **2012,** *109* (34), E2294-303.
211. Thompson, A. A.; Peersen, O. B., Structural basis for proteolysis-dependent activation of the poliovirus RNA-dependent RNA polymerase. *EMBO J* **2004,** *23* (17), 3462-71.
212. Levi, L. I.; Gnadig, N. F.; Beaucourt, S.; McPherson, M. J.; Baron, B.; Arnold, J. J.; Vignuzzi, M., Fidelity variants of RNA dependent RNA polymerases uncover an indirect, mutagenic activity of amiloride compounds. *PLoS pathogens* **2010,** *6* (10), e1001163.

213. Pfeiffer, J. K.; Kirkegaard, K., Increased fidelity reduces poliovirus fitness and virulence under selective pressure in mice. *PLoS pathogens* **2005,** *1* (2), e11.
214. Vignuzzi, M.; Wendt, E.; Andino, R., Engineering attenuated virus vaccines by controlling replication fidelity. *Nature medicine* **2008,** *14* (2), 154-61.
215. Shi, W.; Ye, H. Q.; Deng, C. L.; Li, R.; Zhang, B.; Gong, P., A nucleobase-binding pocket in a viral RNA-dependent RNA polymerase contributes to elongation complex stability. *Nucleic Acids Res* **2020,** *48* (3), 1392-1405.
216. Administration, U. S. F. a. D., Coronavirus (COVID-19) Update: FDA Authorizes Additional Oral Antiviral for Treatment of COVID-19 in Certain Adults. 2021.
217. Jayk Bernal, A.; Gomes da Silva, M. M.; Musungaie, D. B.; Kovalchuk, E.; Gonzalez, A.; Delos Reyes, V.; Martín-Quirós, A.; Caraco, Y.; Williams-Diaz, A.; Brown, M. L.; Du, J.; Pedley, A.; Assaid, C.; Strizki, J.; Grobler, J. A.; Shamsuddin, H. H.; Tipping, R.; Wan, H.; Paschke, A.; Butterton, J. R.; Johnson, M. G.; De Anda, C., Molnupiravir for Oral Treatment of Covid-19 in Nonhospitalized Patients. *New England Journal of Medicine* **2021,** *386* (6), 509-520.
218. Butler, C. C.; Hobbs, F. D. R.; Gbinigie, O. A.; Rahman, N. M.; Hayward, G.; Richards, D. B.; Dorward, J.; Lowe, D. M.; Standing, J. F.; Breuer, J.; Khoo, S.; Petrou, S.; Hood, K.; Nguyen-Van-Tam, J. S.; Patel, M. G.; Saville, B. R.; Marion, J.; Ogburn, E.; Allen, J.; Rutter, H.; Francis, N.; Thomas, N. P. B.; Evans, P.; Dobson, M.; Madden, T. A.; Holmes, J.; Harris, V.; Png, M. E.; Lown, M.; van Hecke, O.; Detry, M. A.; Saunders, C. T.; Fitzgerald, M.; Berry, N. S.; Mwandigha, L.; Galal, U.; Mort, S.; Jani, B. D.; Hart, N. D.; Ahmed, H.; Butler, D.; McKenna, M.; Chalk, J.; Lavallee, L.; Hadley, E.; Cureton, L.; Benysek, M.; Andersson, M.; Coates, M.; Barrett, S.; Bateman, C.; Davies, J. C.; Raymundo-Wood, I.; Ustianowski, A.; Carson-Stevens, A.; Yu, L. M.; Little, P.; Group, P. T. C., Molnupiravir plus usual care versus usual care alone as early treatment for adults with COVID-19 at increased risk of adverse outcomes (PANORAMIC): an open-label, platform-adaptive randomised controlled trial. *Lancet* **2023,** *401* (10373), 281-293.
219. Khoo, S. H.; FitzGerald, R.; Saunders, G.; Middleton, C.; Ahmad, S.; Edwards, C. J.; Hadjiyiannakis, D.; Walker, L.; Lyon, R.; Shaw, V.; Mozgunov, P.; Periselneris, J.; Woods, C.; Bullock, K.; Hale, C.; Reynolds, H.; Downs, N.; Ewings, S.; Buadi, A.; Cameron, D.; Edwards, T.; Knox, E.; Donovan-Banfield, I.; Greenhalf, W.; Chiong, J.; Lavelle-Langham, L.; Jacobs, M.; Northey, J.; Painter, W.; Holman, W.; Lalloo, D. G.; Tetlow, M.; Hiscox, J. A.; Jaki, T.; Fletcher, T.; Griffiths, G.; Group, A. C.-S., Molnupiravir versus placebo in unvaccinated and vaccinated patients with early SARS-CoV-2 infection in the UK (AGILE CST-2): a randomised, placebo-controlled, double-blind, phase 2 trial. *Lancet Infect Dis* **2023,** *23* (2), 183-195.
220. Kobayashi, H.; Mori, Y.; Ahmed, S.; Hirao, Y.; Kato, S.; Kawanishi, S.; Murata, M.; Oikawa, S., Oxidative DNA Damage by N4-hydroxycytidine, a Metabolite of the SARS-CoV-2 Antiviral Molnupiravir. *J Infect Dis* **2023,** *227* (9), 1068-1072.
221. Swanstrom, R.; Schinazi, R. F., Lethal mutagenesis as an antiviral strategy. *Science* **2022,** *375* (6580), 497-498.
222. Stuyver, L. J.; Whitaker, T.; McBrayer, T. R.; Hernandez-Santiago, B. I.; Lostia, S.; Tharnish, P. M.; Ramesh, M.; Chu, C. K.; Jordan, R.; Shi, J.; Rachakonda, S.; Watanabe, K. A.; Otto, M. J.; Schinazi, R. F., Ribonucleoside analogue that blocks replication of bovine viral diarrhea and hepatitis C viruses in culture. *Antimicrobial agents and chemotherapy* **2003,** *47* (1), 244-54.

223. Yoon, J. J.; Toots, M.; Lee, S.; Lee, M. E.; Ludeke, B.; Luczo, J. M.; Ganti, K.; Cox, R. M.; Sticher, Z. M.; Edpuganti, V.; Mitchell, D. G.; Lockwood, M. A.; Kolykhalov, A. A.; Greninger, A. L.; Moore, M. L.; Painter, G. R.; Lowen, A. C.; Tompkins, S. M.; Fearns, R.; Natchus, M. G.; Plemper, R. K., Orally Efficacious Broad-Spectrum Ribonucleoside Analog Inhibitor of Influenza and Respiratory Syncytial Viruses. *Antimicrobial agents and chemotherapy* **2018,** *62* (8).
224. Kabinger, F.; Stiller, C.; Schmitzova, J.; Dienemann, C.; Kokic, G.; Hillen, H. S.; Hobartner, C.; Cramer, P., Mechanism of molnupiravir-induced SARS-CoV-2 mutagenesis. *Nat Struct Mol Biol* **2021,** *28* (9), 740-746.
225. Costantini, V. P.; Whitaker, T.; Barclay, L.; Lee, D.; McBrayer, T. R.; Schinazi, R. F.; Vinjé, J., Antiviral Activity of Nucleoside Analogues against Norovirus. *Antiviral Therapy* **2012,** *17* (6), 981-991.
226. Agostini, M. L.; Pruijssers, A. J.; Chappell, J. D.; Gribble, J.; Lu, X.; Andres, E. L.; Bluemling, G. R.; Lockwood, M. A.; Sheahan, T. P.; Sims, A. C.; Natchus, M. G.; Saindane, M.; Kolykhalov, A. A.; Painter, G. R.; Baric, R. S.; Denison, M. R., Small-Molecule Antiviral beta-d-N(4)-Hydroxycytidine Inhibits a Proofreading-Intact Coronavirus with a High Genetic Barrier to Resistance. *J Virol* **2019,** *93* (24).
227. Ehteshami, M.; Tao, S.; Zandi, K.; Hsiao, H. M.; Jiang, Y.; Hammond, E.; Amblard, F.; Russell, O. O.; Merits, A.; Schinazi, R. F., Characterization of beta-d-N(4)-Hydroxycytidine as a Novel Inhibitor of Chikungunya Virus. *Antimicrobial agents and chemotherapy* **2017,** *61* (4).
228. Li, Y.; Liu, M.; Yan, Y.; Wang, Z.; Dai, Q.; Yang, X.; Guo, X.; Li, W.; Chen, X.; Cao, R.; Zhong, W., Molnupiravir and Its Active Form, EIDD-1931, Show Potent Antiviral Activity against Enterovirus Infections In Vitro and In Vivo. *Viruses* **2022,** *14* (6).
229. Sheahan, T. P.; Sims, A. C.; Zhou, S.; Graham, R. L.; Pruijssers, A. J.; Agostini, M. L.; Leist, S. R.; Schafer, A.; Dinnon, K. H., 3rd; Stevens, L. J.; Chappell, J. D.; Lu, X.; Hughes, T. M.; George, A. S.; Hill, C. S.; Montgomery, S. A.; Brown, A. J.; Bluemling, G. R.; Natchus, M. G.; Saindane, M.; Kolykhalov, A. A.; Painter, G.; Harcourt, J.; Tamin, A.; Thornburg, N. J.; Swanstrom, R.; Denison, M. R.; Baric, R. S., An orally bioavailable broad-spectrum antiviral inhibits SARS-CoV-2 in human airway epithelial cell cultures and multiple coronaviruses in mice. *Science translational medicine* **2020,** *12* (541).
230. Donovan-Banfield, I.; Penrice-Randal, R.; Goldswain, H.; Rzeszutek, A. M.; Pilgrim, J.; Bullock, K.; Saunders, G.; Northey, J.; Dong, X.; Ryan, Y.; Reynolds, H.; Tetlow, M.; Walker, L. E.; FitzGerald, R.; Hale, C.; Lyon, R.; Woods, C.; Ahmad, S.; Hadjiyiannakis, D.; Periselneris, J.; Knox, E.; Middleton, C.; Lavelle-Langham, L.; Shaw, V.; Greenhalf, W.; Edwards, T.; Lalloo, D. G.; Edwards, C. J.; Darby, A. C.; Carroll, M. W.; Griffiths, G.; Khoo, S. H.; Hiscox, J. A.; Fletcher, T., Characterisation of SARS-CoV-2 genomic variation in response to molnupiravir treatment in the AGILE Phase IIa clinical trial. *Nature communications* **2022,** *13* (1), 7284.
231. Sanderson, T.; Hisner, R.; Donovan-Banfield, I.; Hartman, H.; Lochen, A.; Peacock, T. P.; Ruis, C., A molnupiravir-associated mutational signature in global SARS-CoV-2 genomes. *Nature* **2023,** *623* (7987), 594-600.
232. Urakova, N.; Kuznetsova, V.; Crossman, D. K.; Sokratian, A.; Guthrie, D. B.; Kolykhalov, A. A.; Lockwood, M. A.; Natchus, M. G.; Crowley, M. R.; Painter, G. R.; Frolova, E. I.; Frolov, I., beta-d-N(4)-Hydroxycytidine Is a Potent Anti-alphavirus Compound That Induces a High Level of Mutations in the Viral Genome. *J Virol* **2018,** *92* (3).

233. Zibat, A.; Zhang, X.; Dickmanns, A.; Stegmann, K. M.; Dobbelstein, A. W.; Alachram, H.; Soliwoda, R.; Salinas, G.; Gross, U.; Gorlich, D.; Kschischo, M.; Wollnik, B.; Dobbelstein, M., N4-hydroxycytidine, the active compound of Molnupiravir, promotes SARS-CoV-2 mutagenesis and escape from a neutralizing nanobody. *iScience* **2023,** *26* (10), 107786.
234. Standing, J. F.; Buggiotti, L.; Guerra-Assuncao, J. A.; Woodall, M.; Ellis, S.; Agyeman, A. A.; Miller, C.; Okechukwu, M.; Kirkpatrick, E.; Jacobs, A. I.; Williams, C. A.; Roy, S.; Martin-Bernal, L. M.; Williams, R.; Smith, C. M.; Sanderson, T.; Ashford, F. B.; Emmanuel, B.; Afzal, Z. M.; Shields, A.; Richter, A. G.; Dorward, J.; Gbinigie, O.; Van Hecke, O.; Lown, M.; Francis, N.; Jani, B.; Richards, D. B.; Rahman, N. M.; Yu, L. M.; Thomas, N. P. B.; Hart, N. D.; Evans, P.; Andersson, M.; Hayward, G.; Hood, K.; Nguyen-Van-Tam, J. S.; Little, P.; Hobbs, F. D. R.; Khoo, S.; Butler, C.; Lowe, D. M.; Breuer, J.; Group, P. V., Randomized controlled trial of molnupiravir SARS-CoV-2 viral and antibody response in at-risk adult outpatients. *Nature communications* **2024,** *15* (1), 1652.
235. Lu, G.; Bluemling, G. R.; Mao, S.; Hager, M.; Gurale, B. P.; Collop, P.; Kuiper, D.; Sana, K.; Painter, G. R.; De La Rosa, A.; Kolykhalov, A. A., Simple In Vitro Assay To Evaluate the Incorporation Efficiency of Ribonucleotide Analog 5'-Triphosphates into RNA by Human Mitochondrial DNA-Dependent RNA Polymerase. *Antimicrobial agents and chemotherapy* **2018,** *62* (2).
236. Johnson, A. A.; Ray, A. S.; Hanes, J.; Suo, Z.; Colacino, J. M.; Anderson, K. S.; Johnson, K. A., Toxicity of antiviral nucleoside analogs and the human mitochondrial DNA polymerase. *The Journal of biological chemistry* **2001,** *276* (44), 40847-57.
237. Sticher, Z. M.; Lu, G.; Mitchell, D. G.; Marlow, J.; Moellering, L.; Bluemling, G. R.; Guthrie, D. B.; Natchus, M. G.; Painter, G. R.; Kolykhalov, A. A., Analysis of the Potential for N (4)-Hydroxycytidine To Inhibit Mitochondrial Replication and Function. *Antimicrobial agents and chemotherapy* **2020,** *64* (2).
238. Jin, Z.; Kinkade, A.; Behera, I.; Chaudhuri, S.; Tucker, K.; Dyatkina, N.; Rajwanshi, V. K.; Wang, G.; Jekle, A.; Smith, D. B.; Beigelman, L.; Symons, J. A.; Deval, J., Structure-activity relationship analysis of mitochondrial toxicity caused by antiviral ribonucleoside analogs. *Antiviral research* **2017,** *143*, 151-161.
239. Cappellacci, L.; Barboni, G.; Palmieri, M.; Pasqualini, M.; Grifantini, M.; Costa, B.; Martini, C.; Franchetti, P., Ribose-modified nucleosides as ligands for adenosine receptors: synthesis, conformational analysis, and biological evaluation of 1'-C-methyl adenosine analogues. *Journal of medicinal chemistry* **2002,** *45* (6), 1196-202.
240. Cho, A.; Saunders, O. L.; Butler, T.; Zhang, L.; Xu, J.; Vela, J. E.; Feng, J. Y.; Ray, A. S.; Kim, C. U., Synthesis and antiviral activity of a series of 1'-substituted 4-aza-7,9-dideazaadenosine C-nucleosides. *Bioorg Med Chem Lett* **2012,** *22* (8), 2705-7.
241. Siegel, D.; Hui, H. C.; Doerffler, E.; Clarke, M. O.; Chun, K.; Zhang, L.; Neville, S.; Carra, E.; Lew, W.; Ross, B.; Wang, Q.; Wolfe, L.; Jordan, R.; Soloveva, V.; Knox, J.; Perry, J.; Perron, M.; Stray, K. M.; Barauskas, O.; Feng, J. Y.; Xu, Y.; Lee, G.; Rheingold, A. L.; Ray, A. S.; Bannister, R.; Strickley, R.; Swaminathan, S.; Lee, W. A.; Bavari, S.; Cihlar, T.; Lo, M. K.; Warren, T. K.; Mackman, R. L., Discovery and Synthesis of a Phosphoramidate Prodrug of a Pyrrolo[2,1-f][triazin-4-amino] Adenine C-Nucleoside (GS-5734) for the Treatment of Ebola and Emerging Viruses. *Journal of medicinal chemistry* **2017,** *60* (5), 1648-1661.
242. Mulangu, S.; Dodd, L. E.; Davey, R. T., Jr.; Tshiani Mbaya, O.; Proschan, M.; Mukadi, D.; Lusakibanza Manzo, M.; Nzolo, D.; Tshomba Oloma, A.; Ibanda, A.; Ali, R.; Coulibaly, S.; Levine, A. C.; Grais, R.; Diaz, J.; Lane, H. C.; Muyembe-Tamfum, J. J.; Group, P. W.;

Sivahera, B.; Camara, M.; Kojan, R.; Walker, R.; Dighero-Kemp, B.; Cao, H.; Mukumbayi, P.; Mbala-Kingebeni, P.; Ahuka, S.; Albert, S.; Bonnett, T.; Crozier, I.; Duvenhage, M.; Proffitt, C.; Teitelbaum, M.; Moench, T.; Aboulhab, J.; Barrett, K.; Cahill, K.; Cone, K.; Eckes, R.; Hensley, L.; Herpin, B.; Higgs, E.; Ledgerwood, J.; Pierson, J.; Smolskis, M.; Sow, Y.; Tierney, J.; Sivapalasingam, S.; Holman, W.; Gettinger, N.; Vallee, D.; Nordwall, J.; Team, P. C. S., A Randomized, Controlled Trial of Ebola Virus Disease Therapeutics. *The New England journal of medicine* **2019,** *381* (24), 2293-2303.
243. Grein, J.; Ohmagari, N.; Shin, D.; Diaz, G.; Asperges, E.; Castagna, A.; Feldt, T.; Green, G.; Green, M. L.; Lescure, F. X.; Nicastri, E.; Oda, R.; Yo, K.; Quiros-Roldan, E.; Studemeister, A.; Redinski, J.; Ahmed, S.; Bernett, J.; Chelliah, D.; Chen, D.; Chihara, S.; Cohen, S. H.; Cunningham, J.; D'Arminio Monforte, A.; Ismail, S.; Kato, H.; Lapadula, G.; L'Her, E.; Maeno, T.; Majumder, S.; Massari, M.; Mora-Rillo, M.; Mutoh, Y.; Nguyen, D.; Verweij, E.; Zoufaly, A.; Osinusi, A. O.; DeZure, A.; Zhao, Y.; Zhong, L.; Chokkalingam, A.; Elboudwarej, E.; Telep, L.; Timbs, L.; Henne, I.; Sellers, S.; Cao, H.; Tan, S. K.; Winterbourne, L.; Desai, P.; Mera, R.; Gaggar, A.; Myers, R. P.; Brainard, D. M.; Childs, R.; Flanigan, T., Compassionate Use of Remdesivir for Patients with Severe Covid-19. *The New England journal of medicine* **2020,** *382* (24), 2327-2336.
244. U.S. Food and Drug Administration Approves Gilead's Antiviral Veklury® (remdesivir) for Treatment of COVID-19. 2020.
245. Cox, R. M.; Wolf, J. D.; Lieber, C. M.; Sourimant, J.; Lin, M. J.; Babusis, D.; DuPont, V.; Chan, J.; Barrett, K. T.; Lye, D.; Kalla, R.; Chun, K.; Mackman, R. L.; Ye, C.; Cihlar, T.; Martinez-Sobrido, L.; Greninger, A. L.; Bilello, J. P.; Plemper, R. K., Oral prodrug of remdesivir parent GS-441524 is efficacious against SARS-CoV-2 in ferrets. *Nature communications* **2021,** *12* (1), 6415.
246. Cao, L.; Li, Y.; Yang, S.; Li, G.; Zhou, Q.; Sun, J.; Xu, T.; Yang, Y.; Liao, R.; Shi, Y.; Yang, Y.; Zhu, T.; Huang, S.; Ji, Y.; Cong, F.; Luo, Y.; Zhu, Y.; Luan, H.; Zhang, H.; Chen, J.; Liu, X.; Luo, R.; Liu, L.; Wang, P.; Yu, Y.; Xing, F.; Ke, B.; Zheng, H.; Deng, X.; Zhang, W.; Lin, C.; Shi, M.; Li, C. M.; Zhang, Y.; Zhang, L.; Dai, J.; Lu, H.; Zhao, J.; Zhang, X.; Guo, D., The adenosine analog prodrug ATV006 is orally bioavailable and has preclinical efficacy against parental SARS-CoV-2 and variants. *Science translational medicine* **2022,** *14* (661), eabm7621.
247. Mackman, R. L.; Kalla, R. V.; Babusis, D.; Pitts, J.; Barrett, K. T.; Chun, K.; Du Pont, V.; Rodriguez, L.; Moshiri, J.; Xu, Y.; Lee, M.; Lee, G.; Bleier, B.; Nguyen, A. Q.; O'Keefe, B. M.; Ambrosi, A.; Cook, M.; Yu, J.; Dempah, K. E.; Bunyan, E.; Riola, N. C.; Lu, X.; Liu, R.; Davie, A.; Hsiang, T. Y.; Dearing, J.; Vermillion, M.; Gale, M., Jr.; Niedziela-Majka, A.; Feng, J. Y.; Hedskog, C.; Bilello, J. P.; Subramanian, R.; Cihlar, T., Discovery of GS-5245 (Obeldesivir), an Oral Prodrug of Nucleoside GS-441524 That Exhibits Antiviral Efficacy in SARS-CoV-2-Infected African Green Monkeys. *Journal of medicinal chemistry* **2023,** *66* (17), 11701-11717.
248. Martinez, D. R.; Moreira, F. R.; Catanzaro, N. J.; Diefenbacher, M. V.; Zweigart, M. R.; Gully, K. L.; De la Cruz, G.; Brown, A. J.; Adams, L. E.; Yount, B.; Baric, T. J.; Mallory, M. L.; Conrad, H.; May, S. R.; Dong, S.; Scobey, D. T.; Nguyen, C.; Montgomery, S. A.; Perry, J. K.; Babusis, D.; Barrett, K. T.; Nguyen, A. H.; Nguyen, A. Q.; Kalla, R.; Bannister, R.; Feng, J. Y.; Cihlar, T.; Baric, R. S.; Mackman, R. L.; Bilello, J. P.; Schafer, A.; Sheahan, T. P., The oral nucleoside prodrug GS-5245 is efficacious against SARS-CoV-2 and other endemic, epidemic, and enzootic coronaviruses. *Science translational medicine* **2024,** *16* (748), eadj4504.

249. National Library of Medicine, Study of Obeldesivir in participants with COVID-19 who have a high risk of developing serious or severe illness (identifier: NCT05603143). **2023**.
250. Cross, R. W.; Woolsey, C.; Chu, V. C.; Babusis, D.; Bannister, R.; Vermillion, M. S.; Geleziunas, R.; Barrett, K. T.; Bunyan, E.; Nguyen, A. Q.; Cihlar, T.; Porter, D. P.; Prasad, A. N.; Deer, D. J.; Borisevich, V.; Agans, K. N.; Martinez, J.; Harrison, M. B.; Dobias, N. S.; Fenton, K. A.; Bilello, J. P.; Geisbert, T. W., Oral administration of obeldesivir protects nonhuman primates against Sudan ebolavirus. *Science* **2024,** *383* (6688), eadk6176.
251. Agostini, M. L.; Andres, E. L.; Sims, A. C.; Graham, R. L.; Sheahan, T. P.; Lu, X.; Smith, E. C.; Case, J. B.; Feng, J. Y.; Jordan, R.; Ray, A. S.; Cihlar, T.; Siegel, D.; Mackman, R. L.; Clarke, M. O.; Baric, R. S.; Denison, M. R., Coronavirus Susceptibility to the Antiviral Remdesivir (GS-5734) Is Mediated by the Viral Polymerase and the Proofreading Exoribonuclease. *mBio* **2018,** *9* (2).
252. Pruijssers, A. J.; George, A. S.; Schafer, A.; Leist, S. R.; Gralinksi, L. E.; Dinnon, K. H., 3rd; Yount, B. L.; Agostini, M. L.; Stevens, L. J.; Chappell, J. D.; Lu, X.; Hughes, T. M.; Gully, K.; Martinez, D. R.; Brown, A. J.; Graham, R. L.; Perry, J. K.; Du Pont, V.; Pitts, J.; Ma, B.; Babusis, D.; Murakami, E.; Feng, J. Y.; Bilello, J. P.; Porter, D. P.; Cihlar, T.; Baric, R. S.; Denison, M. R.; Sheahan, T. P., Remdesivir Inhibits SARS-CoV-2 in Human Lung Cells and Chimeric SARS-CoV Expressing the SARS-CoV-2 RNA Polymerase in Mice. *Cell reports* **2020,** *32* (3), 107940.
253. Sheahan, T. P.; Sims, A. C.; Graham, R. L.; Menachery, V. D.; Gralinski, L. E.; Case, J. B.; Leist, S. R.; Pyrc, K.; Feng, J. Y.; Trantcheva, I.; Bannister, R.; Park, Y.; Babusis, D.; Clarke, M. O.; Mackman, R. L.; Spahn, J. E.; Palmiotti, C. A.; Siegel, D.; Ray, A. S.; Cihlar, T.; Jordan, R.; Denison, M. R.; Baric, R. S., Broad-spectrum antiviral GS-5734 inhibits both epidemic and zoonotic coronaviruses. *Science translational medicine* **2017,** *9* (396).
254. Sheahan, T. P.; Sims, A. C.; Leist, S. R.; Schafer, A.; Won, J.; Brown, A. J.; Montgomery, S. A.; Hogg, A.; Babusis, D.; Clarke, M. O.; Spahn, J. E.; Bauer, L.; Sellers, S.; Porter, D.; Feng, J. Y.; Cihlar, T.; Jordan, R.; Denison, M. R.; Baric, R. S., Comparative therapeutic efficacy of remdesivir and combination lopinavir, ritonavir, and interferon beta against MERS-CoV. *Nature communications* **2020,** *11* (1), 222.
255. Radoshitzky, S. R.; Iversen, P.; Lu, X.; Zou, J.; Kaptein, S. J. F.; Stuthman, K. S.; Van Tongeren, S. A.; Steffens, J.; Gong, R.; Truong, H.; Sapre, A. A.; Yang, H.; Xie, X.; Chia, J. J.; Song, Z. J.; Leventhal, S. M.; Chan, J.; Shornikov, A.; Zhang, X.; Cowfer, D.; Yu, H.; Warren, T.; Cihlar, T.; Porter, D. P.; Neyts, J.; Shi, P. Y.; Wells, J.; Bilello, J. P.; Feng, J. Y., Expanded profiling of Remdesivir as a broad-spectrum antiviral and low potential for interaction with other medications in vitro. *Sci Rep* **2023,** *13* (1), 3131.
256. Ye, W.; Yao, M.; Dong, Y.; Ye, C.; Wang, D.; Liu, H.; Ma, H.; Zhang, H.; Qi, L.; Yang, Y.; Wang, Y.; Zhang, L.; Cheng, L.; Lv, X.; Xu, Z.; Lei, Y.; Zhang, F., Remdesivir (GS-5734) Impedes Enterovirus Replication Through Viral RNA Synthesis Inhibition. *Front Microbiol* **2020,** *11*, 1105.
257. Lo, M. K.; Jordan, R.; Arvey, A.; Sudhamsu, J.; Shrivastava-Ranjan, P.; Hotard, A. L.; Flint, M.; McMullan, L. K.; Siegel, D.; Clarke, M. O.; Mackman, R. L.; Hui, H. C.; Perron, M.; Ray, A. S.; Cihlar, T.; Nichol, S. T.; Spiropoulou, C. F., GS-5734 and its parent nucleoside analog inhibit Filo-, Pneumo-, and Paramyxoviruses. *Scientific reports* **2017,** *7*, 43395.
258. Mackman, R. L.; Hui, H. C.; Perron, M.; Murakami, E.; Palmiotti, C.; Lee, G.; Stray, K.; Zhang, L.; Goyal, B.; Chun, K.; Byun, D.; Siegel, D.; Simonovich, S.; Du Pont, V.; Pitts, J.; Babusis, D.; Vijjapurapu, A.; Lu, X.; Kim, C.; Zhao, X.; Chan, J.; Ma, B.; Lye, D.;

Vandersteen, A.; Wortman, S.; Barrett, K. T.; Toteva, M.; Jordan, R.; Subramanian, R.; Bilello, J. P.; Cihlar, T., Prodrugs of a 1'-CN-4-Aza-7,9-dideazaadenosine C-Nucleoside Leading to the Discovery of Remdesivir (GS-5734) as a Potent Inhibitor of Respiratory Syncytial Virus with Efficacy in the African Green Monkey Model of RSV. *Journal of medicinal chemistry* **2021,** *64* (8), 5001-5017.
259. Radoshitzky, S. R.; Iversen, P.; Lu, X.; Zou, J.; Kaptein, S. J. F.; Stuthman, K. S.; Van Tongeren, S. A.; Steffens, J.; Gong, R.; Truong, H.; Sapre, A. A.; Yang, H.; Xie, X.; Chia, J. J.; Song, Z. J.; Leventhal, S. M.; Chan, J.; Shornikov, A.; Zhang, X.; Cowfer, D.; Yu, H.; Warren, T.; Cihlar, T.; Porter, D. P.; Neyts, J.; Shi, P.-Y.; Wells, J.; Bilello, J. P.; Feng, J. Y., Expanded profiling of Remdesivir as a broad-spectrum antiviral and low potential for interaction with other medications in vitro. *Scientific reports* **2023,** *13* (1), 3131.
260. Gordon, C. J.; Lee, H. W.; Tchesnokov, E. P.; Perry, J. K.; Feng, J. Y.; Bilello, J. P.; Porter, D. P.; Gotte, M., Efficient incorporation and template-dependent polymerase inhibition are major determinants for the broad-spectrum antiviral activity of remdesivir. *The Journal of biological chemistry* **2022,** *298* (2), 101529.
261. Dangerfield, T. L.; Huang, N. Z.; Johnson, K. A., Remdesivir Is Effective in Combating COVID-19 because It Is a Better Substrate than ATP for the Viral RNA-Dependent RNA Polymerase. *iScience* **2020,** *23* (12), 101849.
262. Gordon, C. J.; Walker, S. M.; Tchesnokov, E. P.; Kocincova, D.; Pitts, J.; Siegel, D. S.; Perry, J. K.; Feng, J. Y.; Bilello, J. P.; Gotte, M., Mechanism and spectrum of inhibition of a 4 -cyano modified nucleotide analog against diverse RNA polymerases of prototypic respiratory RNA viruses. *The Journal of biological chemistry* **2024**, 107514.
263. Bravo, J. P. K.; Dangerfield, T. L.; Taylor, D. W.; Johnson, K. A., Remdesivir is a delayed translocation inhibitor of SARS-CoV-2 replication. *Mol Cell* **2021,** *81* (7), 1548-1552 e4.
264. Wu, J.; Wang, H.; Liu, Q.; Li, R.; Gao, Y.; Fang, X.; Zhong, Y.; Wang, M.; Wang, Q.; Rao, Z.; Gong, P., Remdesivir overcomes the S861 roadblock in SARS-CoV-2 polymerase elongation complex. *Cell reports* **2021,** *37* (4), 109882.
265. Tchesnokov, E. P.; Gordon, C. J.; Woolner, E.; Kocinkova, D.; Perry, J. K.; Feng, J. Y.; Porter, D. P.; Gotte, M., Template-dependent inhibition of coronavirus RNA-dependent RNA polymerase by remdesivir reveals a second mechanism of action. *The Journal of biological chemistry* **2020,** *295* (47), 16156-16165.
266. Kokic, G.; Hillen, H. S.; Tegunov, D.; Dienemann, C.; Seitz, F.; Schmitzova, J.; Farnung, L.; Siewert, A.; Hobartner, C.; Cramer, P., Mechanism of SARS-CoV-2 polymerase stalling by remdesivir. *Nature communications* **2021,** *12* (1), 279.
267. Tchesnokov, E. P.; Feng, J. Y.; Porter, D. P.; Gotte, M., Mechanism of Inhibition of Ebola Virus RNA-Dependent RNA Polymerase by Remdesivir. *Viruses* **2019,** *11* (4).
268. Tchesnokov, E. P.; Obikhod, A.; Schinazi, R. F.; Gotte, M., Delayed chain termination protects the anti-hepatitis B virus drug entecavir from excision by HIV-1 reverse transcriptase. *The Journal of biological chemistry* **2008,** *283* (49), 34218-28.
269. Magee, W. C.; Aldern, K. A.; Hostetler, K. Y.; Evans, D. H., Cidofovir and (S)-9-[3-hydroxy-(2-phosphonomethoxy)propyl]adenine are highly effective inhibitors of vaccinia virus DNA polymerase when incorporated into the template strand. *Antimicrobial agents and chemotherapy* **2008,** *52* (2), 586-97.
270. Chinthapatla, R.; Sotoudegan, M.; Srivastava, P.; Anderson, T. K.; Moustafa, I. M.; Passow, K. T.; Kennelly, S. A.; Moorthy, R.; Dulin, D.; Feng, J. Y.; Harki, D. A.; Kirchdoerfer,

R. N.; Cameron, C. E.; Arnold, J. J., Interfering with nucleotide excision by the coronavirus 3'-to-5' exoribonuclease. *Nucleic Acids Res* **2023,** *51* (1), 315-336.
271. Sexton, N. R.; Smith, E. C.; Blanc, H.; Vignuzzi, M.; Peersen, O. B.; Denison, M. R., Homology-Based Identification of a Mutation in the Coronavirus RNA-Dependent RNA Polymerase That Confers Resistance to Multiple Mutagens. *J Virol* **2016,** *90* (16), 7415-7428.
272. Luo, X.; Wang, X.; Yao, Y.; Gao, X.; Zhang, L., Unveiling the "Template-Dependent" Inhibition on the Viral Transcription of SARS-CoV-2. *J Phys Chem Lett* **2022,** *13* (31), 7197-7205.
273. Stevens, L. J.; Pruijssers, A. J.; Lee, H. W.; Gordon, C. J.; Tchesnokov, E. P.; Gribble, J.; George, A. S.; Hughes, T. M.; Lu, X.; Li, J.; Perry, J. K.; Porter, D. P.; Cihlar, T.; Sheahan, T. P.; Baric, R. S.; Gotte, M.; Denison, M. R., Mutations in the SARS-CoV-2 RNA-dependent RNA polymerase confer resistance to remdesivir by distinct mechanisms. *Science translational medicine* **2022,** *14* (656), eabo0718.
274. Hogan, J. I.; Duerr, R.; Dimartino, D.; Marier, C.; Hochman, S. E.; Mehta, S.; Wang, G.; Heguy, A., Remdesivir Resistance in Transplant Recipients With Persistent Coronavirus Disease 2019. *Clin Infect Dis* **2023,** *76* (2), 342-345.
275. Lo, M. K.; Albarino, C. G.; Perry, J. K.; Chang, S.; Tchesnokov, E. P.; Guerrero, L.; Chakrabarti, A.; Shrivastava-Ranjan, P.; Chatterjee, P.; McMullan, L. K.; Martin, R.; Jordan, R.; Gotte, M.; Montgomery, J. M.; Nichol, S. T.; Flint, M.; Porter, D.; Spiropoulou, C. F., Remdesivir targets a structurally analogous region of the Ebola virus and SARS-CoV-2 polymerases. *Proceedings of the National Academy of Sciences of the United States of America* **2020,** *117* (43), 26946-26954.
276. Sofia, M. J.; Bao, D.; Chang, W.; Du, J.; Nagarathnam, D.; Rachakonda, S.; Reddy, P. G.; Ross, B. S.; Wang, P.; Zhang, H. R.; Bansal, S.; Espiritu, C.; Keilman, M.; Lam, A. M.; Steuer, H. M.; Niu, C.; Otto, M. J.; Furman, P. A., Discovery of a beta-d-2'-deoxy-2'-alpha-fluoro-2'-beta-C-methyluridine nucleotide prodrug (PSI-7977) for the treatment of hepatitis C virus. *Journal of medicinal chemistry* **2010,** *53* (19), 7202-18.
277. Gane, E. J.; Stedman, C. A.; Hyland, R. H.; Ding, X.; Svarovskaia, E.; Symonds, W. T.; Hindes, R. G.; Berrey, M. M., Nucleotide polymerase inhibitor sofosbuvir plus ribavirin for hepatitis C. *The New England journal of medicine* **2013,** *368* (1), 34-44.
278. Xu, H. T.; Colby-Germinario, S. P.; Hassounah, S. A.; Fogarty, C.; Osman, N.; Palanisamy, N.; Han, Y.; Oliveira, M.; Quan, Y.; Wainberg, M. A., Evaluation of Sofosbuvir (beta-D-2'-deoxy-2'-alpha-fluoro-2'-beta-C-methyluridine) as an inhibitor of Dengue virus replication<sup/>. *Scientific reports* **2017,** *7* (1), 6345.
279. Ferreira, A. C.; Zaverucha-do-Valle, C.; Reis, P. A.; Barbosa-Lima, G.; Vieira, Y. R.; Mattos, M.; Silva, P. P.; Sacramento, C.; de Castro Faria Neto, H. C.; Campanati, L.; Tanuri, A.; Bruning, K.; Bozza, F. A.; Bozza, P. T.; Souza, T. M. L., Sofosbuvir protects Zika virus-infected mice from mortality, preventing short- and long-term sequelae. *Scientific reports* **2017,** *7* (1), 9409.
280. Bullard-Feibelman, K. M.; Govero, J.; Zhu, Z.; Salazar, V.; Veselinovic, M.; Diamond, M. S.; Geiss, B. J., The FDA-approved drug sofosbuvir inhibits Zika virus infection. *Antiviral research* **2017,** *137*, 134-140.
281. Binderup, A.; Galli, A.; Fossat, N.; Fernandez-Antunez, C.; Mikkelsen, L. S.; Rivera-Rangel, L. R.; Scheel, T. K. H.; Fahnoe, U.; Bukh, J.; Ramirez, S., Differential activity of nucleotide analogs against tick-borne encephalitis and yellow fever viruses in human cell lines. *Virology* **2023,** *585*, 179-185.

282. LeCher, J. C.; Zandi, K.; Costa, V. V.; Amblard, F.; Tao, S.; Patel, D.; Lee, S.; da Silva Santos, F. R.; Goncalves, M. R.; Queroz-Junior, C. M.; Marim, F. M.; Musall, K.; Goh, S. L.; McBrayer, T.; Downs-Bowen, J.; De, R.; Azadi, N.; Kohler, J.; Teixeira, M. M.; Schinazi, R. F., Discovery of a 2'-Fluoro,2'-Bromouridine Phosphoramidate Prodrug Exhibiting Anti-Yellow Fever Virus Activity in Culture and in Mice. *Microorganisms* **2022,** *10* (11).
283. Mendes, E. A.; Pilger, D. R. B.; Santos Nastri, A. C. S.; Malta, F. M.; Pascoalino, B. D. S.; Carneiro D'Albuquerque, L. A.; Balan, A.; Freitas, L. H. G., Jr.; Durigon, E. L.; Carrilho, F. J.; Rebello Pinho, J. R., Sofosbuvir inhibits yellow fever virus in vitro and in patients with acute liver failure. *Ann Hepatol* **2019,** *18* (6), 816-824.
284. de Freitas, C. S.; Higa, L. M.; Sacramento, C. Q.; Ferreira, A. C.; Reis, P. A.; Delvecchio, R.; Monteiro, F. L.; Barbosa-Lima, G.; James Westgarth, H.; Vieira, Y. R.; Mattos, M.; Rocha, N.; Hoelz, L. V. B.; Leme, R. P. P.; Bastos, M. M.; Rodrigues, G. O. L.; Lopes, C. E. M.; Queiroz-Junior, C. M.; Lima, C. X.; Costa, V. V.; Teixeira, M. M.; Bozza, F. A.; Bozza, P. T.; Boechat, N.; Tanuri, A.; Souza, T. M. L., Yellow fever virus is susceptible to sofosbuvir both in vitro and in vivo. *PLoS neglected tropical diseases* **2019,** *13* (1), e0007072.
285. Elfiky, A. A., Ribavirin, Remdesivir, Sofosbuvir, Galidesivir, and Tenofovir against SARS-CoV-2 RNA dependent RNA polymerase (RdRp): A molecular docking study. *Life Sci* **2020,** *253*, 117592.
286. Shannon, A.; Fattorini, V.; Sama, B.; Selisko, B.; Feracci, M.; Falcou, C.; Gauffre, P.; El Kazzi, P.; Delpal, A.; Decroly, E.; Alvarez, K.; Eydoux, C.; Guillemot, J. C.; Moussa, A.; Good, S. S.; La Colla, P.; Lin, K.; Sommadossi, J. P.; Zhu, Y.; Yan, X.; Shi, H.; Ferron, F.; Canard, B., A dual mechanism of action of AT-527 against SARS-CoV-2 polymerase. *Nature communications* **2022,** *13* (1), 621.
287. Fung, A.; Jin, Z.; Dyatkina, N.; Wang, G.; Beigelman, L.; Deval, J., Efficiency of incorporation and chain termination determines the inhibition potency of 2'-modified nucleotide analogs against hepatitis C virus polymerase. *Antimicrobial agents and chemotherapy* **2014,** *58* (7), 3636-45.
288. Villalba, B.; Li, J.; Johnson, K. A., Resistance to excision determines efficiency of hepatitis C virus RNA-dependent RNA polymerase inhibition by nucleotide analogs. *The Journal of biological chemistry* **2020,** *295* (30), 10112-10124.
289. Dragoni, F.; Boccuto, A.; Picarazzi, F.; Giannini, A.; Giammarino, F.; Saladini, F.; Mori, M.; Mastrangelo, E.; Zazzi, M.; Vicenti, I., Evaluation of sofosbuvir activity and resistance profile against West Nile virus in vitro. *Antiviral research* **2020,** *175*, 104708.
290. Saenger, W., W (1984) Principles of Nucleic Acid Structure. Springer.
291. Klumpp, K.; Kalayanov, G.; Ma, H.; Le Pogam, S.; Leveque, V.; Jiang, W. R.; Inocencio, N.; De Witte, A.; Rajyaguru, S.; Tai, E.; Chanda, S.; Irwin, M. R.; Sund, C.; Winqist, A.; Maltseva, T.; Eriksson, S.; Usova, E.; Smith, M.; Alker, A.; Najera, I.; Cammack, N.; Martin, J. A.; Johansson, N. G.; Smith, D. B., 2'-deoxy-4'-azido nucleoside analogs are highly potent inhibitors of hepatitis C virus replication despite the lack of 2'-alpha-hydroxyl groups. *The Journal of biological chemistry* **2008,** *283* (4), 2167-75.
292. Clark, J. L.; Hollecker, L.; Mason, J. C.; Stuyver, L. J.; Tharnish, P. M.; Lostia, S.; McBrayer, T. R.; Schinazi, R. F.; Watanabe, K. A.; Otto, M. J.; Furman, P. A.; Stec, W. J.; Patterson, S. E.; Pankiewicz, K. W., Design, synthesis, and antiviral activity of 2'-deoxy-2'-fluoro-2'-C-methylcytidine, a potent inhibitor of hepatitis C virus replication. *Journal of medicinal chemistry* **2005,** *48* (17), 5504-8.

293. Gudmundsson, K. S.; Freeman, G. A.; Drach, J. C.; Townsend, L. B., Synthesis of fluorosugar analogues of 2,5,6-trichloro-1-(beta-D-ribofuranosyl)benzimidazole as antivirals with potentially increased glycosidic bond stability. *Journal of medicinal chemistry* **2000,** *43* (12), 2473-8.
294. Migliaccio, G.; Tomassini, J. E.; Carroll, S. S.; Tomei, L.; Altamura, S.; Bhat, B.; Bartholomew, L.; Bosserman, M. R.; Ceccacci, A.; Colwell, L. F.; Cortese, R.; De Francesco, R.; Eldrup, A. B.; Getty, K. L.; Hou, X. S.; LaFemina, R. L.; Ludmerer, S. W.; MacCoss, M.; McMasters, D. R.; Stahlhut, M. W.; Olsen, D. B.; Hazuda, D. J.; Flores, O. A., Characterization of resistance to non-obligate chain-terminating ribonucleoside analogs that inhibit hepatitis C virus replication in vitro. *The Journal of biological chemistry* **2003,** *278* (49), 49164-70.
295. Boehr, A. K.; Arnold, J. J.; Oh, H. S.; Cameron, C. E.; Boehr, D. D., 2'-C-methylated nucleotides terminate virus RNA synthesis by preventing active site closure of the viral RNA-dependent RNA polymerase. *The Journal of biological chemistry* **2019,** *294* (45), 16897-16907.
296. Lam, A. M.; Espiritu, C.; Bansal, S.; Micolochick Steuer, H. M.; Niu, C.; Zennou, V.; Keilman, M.; Zhu, Y.; Lan, S.; Otto, M. J.; Furman, P. A., Genotype and subtype profiling of PSI-7977 as a nucleotide inhibitor of hepatitis C virus. *Antimicrobial agents and chemotherapy* **2012,** *56* (6), 3359-68.
297. Lam, A. M.; Espiritu, C.; Murakami, E.; Zennou, V.; Bansal, S.; Micolochick Steuer, H. M.; Niu, C.; Keilman, M.; Bao, H.; Bourne, N.; Veselenak, R. L.; Reddy, P. G.; Chang, W.; Du, J.; Nagarathnam, D.; Sofia, M. J.; Otto, M. J.; Furman, P. A., Inhibition of hepatitis C virus replicon RNA synthesis by PSI-352938, a cyclic phosphate prodrug of beta-D-2'-deoxy-2'-alpha-fluoro-2'-beta-C-methylguanosine. *Antimicrobial agents and chemotherapy* **2011,** *55* (6), 2566-75.
298. Stuyver, L. J.; McBrayer, T. R.; Tharnish, P. M.; Clark, J.; Hollecker, L.; Lostia, S.; Nachman, T.; Grier, J.; Bennett, M. A.; Xie, M. Y.; Schinazi, R. F.; Morrey, J. D.; Julander, J. L.; Furman, P. A.; Otto, M. J., Inhibition of hepatitis C replicon RNA synthesis by beta-D-2'-deoxy-2'-fluoro-2'-C-methylcytidine: a specific inhibitor of hepatitis C virus replication. *Antivir Chem Chemother* **2006,** *17* (2), 79-87.
299. Dutartre, H.; Bussetta, C.; Boretto, J.; Canard, B., General catalytic deficiency of hepatitis C virus RNA polymerase with an S282T mutation and mutually exclusive resistance towards 2'-modified nucleotide analogues. *Antimicrobial agents and chemotherapy* **2006,** *50* (12), 4161-9.
300. Powdrill, M. H.; Tchesnokov, E. P.; Kozak, R. A.; Russell, R. S.; Martin, R.; Svarovskaia, E. S.; Mo, H.; Kouyos, R. D.; Gotte, M., Contribution of a mutational bias in hepatitis C virus replication to the genetic barrier in the development of drug resistance. *Proceedings of the National Academy of Sciences of the United States of America* **2011,** *108* (51), 20509-13.
301. Xu, H. T.; Hassounah, S. A.; Colby-Germinario, S. P.; Oliveira, M.; Fogarty, C.; Quan, Y.; Han, Y.; Golubkov, O.; Ibanescu, I.; Brenner, B.; Stranix, B. R.; Wainberg, M. A., Purification of Zika virus RNA-dependent RNA polymerase and its use to identify small-molecule Zika inhibitors. *J Antimicrob Chemother* **2017,** *72* (3), 727-734.
302. Kulkarni, A. S.; Damha, M. J.; Schinazi, R. F.; Mo, H.; Doehle, B.; Sagan, S. M.; Gotte, M., A Complex Network of Interactions between S282 and G283 of Hepatitis C Virus Nonstructural Protein 5B and the Template Strand Affects Susceptibility to Sofosbuvir and Ribavirin. *Antimicrobial agents and chemotherapy* **2016,** *60* (4), 2018-27.
303. Appleby, T. C.; Perry, J. K.; Murakami, E.; Barauskas, O.; Feng, J.; Cho, A.; Fox, D., 3rd; Wetmore, D. R.; McGrath, M. E.; Ray, A. S.; Sofia, M. J.; Swaminathan, S.; Edwards, T.

E., Viral replication. Structural basis for RNA replication by the hepatitis C virus polymerase. *Science* **2015,** *347* (6223), 771-5.
304. Good, S. S.; Moussa, A.; Zhou, X. J.; Pietropaolo, K.; Sommadossi, J. P., Preclinical evaluation of AT-527, a novel guanosine nucleotide prodrug with potent, pan-genotypic activity against hepatitis C virus. *PloS one* **2020,** *15* (1), e0227104.
305. Marchand, B.; Gotte, M., Site-specific footprinting reveals differences in the translocation status of HIV-1 reverse transcriptase. Implications for polymerase translocation and drug resistance. *The Journal of biological chemistry* **2003,** *278* (37), 35362-72.
306. Marchand, B.; Tchesnokov, E. P.; Gotte, M., The pyrophosphate analogue foscarnet traps the pre-translocational state of HIV-1 reverse transcriptase in a Brownian ratchet model of polymerase translocation. *The Journal of biological chemistry* **2007,** *282* (5), 3337-46.
307. Sarafianos, S. G.; Clark, A. D., Jr.; Tuske, S.; Squire, C. J.; Das, K.; Sheng, D.; Ilankumaran, P.; Ramesha, A. R.; Kroth, H.; Sayer, J. M.; Jerina, D. M.; Boyer, P. L.; Hughes, S. H.; Arnold, E., Trapping HIV-1 reverse transcriptase before and after translocation on DNA. *The Journal of biological chemistry* **2003,** *278* (18), 16280-8.
308. Sarafianos, S. G.; Clark, A. D., Jr.; Das, K.; Tuske, S.; Birktoft, J. J.; Ilankumaran, P.; Ramesha, A. R.; Sayer, J. M.; Jerina, D. M.; Boyer, P. L.; Hughes, S. H.; Arnold, E., Structures of HIV-1 reverse transcriptase with pre- and post-translocation AZTMP-terminated DNA. *EMBO J* **2002,** *21* (23), 6614-24.
309. Meyer, P. R.; Matsuura, S. E.; Mian, A. M.; So, A. G.; Scott, W. A., A mechanism of AZT resistance: an increase in nucleotide-dependent primer unblocking by mutant HIV-1 reverse transcriptase. *Mol Cell* **1999,** *4* (1), 35-43.
310. Tu, X.; Das, K.; Han, Q.; Bauman, J. D.; Clark, A. D., Jr.; Hou, X.; Frenkel, Y. V.; Gaffney, B. L.; Jones, R. A.; Boyer, P. L.; Hughes, S. H.; Sarafianos, S. G.; Arnold, E., Structural basis of HIV-1 resistance to AZT by excision. *Nat Struct Mol Biol* **2010,** *17* (10), 1202-9.
311. Deval, J.; Powdrill, M. H.; D'Abramo, C. M.; Cellai, L.; Gotte, M., Pyrophosphorolytic excision of nonobligate chain terminators by hepatitis C virus NS5B polymerase. *Antimicrobial agents and chemotherapy* **2007,** *51* (8), 2920-8.
312. Jin, Z.; Leveque, V.; Ma, H.; Johnson, K. A.; Klumpp, K., NTP-mediated nucleotide excision activity of hepatitis C virus RNA-dependent RNA polymerase. *Proceedings of the National Academy of Sciences of the United States of America* **2013,** *110* (5), E348-57.
313. Murakami, E.; Bao, H.; Ramesh, M.; McBrayer, T. R.; Whitaker, T.; Micolochick Steuer, H. M.; Schinazi, R. F.; Stuyver, L. J.; Obikhod, A.; Otto, M. J.; Furman, P. A., Mechanism of activation of beta-D-2'-deoxy-2'-fluoro-2'-c-methylcytidine and inhibition of hepatitis C virus NS5B RNA polymerase. *Antimicrobial agents and chemotherapy* **2007,** *51* (2), 503-9.
314. Wedemeyer, H.; Jensen, D.; Herring, R., Jr.; Ferenci, P.; Ma, M. M.; Zeuzem, S.; Rodriguez-Torres, M.; Bzowej, N.; Pockros, P.; Vierling, J.; Ipe, D.; Munson, M. L.; Chen, Y. C.; Najera, I.; Thommes, J.; Investigators, P., PROPEL: a randomized trial of mericitabine plus peginterferon alpha-2a/ribavirin therapy in treatment-naive HCV genotype 1/4 patients. *Hepatology* **2013,** *58* (2), 524-37.
315. Pockros, P. J.; Jensen, D.; Tsai, N.; Taylor, R.; Ramji, A.; Cooper, C.; Dickson, R.; Tice, A.; Kulkarni, R.; Vierling, J. M.; Lou Munson, M.; Chen, Y. C.; Najera, I.; Thommes, J.; Investigators, J.-C., JUMP-C: a randomized trial of mericitabine plus pegylated interferon alpha-2a/ribavirin for 24 weeks in treatment-naive HCV genotype 1/4 patients. *Hepatology* **2013,** *58* (2), 514-23.

316. Eltahla, A. A.; Luciani, F.; White, P. A.; Lloyd, A. R.; Bull, R. A., Inhibitors of the Hepatitis C Virus Polymerase; Mode of Action and Resistance. *Viruses* **2015,** *7* (10), 5206-24.
317. Good, S. S.; Westover, J.; Jung, K. H.; Zhou, X. J.; Moussa, A.; La Colla, P.; Collu, G.; Canard, B.; Sommadossi, J. P., AT-527, a Double Prodrug of a Guanosine Nucleotide Analog, Is a Potent Inhibitor of SARS-CoV-2 In Vitro and a Promising Oral Antiviral for Treatment of COVID-19. *Antimicrobial agents and chemotherapy* **2021,** *65* (4).
318. Good, S. S.; Shannon, A.; Lin, K.; Moussa, A.; Julander, J. G.; La Colla, P.; Collu, G.; Canard, B.; Sommadossi, J. P., Evaluation of AT-752, a Double Prodrug of a Guanosine Nucleotide Analog with In Vitro and In Vivo Activity against Dengue and Other Flaviviruses. *Antimicrobial agents and chemotherapy* **2021,** *65* (11), e0098821.
319. Lin, K.; Good, S. S.; Julander, J. G.; Weight, A. E.; Moussa, A.; Sommadossi, J. P., AT-752, a double prodrug of a guanosine nucleotide analog, inhibits yellow fever virus in a hamster model. *PLoS neglected tropical diseases* **2022,** *16* (1), e0009937.
320. Feracci, M.; Eydoux, C.; Fattorini, V.; Lo Bello, L.; Gauffre, P.; Selisko, B.; Sutto-Ortiz, P.; Shannon, A.; Xia, H.; Shi, P. Y.; Noel, M.; Debart, F.; Vasseur, J. J.; Good, S.; Lin, K.; Moussa, A.; Sommadossi, J. P.; Chazot, A.; Alvarez, K.; Guillemot, J. C.; Decroly, E.; Ferron, F.; Canard, B., AT-752 targets multiple sites and activities on the Dengue virus replication enzyme NS5. *Antiviral research* **2023,** *212*, 105574.
321. Shannon, A.; Chazot, A.; Feracci, M.; Falcou, C.; Fattorini, V.; Selisko, B.; Good, S.; Moussa, A.; Sommadossi, J. P.; Ferron, F.; Alvarez, K.; Canard, B., An exonuclease-resistant chain-terminating nucleotide analogue targeting the SARS-CoV-2 replicase complex. *Nucleic Acids Res* **2024,** *52* (3), 1325-1340.
322. Wang, G.; Deval, J.; Hong, J.; Dyatkina, N.; Prhavc, M.; Taylor, J.; Fung, A.; Jin, Z.; Stevens, S. K.; Serebryany, V.; Liu, J.; Zhang, Q.; Tam, Y.; Chanda, S. M.; Smith, D. B.; Symons, J. A.; Blatt, L. M.; Beigelman, L., Discovery of 4'-chloromethyl-2'-deoxy-3',5'-di-O-isobutyryl-2'-fluorocytidine (ALS-8176), a first-in-class RSV polymerase inhibitor for treatment of human respiratory syncytial virus infection. *Journal of medicinal chemistry* **2015,** *58* (4), 1862-78.
323. DeVincenzo, J. P.; McClure, M. W.; Symons, J. A.; Fathi, H.; Westland, C.; Chanda, S.; Lambkin-Williams, R.; Smith, P.; Zhang, Q.; Beigelman, L.; Blatt, L. M.; Fry, J., Activity of Oral ALS-008176 in a Respiratory Syncytial Virus Challenge Study. *The New England journal of medicine* **2015,** *373* (21), 2048-58.
324. Oey, A.; McClure, M.; Symons, J. A.; Chanda, S.; Fry, J.; Smith, P. F.; Luciani, K.; Fayon, M.; Chokephaibulkit, K.; Uppala, R.; Bernatoniene, J.; Furuno, K.; Stanley, T.; Huntjens, D.; Witek, J.; Groups, R. S. V. S., Lumicitabine, an orally administered nucleoside analog, in infants hospitalized with respiratory syncytial virus (RSV) infection: Safety, efficacy, and pharmacokinetic results. *PloS one* **2023,** *18* (7), e0288271.
325. Deval, J.; Hong, J.; Wang, G.; Taylor, J.; Smith, L. K.; Fung, A.; Stevens, S. K.; Liu, H.; Jin, Z.; Dyatkina, N.; Prhavc, M.; Stoycheva, A. D.; Serebryany, V.; Liu, J.; Smith, D. B.; Tam, Y.; Zhang, Q.; Moore, M. L.; Fearns, R.; Chanda, S. M.; Blatt, L. M.; Symons, J. A.; Beigelman, L., Molecular Basis for the Selective Inhibition of Respiratory Syncytial Virus RNA Polymerase by 2'-Fluoro-4'-Chloromethyl-Cytidine Triphosphate. *PLoS pathogens* **2015,** *11* (6), e1004995.
326. Deval, J.; Fung, A.; Stevens, S. K.; Jordan, P. C.; Gromova, T.; Taylor, J. S.; Hong, J.; Meng, J.; Wang, G.; Dyatkina, N.; Prhavc, M.; Symons, J. A.; Beigelman, L., Biochemical

Effect of Resistance Mutations against Synergistic Inhibitors of RSV RNA Polymerase. *PloS one* **2016,** *11* (5), e0154097.
327. Sourimant, J.; Lieber, C. M.; Aggarwal, M.; Cox, R. M.; Wolf, J. D.; Yoon, J. J.; Toots, M.; Ye, C.; Sticher, Z.; Kolykhalov, A. A.; Martinez-Sobrido, L.; Bluemling, G. R.; Natchus, M. G.; Painter, G. R.; Plemper, R. K., 4'-Fluorouridine is an oral antiviral that blocks respiratory syncytial virus and SARS-CoV-2 replication. *Science* **2022,** *375* (6577), 161-167.
328. Chen, Y.; Li, X.; Han, F.; Ji, B.; Li, Y.; Yan, J.; Wang, M.; Fan, J.; Zhang, S.; Lu, L.; Zou, P., The nucleoside analog 4'-fluorouridine suppresses the replication of multiple enteroviruses by targeting 3D polymerase. *Antimicrobial agents and chemotherapy* **2024**, e0005424.
329. Lieber, C. M.; Aggarwal, M.; Yoon, J. J.; Cox, R. M.; Kang, H. J.; Sourimant, J.; Toots, M.; Johnson, S. K.; Jones, C. A.; Sticher, Z. M.; Kolykhalov, A. A.; Saindane, M. T.; Tompkins, S. M.; Planz, O.; Painter, G. R.; Natchus, M. G.; Sakamoto, K.; Plemper, R. K., 4'-Fluorouridine mitigates lethal infection with pandemic human and highly pathogenic avian influenza viruses. *PLoS pathogens* **2023,** *19* (4), e1011342.
330. Lieber, C. M.; Kang, H. J.; Aggarwal, M.; Lieberman, N. A.; Sobolik, E. B.; Yoon, J. J.; Natchus, M. G.; Cox, R. M.; Greninger, A. L.; Plemper, R. K., Influenza A virus resistance to 4'-fluorouridine coincides with viral attenuation in vitro and in vivo. *PLoS pathogens* **2024,** *20* (2), e1011993.
331. Berger, I.; Fitzgerald, D. J.; Richmond, T. J., Baculovirus expression system for heterologous multiprotein complexes. *Nat Biotechnol* **2004,** *22* (12), 1583-7.
332. Bieniossek, C.; Richmond, T. J.; Berger, I., MultiBac: multigene baculovirus-based eukaryotic protein complex production. *Curr Protoc Protein Sci* **2008,** *Chapter 5*, Unit 5 20.
333. Warren, T. K.; Jordan, R.; Lo, M. K.; Ray, A. S.; Mackman, R. L.; Soloveva, V.; Siegel, D.; Perron, M.; Bannister, R.; Hui, H. C.; Larson, N.; Strickley, R.; Wells, J.; Stuthman, K. S.; Van Tongeren, S. A.; Garza, N. L.; Donnelly, G.; Shurtleff, A. C.; Retterer, C. J.; Gharaibeh, D.; Zamani, R.; Kenny, T.; Eaton, B. P.; Grimes, E.; Welch, L. S.; Gomba, L.; Wilhelmsen, C. L.; Nichols, D. K.; Nuss, J. E.; Nagle, E. R.; Kugelman, J. R.; Palacios, G.; Doerffler, E.; Neville, S.; Carra, E.; Clarke, M. O.; Zhang, L.; Lew, W.; Ross, B.; Wang, Q.; Chun, K.; Wolfe, L.; Babusis, D.; Park, Y.; Stray, K. M.; Trancheva, I.; Feng, J. Y.; Barauskas, O.; Xu, Y.; Wong, P.; Braun, M. R.; Flint, M.; McMullan, L. K.; Chen, S. S.; Fearns, R.; Swaminathan, S.; Mayers, D. L.; Spiropoulou, C. F.; Lee, W. A.; Nichol, S. T.; Cihlar, T.; Bavari, S., Therapeutic efficacy of the small molecule GS-5734 against Ebola virus in rhesus monkeys. *Nature* **2016,** *531* (7594), 381-5.
334. Brown, A. J.; Won, J. J.; Graham, R. L.; Dinnon, K. H., 3rd; Sims, A. C.; Feng, J. Y.; Cihlar, T.; Denison, M. R.; Baric, R. S.; Sheahan, T. P., Broad spectrum antiviral remdesivir inhibits human endemic and zoonotic deltacoronaviruses with a highly divergent RNA dependent RNA polymerase. *Antiviral research* **2019,** *169*, 104541.
335. Jordan, P. C.; Liu, C.; Raynaud, P.; Lo, M. K.; Spiropoulou, C. F.; Symons, J. A.; Beigelman, L.; Deval, J., Initiation, extension, and termination of RNA synthesis by a paramyxovirus polymerase. *PLoS pathogens* **2018,** *14* (2), e1006889.
336. Muhlberger, E.; Weik, M.; Volchkov, V. E.; Klenk, H. D.; Becker, S., Comparison of the transcription and replication strategies of marburg virus and Ebola virus by using artificial replication systems. *J Virol* **1999,** *73* (3), 2333-42.
337. Tchesnokov, E. P.; Raeisimakiani, P.; Ngure, M.; Marchant, D.; Gotte, M., Recombinant RNA-Dependent RNA Polymerase Complex of Ebola Virus. *Scientific reports* **2018,** *8* (1), 3970.

338. Deval, J.; Hong, J.; Wang, G.; Taylor, J.; Smith, L. K.; Fung, A.; Stevens, S. K.; Liu, H.; Jin, Z.; Dyatkina, N.; Prhavc, M.; Stoycheva, A. D.; Serebryany, V.; Liu, J.; Smith, D. B.; Tam, Y.; Zhang, Q.; Moore, M. L.; Fearns, R.; Chanda, S. M.; Blatt, L. M.; Symons, J. A.; Beigelman, L., Molecular Basis for the Selective Inhibition of Respiratory Syncytial Virus RNA Polymerase by 2'-Fluoro-4'-Chloromethyl-Cytidine Triphosphate. *PLoS pathogens* **2015,** *11* (6).
339. Noton, S. L.; Deflube, L. R.; Tremaglio, C. Z.; Fearns, R., The respiratory syncytial virus polymerase has multiple RNA synthesis activities at the promoter. *PLoS pathogens* **2012,** *8* (10), e1002980.
340. Kirchdoerfer, R. N.; Ward, A. B., Structure of the SARS-CoV nsp12 polymerase bound to nsp7 and nsp8 co-factors. *Nature communications* **2019,** *10* (1), 2342.
341. Ferron, F.; Subissi, L.; Silveira De Morais, A. T.; Le, N. T. T.; Sevajol, M.; Gluais, L.; Decroly, E.; Vonrhein, C.; Bricogne, G.; Canard, B.; Imbert, I., Structural and molecular basis of mismatch correction and ribavirin excision from coronavirus RNA. *Proceedings of the National Academy of Sciences of the United States of America* **2017**.
342. Subissi, L.; Posthuma, C. C.; Collet, A.; Zevenhoven-Dobbe, J. C.; Gorbalenya, A. E.; Decroly, E.; Snijder, E. J.; Canard, B.; Imbert, I., One severe acute respiratory syndrome coronavirus protein complex integrates processive RNA polymerase and exonuclease activities. *Proceedings of the National Academy of Sciences of the United States of America* **2014,** *111* (37), E3900-9.
343. Poch, O.; Sauvaget, I.; Delarue, M.; Tordo, N., Identification of four conserved motifs among the RNA-dependent polymerase encoding elements. *EMBO J* **1989,** *8* (12), 3867-74.
344. Imbert, I.; Guillemot, J. C.; Bourhis, J. M.; Bussetta, C.; Coutard, B.; Egloff, M. P.; Ferron, F.; Gorbalenya, A. E.; Canard, B., A second, non-canonical RNA-dependent RNA polymerase in SARS coronavirus. *EMBO J* **2006,** *25* (20), 4933-42.
345. Mulangu, S.; Dodd, L. E.; Davey, R. T., Jr.; Tshiani Mbaya, O.; Proschan, M.; Mukadi, D.; Lusakibanza Manzo, M.; Nzolo, D.; Tshomba Oloma, A.; Ibanda, A.; Ali, R.; Coulibaly, S.; Levine, A. C.; Grais, R.; Diaz, J.; Lane, H. C.; Muyembe-Tamfum, J. J.; Sivahera, B.; Camara, M.; Kojan, R.; Walker, R.; Dighero-Kemp, B.; Cao, H.; Mukumbayi, P.; Mbala-Kingebeni, P.; Ahuka, S.; Albert, S.; Bonnett, T.; Crozier, I.; Duvenhage, M.; Proffitt, C.; Teitelbaum, M.; Moench, T.; Aboulhab, J.; Barrett, K.; Cahill, K.; Cone, K.; Eckes, R.; Hensley, L.; Herpin, B.; Higgs, E.; Ledgerwood, J.; Pierson, J.; Smolskis, M.; Sow, Y.; Tierney, J.; Sivapalasingam, S.; Holman, W.; Gettinger, N.; Vallee, D.; Nordwall, J., A Randomized, Controlled Trial of Ebola Virus Disease Therapeutics. *The New England journal of medicine* **2019,** *381* (24), 2293-2303.
346. de Wit, E.; Feldmann, F.; Cronin, J.; Jordan, R.; Okumura, A.; Thomas, T.; Scott, D.; Cihlar, T.; Feldmann, H., Prophylactic and therapeutic remdesivir (GS-5734) treatment in the rhesus macaque model of MERS-CoV infection. *Proceedings of the National Academy of Sciences* **2020**, 201922083.
347. de Wilde, A. H.; Jochmans, D.; Posthuma, C. C.; Zevenhoven-Dobbe, J. C.; van Nieuwkoop, S.; Bestebroer, T. M.; van den Hoogen, B. G.; Neyts, J.; Snijder, E. J., Screening of an FDA-approved compound library identifies four small-molecule inhibitors of Middle East respiratory syndrome coronavirus replication in cell culture. *Antimicrobial agents and chemotherapy* **2014,** *58* (8), 4875-84.
348. Arabi, Y. M.; Asiri, A. Y.; Assiri, A. M.; Aziz Jokhdar, H. A.; Alothman, A.; Balkhy, H. H.; AlJohani, S.; Al Harbi, S.; Kojan, S.; Al Jeraisy, M.; Deeb, A. M.; Memish, Z. A.; Ghazal, S.; Al Faraj, S.; Al-Hameed, F.; AlSaedi, A.; Mandourah, Y.; Al Mekhlafi, G. A.;

Sherbeeni, N. M.; Elzein, F. E.; Almotairi, A.; Al Bshabshe, A.; Kharaba, A.; Jose, J.; Al Harthy, A.; Al Sulaiman, M.; Mady, A.; Fowler, R. A.; Hayden, F. G.; Al-Dawood, A.; Abdelzaher, M.; Bajhmom, W.; Hussein, M. A., Treatment of Middle East respiratory syndrome with a combination of lopinavir/ritonavir and interferon-beta1b (MIRACLE trial): statistical analysis plan for a recursive two-stage group sequential randomized controlled trial. *Trials* **2020,** *21* (1), 8.
349. Zhu, N.; Zhang, D.; Wang, W.; Li, X.; Yang, B.; Song, J.; Zhao, X.; Huang, B.; Shi, W.; Lu, R.; Niu, P.; Zhan, F.; Ma, X.; Wang, D.; Xu, W.; Wu, G.; Gao, G. F.; Tan, W., A Novel Coronavirus from Patients with Pneumonia in China, 2019. *The New England journal of medicine* **2020,** *382* (8), 727-733.
350. WHO, World Health Organization: Coronavirus Disease 2019 (COVID-19) Situation Report-50, March 10. **2020,** (50).
351. Li, H.; Zhou, Y.; Zhang, M.; Wang, H.; Zhao, Q.; Liu, J., Updated approaches against SARS-CoV-2. *Antimicrobial agents and chemotherapy* **2020**.
352. Lo, M. K.; Feldmann, F.; Gary, J. M.; Jordan, R.; Bannister, R.; Cronin, J.; Patel, N. R.; Klena, J. D.; Nichol, S. T.; Cihlar, T.; Zaki, S. R.; Feldmann, H.; Spiropoulou, C. F.; de Wit, E., Remdesivir (GS-5734) protects African green monkeys from Nipah virus challenge. *Science translational medicine* **2019,** *11* (494).
353. Gordon, C. J.; Tchesnokov, E. P.; Feng, J. Y.; Porter, D. P.; Gotte, M., The antiviral compound remdesivir potently inhibits RNA-dependent RNA polymerase from Middle East respiratory syndrome coronavirus. *The Journal of biological chemistry* **2020**.
354. Stuyver, L. J.; McBrayer, T. R.; Whitaker, T.; Tharnish, P. M.; Ramesh, M.; Lostia, S.; Cartee, L.; Shi, J.; Hobbs, A.; Schinazi, R. F.; Watanabe, K. A.; Otto, M. J., Inhibition of the subgenomic hepatitis C virus replicon in huh-7 cells by 2'-deoxy-2'-fluorocytidine. *Antimicrobial agents and chemotherapy* **2004,** *48* (2), 651-4.
355. Welch, S. R.; Scholte, F. E. M.; Flint, M.; Chatterjee, P.; Nichol, S. T.; Bergeron, E.; Spiropoulou, C. F., Identification of 2'-deoxy-2'-fluorocytidine as a potent inhibitor of Crimean-Congo hemorrhagic fever virus replication using a recombinant fluorescent reporter virus. *Antiviral research* **2017,** *147*, 91-99.
356. Kumaki, Y.; Day, C. W.; Smee, D. F.; Morrey, J. D.; Barnard, D. L., In vitro and in vivo efficacy of fluorodeoxycytidine analogs against highly pathogenic avian influenza H5N1, seasonal, and pandemic H1N1 virus infections. *Antiviral research* **2011,** *92* (2), 329-40.
357. Welch, S. R.; Guerrero, L. W.; Chakrabarti, A. K.; McMullan, L. K.; Flint, M.; Bluemling, G. R.; Painter, G. R.; Nichol, S. T.; Spiropoulou, C. F.; Albarino, C. G., Lassa and Ebola virus inhibitors identified using minigenome and recombinant virus reporter systems. *Antiviral research* **2016,** *136*, 9-18.
358. Furuta, Y.; Komeno, T.; Nakamura, T., Favipiravir (T-705), a broad spectrum inhibitor of viral RNA polymerase. *Proceedings of the Japan Academy. Series B, Physical and biological sciences* **2017,** *93* (7), 449-463.
359. Hawman, D. W.; Haddock, E.; Meade-White, K.; Williamson, B.; Hanley, P. W.; Rosenke, K.; Komeno, T.; Furuta, Y.; Gowen, B. B.; Feldmann, H., Favipiravir (T-705) but not ribavirin is effective against two distinct strains of Crimean-Congo hemorrhagic fever virus in mice. *Antiviral research* **2018,** *157*, 18-26.
360. Oestereich, L.; Rieger, T.; Neumann, M.; Bernreuther, C.; Lehmann, M.; Krasemann, S.; Wurr, S.; Emmerich, P.; de Lamballerie, X.; Olschlager, S.; Gunther, S., Evaluation of

antiviral efficacy of ribavirin, arbidol, and T-705 (favipiravir) in a mouse model for Crimean-Congo hemorrhagic fever. *PLoS neglected tropical diseases* **2014,** *8* (5), e2804.
361. Zamyatkin, D. F.; Parra, F.; Alonso, J. M.; Harki, D. A.; Peterson, B. R.; Grochulski, P.; Ng, K. K., Structural insights into mechanisms of catalysis and inhibition in Norwalk virus polymerase. *The Journal of biological chemistry* **2008,** *283* (12), 7705-12.
362. Traut, T. W., Physiological concentrations of purines and pyrimidines. *Molecular and cellular biochemistry* **1994,** *140* (1), 1-22.
363. Kennedy, E. M.; Gavegnano, C.; Nguyen, L.; Slater, R.; Lucas, A.; Fromentin, E.; Schinazi, R. F.; Kim, B., Ribonucleoside triphosphates as substrate of human immunodeficiency virus type 1 reverse transcriptase in human macrophages. *The Journal of biological chemistry* **2010,** *285* (50), 39380-91.
364. Posthuma, C. C.; Te Velthuis, A. J. W.; Snijder, E. J., Nidovirus RNA polymerases: Complex enzymes handling exceptional RNA genomes. *Virus research* **2017,** *234*, 58-73.
365. Minskaia, E.; Hertzig, T.; Gorbalenya, A. E.; Campanacci, V.; Cambillau, C.; Canard, B.; Ziebuhr, J., Discovery of an RNA virus 3'->5' exoribonuclease that is critically involved in coronavirus RNA synthesis. *Proceedings of the National Academy of Sciences of the United States of America* **2006,** *103* (13), 5108-13.
366. Pruijssers, A. J.; Denison, M. R., Nucleoside analogues for the treatment of coronavirus infections. *Current opinion in virology* **2019,** *35*, 57-62.
367. Uebelhoer, L. S.; Albarino, C. G.; McMullan, L. K.; Chakrabarti, A. K.; Vincent, J. P.; Nichol, S. T.; Towner, J. S., High-throughput, luciferase-based reverse genetics systems for identifying inhibitors of Marburg and Ebola viruses. *Antiviral research* **2014,** *106*, 86-94.
368. Schinazi, R.; Halfon, P.; Marcellin, P.; Asselah, T., HCV direct-acting antiviral agents: the best interferon-free combinations. *Liver international : official journal of the International Association for the Study of the Liver* **2014,** *34 Suppl 1*, 69-78.
369. Feld, J. J.; Hoofnagle, J. H., Mechanism of action of interferon and ribavirin in treatment of hepatitis C. *Nature* **2005,** *436* (7053), 967-72.
370. https://www.fda.gov/media/137566/download, Food and Drug Administration: Fact Sheet for Health Care Providers Eergency Use Authorization (EUA) of Veklury® (remdesivir). 2020.
371. Wang, Y.; Zhang, D.; Du, G.; Du, R.; Zhao, J.; Jin, Y.; Fu, S.; Gao, L.; Cheng, Z.; Lu, Q.; Hu, Y.; Luo, G.; Wang, K.; Lu, Y.; Li, H.; Wang, S.; Ruan, S.; Yang, C.; Mei, C.; Wang, Y.; Ding, D.; Wu, F.; Tang, X.; Ye, X.; Ye, Y.; Liu, B.; Yang, J.; Yin, W.; Wang, A.; Fan, G.; Zhou, F.; Liu, Z.; Gu, X.; Xu, J.; Shang, L.; Zhang, Y.; Cao, L.; Guo, T.; Wan, Y.; Qin, H.; Jiang, Y.; Jaki, T.; Hayden, F. G.; Horby, P. W.; Cao, B.; Wang, C., Remdesivir in adults with severe COVID-19: a randomised, double-blind, placebo-controlled, multicentre trial. *Lancet* **2020,** *395* (10236), 1569-1578.
372. de Wit, E.; Feldmann, F.; Cronin, J.; Jordan, R.; Okumura, A.; Thomas, T.; Scott, D.; Cihlar, T.; Feldmann, H., Prophylactic and therapeutic remdesivir (GS-5734) treatment in the rhesus macaque model of MERS-CoV infection. *Proc Natl Acad Sci U S A* **2020,** *117* (12), 6771-6776.
373. Wang, Q.; Wu, J.; Wang, H.; Gao, Y.; Liu, Q.; Mu, A.; Ji, W.; Yan, L.; Zhu, Y.; Zhu, C.; Fang, X.; Yang, X.; Huang, Y.; Gao, H.; Liu, F.; Ge, J.; Sun, Q.; Xu, W.; Liu, Z.; Yang, H.; Lou, Z.; Jiang, B.; Guddat, L. W.; Gong, P.; Rao, Z., Structural Basis for RNA Replication by the SARS-CoV-2 Polymerase. *Cell* **2020,** *182* (2), 417-428 e13.

374. Wiersinga, W. J.; Rhodes, A.; Cheng, A. C.; Peacock, S. J.; Prescott, H. C., Pathophysiology, Transmission, Diagnosis, and Treatment of Coronavirus Disease 2019 (COVID-19): A Review. *JAMA* **2020**.
375. Seifert, M.; Bera, S. C.; van Nies, P.; Kirchdoerfer, R. N.; Shannon, A.; Le, T.-T.-N.; Grove, T. L.; Papini, F. S.; Arnold, J. J.; Almo, S. C.; Canard, B.; Depken, M.; Cameron, C. E.; Dulin, D., Signatures and mechanisms of efficacious therapeutic ribonucleotides against SARS-CoV-2 revealed by analysis of its replicase using magnetic tweezers. *bioRxiv* **2020**, 2020.08.06.240325.
376. U.S. Food and Drug Administration. (2020) *Fact sheet for health care providers Emergency Use Authorization (EUA) of remdesivir (GS-5734™)*, Food and Drug Administration, Silver Spring, MD. https://www.fda.gov/media/137566/download.
377. U.S. Food and Drug Administration. (2020) *Fact sheet for health care providers Emergency Use Authorization (EUA) of Casirivimab and Imdevimab*, Food and Drug Administration, Silver Spring, MD. https://www.fda.gov/media/143892/download.
378. Vasudevan, N.; Ahlqvist, G. P.; McGeough, C. P.; Paymode, D. J.; Cardoso, F. S. P.; Lucas, T.; Dietz, J. P.; Opatz, T.; Jamison, T. F.; Gupton, F. B.; Snead, D. R., A concise route to MK-4482 (EIDD-2801) from cytidine. *Chem Commun (Camb)* **2020,** *56* (87), 13363-13364.
379. Costantini, V. P.; Whitaker, T.; Barclay, L.; Lee, D.; McBrayer, T. R.; Schinazi, R. F.; Vinje, J., Antiviral activity of nucleoside analogues against norovirus. *Antivir Ther* **2012,** *17* (6), 981-91.
380. Reynard, O.; Nguyen, X. N.; Alazard-Dany, N.; Barateau, V.; Cimarelli, A.; Volchkov, V. E., Identification of a New Ribonucleoside Inhibitor of Ebola Virus Replication. *Viruses* **2015,** *7* (12), 6233-40.
381. Urakova, N.; Kuznetsova, V.; Crossman, D. K.; Sokratian, A.; Guthrie, D. B.; Kolykhalov, A. A.; Lockwood, M. A.; Natchus, M. G.; Crowley, M. R.; Painter, G. R.; Frolova, E. I.; Frolov, I., beta-d-N (4)-Hydroxycytidine Is a Potent Anti-alphavirus Compound That Induces a High Level of Mutations in the Viral Genome. *Journal of virology* **2018,** *92* (3).
382. Agostini, M. L.; Pruijssers, A. J.; Chappell, J. D.; Gribble, J.; Lu, X.; Andres, E. L.; Bluemling, G. R.; Lockwood, M. A.; Sheahan, T. P.; Sims, A. C.; Natchus, M. G.; Saindane, M.; Kolykhalov, A. A.; Painter, G. R.; Baric, R. S.; Denison, M. R., Small-Molecule Antiviral beta-d-N (4)-Hydroxycytidine Inhibits a Proofreading-Intact Coronavirus with a High Genetic Barrier to Resistance. *Journal of virology* **2019,** *93* (24).
383. Rosenke, K.; Hansen, F.; Schwarz, B.; Feldmann, F.; Haddock, E.; Rosenke, R.; Barbian, K.; Meade-White, K.; Okumura, A.; Leventhal, S.; Hawman, D. W.; Ricotta, E.; Bosio, C. M.; Martens, C.; Saturday, G.; Feldmann, H.; Jarvis, M. A., Orally delivered MK-4482 inhibits SARS-CoV-2 replication in the Syrian hamster model. *Nature communications* **2021,** *12* (1), 2295.
384. Cox, R. M.; Wolf, J. D.; Plemper, R. K., Therapeutically administered ribonucleoside analogue MK-4482/EIDD-2801 blocks SARS-CoV-2 transmission in ferrets. *Nat Microbiol* **2021,** *6* (1), 11-18.
385. Wahl, A.; Gralinski, L. E.; Johnson, C. E.; Yao, W.; Kovarova, M.; Dinnon, K. H., 3rd; Liu, H.; Madden, V. J.; Krzystek, H. M.; De, C.; White, K. K.; Gully, K.; Schafer, A.; Zaman, T.; Leist, S. R.; Grant, P. O.; Bluemling, G. R.; Kolykhalov, A. A.; Natchus, M. G.; Askin, F. B.; Painter, G.; Browne, E. P.; Jones, C. D.; Pickles, R. J.; Baric, R. S.; Garcia, J. V., SARS-CoV-2 infection is effectively treated and prevented by EIDD-2801. *Nature* **2021,** *591* (7850), 451-457.

386. Sledziewska, E.; Janion, C., Mutagenic specificity of N4-hydroxycytidine. *Mutat Res* **1980,** *70* (1), 11-6.
387. Janion, C.; Glickman, B. W., N-4-Hydroxycytidine - a Mutagen Specific for at to Gc Transitions. *Mutation Research* **1980,** *72* (1), 43-47.
388. Hernandez-Santiago, B. I.; Beltran, T.; Stuyver, L.; Chu, C. K.; Schinazi, R. F., Metabolism of the anti-hepatitis C virus nucleoside beta-D-N4-hydroxycytidine in different liver cells. *Antimicrobial agents and chemotherapy* **2004,** *48* (12), 4636-42.
389. Janion, C., On the different response of Salmonella typhimurium hisG46 and TA1530 to mutagenic action of base analogues. *Acta Biochim Pol* **1979,** *26* (1-2), 171-7.
390. Painter, W. P.; Holman, W.; Bush, J. A.; Almazedi, F.; Malik, H.; Eraut, N.; Morin, M. J.; Szewczyk, L. J.; Painter, G. R., Human Safety, Tolerability, and Pharmacokinetics of Molnupiravir, a Novel Broad-Spectrum Oral Antiviral Agent with Activity Against SARS-CoV-2. *Antimicrobial agents and chemotherapy* **2021**.
391. Tchesnokov, E. P.; Bailey-Elkin, B. A.; Mark, B. L.; Gotte, M., Independent inhibition of the polymerase and deubiquitinase activities of the Crimean-Congo Hemorrhagic Fever Virus full-length L-protein. *PLoS neglected tropical diseases* **2020,** *14* (6), e0008283.
392. Tvarogova, J.; Madhugiri, R.; Bylapudi, G.; Ferguson, L. J.; Karl, N.; Ziebuhr, J., Identification and Characterization of a Human Coronavirus 229E Nonstructural Protein 8-Associated RNA 3'-Terminal Adenylyltransferase Activity. *J Virol* **2019,** *93* (12).
393. Zhu, N.; Zhang, D.; Wang, W.; Li, X.; Yang, B.; Song, J.; Zhao, X.; Huang, B.; Shi, W.; Lu, R.; Niu, P.; Zhan, F.; Ma, X.; Wang, D.; Xu, W.; Wu, G.; Gao, G. F.; Tan, W.; China Novel Coronavirus, I.; Research, T., A Novel Coronavirus from Patients with Pneumonia in China, 2019. *The New England journal of medicine* **2020,** *382* (8), 727-733.
394. Baden, L. R.; El Sahly, H. M.; Essink, B.; Kotloff, K.; Frey, S.; Novak, R.; Diemert, D.; Spector, S. A.; Rouphael, N.; Creech, C. B.; McGettigan, J.; Khetan, S.; Segall, N.; Solis, J.; Brosz, A.; Fierro, C.; Schwartz, H.; Neuzil, K.; Corey, L.; Gilbert, P.; Janes, H.; Follmann, D.; Marovich, M.; Mascola, J.; Polakowski, L.; Ledgerwood, J.; Graham, B. S.; Bennett, H.; Pajon, R.; Knightly, C.; Leav, B.; Deng, W.; Zhou, H.; Han, S.; Ivarsson, M.; Miller, J.; Zaks, T.; Group, C. S., Efficacy and Safety of the mRNA-1273 SARS-CoV-2 Vaccine. *The New England journal of medicine* **2021,** *384* (5), 403-416.
395. Polack, F. P.; Thomas, S. J.; Kitchin, N.; Absalon, J.; Gurtman, A.; Lockhart, S.; Perez, J. L.; Perez Marc, G.; Moreira, E. D.; Zerbini, C.; Bailey, R.; Swanson, K. A.; Roychoudhury, S.; Koury, K.; Li, P.; Kalina, W. V.; Cooper, D.; Frenck, R. W., Jr.; Hammitt, L. L.; Tureci, O.; Nell, H.; Schaefer, A.; Unal, S.; Tresnan, D. B.; Mather, S.; Dormitzer, P. R.; Sahin, U.; Jansen, K. U.; Gruber, W. C.; Group, C. C. T., Safety and Efficacy of the BNT162b2 mRNA Covid-19 Vaccine. *The New England journal of medicine* **2020,** *383* (27), 2603-2615.
396. Voysey, M.; Clemens, S. A. C.; Madhi, S. A.; Weckx, L. Y.; Folegatti, P. M.; Aley, P. K.; Angus, B.; Baillie, V. L.; Barnabas, S. L.; Bhorat, Q. E.; Bibi, S.; Briner, C.; Cicconi, P.; Collins, A. M.; Colin-Jones, R.; Cutland, C. L.; Darton, T. C.; Dheda, K.; Duncan, C. J. A.; Emary, K. R. W.; Ewer, K. J.; Fairlie, L.; Faust, S. N.; Feng, S.; Ferreira, D. M.; Finn, A.; Goodman, A. L.; Green, C. M.; Green, C. A.; Heath, P. T.; Hill, C.; Hill, H.; Hirsch, I.; Hodgson, S. H. C.; Izu, A.; Jackson, S.; Jenkin, D.; Joe, C. C. D.; Kerridge, S.; Koen, A.; Kwatra, G.; Lazarus, R.; Lawrie, A. M.; Lelliott, A.; Libri, V.; Lillie, P. J.; Mallory, R.; Mendes, A. V. A.; Milan, E. P.; Minassian, A. M.; McGregor, A.; Morrison, H.; Mujadidi, Y. F.; Nana, A.; O'Reilly, P. J.; Padayachee, S. D.; Pittella, A.; Plested, E.; Pollock, K. M.; Ramasamy, M. N.; Rhead, S.; Schwarzbold, A. V.; Singh, N.; Smith, A.; Song, R.; Snape, M.

D.; Sprinz, E.; Sutherland, R. K.; Tarrant, R.; Thomson, E. C.; Torok, M. E.; Toshner, M.; Turner, D. P. J.; Vekemans, J.; Villafana, T. L.; Watson, M. E. E.; Williams, C. J.; Douglas, A. D.; Hill, A. V. S.; Lambe, T.; Gilbert, S. C.; Pollard, A. J.; Oxford, C. V. T. G., Safety and efficacy of the ChAdOx1 nCoV-19 vaccine (AZD1222) against SARS-CoV-2: an interim analysis of four randomised controlled trials in Brazil, South Africa, and the UK. *Lancet* **2021,** *397* (10269), 99-111.
397. Sadoff, J.; Le Gars, M.; Shukarev, G.; Heerwegh, D.; Truyers, C.; de Groot, A. M.; Stoop, J.; Tete, S.; Van Damme, W.; Leroux-Roels, I.; Berghmans, P. J.; Kimmel, M.; Van Damme, P.; de Hoon, J.; Smith, W.; Stephenson, K. E.; De Rosa, S. C.; Cohen, K. W.; McElrath, M. J.; Cormier, E.; Scheper, G.; Barouch, D. H.; Hendriks, J.; Struyf, F.; Douoguih, M.; Van Hoof, J.; Schuitemaker, H., Interim Results of a Phase 1-2a Trial of Ad26.COV2.S Covid-19 Vaccine. *The New England journal of medicine* **2021,** *384* (19), 1824-1835.
398. Food, U.; Administration, D., Fact sheet for health care providers. Emergency Use Authorization (EUA) of Veklury (remdesivir). *Food and Drug Administration, Silver Spring, MD* **2020**, 1-20.
399. Grein, J.; Ohmagari, N.; Shin, D.; Diaz, G.; Asperges, E.; Castagna, A.; Feldt, T.; Green, G.; Green, M. L.; Lescure, F.-X.; Nicastri, E.; Oda, R.; Yo, K.; Quiros-Roldan, E.; Studemeister, A.; Redinski, J.; Ahmed, S.; Bernett, J.; Chelliah, D.; Chen, D.; Chihara, S.; Cohen, S. H.; Cunningham, J.; D'Arminio Monforte, A.; Ismail, S.; Kato, H.; Lapadula, G.; L'Her, E.; Maeno, T.; Majumder, S.; Massari, M.; Mora-Rillo, M.; Mutoh, Y.; Nguyen, D.; Verweij, E.; Zoufaly, A.; Osinusi, A. O.; DeZure, A.; Zhao, Y.; Zhong, L.; Chokkalingam, A.; Elboudwarej, E.; Telep, L.; Timbs, L.; Henne, I.; Sellers, S.; Cao, H.; Tan, S. K.; Winterbourne, L.; Desai, P.; Mera, R.; Gaggar, A.; Myers, R. P.; Brainard, D. M.; Childs, R.; Flanigan, T., Compassionate Use of Remdesivir for Patients with Severe Covid-19. *New England Journal of Medicine* **2020,** *382* (24), 2327-2336.
400. Beigel, J. H.; Tomashek, K. M.; Dodd, L. E.; Mehta, A. K.; Zingman, B. S.; Kalil, A. C.; Hohmann, E.; Chu, H. Y.; Luetkemeyer, A.; Kline, S.; Lopez de Castilla, D.; Finberg, R. W.; Dierberg, K.; Tapson, V.; Hsieh, L.; Patterson, T. F.; Paredes, R.; Sweeney, D. A.; Short, W. R.; Touloumi, G.; Lye, D. C.; Ohmagari, N.; Oh, M. D.; Ruiz-Palacios, G. M.; Benfield, T.; Fatkenheuer, G.; Kortepeter, M. G.; Atmar, R. L.; Creech, C. B.; Lundgren, J.; Babiker, A. G.; Pett, S.; Neaton, J. D.; Burgess, T. H.; Bonnett, T.; Green, M.; Makowski, M.; Osinusi, A.; Nayak, S.; Lane, H. C.; Members, A.-S. G., Remdesivir for the Treatment of Covid-19 - Final Report. *The New England journal of medicine* **2020,** *383* (19), 1813-1826.
401. Consortium, W. S. T., Repurposed antiviral drugs for COVID-19—interim WHO SOLIDARITY trial results. *New England journal of medicine* **2021,** *384* (6), 497-511.
402. Boyer, P. L.; Julias, J. G.; Marquez, V. E.; Hughes, S. H., Fixed conformation nucleoside analogs effectively inhibit excision-proficient HIV-1 reverse transcriptases. *J Mol Biol* **2005,** *345* (3), 441-50.
403. Boyer, P. L.; Julias, J. G.; Ambrose, Z.; Siddiqui, M. A.; Marquez, V. E.; Hughes, S. H., The nucleoside analogs 4'C-methyl thymidine and 4'C-ethyl thymidine block DNA synthesis by wild-type HIV-1 RT and excision proficient NRTI resistant RT variants. *J Mol Biol* **2007,** *371* (4), 873-82.
404. Langley, D. R.; Walsh, A. W.; Baldick, C. J.; Eggers, B. J.; Rose, R. E.; Levine, S. M.; Kapur, A. J.; Colonno, R. J.; Tenney, D. J., Inhibition of hepatitis B virus polymerase by entecavir. *J Virol* **2007,** *81* (8), 3992-4001.

405. Deval, J., Antimicrobial strategies: inhibition of viral polymerases by 3'-hydroxyl nucleosides. *Drugs* **2009,** *69* (2), 151-66.
406. Michailidis, E.; Huber, A. D.; Ryan, E. M.; Ong, Y. T.; Leslie, M. D.; Matzek, K. B.; Singh, K.; Marchand, B.; Hagedorn, A. N.; Kirby, K. A.; Rohan, L. C.; Kodama, E. N.; Mitsuya, H.; Parniak, M. A.; Sarafianos, S. G., 4'-Ethynyl-2-fluoro-2'-deoxyadenosine (EFdA) inhibits HIV-1 reverse transcriptase with multiple mechanisms. *The Journal of biological chemistry* **2014,** *289* (35), 24533-48.
407. Chen, H.; Lawler, J. L.; Filman, D. J.; Hogle, J. M.; Coen, D. M., Resistance to a Nucleoside Analog Antiviral Drug from More Rapid Extension of Drug-Containing Primers. *mBio* **2021,** *12* (1).
408. Lu, G.; Zhang, X.; Zheng, W.; Sun, J.; Hua, L.; Xu, L.; Chu, X. J.; Ding, S.; Xiong, W., Development of a Simple In Vitro Assay To Identify and Evaluate Nucleotide Analogs against SARS-CoV-2 RNA-Dependent RNA Polymerase. *Antimicrobial agents and chemotherapy* **2020,** *65* (1).
409. Wang, J.; Reiss, K.; Shi, Y.; Lolis, E.; Lisi, G. P.; Batista, V. S., Mechanism of Inhibition of the Reproduction of SARS-CoV-2 and Ebola Viruses by Remdesivir. *Biochemistry* **2021,** *60* (24), 1869-1875.
410. Young, T.; Abel, R.; Kim, B.; Berne, B. J.; Friesner, R. A., Motifs for molecular recognition exploiting hydrophobic enclosure in protein-ligand binding. *Proceedings of the National Academy of Sciences of the United States of America* **2007,** *104* (3), 808-13.
411. Abel, R.; Young, T.; Farid, R.; Berne, B. J.; Friesner, R. A., Role of the active-site solvent in the thermodynamics of factor Xa ligand binding. *J Am Chem Soc* **2008,** *130* (9), 2817-31.
412. Romero, J. R.; Newland, J. G., Viral meningitis and encephalitis: traditional and emerging viral agents. *Semin Pediatr Infect Dis* **2003,** *14* (2), 72-82.
413. Royston, L.; Tapparel, C., Rhinoviruses and Respiratory Enteroviruses: Not as Simple as ABC. *Viruses* **2016,** *8* (1).
414. Wang, X.; Li, Y.; Deloria-Knoll, M.; Madhi, S. A.; Cohen, C.; Arguelles, V. L.; Basnet, S.; Bassat, Q.; Brooks, W. A.; Echavarria, M.; Fasce, R. A.; Gentile, A.; Goswami, D.; Homaira, N.; Howie, S. R. C.; Kotloff, K. L.; Khuri-Bulos, N.; Krishnan, A.; Lucero, M. G.; Lupisan, S.; Mathisen, M.; McLean, K. A.; Mira-Iglesias, A.; Moraleda, C.; Okamoto, M.; Oshitani, H.; O'Brien, K. L.; Owor, B. E.; Rasmussen, Z. A.; Rath, B. A.; Salimi, V.; Sawatwong, P.; Scott, J. A. G.; Simoes, E. A. F.; Sotomayor, V.; Thea, D. M.; Treurnicht, F. K.; Yoshida, L. M.; Zar, H. J.; Campbell, H.; Nair, H.; Respiratory Virus Global Epidemiology, N., Global burden of acute lower respiratory infection associated with human parainfluenza virus in children younger than 5 years for 2018: a systematic review and meta-analysis. *Lancet Glob Health* **2021,** *9* (8), e1077-e1087.
415. Wang, X.; Li, Y.; Deloria-Knoll, M.; Madhi, S. A.; Cohen, C.; Ali, A.; Basnet, S.; Bassat, Q.; Brooks, W. A.; Chittaganpitch, M.; Echavarria, M.; Fasce, R. A.; Goswami, D.; Hirve, S.; Homaira, N.; Howie, S. R. C.; Kotloff, K. L.; Khuri-Bulos, N.; Krishnan, A.; Lucero, M. G.; Lupisan, S.; Mira-Iglesias, A.; Moore, D. P.; Moraleda, C.; Nunes, M.; Oshitani, H.; Owor, B. E.; Polack, F. P.; O'Brien, K. L.; Rasmussen, Z. A.; Rath, B. A.; Salimi, V.; Scott, J. A. G.; Simoes, E. A. F.; Strand, T. A.; Thea, D. M.; Treurnicht, F. K.; Vaccari, L. C.; Yoshida, L. M.; Zar, H. J.; Campbell, H.; Nair, H.; Respiratory Virus Global Epidemiology, N., Global burden of acute lower respiratory infection associated with human metapneumovirus in children under 5 years in 2018: a systematic review and modelling study. *Lancet Glob Health* **2021,** *9* (1), e33-e43.

416. Collaborators, G. B. D. I., Mortality, morbidity, and hospitalisations due to influenza lower respiratory tract infections, 2017: an analysis for the Global Burden of Disease Study 2017. *Lancet Respir Med* **2019,** *7* (1), 69-89.
417. [preprint]; Siegel, D. S.; Hui, H. C.; Pitts, J.; Vermillion, M. S.; Ishida, K.; Rautiola, D.; Keeney, M.; Irshad, H.; Zhang, L.; Chun, K.; Chin, G.; Goyal, B.; Doerffler, E.; Yang, H.; Clarke, M. O.; Palmiotti, C.; Vijjapurapu, A.; Riola, N. C.; Stray, K.; Murakami, E.; Ma, B.; Wang, T.; Zhao, X.; Xu, Y.; Lee, G.; Marchand, B.; Seung, M.; Nayak, A.; Tomkinson, A.; Kadrichu, N.; Ellis, S.; Barauskas, O.; Feng, J. Y.; Perry, J. K.; Perron, M.; Bilello, J.; Kuehl, P. J.; Subramanian, R.; Cihlar, T.; Mackman, R. L., Discovery and Synthesis of GS-7682, a Novel Prodrug of a 4'-CN-4-Aza-7,9-Dideazaadenosine C-Nucleoside with Broad-Spectrum Potency Against Pneumo- and Picornaviruses and Efficacy in RSV-Infected African Green Monkeys. *bioRxiv* **2024**, 2024.04.17.589937.
418. Schwinghammer, K.; Cheung, A. C.; Morozov, Y. I.; Agaronyan, K.; Temiakov, D.; Cramer, P., Structure of human mitochondrial RNA polymerase elongation complex. *Nat Struct Mol Biol* **2013,** *20* (11), 1298-303.
419. Peersen, O. B., A Comprehensive Superposition of Viral Polymerase Structures. *Viruses* **2019,** *11* (8).
420. Michailidis, E.; Marchand, B.; Kodama, E. N.; Singh, K.; Matsuoka, M.; Kirby, K. A.; Ryan, E. M.; Sawani, A. M.; Nagy, E.; Ashida, N.; Mitsuya, H.; Parniak, M. A.; Sarafianos, S. G., Mechanism of inhibition of HIV-1 reverse transcriptase by 4'-Ethynyl-2-fluoro-2'-deoxyadenosine triphosphate, a translocation-defective reverse transcriptase inhibitor. *The Journal of biological chemistry* **2009,** *284* (51), 35681-91.
421. Salie, Z. L.; Kirby, K. A.; Michailidis, E.; Marchand, B.; Singh, K.; Rohan, L. C.; Kodama, E. N.; Mitsuya, H.; Parniak, M. A.; Sarafianos, S. G., Structural basis of HIV inhibition by translocation-defective RT inhibitor 4'-ethynyl-2-fluoro-2'-deoxyadenosine (EFdA). *Proceedings of the National Academy of Sciences of the United States of America* **2016,** *113* (33), 9274-9.
422. Jordan, P. C.; Stevens, S. K.; Deval, J., Nucleosides for the treatment of respiratory RNA virus infections. *Antivir Chem Chemother* **2018,** *26*, 2040206618764483.
423. Biteau, N. G.; Amichai, S. A.; Azadi, N.; De, R.; Downs-Bowen, J.; Lecher, J. C.; MacBrayer, T.; Schinazi, R. F.; Amblard, F., Synthesis of 4'-Substituted Carbocyclic Uracil Derivatives and Their Monophosphate Prodrugs as Potential Antiviral Agents. *Viruses* **2023,** *15* (2).
424. Wang, G.; Dyatkina, N.; Prhavc, M.; Williams, C.; Serebryany, V.; Hu, Y.; Huang, Y.; Wan, J.; Wu, X.; Deval, J.; Fung, A.; Jin, Z.; Tan, H.; Shaw, K.; Kang, H.; Zhang, Q.; Tam, Y.; Stoycheva, A.; Jekle, A.; Smith, D. B.; Beigelman, L., Synthesis and Anti-HCV Activities of 4'-Fluoro-2'-Substituted Uridine Triphosphates and Nucleotide Prodrugs: Discovery of 4'-Fluoro-2'- C-methyluridine 5'-Phosphoramidate Prodrug (AL-335) for the Treatment of Hepatitis C Infection. *Journal of medicinal chemistry* **2019,** *62* (9), 4555-4570.
425. Takamatsu, Y.; Tanaka, Y.; Kohgo, S.; Murakami, S.; Singh, K.; Das, D.; Venzon, D. J.; Amano, M.; Higashi-Kuwata, N.; Aoki, M.; Delino, N. S.; Hayashi, S.; Takahashi, S.; Sukenaga, Y.; Haraguchi, K.; Sarafianos, S. G.; Maeda, K.; Mitsuya, H., 4'-modified nucleoside analogs: potent inhibitors active against entecavir-resistant hepatitis B virus. *Hepatology* **2015,** *62* (4), 1024-36.
426. Gottlieb, R. L.; Vaca, C. E.; Paredes, R.; Mera, J.; Webb, B. J.; Perez, G.; Oguchi, G.; Ryan, P.; Nielsen, B. U.; Brown, M.; Hidalgo, A.; Sachdeva, Y.; Mittal, S.; Osiyemi, O.;

Skarbinski, J.; Juneja, K.; Hyland, R. H.; Osinusi, A.; Chen, S.; Camus, G.; Abdelghany, M.; Davies, S.; Behenna-Renton, N.; Duff, F.; Marty, F. M.; Katz, M. J.; Ginde, A. A.; Brown, S. M.; Schiffer, J. T.; Hill, J. A.; Investigators, G.-U.-. Early Remdesivir to Prevent Progression to Severe Covid-19 in Outpatients. *The New England journal of medicine* **2022,** *386* (4), 305-315.
427. Ikematsu, H.; Hayden, F. G.; Kawaguchi, K.; Kinoshita, M.; de Jong, M. D.; Lee, N.; Takashima, S.; Noshi, T.; Tsuchiya, K.; Uehara, T., Baloxavir Marboxil for Prophylaxis against Influenza in Household Contacts. *The New England journal of medicine* **2020,** *383* (4), 309-320.
428. Hayden, F. G.; Sugaya, N.; Hirotsu, N.; Lee, N.; de Jong, M. D.; Hurt, A. C.; Ishida, T.; Sekino, H.; Yamada, K.; Portsmouth, S.; Kawaguchi, K.; Shishido, T.; Arai, M.; Tsuchiya, K.; Uehara, T.; Watanabe, A.; Baloxavir Marboxil Investigators, G., Baloxavir Marboxil for Uncomplicated Influenza in Adults and Adolescents. *The New England journal of medicine* **2018,** *379* (10), 913-923.
429. Eggleton, J. S.; Nagalli, S., Highly Active Antiretroviral Therapy (HAART). In *StatPearls*, Treasure Island (FL) ineligible companies. Disclosure: Shivaraj Nagalli declares no relevant financial relationships with ineligible companies., 2024.
430. Adedeji, A. O.; Marchand, B.; Te Velthuis, A. J.; Snijder, E. J.; Weiss, S.; Eoff, R. L.; Singh, K.; Sarafianos, S. G., Mechanism of nucleic acid unwinding by SARS-CoV helicase. *PloS one* **2012,** *7* (5), e36521.
431. Jia, Z.; Yan, L.; Ren, Z.; Wu, L.; Wang, J.; Guo, J.; Zheng, L.; Ming, Z.; Zhang, L.; Lou, Z.; Rao, Z., Delicate structural coordination of the Severe Acute Respiratory Syndrome coronavirus Nsp13 upon ATP hydrolysis. *Nucleic Acids Res* **2019,** *47* (12), 6538-6550.
432. Sommers, J. A.; Loftus, L. N.; Jones, M. P., 3rd; Lee, R. A.; Haren, C. E.; Dumm, A. J.; Brosh, R. M., Jr., Biochemical analysis of SARS-CoV-2 Nsp13 helicase implicated in COVID-19 and factors that regulate its catalytic functions. *The Journal of biological chemistry* **2023,** *299* (3), 102980.
433. Wang, M.; Wu, C.; Liu, N.; Zhang, F.; Dong, H.; Wang, S.; Chen, M.; Jiang, X.; Zhang, K.; Gu, L., SARS-CoV-2 RdRp uses NDPs as a substrate and is able to incorporate NHC into RNA from diphosphate form molnupiravir. *Int J Biol Macromol* **2023,** *226*, 946-955.

Appendices

## Appendix A: Supporting information for Chapter 4

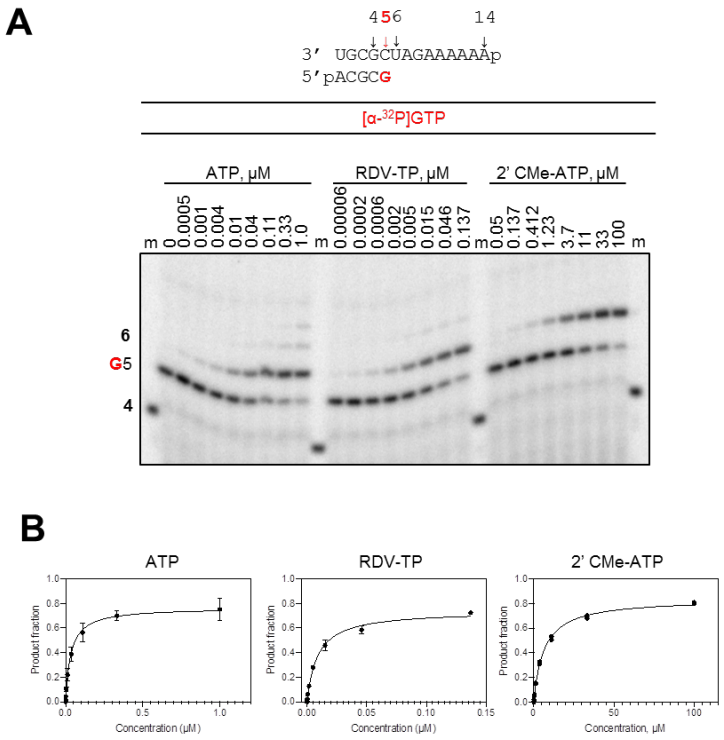


**Figure A1. Selective incorporation of ATP analogs**. ***A***, RNA primer/template substrate used in the RNA synthesis assays to test RDV-TP and 2'CMe-ATP as substrates for incorporation as ATP -analogs is shown above the gel. G indicates incorporation of the radiolabeled nucleotide opposite template position 5. Position i allows incorporation of ATP or ATP analogs. NTP incorporation was monitored with purified SARS-CoV-2 RdRp complex in the presence of [α-$^{32}$P]GTP, RNA primer/template, $MgCl_2$ and increasing concentrations of ATP and ATP substrate analogs. Lane m illustrates the migration pattern of the radiolabeled 4 nucleotide-long primer. ***B***, Graphic representation of the data for incorporation of ATP and ATP-analogs. Error bars represent standard deviation of the data within at least three independent experiments.

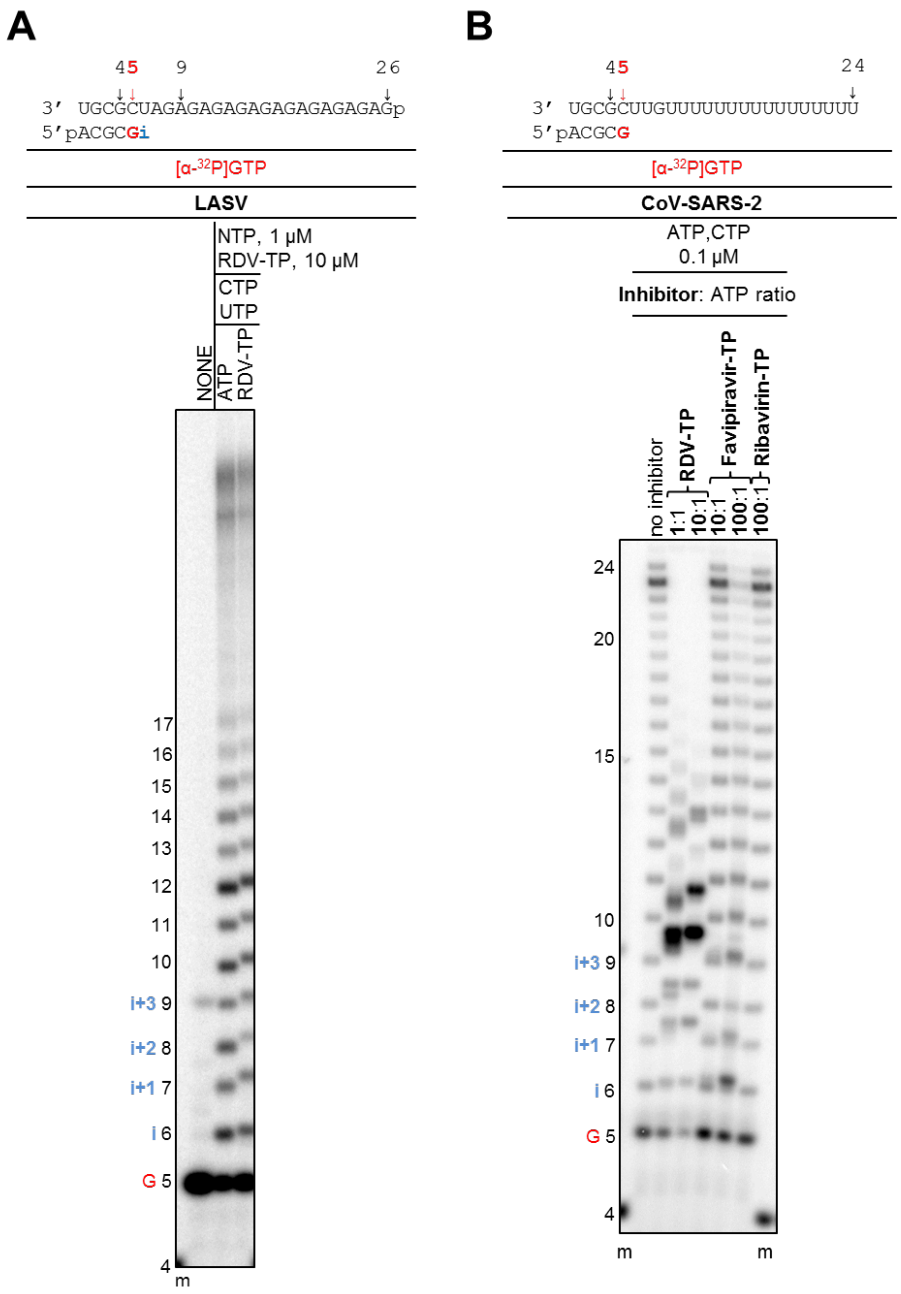


**Figure A2: Patterns of inhibition of RNA synthesis by LASV and CoV-SARS-2 RdRp**. ***A***, The RNA primer/template used in this experiment is shown above the gel. A single incorporation event of RDV-TP is supported by this template. G indicates incorporation of the radiolabeled nucleotide opposite template position 5. RDV-TP incorporation is indicated by "i". RDV-TP incorporation was monitored with purified LASV RdRp in the presence of indicated combinations of NTPs and RDV-TP. ***B***, Multiple incorporations RDV-TP are supported by this template. G indicates incorporation of the radiolabeled nucleotide opposite template position 5. The first RDV-TP incorporation is indicated by "i". RDV-TP incorporation was monitored with purified SARS-CoV-2 RdRp in the presence of indicated combinations of NTPs, RDV-TP or favipiravir-TP and ribavirin-TP, respectively.

*EPT contributed to this figure.

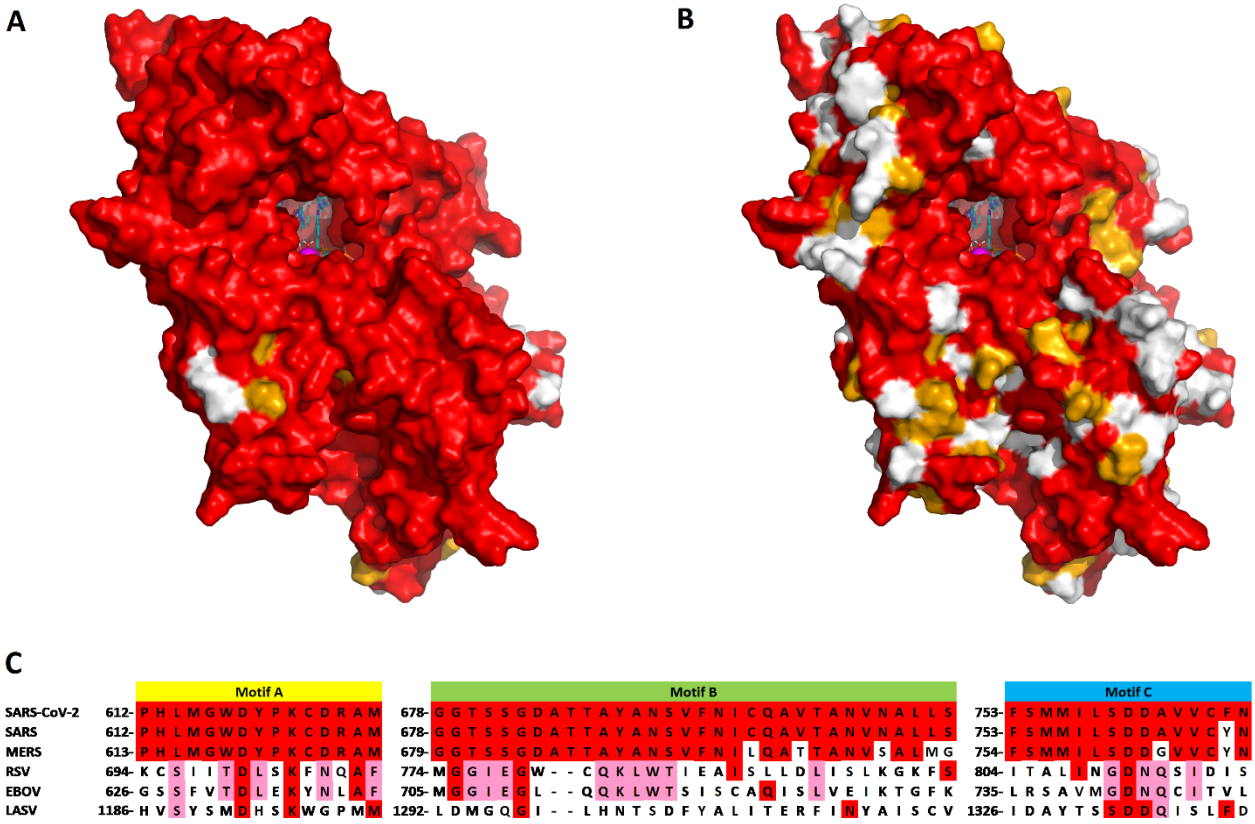


**Figure A3. The nsp12 active site is well conserved between SARS-CoV-2 and (*A*) SARS-CoV and (*B*) MERS**. Residues shown in red are identical, yellow similar and white dissimilar. The active site is visible near the center of each image. C, The active site of other polymerases, while maintaining the same basic structure defined by motifs A, B and C, is only conserved at key residues (highlighted in red). RSV and EBOV are similar in the nature of their active sites (highlighted in pink), while LASV is different from both CoV and RSV-like structures in key aspects.

*JKP contributed this figure.

## Appendix B: Supporting information for Chapter 5

Table B1. UTP and ATP relative efficiency of incorporation opposite or after remdesivir in the template, respectively, catalyzed by SARS-CoV-2 WT and V557L mutant RdRp complexes.

| Incorporation opposite RDV in the template | | |
|---|---|---|
| | | UTP |
| wild type | $V_{max}$ [a] (product fraction) | 0.76[d] ±0.010[e] |
| | $K_m$ [b], μM | 3.6 ±0.24 |
| | $V_{max}/K_m$ [c] | 0.21 |
| | | |
| V557L | $V_{max}$ (product fraction) | 0.67 ±0.019 |
| | $K_m$, μM | 0.64 ±0.13 |
| | $V_{max}/K_m$ | 1.0 |
| | $\frac{\mathbf{V557L}\ (\frac{V_{max}}{K_m})}{\mathbf{wild\ type}\ (\frac{V_{max}}{K_m})}$ | 5 |
| | | |
| Incorporation after RDV in the template | | |
| | | ATP |
| wild type | $V_{max}$ (product fraction) | 0.31 ±0.0021 |
| | $K_m$, μM | 2.1 ±0.068 |
| | $V_{max}/K_m$ | 0.15 |
| | | |
| V557L | $V_{max}$ (product fraction) | 0.33 ±0.013 |
| | $K_m$, μM | 1.9 ±0.037 |
| | $V_{max}/K_m$ | 0.17 |
| | $\frac{\mathbf{V557L}\ (\frac{V_{max}}{K_m})}{\mathbf{wild\ type}\ (\frac{V_{max}}{K_m})}$ | 1.2 |

[a] $V_{max}$ is a Michaelis–Menten parameter reflecting the maximal velocity of nucleotide incorporation.
[b] $K_m$ is a Michaelis–Menten parameter reflecting the concentration of the nucleotide substrate at which the velocity of nucleotide incorporation is half of $V_{max.}$
[c] Efficiency of nucleotide incorporation.
[d] All reported values have been calculated on the basis of an 8- or 10-data point experiments.
[e] Standard error associated with the fit.

Table B2. Remdesivir-TP (RDV-TP) selectivity values of for incorporation opposite U in the template catalyzed by SARS-CoV-2 wild-type and V557L mutant RdRp complexes.

| Incorporation opposite U | | | |
|---|---|---|---|
| | | ATP | RDV-TP |
| wild type | $V_{max}$ [a] (product fraction) | 0.90[d] ±0.0081[f] | 0.87 ±0.018 |
| | $K_m$ [b], μM | 0.033 ±0.0012 | 0.013 ±0.00098 |
| | $V_{max}/K_m$ [c] | 27 | 67 |
| | Selectivity, fold [d] | | 0.41 |
| | | | |
| V557L | $V_{max}$ (product fraction) | 0.76 ±0.020 | 0.66 ±0.029 |
| | $K_m$, μM | 0.091 ±0.012 | 0.033 ±0.0061 |
| | $V_{max}/K_m$ | 8.4 | 20 |
| | Selectivity, fold | | 0.42 |

[a] $V_{max}$ is a Michaelis–Menten parameter reflecting the maximal velocity of nucleotide incorporation.
[b] $K_m$ is a Michaelis–Menten parameter reflecting the concentration of the nucleotide substrate at which the velocity of nucleotide incorporation is half of $V_{max}$.
[c] Efficiency of nucleotide incorporation.
[d] Selectivity of a viral RNA polymerase for a nucleotide substrate analogue is calculated as the ratio of the $V_{max}/K_m$ values for NTP and NTP analogue, respectively.
[e] All reported values have been calculated on the basis of an 8- or 10-data point experiment.
[f] Standard error associated with the fit.

**A**

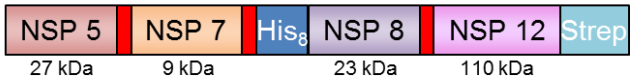


**B**

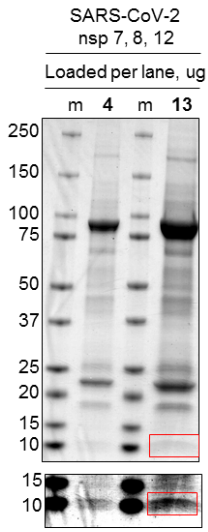


**C**

| Accession | Description | Score | Coverage | # Proteins | # Unique Peptides | # Peptides |
|---|---|---|---|---|---|---|
| sp\|7 | sp\|7 | 30.53 | 84.34 | 1 | 6 | 6 |

| A3 | Sequence | # PSMs | # Proteins | # Protein Groups | Protein Group Accessions |
|---|---|---|---|---|---|
| High | LWAQcVQLHNDILLAK | 3 | 1 | 1 | sp\|7 |
| High | cTSVVLLSVLQQLR | 4 | 1 | 1 | sp\|7 |
| High | LcEEmLDNR | 12 | 1 | 1 | sp\|7 |
| High | LcEEmLDnRATLQ | 2 | 1 | 1 | sp\|7 |
| High | LcEEMLDNR | 2 | 1 | 1 | sp\|7 |
| High | DTTEAFEK | 4 | 1 | 1 | sp\|7 |
| High | mVSLLSVLLSMQGAVDINK | 1 | 1 | 1 | sp\|7 |
| High | mVSLLSVLLSmQGAVDINK | 1 | 1 | 1 | sp\|7 |
| High | LWAQcVQLHnDILLAK | 6 | 1 | 1 | sp\|7 |

**Figure B1. Expression construct, SDS PAGE and mass spectroscopic analyses of the SARS-CoV-2 RdRp complexes**. ***A***, Schematic representaion of the expression construct (pFastBac1/nsp5-7-8-12) used to produce SARS-CoV-2 nsp7/nsp8/nsp12 RdRp complex. Genes coding for non-structural proteins, molecular weight of the expressed proteins in kDa and affinity tags ($His_8$ and Strep, histidine and strep tags, respectively) are indicated. Red rectangles indicate the nsp5 protease cognate cleavage sites. ***B***, SDS PAGE migration pattern of the purified enzyme preparations stained with Coomassie Brilliant Blue G-250 dye. Bands migrating at ~100 kDa and ~25 kDa contain nsp12 and nsp8, respectively. Red rectangle defines the location on the gel which was submitted to the mass spectroscopic analysis. Bottom subpanel illustrates the portion of the gel where nsp7 is expected to migrate; in order to facilitate the visualization the contrast of the image was uniformly increased. ***C***, A snapshot of the mass spectroscopy data file of the portion of the gel illustrated by the red rectangle in panel ***B***.

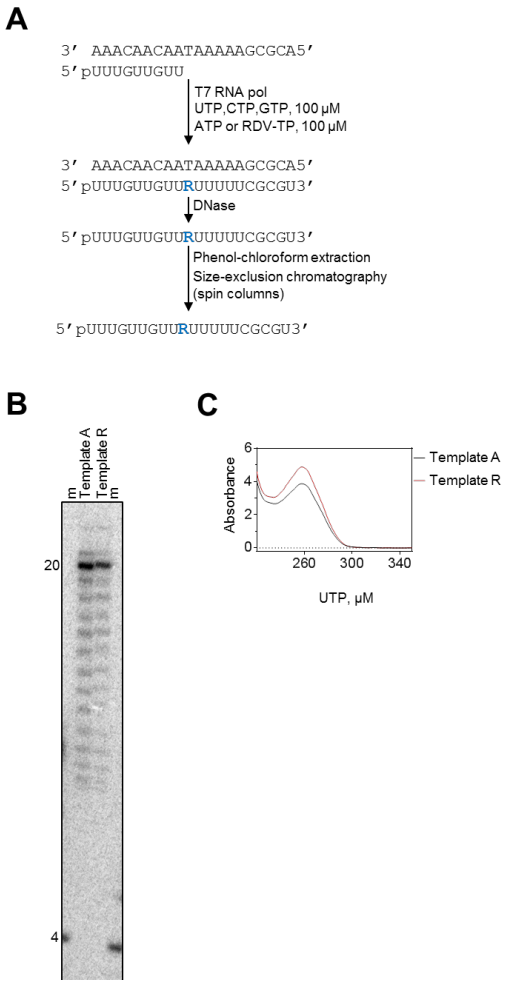


**Figure B2. Quality of the RNA templates produced by T7 RNA polymerase**. ***A***, Schematic representation of the T7 RNA polymerase reaction used to produce an RNA template with template-embedded RDV (R). ***B***, Migration pattern of RNA template preparations (after phenol/chloroform extraction and spin-column size-exclusion chromatography) subjected to denaturing 8M urea PAGE. Trace amounts of [α-$^{32}$P]-CTP were added to the T7 RNA polymerase reactions to allow the visualization of the final reaction products. Template A and R refers to T7 RNA polymerase reaction conditions where UTP/CTP/GTP nucleotide cocktail was supplemented with ATP or RDV-TP, respectively. Full template-length product (20) fraction in Template A preparation is 1.2-fold higher than in Template R preparation. Template A and R exhibit identical and uniform RNA degradation products with the full template-length (20) product containing the strongest signal in the lane. These RNA template preparations were used only for the illustration of their migration pattern; they were not used in reactions with SARS-CoV-2 RdRp complex. 4 indicates the migration pattern of 5'-$^{32}$P-labeled 4-nt primer used here as a marker (m). ***C***, Example of an absorbance spectra of the RNA template preparations used in the reactions with SARS-CoV-2 RdRp complex after phenol/chloroform extraction and spin-column size-exclusion chromatography. These RNA templates were synthesized by T7 RNA polymerase using ATP/UTP/CTP/GTP or RDV-TP/ UTP/CTP/GTP cocktails in the absence of [α-$^{32}$P]-CTP. The a260 absorbance of Template R is 1.3-fold higher than of Template A.

*EPT contributed to this figure.

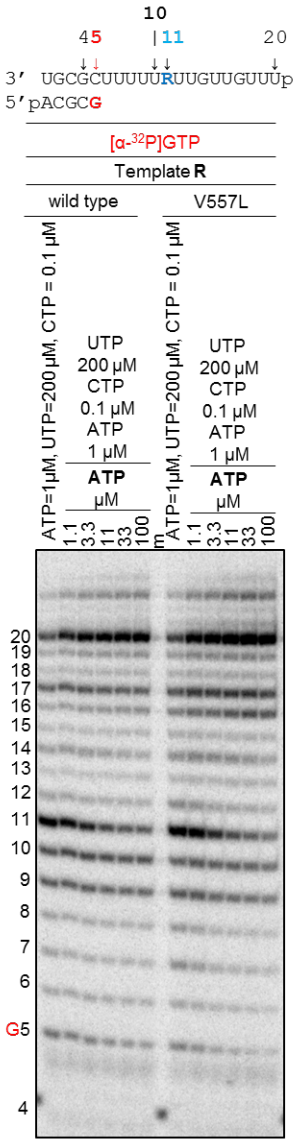


**Figure B3. RNA synthesis catalyzed by SARS-CoV-2 RdRp wild type and V557L complexes on an RNA template containing remdesivir embedded in the template**. RNA primer/template with template-embedded remdesivir (R) at position 11 is shown on top. G5 indicates the incorporation of [α-$^{32}$P]-GTP opposite template position 5. Below the primer/template sequence is the migration pattern of the products of RNA synthesis catalyzed by CoV-SARS-2 RdRp complexes in the presence of RNA primer/template, $MgCl_2$, indicated concentrations of NTP cocktail supplemented with indicated concentrations of UTP after 30 minutes. 4 indicates the migration pattern of 5'-$^{32}$P-labeled 4-nt primer used here as a marker.

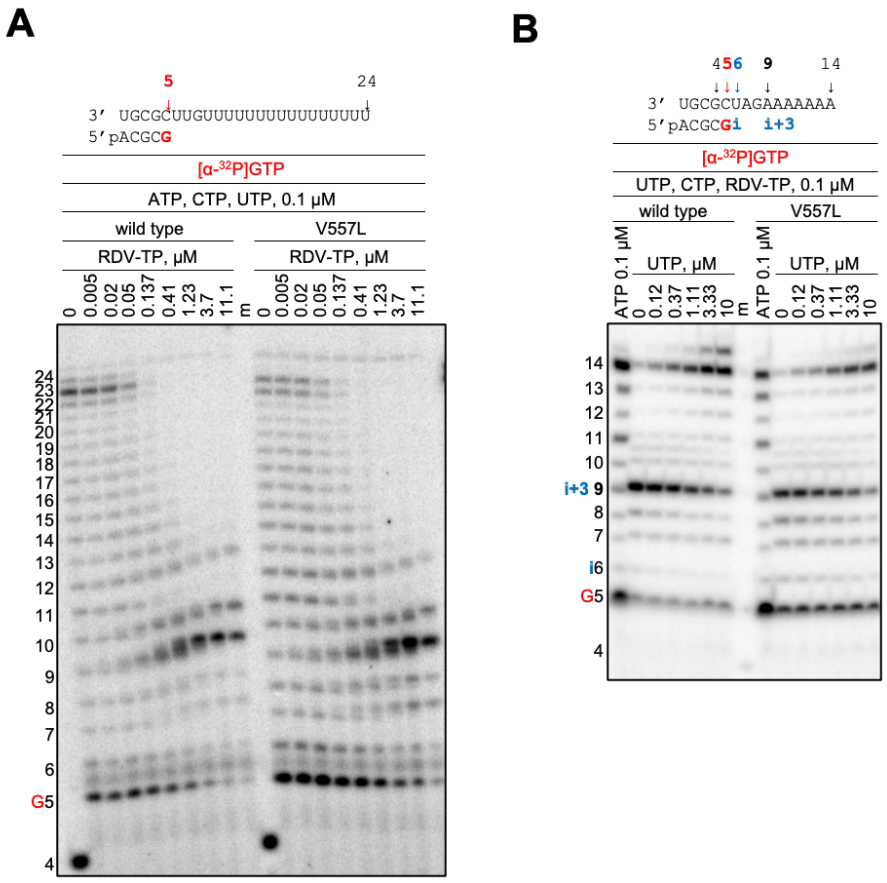


**Figure B4. RNA synthesis catalyzed by SARS-CoV-2 RdRp wild-type and V557L mutant complexes on an RNA template containing multiple or a single site for RDV-TP incorporation**. ***A***, Inhibition of RNA synthesis with increasing concentrations of RDV-TP. RNA primer/template supporting multiple incorporations of RDV-TP shown on top of the panel. G5 indicates the incorporation of [α-$^{32}$P]-GTP opposite template position 5. RNA synthesis was catalyzed by CoV-SARS-2 RdRp wild-type and mutant complexes in the presence of RNA primer/template, $MgCl_2$, indicated concentrations of NTP cocktail and increasing concentrations of RDV-TP for 30 minutes. "4" indicates the migration pattern of 5'-$^{32}$P-labeled 4-nt primer used here as a size marker. ***B***, Overcoming the delayed chain-termination at position i+3. RNA primer/template supporting incorporation of RDV-TP (i) at position 6 (i = 6) is shown on top. i+3 illustrates a delayed chain termination at position 9 when RDV-TP is incorporated at position 6. G5 indicates the incorporation of [α-$^{32}$P]-GTP opposite template position 5. RNA synthesis was catalyzed by CoV-SARS-2 RdRp wild type and mutant complexes in the presence of RNA primer/template, $MgCl_2$ and indicated concentrations of NTP supplemented with increasing concentrations of UTP for 30 minutes. "4" indicates the migration pattern of 5'-$^{32}$P-labeled 4-nt primer used here as a size marker.

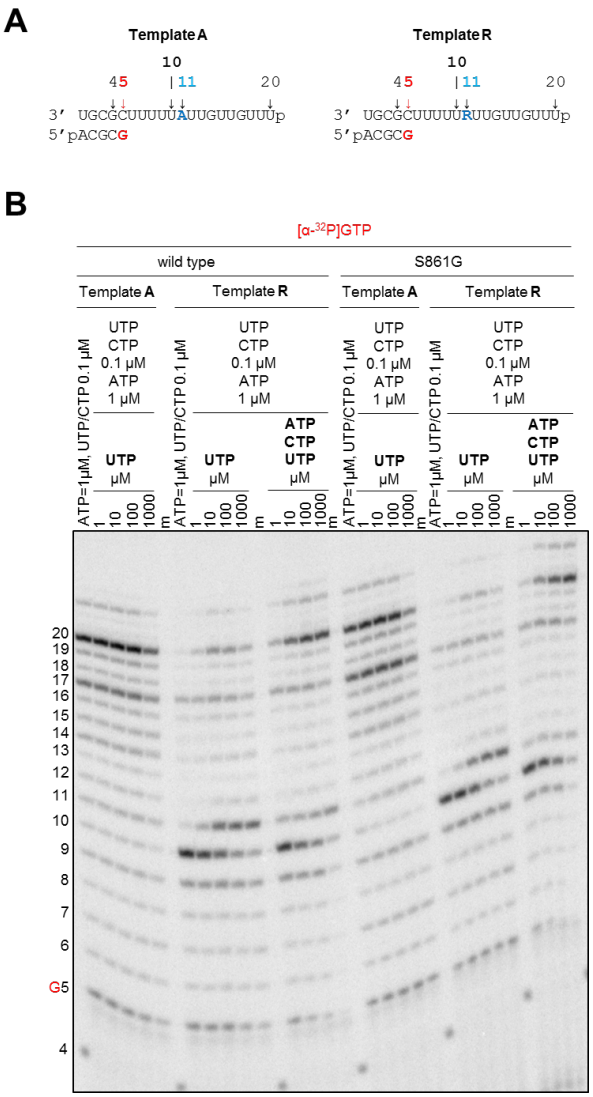


**Figure B5. RNA synthesis catalyzed by SARS-CoV-2 wild type and S861G mutant RdRp complexes**. ***A***, RNA primer/template with template-embedded RDV (Template R) at position 11; the corresponding primer/template with adenosine at this position (Template A) is shown on the left. G5 indicates the incorporation of [α-$^{32}$P]-GTP opposite template position 5. ***B***, Migration pattern of the products of RNA synthesis catalyzed by CoV-SARS-2 RdRp wildtype and S861G mutant RdRp complexes in the presence of RNA primer/templates shown in panel A, $MgCl_2$ and indicated concentrations of NTP cocktails after 30 minutes. "4" indicates the migration pattern of 5'-$^{32}$P-labeled 4-nt primer used here as a size marker.

## Appendix C: Supporting information for Chapter 6

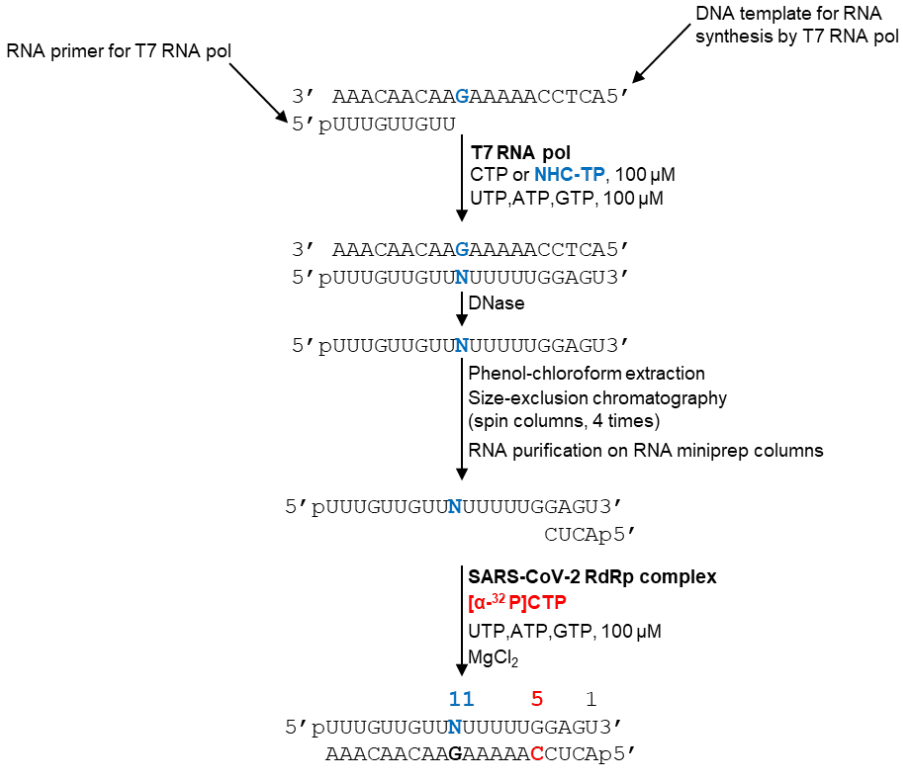


**Figure C1. Schematic representation of the T7 RNA polymerase system used to synthesize the RNA template with NHC-MP embedded at position 11**. The scheme illustrates the modifications necessary for the synthesis of an NHC-embedded RNA template. T7 RNA polymerase (Thermo Fisher Scientific, Waltham, MA, USA) was used to initiate the RNA synthesis from a 5′-pyosphorylated RNA primer: 5'-pUUUGUUGUU which is complementary to the 3′-end of the DNA template (Dharmacon (Lafayette, CO, USA)): 3′-AAACAACAAGAAAAACCTCA-5'. Underlined portion indicates the region which is complementary to the RNA primer. The template residue "G" indicates the site of the NHC_MP incorporation into the RNA primer. Therefore, the fully extended primer will contain an embedded NHC-MP (N) and may serve as a 20-nt RNA template for the RNA synthesis by SARS-CoV-2 RdRp complex: 5′-pUUUGUUGUUNUUUUUGGAGU-3', where underlined portion is complementary to the RNA primer 5′-pACUC used in SARS-CoV-2 RNA synthesis reactions. Note that this RNA primer can only anneal to a fully-synthesized 20-nt RNA template. The T7 RNA polymerase reaction mixtures contained 30 units of the polymerase, 300 µM RNA primer, 100 µM DNA template, 100 µM UTP/ATP/GTP cocktail, and 100 µM CTP or NHC-TP in a 25 mM Tris-HCl buffer (pH 8). Reactions were started with 5 mM $MgCl_2$, incubated at 37 ºC for 90 minutes, boiled for 10 minutes, and incubated with 2 units of Turbo DNase (Thermo Fisher Scientific, Waltham, MA, USA) at 37 ºC for 30 minutes. The reaction mixtures were then extracted with phenol/chlorophorm (premixed with Isoamyl Alcohol 25:24:1, (BioShop (Burlington, ON, Canada)) and buffer-exchanged consecutively four times through the size-exclusion chromatography on PD SpinTrap G-25 spin columns (Cytiva, Little Chalfont, UK). The fourth column eluate was further purified using a Direct-zol RNA MiniPrep Plus kit (ZYMO Research, Tustin, CA, USA). *EPT Contributed to this figure.

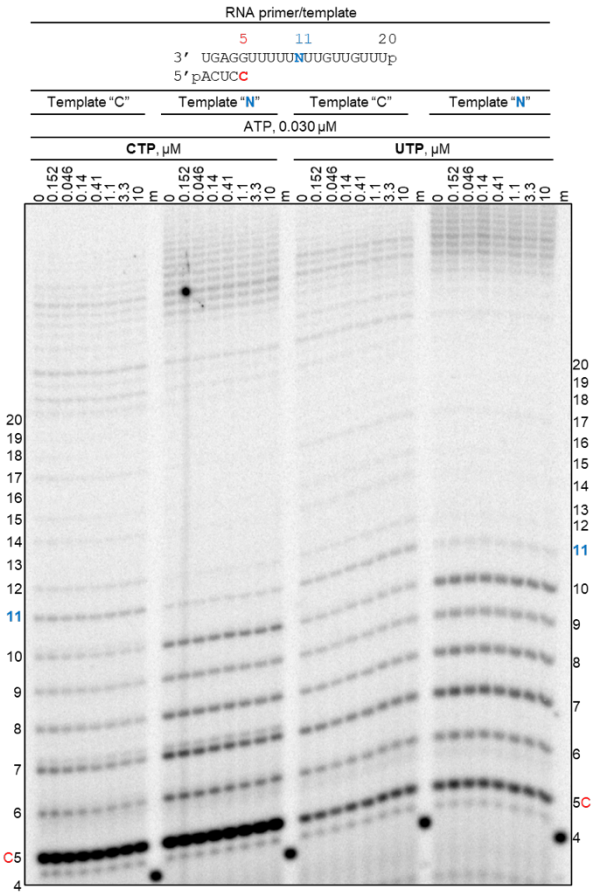


**Figure C2. CTP and UTP incorporation opposite templating NHC-MP during viral RNA synthesis along a template with a single NHC-MP residue**. Migration pattern of the products of RNA synthesis catalyzed by SARS-CoV-2 RdRp complex along the RNA primer/template with a strategic residue at position 11 as shown at the top of the panel. RNA primer/template contains an embedded NHC-MP at position 11 (Template "N") or CMP (Template "C"). Figure notations are as in Figure 1. Signal at position 11 in panels Template "C" is due to C:A misincorporation. Signal accumulation of position 10 in panels Template "N" illustrates the inability of SARS-CoV-2 RdRp complex to generate NHC-MP:A misincorporation. Persistence of the signal at position 11 and 10 at increasing concentrations of CTP or UTP in panels "C" and "N", respectively, illustrate the inability of the enzyme to generate C:C, U:U, and NHC-MP:C, NHC-MP:U misincorporations. Note that in order to avoid CTP competition with [α-$^{32}$P]CTP the reactions were run for 8 minutes with [α-$^{32}$P]CTP only, then increasing concentrations of CTP in the presence of 0.030 µM ATP we added and the reactions were further incubated at 30°C for another 10 minutes.

## Appendix D: Supporting information for Chapter 7

Table D1. $V_{max}$ and $K_m$ values associated with newly reported selectivity values for the triphosphate metabolite of remdesivir (RDV-TP) with RdRp enzymes as it relates to table 7.1 in the main text.

| | **ATP** | | | | **RDV-TP** | | | |
|---|---|---|---|---|---|---|---|---|
| | **$V_{max}$**[a] (product fraction) | **$K_m$**[b] (μM) | **$\frac{V_{max}}{K_m}$** | | **$V_{max}$** (product fraction) | **$K_m$** (μM) | **$\frac{V_{max}}{K_m}$** | **Selectivity**[c] (fold) |
| **HCV** | n=3 [d] | | | | n = 3 | | | **0.93** |
| | 0.55 | 0.012 | 46 | | 0.59 | 0.012 | 49 | |
| ±[e] | 0.018 | 0.0019 | | | 0.023 | 0.0021 | | |
| | | | | | | | | |
| **Nipah** | n = 3 | | | | n = 3 | | | **1.6** |
| | 0.89 | 0.034 | 26 | | 0.90 | 0.056 | 16 | |
| ± | 0.014 | 0.020 | | | 0.023 | 0.0047 | | |
| | | | | | | | | |
| **CCHFV** | n = 4 | | | | n = 4 | | | **41** |
| | 0.69 | 0.063 | 11 | | 0.54 | 2.0 | 0.27 | |
| ± | 0.019 | 0.0092 | | | 0.017 | 0.26 | | |
| | | | | | | | | |
| **FluB** | n=3 | | | | n=3 | | | **68** |
| | 0.73 | 0.23 | 3.2 | | 0.45 | 9.7 | 0.046 | |
| ± | 0.014 | 0.020 | | | 0.0064 | 0.42 | | |
| | | | | | | | | |

[a] $V_{max}$ is a Michaelis–Menten parameter reflecting the maximal velocity of nucleotide incorporation. The ATP or RDV-TP incorporation is measured by quantifying the signal corresponding to the product of incorporated AMP or RDV-MP and dividing it by the total signal in the reaction (the sum of signals corresponding to un-extended primer and AMP- or RDV-MP-extended primer). This defines the product fraction at the end of the reaction time.
[b] $K_m$ is a Michaelis–Menten parameter reflecting the concentration of the nucleotide substrate at which the velocity of nucleotide incorporation is half of $V_{max.}$
[c] Selectivity of a viral RNA polymerase for a nucleotide substrate analogue is calculated as the ratio of the $V_{max}/K_m$ values for NTP and NTP analogue, respectively, and it is a unitless parameter.
[d] All reported values have been calculated on the basis of a 8-data point experiment repeated indicated number of times (n).
[e] Standard error associated with the fit.
*Nipah selectivity values were generated by HWL
*CCHFV and FluB selectivity values were generated by EPT

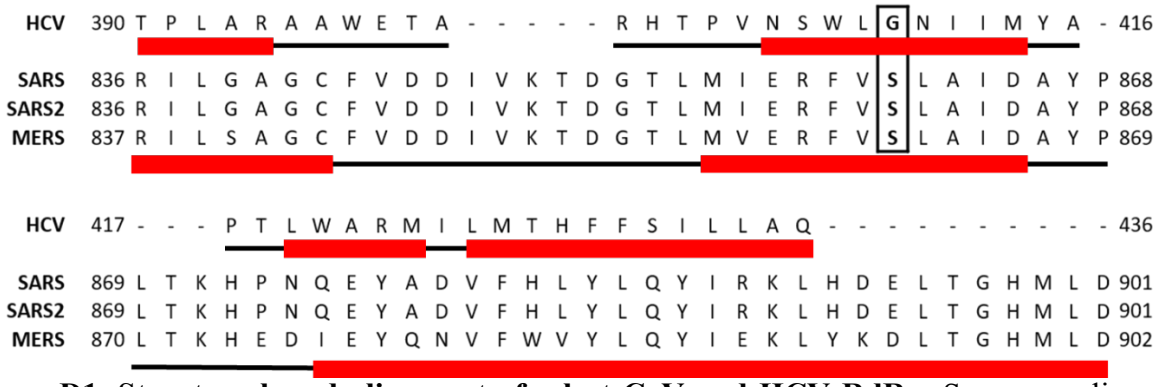


**Figure D1. Structure-based alignment of select CoV and HCV RdRp**. Sequence alignment based on a 3D structural overlay of HCV ns5b (PDB:4WTA) and SARS-CoV-2 nsp12 (PDB:6XEZ). Secondary structure is shown below the HCV sequence and below the three coronavirus sequences. Helix secondary structure elements are indicated by the red bars, while loops are indicated by solid black lines. While the three coronaviruses have high homology, the HCV sequence has fairly low homology. Despite this, it shares a common secondary structure in the thumb sub-domain such that Ser-861 in SARS-CoV-2 is seen to correspond to Gly-410 in HCV.

*EPT contributed this figure.

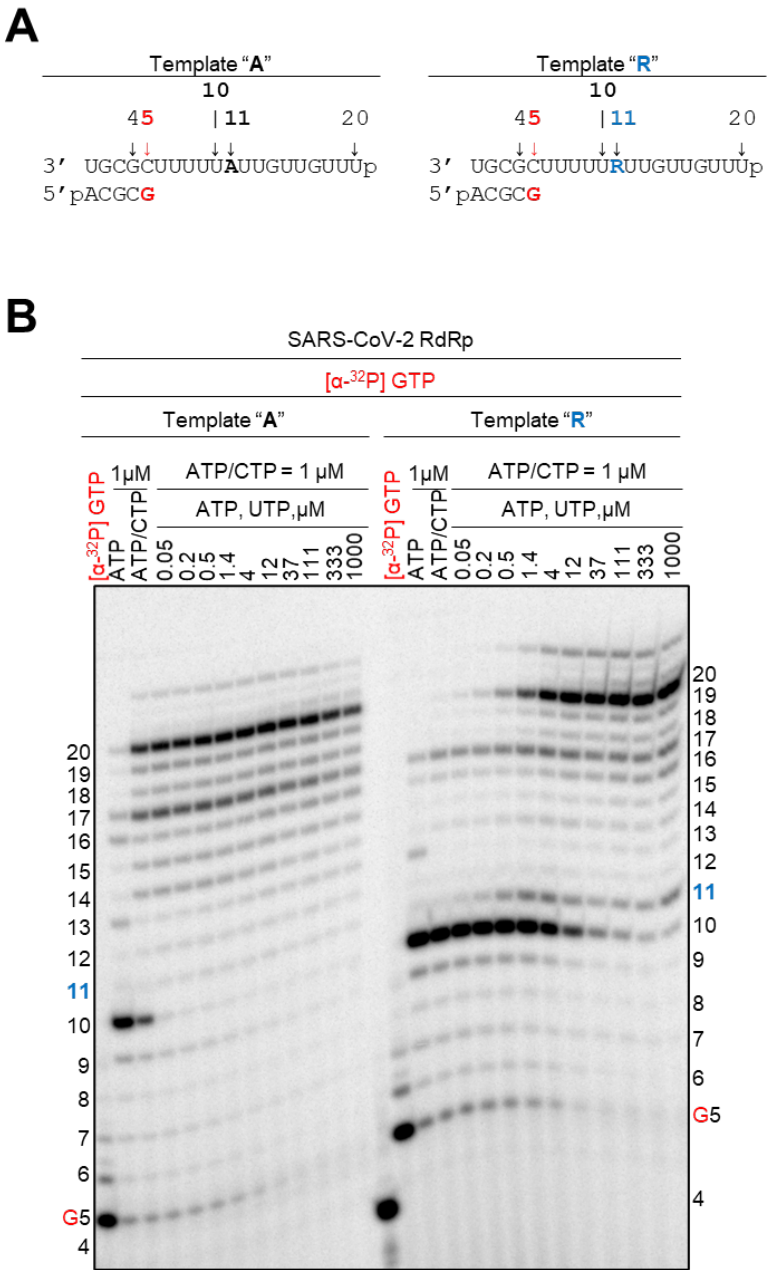


**Figure D2. Template-dependent inhibition of SARS-CoV-2 RdRp**. ***A***, RNA primer/template with a template-embedded AMP (Template "A", *left*) and RDV-MP (Template "R", *right*) at position 11. ***B***, Migration pattern of products of RNA synthesis catalyzed by SARS-CoV-2 RdRp, incorporation of UTP opposite RDV-MP is inhibited (signal accumulation at p10), but is overcome with increasing concentrations of ATP, UTP nucleotide mix.

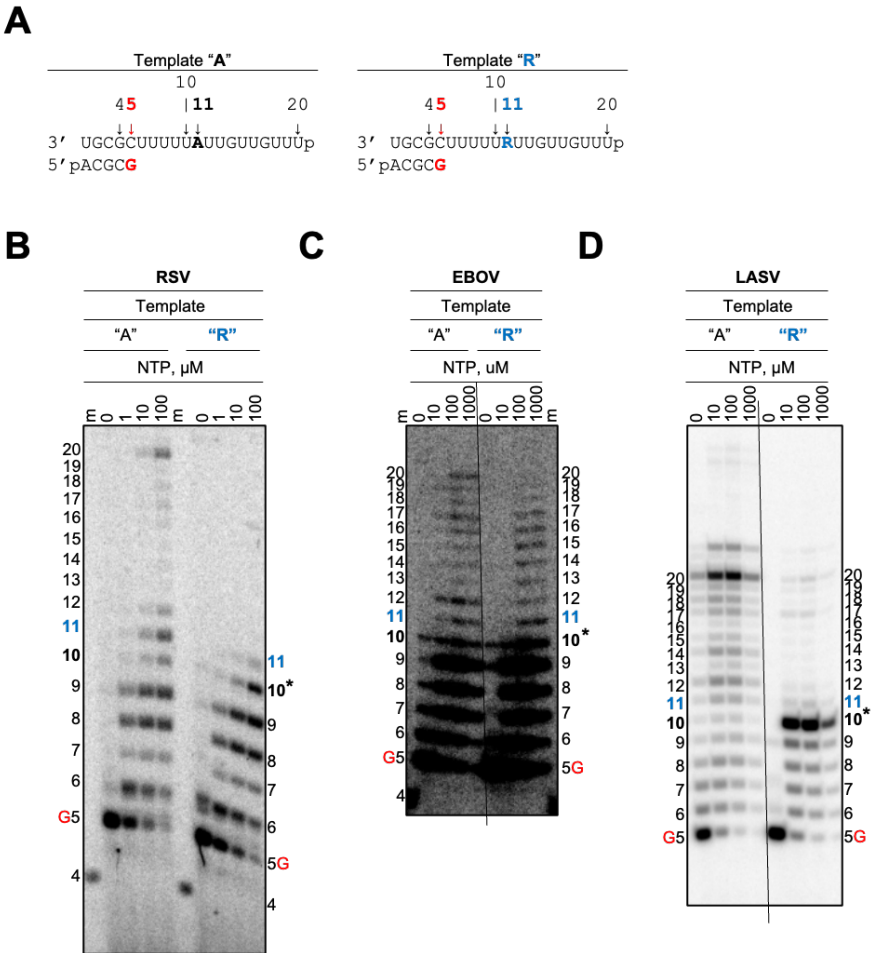


**Figure D3. Template-dependent inhibition of RSV, EBOV, and LASV RdRp by an embedded RDV-MP**. ***A***, RNA primer/template as indicated in Fig. 3. ***B***, Migration pattern of RSV RdRp-catalyzed RNA synthesis supplemented with increasing NTP concentrations opposite AMP (*left*) or RDV-MP (*right*). ***C***, Migration pattern of EBOV RdRp-catalyzed RNA synthesis in which the conditions are the same as described in ***B***. ***D***, Migration pattern of RSV RdRp-catalyzed RNA synthesis in which the conditions are the same as described in B and C. The asterisk at position 10 indicates point of inhibition as a result of the embedded RDV-MP at position 11.

*EPT Contributed this figure.

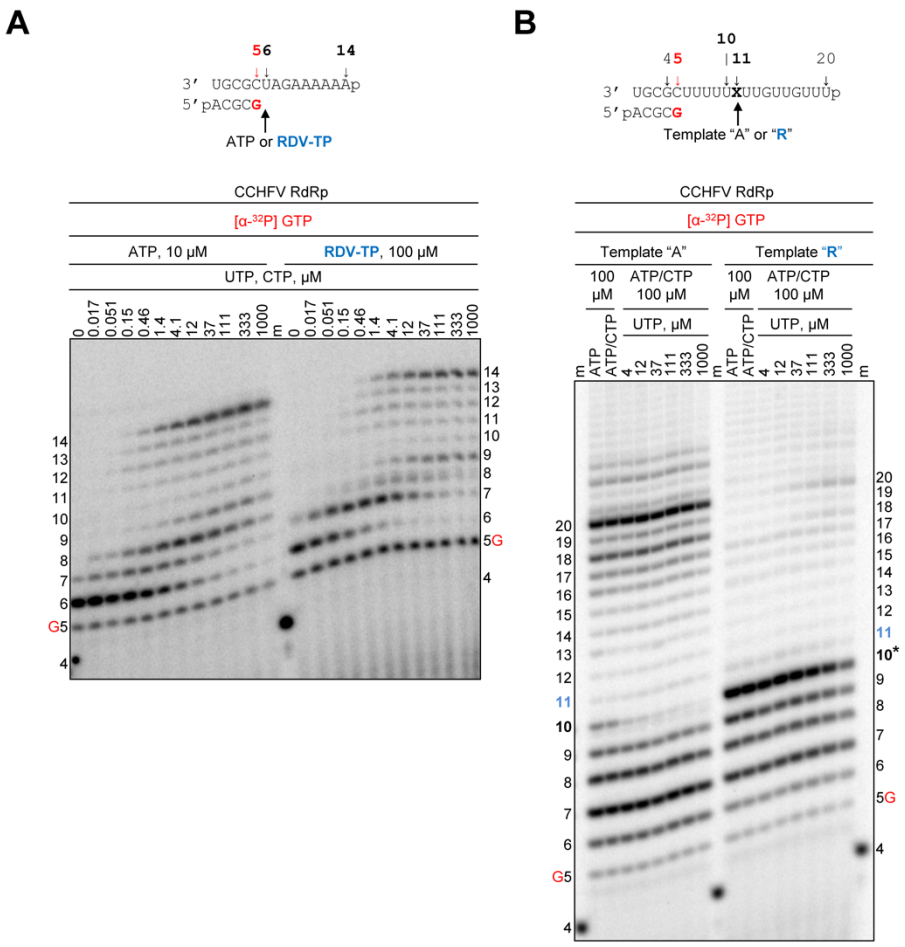


**Figure D4. RNA synthesis patterns following AMP and RDV-MP incorporation and template-dependent inhibition of CCHFV RdRp**. ***A***, RNA primer/ template, as indicated in Figure 6.1 and migration pattern of products of RNA following the incorporation of AMP or RDV-MP. No inhibition is evident. ***B***, RNA primer/template, as indicated in Figure 6.3 and migration pattern of RNA synthesis opposite AMP (*left*) or RDV-MP (*right*). The asterisk at position 10 indicates the point of inhibition as a result of the embedded RDV-MP at position 11.

*EPT Contributed to this figure.

## Appendix E: Supporting information for Chapter 8

Table E1: Selective incorporation of GS-443902, a 1′-cyano purine NTP analog, by selected RdRp enzymes

| | | | ATP | | | GS-443902 | | | |
|---|---|---|---|---|---|---|---|---|---|
| RNA Sense | Family (-viridae) | Virus | $V_{max}$[a] (product fraction) | $K_m$[b] (μM) | $V_{max}/K_m$ | $V_{max}$ (product fraction) | $K_m$ (μM) | $V_{max}/_m$ | Selectivity[f] (fold) |
| Positive ssRNA | Corona- | **SARS-CoV-2** | | | | | | | **0.30**[1] |
| | | P.R.[c] | 0.75[d] | 0.03 | 25 | 0.74 | 0.0089 | 83 | |
| | | ±[e] | 0.019 | 0.003 | | 0.023 | 0.0020 | | |
| | | **SARS-CoV** | | | | | | | **0.34**[1] |
| | | P.R. | 0.73 | 0.03 | 24 | 0.70 | 0.010 | 70 | |
| | | ± | 0.017 | 0.003 | | 0.015 | 0.0008 | | |
| | | **MERS-CoV** | | | | | | | **0.35**[1] |
| | | P.R. | 0.47 | 0.017 | 28 | 0.50 | 0.0063 | 79 | |
| | | ± | 0.011 | 0.019 | | 0.012 | 0.0006 | | |
| | Picorna- | **HRV-16** | | | | | | | **1.03** |
| | | | 0.90 | 4.52 | 0.20 | 0.96 | 4.96 | 0.19 | |
| | | ± | 0.017 | 0.31 | | 0.015 | 0.27 | | |
| | | **EV-71** | | | | | | | **0.93** |
| | | | 0.96 | 0.96 | 1.0 | 0.93 | 0.86 | 1.08 | |
| | | ± | 0.021 | 0.066 | | 0.027 | 0.081 | | |
| Nonsegemented negative ssRNA | Pneumo- | **RSV** | | | | | | | **2.73**[2] |
| | | P.R. | 0.76 | 0.17 | 4.5 | 0.82 | 0.50 | 1.6 | |
| | | ± | 0.022 | 0.023 | | 0.027 | 0.089 | | |
| | | **HMPV** | | | | | | | **6.71** |
| | | | 0.60 | 6.40 | 0.094 | 0.57 | 42.19 | 0.014 | |
| | | ± | 0.024 | 0.98 | | 0.045 | 7.79 | | |
| | Paramyxo- | **HPIV-3** | | | | | | | **7.20** |
| | | | 0.63 | 0.061 | 10.3 | 0.63 | 0.44 | 1.43 | |
| | | ± | 0.025 | 0.015 | | 0.010 | 0.040 | | |
| | | **PIV-5** | | | | | | | **8.31** |
| | | | 0.74 | 1.5 | 0.49 | 0.77 | 13 | 0.059 | |
| | | ± | 0.026 | 0.25 | | 0.042 | 2.3 | | |
| Segmented Negative ssRNA | Orthomyxo- | **FluB** | | | | | | | **70**[1] |
| | | P.R. | 0.73 | 0.23 | 3.2 | 0.45 | 9.7 | 0.046 | |
| | | ± | 0.014 | 0.020 | | 0.0064 | 0.42 | | |
| | Arena- | **LASV** | | | | | | | **19**[1] |
| | | P.R. | 0.57 | 0.11 | 5.2 | 0.35 | 1.3 | 0.27 | |
| | | ± | 0.032 | 0.020 | | 0.016 | 0.18 | | |
| Human DNA-dependent RNA polymerase | | **h-mtRNAP** | | | | | | | **503**[2] |
| | | P.R. | 0.98 | 0.050 | 19.6 | 0.81 | 21 | 0.039 | |
| | | ± | 0.018 | 0.0037 | | 0.013 | 0.096 | | |

[a] $V_{max}$ is a Michaelis–Menten parameter reflecting the maximal velocity of nucleotide incorporation.

[b] $K_m$ is a Michaelis–Menten parameter reflecting the concentration of the nucleotide substrate at which the velocity of nucleotide incorporation is half of $V_{max}$

[c] Previously reported

[d] All reported values have been calculated based on an 8–data point experiment repeated at least 3 times (n=3).

[e] Standard error associated with the fit.

[f] Selectivity of a viral RNA polymerase for a nucleotide substrate analog is calculated as the ratio of the $V_{max}/K_m$ values for ATP and GS-443902 analog, respectively.

[1] Data from Gordon et al.[260]

[2] Data from Tchesnokov et al.[267]

*HPIV-3 and HPIV-5 selectivity values were generated by SMW

Table E2: Selective incorporation of GS-646939, a 4′-cyano purine NTP analog, by selected RdRp enzymes

| | | | ATP | | | GS-646939 | | | |
|---|---|---|---|---|---|---|---|---|---|
| RNA Sense | Family (-viridae) | Virus | $V_{max}$[a] (product fraction) | $K_m$[b] (μM) | $V_{max}/K_m$ | $V_{max}$ (product fraction) | $K_m$ (μM) | $V_{max}/K_m$ | Selectivity[e] (fold) |
| Positive ssRNA | Corona- | **SARS-CoV-2** | | | | | | | **1.37** |
| | | 0.84[c] | 0.057 | 14.74 | 0.88 | 0.082 | 10.73 | |
| | | ±[d] | 0.030 | 0.0078 | | 0.015 | 0.0070 | | |
| | | **MERS-CoV** | | | | | | | **1.17** |
| | | 0.84 | 0.032 | 26.25 | 0.90 | 0.040 | 22.50 | |
| | | ± | 0.0090 | 0.0014 | | 0.012 | 0.0031 | | |
| | Picorna- | **HRV-16** | | | | | | | **0.018** |
| | | 0.90 | 4.52 | 0.20 | 0.80 | 0.072 | 11.11 | |
| | | ± | 0.017 | 0.31 | | 0.021 | 0.0097 | | |
| | | **EV-71** | | | | | | | **0.051** |
| | | 0.96 | 0.96 | 1.0 | 0.93 | 0.047 | 19.79 | |
| | | ± | 0.021 | 0.066 | | 0.019 | 0.0034 | | |
| Nonsegemented negative ssRNA | Pneumo- | **RSV** | | | | | | | **1.58** |
| | | 0.61 | 0.97 | 0.63 | 0.80 | 2.0 | 0.40 | |
| | | ± | 0.065 | 0.36 | | 0.059 | 0.52 | | |
| | | **HMPV** | | | | | | | **1.73** |
| | | 0.39 | 2.1 | 0.19 | 0.53 | 4.8 | 0.11 | |
| | | ± | 0.028 | 0.41 | | 0.027 | 0.99 | | |
| | Paramyxo- | **HPIV-3** | | | | | | | **10.3** |
| | | 0.63 | 0.061 | 10.3 | 0.78 | 0.78 | 1.0 | |
| | | ± | 0.025 | 0.015 | | 0.012 | 0.059 | | |
| | | **PIV-5** | | | | | | | **5.05** |
| | | 0.74 | 1.5 | 0.49 | 0.69 | 7.1 | 0.097 | |
| | | ± | 0.026 | 0.25 | | 0.013 | 0.49 | | |
| Segmented Negative ssRNA | Orthomyxo- | **FluB** | | | | | | | **2288** |
| | | 0.68 | 0.11 | 6.18 | 0.18 | 66 | 0.0027 | |
| | | ± | 0.014 | 0.0077 | | 0.0057 | 4.1 | | |
| | Arena- | **LASV** | | | | | | | **225** |
| | | 0.80 | 0.39 | 2.05 | 0.29 | 31.95 | 0.0091 | |
| | | ± | 0.0037 | 0.075 | | 0.091 | 25.15 | | |
| Human DNA-dependent RNA polymerase | | **h-mtRNAP** | | | | | | | **1538** |
| | | 0.93 | 0.096 | 9.69 | 0.67 | 107 | 0.0063 | |
| | | ± | 0.026 | 0.0091 | | 0.22 | 60.71 | | |

[a] $V_{max}$ is a Michaelis–Menten parameter reflecting the maximal velocity of nucleotide incorporation.
[b] $K_m$ is a Michaelis–Menten parameter reflecting the concentration of the nucleotide substrate at which the velocity of nucleotide incorporation is half of $V_{max}$.
[c] All reported values have been calculated based on an 8–data point experiment repeated at least 3 times (n=3).
[d] Standard error associated with the fit.
[e] Selectivity of a viral RNA polymerase for a nucleotide substrate analog is calculated as the ratio of the $V_{max}/K_m$ values for ATP and GS-646939, respectively.
*HPIV-3 and HPIV-5 selectivity values were generated by SMW

Table E3: Inhibitory effect of the incorporated analog-monophosphate on incorporation of the subsequent nucleotide

| Virus | Primer 3'-end (base) | Substrate | $V_{max}$[b] (product fraction) | $K_m$[c] (μM) | $V_{max}/K_m$ | Inhibition[d] (fold) |
|---|---|---|---|---|---|---|
| **SARS-CoV-2** | AMP | UTP | 1.10[e] ±[f] 0.043 | 0.009 ± 0.0015 | 122 | Ref[g] |
| | GS-646939 (MP[a]) | | 0.79 ± 0.036 | 16.42 ± 2.67 | 0.048 | **2542** |
| | GS-443902 (MP) | | 1.13 ± 0.047 | 0.0082 ± 0.0013 | 138 | **0.88** |
| **MERS-CoV** | AMP | UTP | 1.03 ± 0.016 | 0.0016 ± 0.0001 | 644 | Ref. |
| | GS-646939 (MP) | | 0.91 ± 0.10 | 24.68 ± 9.19 | 0.037 | **17,405** |
| | GS-443902 (MP) | | 0.98 ± 0.018 | 0.0009 ± 0.0001 | 1089 | **0.59** |
| **HRV-16** | AMP | UTP | 0.76 ± 0.015 | 0.023 ± 0.002 | 33.04 | Ref. |
| | GS-646939 (MP) | | 0.83 ± 0.012 | 18.88 ± 1.22 | 0.044 | **751** |
| | GS-443902 (MP) | | 0.67 ± 0.015 | 0.057 ± 0.005 | 11.75 | **2.81** |
| **EV-71** | AMP | UTP | 0.65 ± 0.003 | 0.028 ± 0.0006 | 23.21 | Ref. |
| | GS-646939 (MP) | | 0.81 ± 0.017 | 157 ± 10.25 | 0.005 | **4,642** |
| | GS-443902 (MP) | | 0.48 ± 0.005 | 0.093 ± 0.003 | 5.16 | **4.50** |
| **RSV** | AMP | UTP | 0.70 ± 0.037 | 1.6 ± 0.41 | 0.44 | Ref. |
| | GS-646939 (MP) | | 0.15 ± 0.0029 | 354 ± 16 | 0.00042 | **1,048** |
| | GS-443902 (MP) | | | | | **6.27[1]** |
| **HMPV** | AMP | UTP | 0.48 ± 0.026 | 7.8 ± 2.2 | 0.062 | Ref. |
| | GS-646939 (MP) | | 0.087 ± 0.030 | 732 ± 488 | 0.00012 | **517** |
| | GS-443902 (MP) | | 0.28 ± 0.018 | 22 ± 6.2 | 0.013 | **4.77** |
| **HPIV-3** | AMP | UTP | 0.56 ± 0.0097 | 0.073 ± 0.0093 | 7.67 | Ref. |
| | GS-646939 (MP) | | 0.61 ± 0.0099 | 268 ± 11 | 0.0023 | **3,334** |
| | GS-443902 (MP) | | 0.58 ± 0.011 | 0.076 ± 0.011 | 7.63 | **1.01** |
| **PIV-5** | AMP | UTP | 0.51 ± 0.022 | 5.8 ± 1.3 | 0.088 | Ref. |
| | GS-646939 (MP) | | 0.058 ± 0.080 | 2740 ± 4899 | 0.000021 | **4,190** |
| | GS-443902 (MP) | | 0.48 ± 0.0089 | 2.2 ± 0.26 | 0.22 | **0.40** |

[a] Denotes that the 3′-end of the primer is terminated by the monophosphate form of the respective nucleotide.
[b] $V_{max}$ is a Michaelis–Menten parameter reflecting the maximal velocity of nucleotide incorporation.
[c] $K_m$ is a Michaelis–Menten parameter reflecting the concentration of the nucleotide substrate at which the velocity of nucleotide incorporation is half of $V_{max}$
[d] Inhibition of subsequent nucleotide incorporation is calculated as the ratio of $V_{max}/K_m$ values for UTP determined on primers terminated with AMP, GS-646939, or GS-443902.
[e] All reported values have been calculated based on an 8–data point experiment repeated at least 3 times (n=3).
[f] Standard error associated with the fit.
[g] Reference.
[1] Data from Tchesnokov et al.[267]
*HPIV-3 and HPIV-5 values were generated by SMW

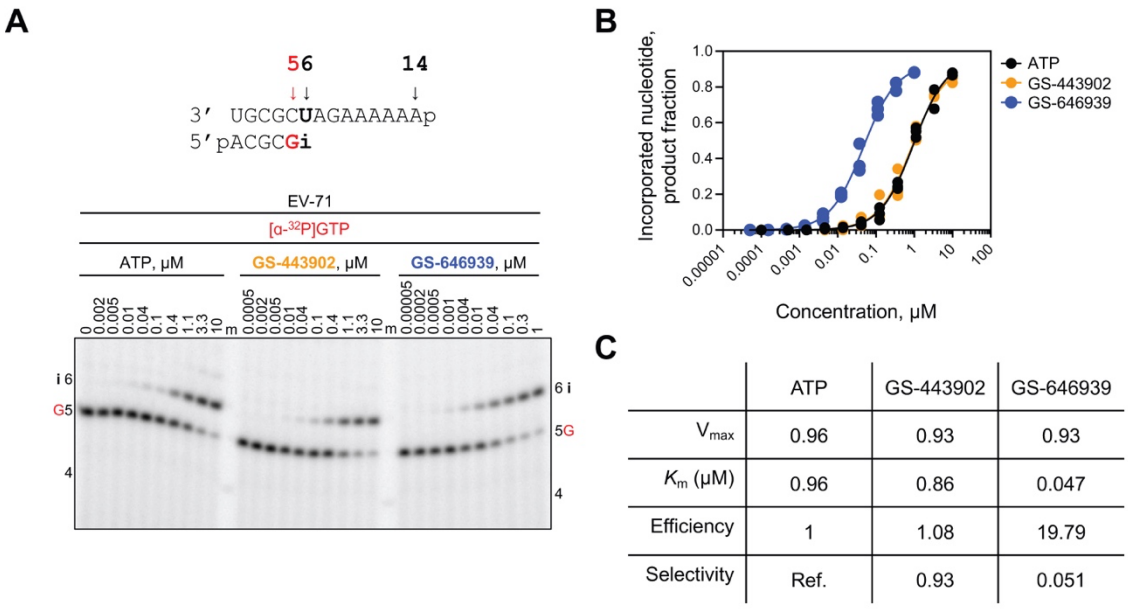


| | ATP | GS-443902 | GS-646939 |
|---|---|---|---|
| $V_{max}$ | 0.96 | 0.93 | 0.93 |
| $K_m$ (μM) | 0.96 | 0.86 | 0.047 |
| Efficiency | 1 | 1.08 | 19.79 |
| Selectivity | Ref. | 0.93 | 0.051 |

**Figure E1. Selective incorporation of GS-443902 and GS-646939 by EV-71 RdRp**. ***A***, RNA primer/template substrate used in the RNA synthesis assays to test GS-443902 and GS-646939 as substrates for incorporation at position 6 ("i") is shown above the gel. G indicates incorporation of the radiolabelled nucleotide opposite template position 5. NTP incorporation was monitored with purified EV-71 RdRp in the presence of [α-$^{32}$P]-GTP, RNA primer/template, $MgCl_2$ and increasing concentrations of ATP or the respective ATP analog substrate. Lane m illustrates the migration pattern of the radiolabelled 4 nucleotide-long primer. ***B***, Graphical representation of the incorporation of ATP and ATP analogs shown in A, fitting the data points to the Michaelis-Menten function to determine $V_{max}$ and $K_m$. Independent 8-data point experiments were performed at least three times (n=3), each replicate is plotted to represent the variation between experiments. ***C***, Kinetic parameters and efficiency of ATP, GS-443902, and GS-646939 incorporation by EV-71 RdRp. Efficiency is determined as the quotient of $V_{max}$ over $K_m$ and selectivity as the quotient of natural ATP efficiency over the efficiency of the ATP analog.

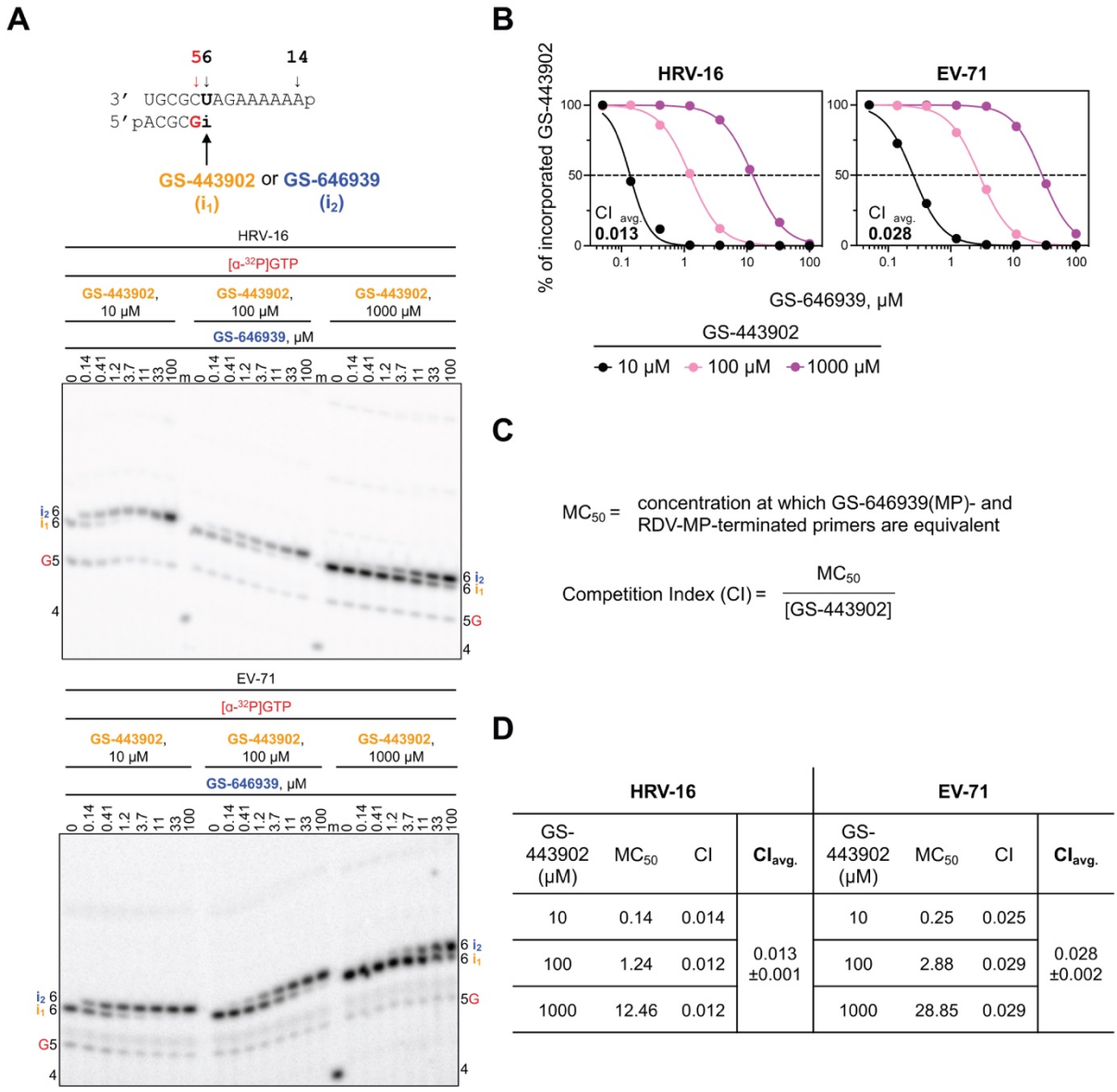


| HRV-16 | | | | EV-71 | | | |
|---|---|---|---|---|---|---|---|
| GS-443902 (µM) | $MC_{50}$ | CI | $CI_{avg.}$ | GS-443902 (µM) | $MC_{50}$ | CI | $CI_{avg.}$ |
| 10 | 0.14 | 0.014 | 0.013 ±0.001 | 10 | 0.25 | 0.025 | 0.028 ±0.002 |
| 100 | 1.24 | 0.012 | | 100 | 2.88 | 0.029 | |
| 1000 | 12.46 | 0.012 | | 1000 | 28.85 | 0.029 | |

**Figure E2. Competitive incorporation of GS-646939 versus GS-443902 by HRV-16 and EV-71 RdRp**. ***A***, RNA primer/template (*top*) supporting a single incorporation of GS-443902 ("$i_1$") or GS-646939 ("$i_2$") at position 6. G indicates incorporation of [α-$^{32}$P]-GTP at position 5. Migration pattern of RNA synthesis products catalyzed by HRV-16 (*middle*) and EV-71 RdRp (*bottom*). Product formation resulting in GS-443902- or GS-646939-terminated primers were compared across increasing GS-646939 concentrations at GS-443902 concentrations of 10, 100, and 1000 µM. A 5′-$^{32}$P-labeled 4-nt primer serves as a size marker. ***B***, Graphical representation of GS-443902-terminated primers (%) at increasing GS-646939 concentrations as shown in A. ***C***, The $MC_{50}$ value is defined as the concentration at which GS-646939 outcompetes GS-443902 for incorporation at position 6. The competition index (CI) is the ratio of the $MC_{50}$ value to the GS-443902 concentration present in the reaction. ***D***, CI values determined for HRV-16 and EV-71 RdRp and the CI average ($CI_{avg}$) and standard deviation (±) across all GS-443902 concentrations.

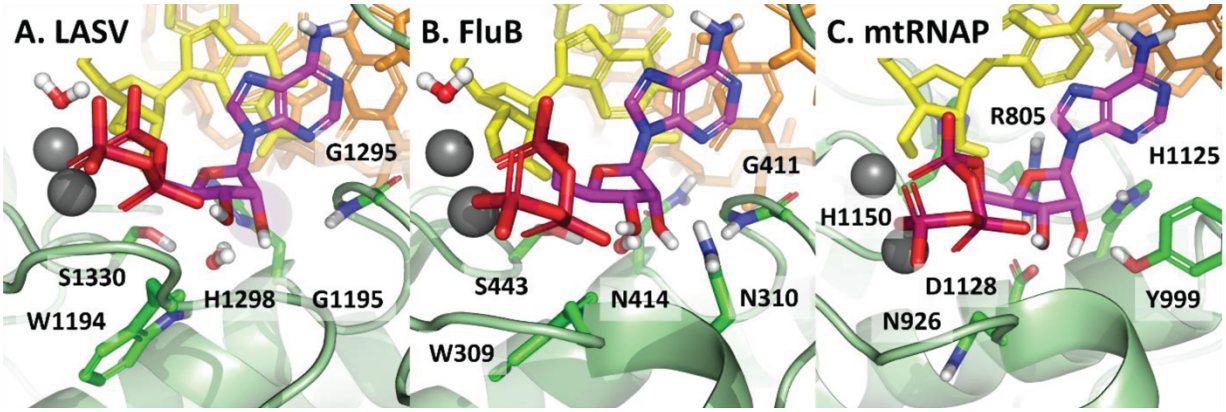


**Figure E3. Models of ATP in its pre-incorporated state for A, LASV, B, FluB, and C, h-mtRNAP**. The active sites of LASV and FluB are similar to RSV and PIV5, but differ significantly in the specific residues which recognize the 2′-OH and define the 4' pocket. In particular, a bridging water molecule is predicted to be a key element in the recognition of the 2′-OH. This is likely displaced by the 4′-cyano of GS-646939, compromising its affinity for these polymerases. The active site for h-mtRNAP is structurally very different from the viral polymerases. The 4′-cyano of GS-646939 appears to conflict with a salt bridge formed by Arg-805 and Asp-1128, which sit just below the ribose, making it a poor inhibitor.

*JKP contributed this figure

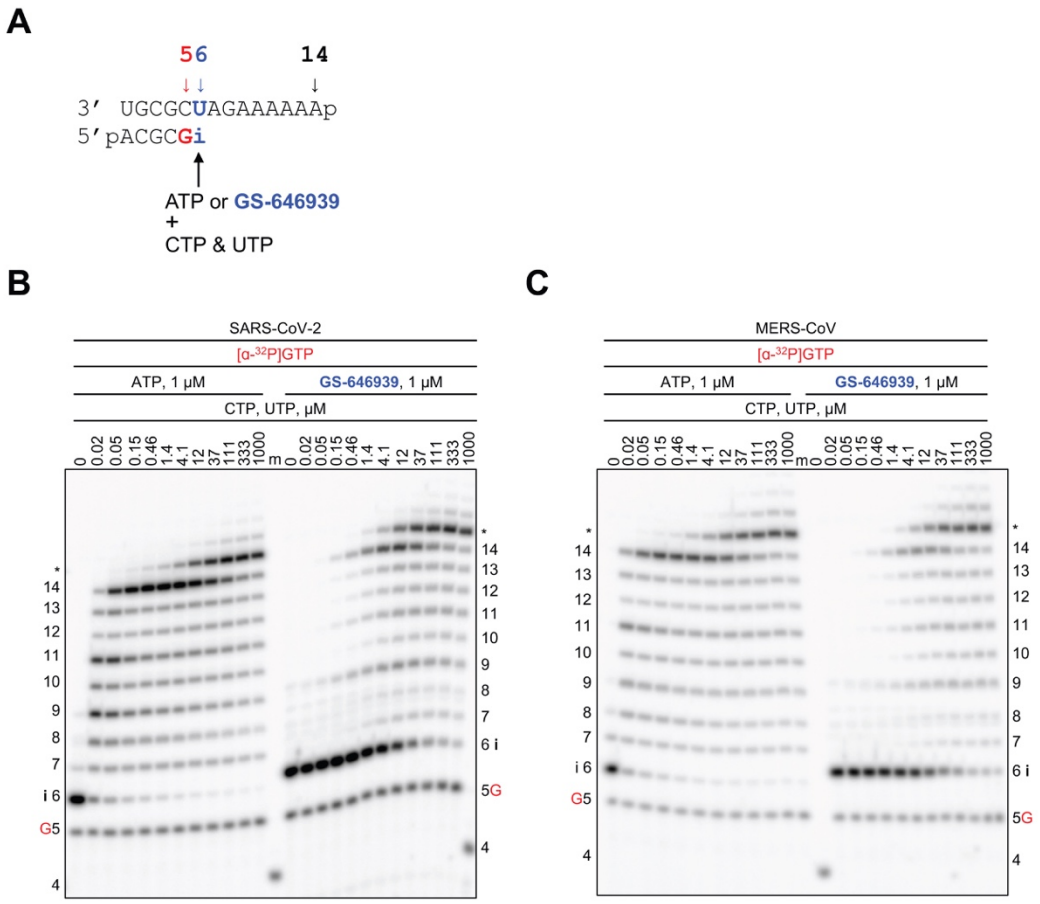


**Figure E4. SARS-CoV-2 and MERS-CoV RdRp-catalyzed RNA synthesis and inhibition patterns following a single incorporation of ATP or GS-646939 as a function of nucleotide concentration**. ***A***, RNA primer/template supporting RNA synthesis and single incorporation of ATP or GS-646939 at position 6 ("i"). G indicates incorporation of [α-$^{32}$P]-GTP at position 5. ***B***, Migration pattern of RNA products resulting from SARS-CoV-2 RdRp catalyzed RNA extension of AMP (*left*) of GS-646939 (*right*) at increasing concentrations of CTP and UTP. A 5′-$^{32}$P-labeled 4-nt primer serves as a size marker. Product formation at and beyond the asterisk indicate RNA products that are likely a result of sequence-dependent slippage events. ***C***, Reactions with MERS-CoV RdRp, incomplete inhibition of RNA synthesis occurs at the site of GS-646939 incorporation, full template-length product is generated at elevated nucleotide concentrations.

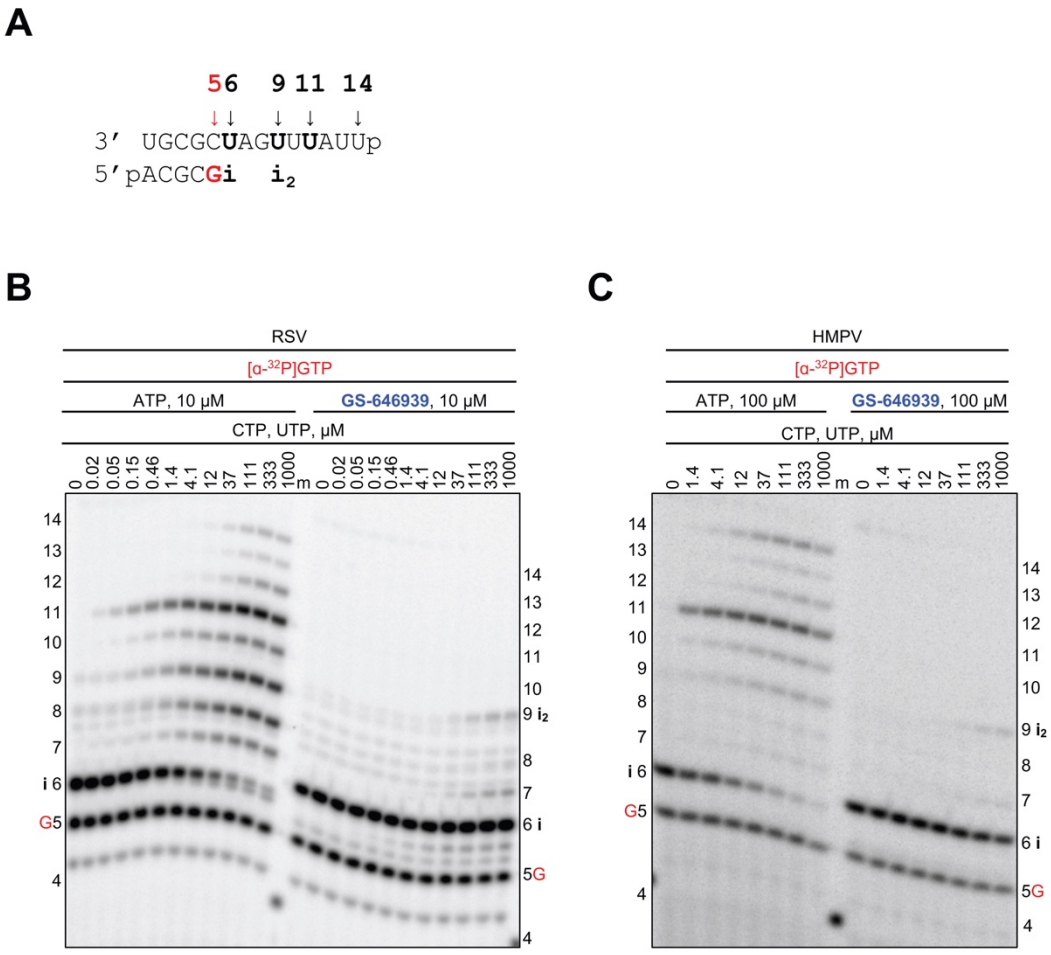


**Figure E5. RSV or HMPV RdRp-catalyzed RNA synthesis and inhibition patterns following the incorporation of GS-646939 as a function of nucleotide concentration**. ***A***, RNA primer/template supporting RNA synthesis and a first and second incorporation of ATP or GS-646939 by RSV and HMPV RdRp at position 6 ("i") and 9 ("$i_2$"). G indicates incorporation of [α-$^{32}$P]-GTP at position 5. ***B***, Migration pattern of RNA products resulting from RSV RdRp-catalyzed RNA extension of AMP (*left*) or GS-646939 (*right*) at increasing concentrations of CTP and UTP. A 5′-$^{32}$P-labeled 4-nt primer serves as a size marker. ***C***, Migration patterns of RNA products catalyzed HMPV RdRp, RNA synthesis was monitored at increasing CTP and UTP concentrations when ATP (*left*) or GS-646939 (*right*) were incorporated at position 6. GS-646939-terminated primers fail to be extended.

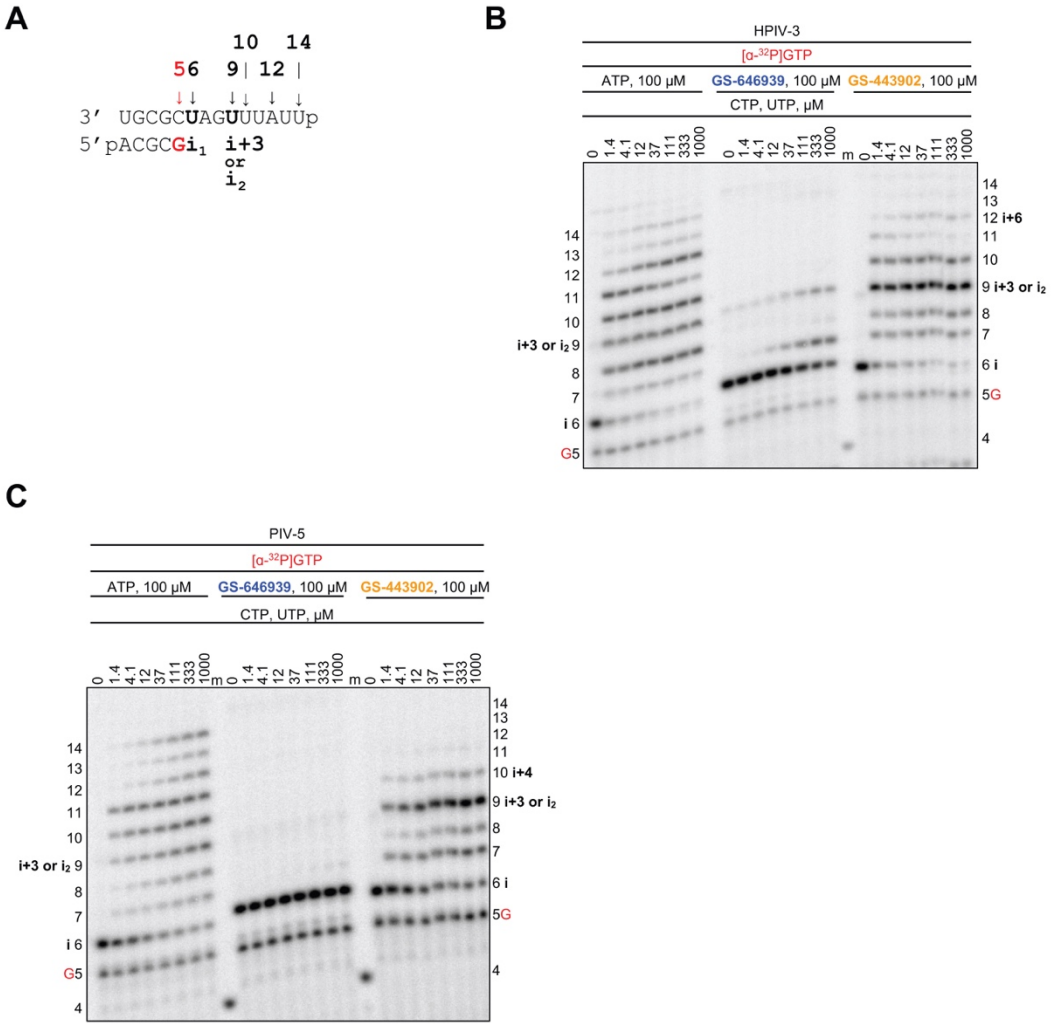


**Figure E6. HPIV-3 or PIV-5 RdRp-catalyzed RNA synthesis and inhibition patterns following the incorporation of ATP, GS-646939, or GS-443902**. ***A***, RNA primer/template supporting RNA synthesis and a first and second incorporation of ATP or GS-646939 or GS-443902 at position 6 ("i") and 9 ("$i_2$"). G indicates incorporation of [α-$^{32}$P]-GTP at position 5. ***B***, Migration patterns of RNA products catalyzed HPIV-3 RdRp. RNA synthesis was monitored at increasing CTP and UTP concentrations when natural ATP (*left*), GS-646939 (*middle*), or GS-443902 (*right*) were incorporated at position 6. GS-646939 termination was nearly absolute, whereas RNA products can be observed up to position 12 following the incorporation of GS-443902. ***C***, Migration patterns of RNA products catalyzed PIV-5 RdRp, RNA synthesis was monitored at increasing CTP and UTP concentrations when natural ATP (*left*), GS-646939 (*middle*), or GS-443902 (*right*) were incorporated at position 6. PIV-5 RdRp failed to catalyze RNA products beyond an incorporated GS-646939, while GS-443902 could be readily extended to position 9 ("i+3" or "$i_2$").

*SMW contributed to this figure

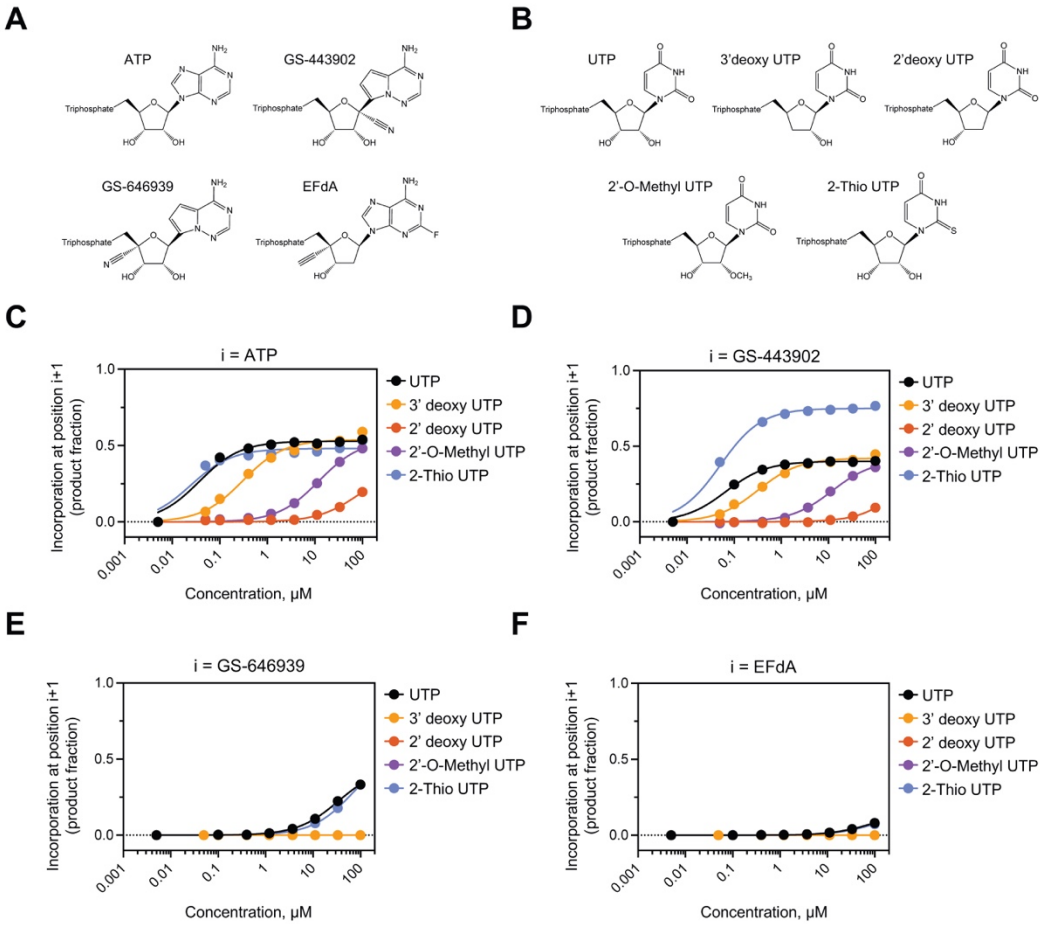


**Figure E7. GS-646939 inhibits subsequent nucleotide incorporation catalyzed by HRV-16 RdRp in a manner resembling EFdA**. ***A***, chemical structures of ATP and ATP analogs. ***B***, Chemical structures of UTP and UTP analogs. UTP and UTP analog incorporation at position 'i+1' was examined at increasing concentrations immediately following incorporation of ATP (***C***), GS-443902 (***D***), GS-646939 (***E***), or EFdA (***F***) at position "i". Product fraction was calculated as the signal generated beyond position "i" divided by the total signal in the lane.

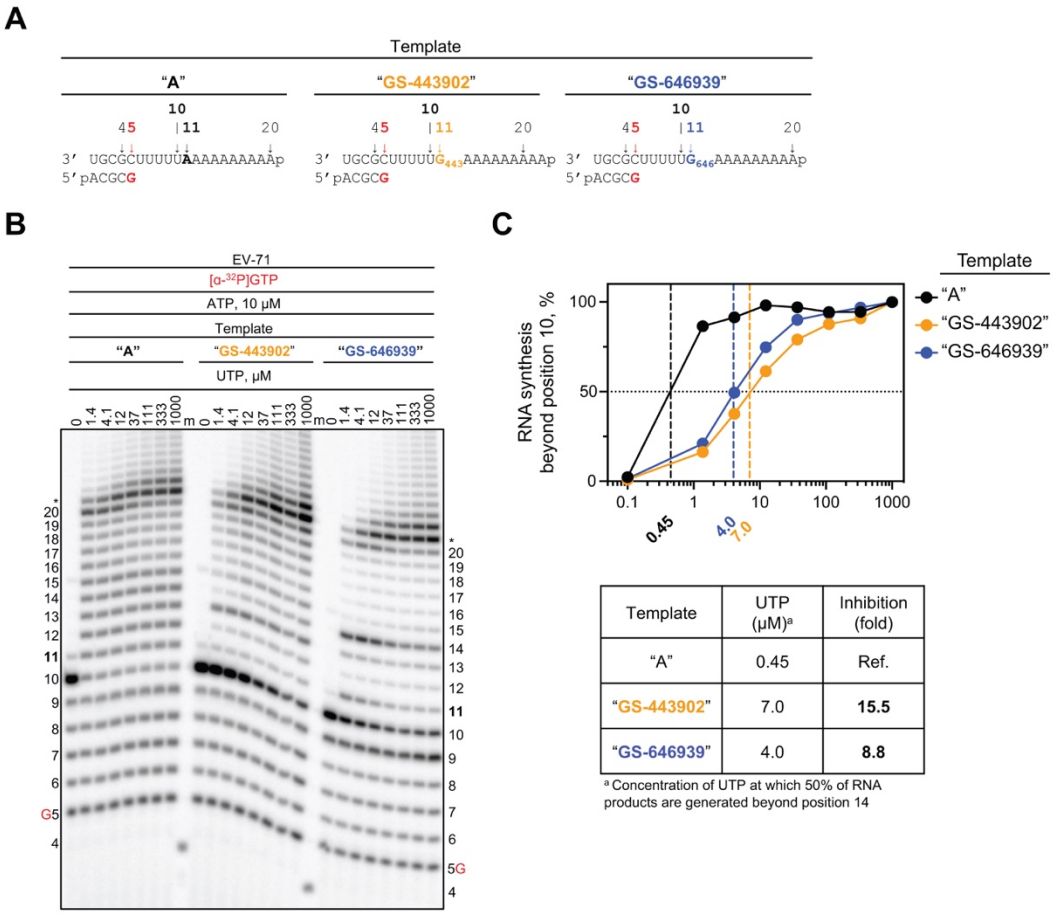


**Figure E8. RNA synthesis catalyzed by EV-71 RdRp using a template with a single GS-443902 or GS-646939 residue in the template at position 11**. ***A***, RNA primer/template with a template-embedded GS-443902 (Template "GS-443902", *middle*) or GS-646939 (Template "GS-646939", *right*) at position 11; the corresponding primer/template with adenosine (Template "A") at this position is shown on the left. G5 indicates incorporation of [α-$^{32}$P]-GTP at position 5. ***B***, Migration pattern of the products of RNA synthesis catalyzed by EV-71 RdRp. $MgCl_2$, [α-$^{32}$P]-GTP, and ATP were provided to the reaction to support RNA synthesis up to position 10. Increasing concentrations of UTP were supplemented to the reactions to monitor incorporation opposite adenosine, GS-443902, or GS646939 at position 11, and templated adenosines from position 12 to 20. For Template "GS-443902", intermediate products are observed at position 10. For Template "GS-646939", additional sites of inhibition are indicated by the formation of intermediate products at positions 9 and 14. Product formation at and beyond the asterisk indicates RNA products that are likely a result of sequence-dependent slippage events. A 5′-$^{32}$P-labeled 4-nt primer serves as a size marker ***C***, Quantification of *B* (*top*) where the sum of RNA products generated beyond position 10 was divided by the total signal in the lane and normalized as a percentage, fold-inhibition resulting from a templated GS-443902 and GS-646939 (*bottom*). To account for template-dependent differences in activity, product fraction was normalized as a percentage to the product fraction observed at 1000 μM UTP for that template.

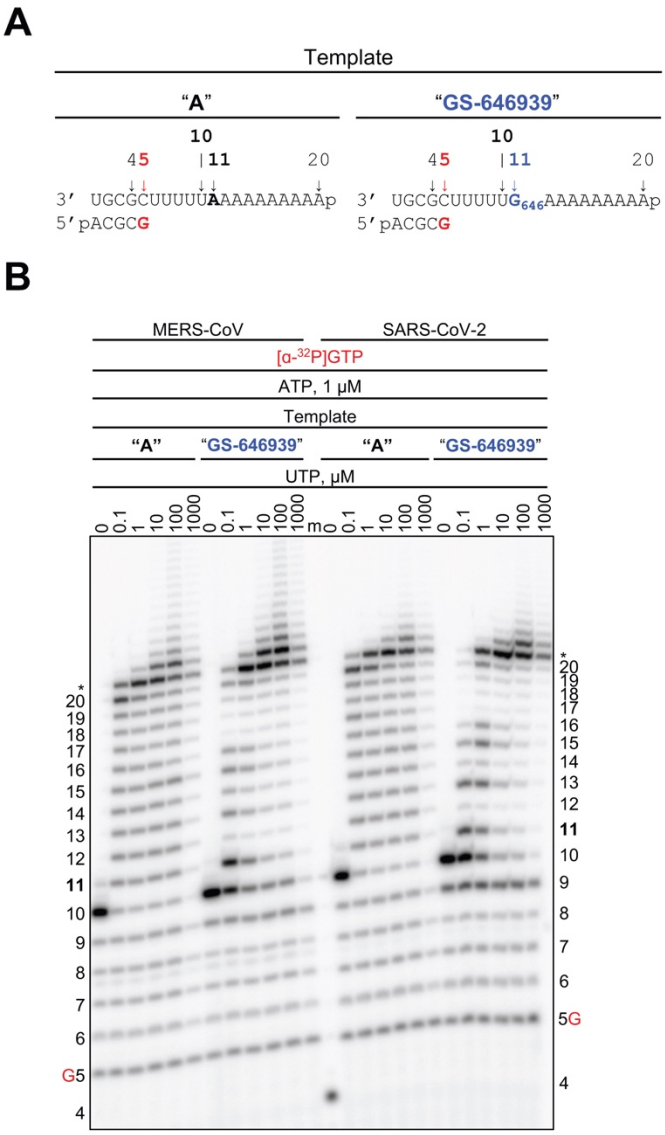


**Figure E9. RNA synthesis catalyzed by MERS-CoV and SARS-CoV-2 RdRp using a template with a single GS-646939 residue embedded at position 11**. ***A***, RNA primer/template with template-embedded GS-646939 (Template "GS-646939", *right*); the corresponding primer/template with adenosine (Template "A") at this position is shown on the left. G5 indicates incorporation of [α-$^{32}$P]-GTP at position 5. ***B***, Migration pattern of the products of RNA synthesis catalyzed by MERS-CoV and SARS-CoV-2 RdRp. $MgCl_2$, [α-$^{32}$P]-GTP, and ATP were provided to the reaction to support RNA synthesis up to position 10. Increasing concentrations of UTP were supplemented to the reactions to monitor incorporation opposite an embedded AMP, or GS-646939, at position 11, and templated adenosines from position 12 to 20. A 5′-$^{32}$P-labeled 4-nt primer serves as a size marker.